Analysis of highly dynamic mooring systems: peak mooring loads in realistic sea conditions

Submitted in September 2014 by

Violette Rozenn Harnois

to the University of Exeter,

College of Engineering, Mathematics and Physical Sciences

as a thesis for the degree of

Doctor of Philosophy in Renewable Energy

I certify that all material in this thesis which is not my own work has been identified and that no material has previously been submitted and approved for the award of a degree by this or any other University.

Abstract

Marine Renewable Energy (MRE) is a promising source of energy for the future. However, it is still under development and many challenges need to be overcome to develop competitive solutions. While the design of the station keeping system of traditional offshore oil and gas structures is driven mainly by their low frequency motions, MRE devices are installed at nearshore locations and move dynamically.

Because of these criteria, MRE mooring systems require novel mooring systems and associated standards. MRE mooring standards need to take into account the highly dynamic behaviour of these systems, which can lead to large mooring loads. The nature of these loads needs to be investigated to improve the confidence in mooring design and to improve cost-effectiveness. The aim of this thesis is to develop the understanding of peak mooring loads on highly dynamic mooring systems, in particular, the environmental conditions associated with the loads. In addition, preliminary research into the response of the mooring systems to environmental conditions is presented.

Both field tests and tank tests have been conducted. Field tests give insight into the behaviour of a dynamic mooring system in real sea conditions. Measuring the mooring loads and the environmental conditions - wave, and current if available – for several months, a methodology has been developed to detect peak mooring loads and identify the associated environmental conditions in order to compare them with the environmental conditions recorded throughout the field tests. The principal finding is that peak mooring loads occur for sea states with large but not always the highest significant wave height H_S. The understanding of the effect of tidal conditions on peak mooring loads requires further work.

A tank test of a dynamic mooring system in moderate sea states has been conducted to observe the dynamic behaviour of the mooring system. Tank tests enable detailed observations of the dynamic behaviour of a system in a well controlled environment and allow the calibration of a numerical model. The model can be used to investigate separate physical parameters.

The results from this thesis will assist in the development of specific standards for MRE mooring systems. These standards are essential for the evolution of the MRE industry.

Keywords

Marine Renewable Energy (MRE)

mooring systems

standards

peak mooring loads

highly dynamic mooring systems

field tests

tank tests

numerical model

mooring loads

environmental conditions

To my Dad

Acknowledgments

To start with, I want to thank Prof. Lars Johanning, who gave me the opportunity to undertake this PhD in parallel with my Research Associate position, for his enthusiasm and determination. My thoughts also turn to my second supervisor, the late Prof. George Smith, who was a great support during the start of my PhD. And I want to thank Dr Philipp Thies, who stepped in, for his energy and scientific rigour. I am extremely grateful for the patience and invaluable advice of all my supervisors.

Further, I want to acknowledge my internal examiner, Dr Gavin Tabor, and my external examiners, Prof. Lars Bergdahl and Prof. Nigel Barltrop.

I would like to thank the Renewable Energy team at the University of Exeter, in particular David Parish who built the SWMTF buoy and always took the time to reply to my (many) questions. I also want to thank Isabel Noon, from the ASK academics skills team, who significantly contributed to the improvement of my English and to the development of my academic English.

I would like to acknowledge the support of the organisations I worked with: Fred Olsen, Ifremer, Orcina, and Teledyne RDI.

This research was made possible through a fee waiver authorised by the College of Engineering, Mathematics and Physical Sciences of the University of Exeter, and through my Research Associate position paid by the Technology Strategy Board for the Fred-Olsen Bolt-2 Lifesaver project, by MARINET and MERiFIC for the SWMTF tank tests, and by the Regional Growth Fund (RGF) for the FaBTest project.

I am also grateful to my colleagues at AWS Ocean Energy, in particular Dr John Fitzgerald and Ben Yeats, who developed my interest in mooring systems. And I want to thank my teachers in higher education, in Classes Préparatoires (equivalent to a BSc) and at Ecole Centrale Marseille (equivalent to a MSc), who gave me a solid and wide scientific knowledge base.

Finally, on a personal note, I want to thank my friends (especially Dan, Niall, Tom, Ally and Tim for the proof-reading and comments) and family for their support through four hectic years.

List of Contents

List of figures

List of Tables

Author's declaration

The South West Mooring Test Facility (SWMTF) has been installed in March 2010 before the author joined the University of Exeter. The buoy and its mooring have been designed by David Parish and Prof. Lars Johanning from University of Exeter. The code to organise the data have been developed in close collaboration with the Computing development officer of the Renewable Energy team. The author was not involved with the practical work but has been focusing on the analysis of the data.

The Fred Olsen Bolt-2 Lifesaver is a commercial project led by Fred Olsen with University of Exeter as part of a consortium. The author of this thesis has been involved in various aspects of the Bolt-2 Lifesaver project for two years as part of her Research Associate (RA) position. In particular, the author of this thesis has contributed to the mooring design of this device. For this thesis, the major input from the Fred Olsen project is the mooring load data which have been analysed and the major output is the peak mooring load assessment for different wave conditions.

The author of this thesis had the opportunity to conduct tank tests as part of her involvement with her Research Associate position in the MARINET (three month RA contract) and MERiFIC (six month RA contract) projects. The Ifremer team built the physical model of the buoy and its mooring and ran the tank tests. The author visited Ifremer for one week during the tank tests. Hydrodynamic parameters of the buoy (e.g. AQUAPLUS output: RAO, QTF, radiation damping, added mass) were provided by Ifremer team as an input to OrcaFlex numerical model. The author developed a Matlab code to analyse the tank test data and used it to analyse the mooring behaviour. The analysis of the data (wave elevation, buoy motion, mooring load) has been integrally conducted by the author of this thesis. These tests lead to a journal paper (Harnois et al., 2014).

Nomenclature

Roman symbols

C current velocity

C_{Mag} current magnitude

C_{Dir} current direction

C_D drag coefficient

C_M inertia coefficient

D buoy diameter

D_{mean} mean wave direction

D_P peak wave direction

f frequency

H wave height in regular waves

h water depth

H_{max} maximal wave height

H_{mean} mean significant wave height

H_S significant wave height

$H_{1/3}$ the mean height of the highest one-third of the zero up-crossing waves

$H_{1/10}$ the mean height of the highest one-tenth of the zero up-crossing waves

I Moment of inertia

K peak mooring load factor

K_C Keulegan-Carpenter number

m_x xth order moment of a spectrum

p_1 linear damping

p_2 quadratic damping

Q_p spectral peakedness parameter

S_{max} standard score of the maximum

S_P average wave steepness using T_P

S_S average wave steepness using T_Z

t time

T wave period in regular waves

$T_{1/3}$ period associated with $H_{1/3}$

$T_{1/10}$ period associated with $H_{1/10}$

T_m natural period

T_{mm10} wave energy period

T_{mean} period associated with H_{mean}

T_P peak period

T_Z mean zero up-crossing period

Ur Ursell number

X_n amplitude of the nth oscillation

Greek symbols

λ wave length

ξ motion amplitude in one degree of freedom

ω angular frequency

φ Phase

τ minimum threshold

Subscripts

$_a$ axial

$_{bin}$ bin size

$_m$ motion

$_n$ normal

$_{peak}$ peak mooring load

$_{vec}$ vector

$_w$ wave

$_0$ minimum value

$_{max}$ maximum current magnitude

Acronyms

ADCP acoustic Doppler current profiler

ALS accidental limit state

CALM catenary anchor leg mooring

CFD computational fluid dynamics

COG centre of gravity

CTD conductivity, temperature, density (and salinity)

DMaC Dynamic Marine Component

DN nominal diameter

DOF degree of freedom

EIA environmental impact assessment

FEM finite element method

FFT fast Fourier transform

FLS fatigue limit state

HF high frequency

JPO joint percentage of occurrences

LCOE levelised costs of energy

LF low frequency

MBL minimum breaking load

MRE marine renewable energy

OPT Ocean Power Technologies

OWC oscillating water column

PTO power take-off

QTF quadratic transfer function

RAO response amplitude operators

SALM single anchor leg mooring

SD scatter diagram

SWMTF South West Mooring Test Facility

TRL technology readiness level

ULS ultimate limit state

VLA vertically loaded anchor

WAFO wave analysis for fatigue and oceanography

WEC wave energy convertors

WF wave frequency

Chapter 1. Aims, objectives and methods

1.1 Motivation, aims and objectives

The motivation of this work is to contribute to advance the Marine Renewable Energy (MRE) sector, in particular the wave energy sector, towards commercial realisation. If design uncertainties are reduced, more cost effective designs could be developed.

In terms of technology readiness level (TRL), most of the devices are between TRL 5, “Component and/or breadboard validation in relevant environment”, and TRL 7, ”System prototype demonstration in an operational environment”. At these stages, specific requirements in terms of moorings need to be fulfilled. Mooring requirements present a challenge where over-designing the mooring incurs a cost penalty, while under-designing the mooring may lead to a failure. Furthermore, a mooring design that would result in reduced response characteristics within power-take-off (PTO) response modes, in the case of a motion-dependent wave energy device, will also lower the power production. The requirement for free movement implies novelty in the mooring design and materials because conventional mooring systems try to achieve different aims. It is therefore important to develop specific dynamic mooring systems and corresponding guidelines for MRE applications.

In particular, the characteristics and occurrence of peak mooring tensions over a wide range of environmental conditions need to be better understood, leading to the research question: **“when and why do peak mooring loads occur?”**

The aim of this research is to develop and apply novel methods to improve the understanding of MRE mooring response to environmental conditions. These new methods would lead to the improvement of MRE mooring designs and would inform MRE guidelines.

The objectives of the collection of extensive field load measurements of floating motion-dependent wave energy devices or similar devices were:

- To assess environmental conditions which trigger peak mooring loads: to obtain better understanding of occurrence and severity of mooring line tension characteristics over a range of sea states
- To develop a procedure for analysis techniques for large datasets obtained from field tests
- To evaluate what sample frequency is required by loadcells to accurately detect peak mooring loads
- To gain experience on MRE mooring deployment and operation to inform guidelines

Focused tank tests of a floating wave energy device and its mooring have been used:

- To develop a procedure to test mooring system in a controlled environment
- To calibrate and validate a numerical mooring model using tank test data
- To individually assess different physical parameters

1.2 Methods

Extensive field load measurements of devices with a dynamic behaviour were collected using two compliant catenary mooring systems with fibre ropes, one for a research facility, and the other for a wave energy device. This type of mooring is commonly used for motion-dependent wave energy mooring systems.

Both mooring systems were installed at locations representative of full scale or scaled wave energy site. The mooring systems used accurate instruments which sampled data at sufficiently high frequencies that are likely to ensure the peak mooring loads were accurately measured and not missed. Large datasets of mooring loads and environmental conditions (months of data) were collected to observe a sufficient amount of peak mooring loads and a significant range of sea states. Methodologies were developed to handle these large datasets, to identify anomalies such as unexpected change in the pre-tension (tension in the mooring at the equilibrium position, without environmental effects), to detect peak mooring loads and to associate them with environmental conditions. The aim of this field work is to identify which environmental conditions are likely to trigger peak mooring loads.

The main objective of the thesis was to investigate statistical values (mean, maximum...) of mooring line tension and relate these values to the associated sea-states. A correlation between the time series of the surface elevation and of the buoy motions was not achievable because of insufficient information about the surface elevation at the buoy position. Consequently, a time domain analysis was not implemented. More details below are given about the difficulties associated with the time series of surface elevation and of the buoy position:

- Surface elevation: In order to analyse correctly the response to the waves of the moored instrumented buoy at a given time step, it would have been essential to predict accurately the wave propagation from the point of measurement to the buoy position. This would first require knowing the exact point of measurement – the exact position of the ADCP used to measure the wave and current. However, there are significant uncertainties about this

position due to the nature of field testing. This would also require knowing the position of the buoy, which is discussed in the following bullet point. Then, a lengthy study would be required to correlate wave propagation between the ADCP location and the buoy position at a given time step.

- Buoy position: the buoy motion was known using GPS data or accelerometer/gyroscope data. The GPS was off centred and higher than the centre of gravity of the buoy, so the 3 DOF rotations of the buoy should be known in order to calculate the position of the centre of gravity of the buoy or the position of a mooring line attachment point. However, the only available data for rotations are angular velocities, which need to be integrated, but their constant of integration is not known. The accelerations could also be integrated twice to estimate the buoy motion, but similarly, the constants of integrations are not known. A complex algorithm using the GPS and the accelerometer/gyroscope data could be created (for example using a Kalman filter) requiring significant further work that was not within the achievable scope.

In order to gain a better understanding of the dynamics of the mooring system and of peak mooring load occurrences, tank tests of the mooring of the research facility were conducted using a 1:5 scale model. The scale has been chosen as large as the basin allowed it to limit scaling effects. These tests were conducted in moderate waves, not focusing on extreme responses. Tests have been conducted step by step, with each step clearly identifying separate hydrodynamic parameters: static and quasi static tests validated the buoy draft, pre-tension and mooring stiffness; decay tests verified the added mass of the buoy and damping of the system; regular wave tests with a large range of wave height and period identified resonance and investigated non-linear behaviour with steep waves; and irregular wave tests indicated the ability of the numerical model to replicate the mooring behaviour under real excitations. A procedure has been developed for wave energy mooring tank tests and for the calibration and validation of a numerical mooring model.

1.3 Content and structure

Each chapter of this thesis aims to focus on a different element of the research question (Figure 1.1).

Chapter 1 defines the motive, research question and the methodology while Chapter 2 sets the research context and identifies the related work.

Chapter 3 presents the field work. Sea trials have been conducted a) at the South West Mooring Test Facility (SWMTF) using an instrumented moored buoy and an Acoustic Doppler Current Profiler (ADCP) and b) at FaBTest using Fred Olsen Bolt-2 LifeSaver device and a wave buoy. This chapter explains why these locations have been chosen for field tests, which mooring layout and instrumentation have been used, how the raw data were organised, and which data are available (field test and hindcast data).

Chapter 4 shows in detail the collected data at both facilities. The data pre-processing, correction and validation is explained. Example of time series and summarised data are shown in order to indicate the dynamic behaviour and the orders of magnitude. The summary of all collected data is then presented. In particular, the percentage of occurrences of environmental conditions and mooring loads is highlighted in order to identify the frequent and infrequent behaviours.

Chapter 5 describes the method which has been developed to detect peak mooring loads from the summary of collected field data. The environmental conditions which occur when peak mooring loads were detected are observed and compared with the measured data recorded throughout the field tests. The results are presented for two different case studies: SWMTF and Bolt-2 Lifesaver.

Chapter 6 introduces the methodology and results of laboratory work and associated building, calibration and validation of a numerical model. Tank tests of a 1:5 model of the SWMTF buoy and mooring have been conducted in the Ifremer basin. The usual tank test methodology has been followed: static and quasi-static tests, decay tests, regular wave and irregular wave tests.

Chapter 7 discusses the findings and states the impact of the scientific findings towards the wave energy development.

Chapter 8 identifies areas for further investigations and concludes.

Appendix 1 presents the publications which have been written during this PhD.

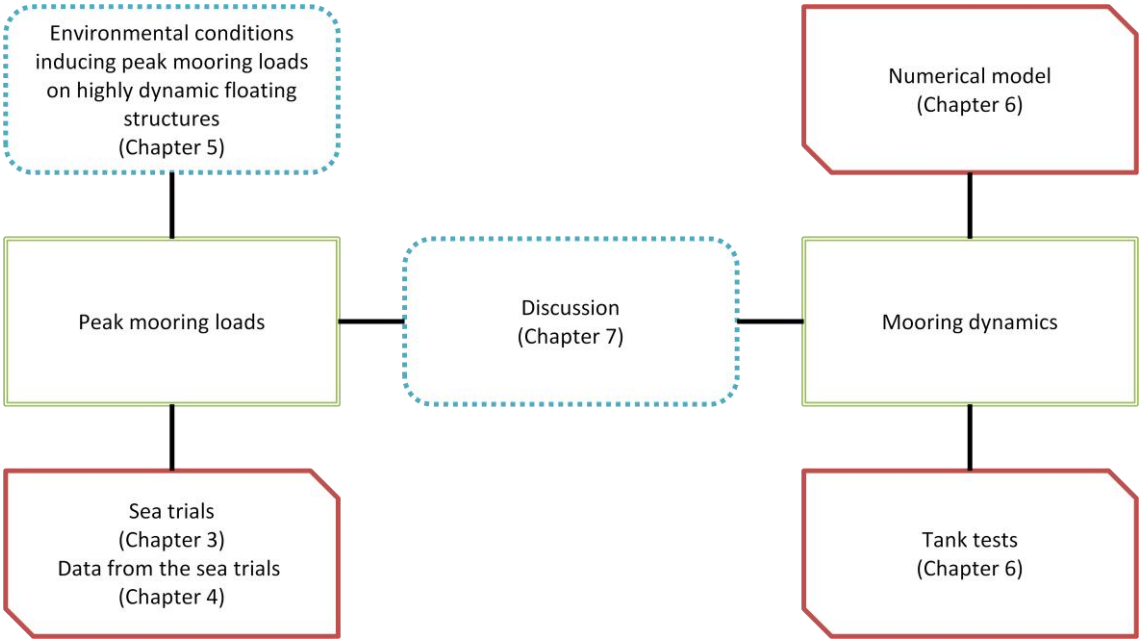

Figure 1.1: Scope of the thesis and links between the different chapters

Chapter 2. Literature review

This chapter reviews the state of the art in the field of moorings for wave energy converters.

This chapter starts by presenting wave, hydrodynamics and wave energy. Basic knowledge about waves and hydrodynamics which is necessary for the understanding of this thesis is outlined. This section also puts wave energy in context.

Mooring analysis is introduced: environmental data required for design calculations are described; design calculations are explained; the safety factors applied on the results of these design calculations are discussed; the additional fatigue calculations are presented; and the lack of accurate and specific Marine Renewable Energy (MRE) guidelines is discussed.

Mooring configurations and components which have been used for years in the traditional oil and gas sector are described. The specific needs, the potential solutions and the methods to design specific moorings for wave energy devices using existing and novel mooring configurations and components are highlighted.

2.1 Wave and hydrodynamics

This section summarises basic knowledge about waves and hydrodynamics: statistical parameters describing ocean waves, regular waves applied in laboratory to study behaviour of floating structure at a given frequency, static catenary equations, equation of motion of moored systems, snap mooring loads, and different theories to represent the motion of a floating body.

This section also introduces wave energy and its context: the diversity of wave energy technologies, the complexity of the wave energy resource, the challenging energy transition in the UK and the place of wave energy in this transition, and the difficulties faced by wave energy projects are presented.

2.1.1 Sea states and wave theory

This subsection describes several wave parameters which are commonly used to describe a sea state. The method to arrange these parameters into a scatter diagram is explained. The wave theories associated with regular waves are also introduced.

2.1.1.1 From wave parameters to scatter diagrams

A stationary period of three hours is usually considered for sea states (Molin, 2002). Spectrum analysis during a sea state is commonly conducted using the spectral density $S(\omega)$. The wave spectrum can also be directional $S(\omega,\vartheta)$ or expressed using the wave frequency f instead of the angular frequency ω: $S(f,\vartheta)$ or $S(f)$. Moments are calculated based on the wave spectrum: $m_n = \int_0^\infty \omega^n S(\omega) d\omega$ or $m_n = \int_0^\infty f^n S(f) df$ (these two values are different for $n \neq 0$)

Spectral parameters are then calculated:

- The significant wave height H_S - originally defined as the mean height of the highest one-third waves in a sea state - estimated as $4\sqrt{m_0}$, for a narrow spectrum, with m_0 the zeroth order moment of the spectrum $S(\omega)$

- The spectral peak period T_P at which the wave spectrum $S(\omega)$ reaches its maximum value. Consequently, this period cannot be defined satisfactorily in multi-peaked spectra.

- The mean zero up-crossing period T_Z - initially the mean time between the wave elevation crossing zero - estimated as $2\pi\sqrt{\frac{m_0}{m_2}}$. In this equation, m_2 is calculated using ω and not f. m_2 is highly dependent on the higher frequencies of the wave spectrum and consequently T_Z may not be very stable.

- The wave energy period T_{mm10} estimated as $2\pi\frac{m_{-1}}{m_0}$ is the period at which the wave power is transported. m_{-1} was calculated using ω.

- The peak direction D_P associated with the spectral peak period T_P

- The mean wave direction D_{mean} (Kuik et al., 1988) equal to $arctan\left(\frac{\int_0^{2\pi}\int_0^{\infty}\cos(\theta)S(f,\theta)dfd\theta}{\int_0^{2\pi}\int_0^{\infty}\sin(\theta)S(f,\theta)dfd\theta}\right)$

- Q_P the spectral bandwidth, equal to $\frac{2}{m_0^2\int_0^{\infty}fS^2(f)df}$ (Goda, 1976)

H_S and T_Z were originally (in the absence of computing tools) calculated using a zero crossing method. They are now mainly defined using spectrum calculations. Other parameters can also be estimated with zero crossing method such as

- H_{max}, the maximum wave height, or T_{max} its associated wave period,
- $H_{1/10}$, the mean height of the highest one-tenth of the zero up-crossing waves in a sea state and its associated period $T_{1/10}$,
- H_{mean}, the mean significant wave height and its associated period $T_{mean.}$

H_S and T_P, or H_S and T_Z, are related by a steepness criterion. The average wave steepnesses are defined as $S_S = \frac{2\pi}{g}\frac{H_S}{{T_Z}^2}$ and $S_P = \frac{2\pi}{g}\frac{H_S}{{T_P}^2}$.

The limiting values in absence of better sources are

- S_S = 1/10 for $T_Z \leq 6$ s and S_S = 1/15 for $T_Z \geq 12$ s, and linearly interpolated values in between,
- and S_P = 1/15 for $T_P \leq 8$ s and S_P= 1/25 for $T_Z \geq 15$ s, and linearly interpolated values in between (DNV-RP-C205, from DNV, 2010).

In order to identify the range of sea states occurring at a site, and the frequency of occurrences of these sea states, scatter diagrams are built using long term measurements of waves. The number of occurrences of two wave parameters *x* and *y* in a given range is summed as shown in Eq. (2.1).

$$SD(x,y)_{i,j} = \sum_{k=1}^{nb\_data} \left\langle \begin{array}{c} x_0 + (i-1)x_{bin} \le x_k < x_0 + ix_{bin} \\ and \\ y_0 + (j-1)y_{bin} \le y_k < y_0 + jy_{bin} \end{array} \right\rangle \quad (2.1)$$

With *SD* the scatter diagram and x_k and y_k the couple describing the environmental conditions for a given sea state *k.*

If for a given *i*, *j* and *k* both conditions $x_0 + (i-1)x_{bin} \le x_k < x_0 + ix_{bin}$ and $y_0 + (j-1)y_{bin} \le y_k < y_0 + jy_{bin}$ are gathered, then the value between the bracket is equal to 1, else it is equal to 0.

If there is no measurement available, or the number of measurement is too low, a hindcast model can be used to build a scatter diagram. For example, SWAN (Simulating Waves Nearshore), a spectral wave model, can be used to build a hindcast model.

2.1.1.2 Regular waves and wave theory

Regular waves are commonly used in tank tests to improve the understanding of the tested system at a given frequency. The wave height *H*, the linear deep water wave length λ_0, the wave length λ and the water depth *h* are required to calculate different parameters which indicate which theory is the most appropriate to describe the waves (Figure 2.1, DNV-RP-C205, from DNV, 2010):

- The wave steepness parameter H/λ_0. In deep waters, the waves are breaking if H/λ is over 0.14. In reality waves are breaking for lower values, around 0.1.
- The shallow water parameter h/λ_0, with *h* the water depth,
- The Ursell number *Ur*, as defined in Eq. (2.2) (Molin, 2002).

$$Ur = \frac{H\lambda^2}{8\pi^2 h^3} \quad (2.2)$$

Only two of these parameters are required, the third one is depending on the other ones.

Figure 2.1 indicates which wave theory is the most appropriate depending on shalowness and wave steepness.

The knowledge of the water depth and of the wave theory is required for hydrodynamics calculations.

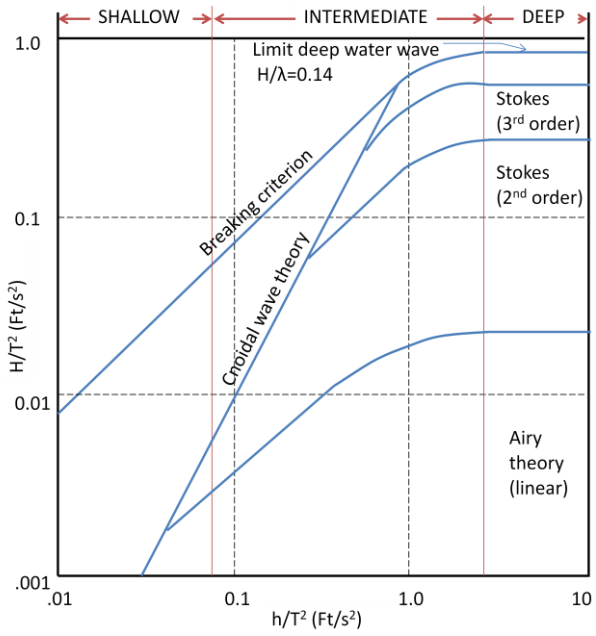

Figure 2.1: Range of validity of the different wave theories adapted from Le Méhauté (1976), with *H* the wave height, *T* the wave period and *h* the water depth

2.1.2 Hydrodynamics

Hydrodynamics is the branch of physics which deals with the motion of fluids and the forces acting on immersed structures. Catenary equations describe catenary lines forces and shape and can be used in a quasi-static approach. An equation of motion can describe the different forces on a traditional moored oil and gas structure. This equation helps to understand some dynamic behaviour such as snap loads on the mooring lines. The different parameters in the equation of motion can be modelled using several theories, depending on the relative size of the floating structure and of the waves, and of the shape of the waves.

2.1.2.1 Static catenary mooring behaviour

The static behaviour of a catenary line is given in Figure 2.2 and below. T is the tension in the catenary line, L the catenary length and L_s the length of the catenary hanging in the water column (lifted line length), h the water depth, Φ the upper angle of incidence of the line with horizontal in radians, x the horizontal scope, which is the horizontal distance between the catenary touchdown point and the floating structure,

and *X* the horizontal distance between the anchor point and the attachment point on the floating structure.

In addition, the parameter *a* is defined as $a = T_H/w$, with T_H the horizontal part of the line tension, and *w* the submerged weight by unit length of the mooring line.

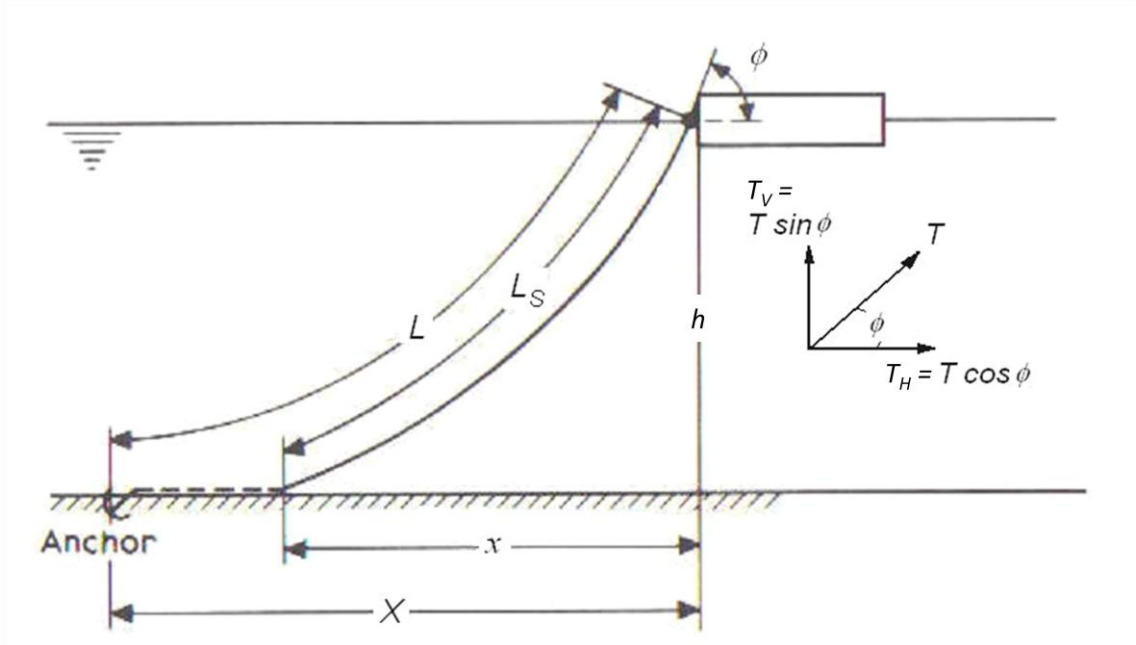

Figure 2.2: Example of a catenary line adapted from Johanning (n.d. a)

These parameters are linked with the following relationships. T_V is the vertical part of the mooring load, L_{min} the minimum line length required for a given maximum horizontal tension T_{H_max}.

$$x = a.cosh^{-1}\left(1 + \frac{h}{a}\right) \tag{2.3}$$

$$L_S = h\left(1 + 2\frac{a}{h}\right)^{\frac{1}{2}} \text{or } L_S = a.sinh\frac{x}{a} \tag{2.4}$$

$$T_H = \frac{wh}{2}\left[\left(\frac{L_S}{h}\right)^2 - 1\right] \tag{2.5}$$

$$T_V = wL_S \tag{2.6}$$

$$L_{min} = h\left(2\frac{T_{H\_max}}{wh} + 1\right)^{\frac{1}{2}} \tag{2.7}$$

$$X = L - L_S + x \tag{2.8}$$

From these equations, the relationship between the mooring load and the horizontal distance between the anchor and the floating structure can be calculated for a static case. An example is presented in Figure 2.3 for a given catenary line and water depth. If the horizontal distance between the buoy and the anchor is small, in this case

X/h < 2.1, the tension linearly increases with the horizontal distance and the cable is slightly lifted from the seabed. If the horizontal distance between the buoy and the anchor is large, in this case *X/h* > 2.1, the tension steeply and non-linearly increases with the horizontal distance until the cable is fully lifted and the line is taut.

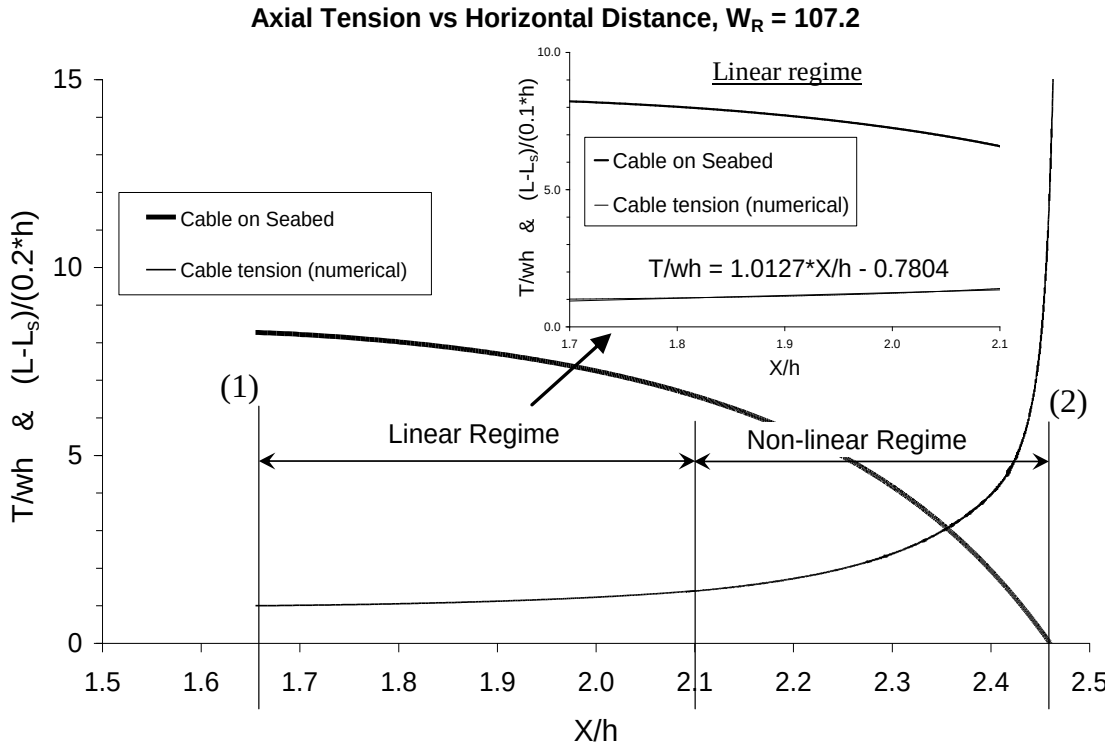

Figure 2.3: Catenary mooring line stiffness characteristics: static load excursion curve from Johanning (n.d.)

In the absence of external loading on the system, the vessel and mooring will not move from its equilibrium position. When external loads are applied on the system, an imbalance in the system occurs and the mooring system provides a restoring force.

For slow motions of the floating structure, a quasi-static approach could be followed to estimate the mooring behaviour. In this case, for each buoy position, the shape and tension of the mooring lines is directly derived from the catenary equations, which account for the weight and axial stiffness of the mooring lines but not for their inertia and for the current and wave forces. In addition, non-linear damping effects (viscous effects) are not taken into account.

2.1.2.2 Equation of motion of a moored floating structure

The dynamic approach is followed to get a more accurate representation of the dynamic response of the mooring system (Figure 2.4). Time domain or frequency domain analysis can be conducted. A software package such as OrcaFlex can be used

to calculate the dynamic behaviour of the mooring system using time domain analysis as explained in 2.4.3.3.

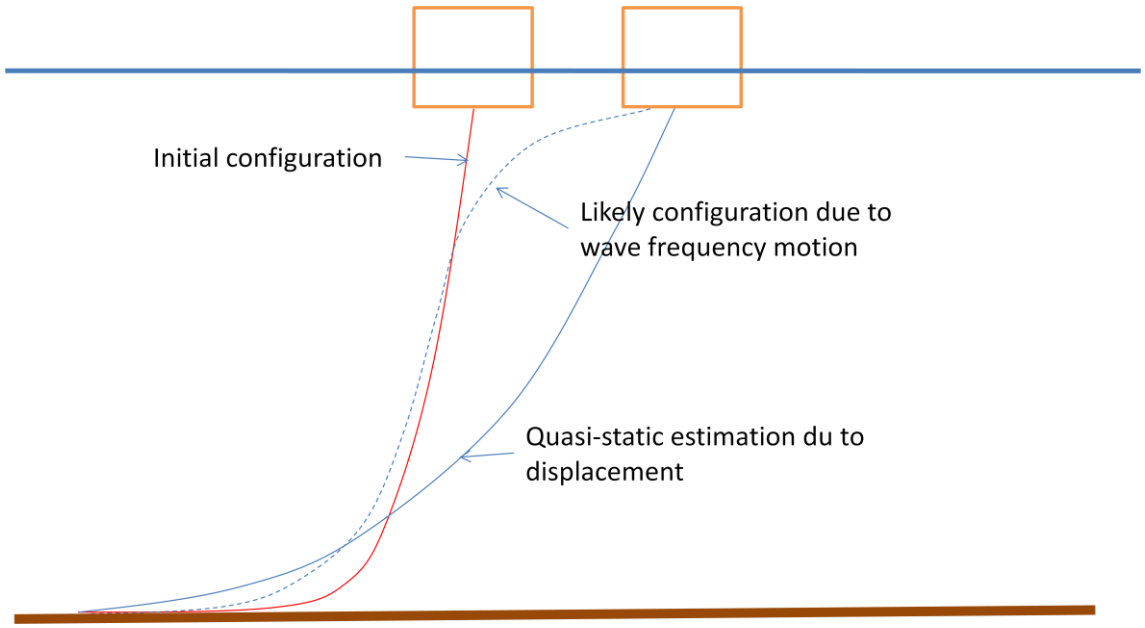

Figure 2.4: Difference between the quasi-static and dynamic model of a mooring line. From Johanning (n.d. b)

Assuming harmonic excitations forces, the dynamic response ξ of the floating structure in a degree of motion can be expressed by Eq. (2.9) (Chakrabarti, 1987):

$$\sum_{j=1}^{6}\begin{bmatrix} -\omega^2\left(M_{ij}^{Structure}+M_{ij}^{Mooring}\right) \\ -i\omega\left(B_{ij}^{Structure}+B_{ij}^{Mooring}\right) \\ +\left(K_{ij}^{Structure}+K_{ij}^{Mooring}\right) \end{bmatrix}\xi_j = F_i \tag{2.9}$$

with *j* =1,…,6 and *i* corresponding to the degree of freedom of the floating structure. Non diagonal terms of the matrixes are corresponding to coupling effects.

- ξ_j is the complex amplitude of motion,
- F_i is the complex amplitude of the exciting forces, which can be created by winds, waves or currents,
- ω is the excitation frequency,

- $M_{ij}^{Structure}$ is the mass, added mass and inertia matrix of the floating structure,
- $M_{ij}^{Mooring}$ is the external mass, added mass and inertia matrix caused by the mooring system,

- $B_{ij}^{Structure}$ is the damping matrix of the floating structure and represents the radiation damping and viscous damping,
- $B_{ij}^{Mooring}$ is the external damping matrix of the mooring system,

- $K_{ij}^{Structure}$ represents the hydrostatic and gravitational stiffness of the floating structure,
- $K_{ij}^{Mooring}$ is the external restoring force and moment matrix of the mooring system caused by the weight in water of the mooring line, its linear elasticity and non-linear dynamic stretching.

The exciting forces F_i are a combination of three excitation modes as described in DNV-RP-F205 (DNV, 2010):

- Steady current, mean wind and mean wave drift forces are creating a mean force, or static loading;
- Low Frequency (LF) forces (0-0.02 Hz) are induced by slowly varying wave drift forces, unsteady wind forces, and slowly varying tidal forces;
- Wave Frequency (WF) forces (0.03-0.3 Hz) are induced by first order wave forces.

Traditional offshore structures are designed to have their resonant frequencies significantly different from the WF in order to avoid large resonant effects (DNV-RP-F205 from DNV, 2010).

Four different non-linear effects can be included in dynamic analysis:

- Geometric non-linearity that is associated with changes in the shape of the mooring line caused by vertical force components (see static analysis in 2.1.2.1)
- Non-linear stretching of synthetic ropes (see Figure 2.10)
- Non-linear seabed friction
- Non-linear viscous damping of the mooring line, which may cause snap loads. Snap loads will be discussed in the next sub-section 2.1.2.3.

2.1.2.3 Snap loads on mooring lines

Snap loads are mooring loads with an amplitude considerably higher than static and dynamic mooring loads. They occur when a mooring line becomes slack (zero or negative tension) and is suddenly re-tensioned. They are particularly frequent in towing lines, but also need to be considered for compliant lines in catenary mooring systems.

The dynamic process leading to snap loads is the following:

a) high velocity amplitudes excite the mooring line at its top end;

b) large perpendicular motions at the midpoint of the line create large drag forces until a part of the line almost “freezes” in its equilibrium position (Aranha and Pinto, 2001). The line becomes slack because the top section of the line keeps moving while one section is frozen;

c) the floating structure accelerates because of hydrodynamics forces and is not pulled back by the slack line. Consequently, the line becomes suddenly re-tensioned which leads to a steep increase in the mooring load.

The stiffness and the pre-tension of the mooring system can significantly modify the mooring damping and the natural response frequency of the mooring system, these parameters being highly interdependent (Johanning, Smith and Wolfram, 2006). Mooring damping includes friction on the seabed, internal friction and drag.

Webster (1995) investigated the effects of mooring scope, drag coefficient, excitation period, stiffness or current and found that the contributions of drag damping and internal damping compete: drag damping is associated with motions transverse to the mooring lines, while internal damping is associated with motions along the mooring line.

The influence of the mooring line damping on the total damping of a mooring system has been first evaluated by Huse (1991) and indicates that for a conventional oil and gas floating structure, the mooring line drag forces can provide the highest contribution to the surge damping of the moored system.

Further investigations have been conducted to isolate parameters which have an influence on the mooring damping and to tune the mooring system to optimise the mooring damping and avoid snap loads. Model tests (HSE, 1998) and numerical models using for example a fully dynamic finite element method (Webster, 1995) or a lumped

mass and spring method (HSE, 1998) can be used to estimate the amplitude of snap loads.

2.1.2.4 Small and large bodies

The exciting forces on a floating structure are calculated depending on the relative size of the wave length and of the floating structure.

If the body is small compared to the wave length ($D/\lambda < 6$ with D the body significant dimension and λ the wave length), the floating structure is considered as a small-volume body, and its diffraction is small, the body does not significantly modify the waves but follows the waves, and the Morison equation can then be used. This approach links local loads with acceleration and velocity of the incident flow: the wave contribution is the sum of an inertia term $\rho C_M S dU/dt$ and of a drag term $1/2\rho C_D D U|U|$, with ρ the water density, C_M the added mass coefficient, S the cross-sectional area of the body perpendicular to the flow direction, U the flow velocity, C_D the drag coefficient and D the body significant dimension. Inertia and drag coefficients are known for simple shapes (e.g. a cylinder) and are generally calculated from trials for more complex shapes.

The Keulegan-Carpenter number K_C can then be used to describe the relative importance of the drag forces over inertia forces, using the body significant dimension D and the wave height H (Molin, 2002).

$$K_C = \frac{\pi H}{D} \tag{2.10}$$

Flows are classified into inertia ($K_C < 4 - 5$)- or drag- dominated regimes ($K_C > 4 - 5$). For $K_C < 1/2$, there is no separation in the flow caused by a cylinder, while for $K_C > 15$ the separation is fully developed (Frigaard, 1989).

If the body is large compared to the wave length ($D/\lambda > 6$), then it has an influence on the waves, diffraction (modification of the incident flow) and radiation (generation of waves from the floating structure) are significant, and a potential radiation-diffraction analysis should be used.

A potential flow radiation-diffraction program such as Hydrostar, WAMIT, AQWA or AQUAPLUS can be used to calculate the hydrodynamic properties of the floating structure:

- added mass: the mass of water set in motion by the moving structure
- radiation damping: damping due to the waves generated by the moving structure
- Response Amplitude Operators (RAOs) : the first order transfer functions of the motions of the moving structure
- Quadratic Transfer Function (QTFs): coefficients for second-order mean forces to estimate the mean drift forces in regular waves and slowly varying drift forces in irregular waves

The main drawback of these potential radiation-diffraction codes is that a) they do not include viscous contributions –a drag force should be added and the drag coefficient is difficult to calculate for a complex shape; b) they are based on linear wave theory - the parameters have been calculated for infinitely low i.e. small-amplitude waves, but the vessel response becomes non-linear when the wave height is increasing; c) they calculate these parameters for a given draft; in the case of a highly dynamic structure, with significant heave or pitch motions, the hull will be inaccurately represented.

2.1.2.5 Hydrodynamics and wave theory

Morison equation can be used in combination with waves following any wave theory, but the potential radiation-diffraction requires the waves to follow a Stokes 1^{st} or 2^{nd} order theory because at the moment diffraction cannot be solved for higher order waves (Molin, 2002).

The water depth also needs to be considered. If the potential radiation-diffraction theory is used, QTFs are used to model the second order (LF) motion of the floating structure. QTFs should be provided for all pairs of wave frequency and wave directions. However full QTFs may not always be available and the use of full QTFs lead to computationally intensive calculations. The Newman's approximation uses QTF data for equal pairs of wave frequency and directions. However, the Newman's approximation can be poor in shallow water (Orcina, 2014).

2.2 Wave energy

2.2.1 Wave energy technologies

The first recorded development of wave energy converters (WECs) was in 1799 by Frenchman Girard (Clement, et al. 2002). After the second oil shock in 1973, wave energy research sporadically progressed depending on intermittent government policy and R&D support (Carbon Trust, 2006).

There are now more than 200 different wave energy converters in various stages of development (Hayward and Osman, 2011). None of them have yet been deployed in commercial scale arrays. The most common technologies are (Clement, 2002; Falcao, 2010):

- *Oscillating water columns (OWC):* oscillating water (due to wave action) acting as a piston forcing air in and out of a column. This air turns a bidirectional turbine;
  example: OE Buoy by OceanEnergy
- *Overtopping devices:* collecting water in a reservoir and letting out water through conventional low head turbine;
  example: Wave Dragon
- *Point absorbers:* directly converting floating structure motion;
  example: Bolt-2 LifeSaver by Fred Olsen
- *Surging devices*: using wave surge motion to push a membrane or a vertical plate;
  example: Oyster by Aquamarine
- *Self-reacting devices*: riding the waves in a parallel direction with articulated arms and capturing energy from the relative motion of the arms;
  example: *Pelamis* by E.ON and ScottishPower Renewables

An example of some wave energy devices, their type, shape and dimensions is given in Table 2.1. This table also includes some floating wind and floating tidal devices for comparison purposes.

There is no clear way to predict which wave energy technology will be market leading in the next few years, because of the complex political, social and economical context which will be discussed below.

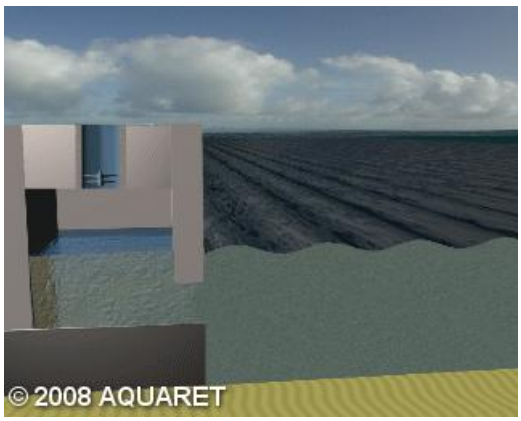

(a)

(b)

(c)

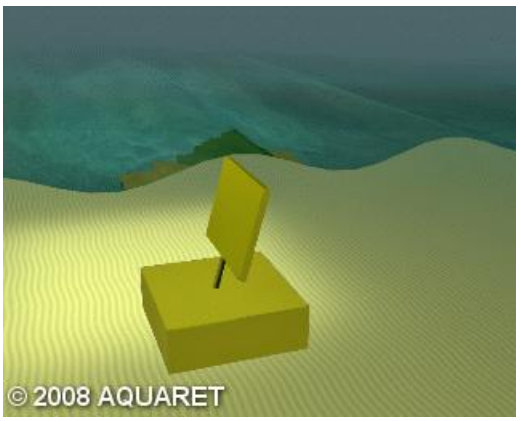

(d)

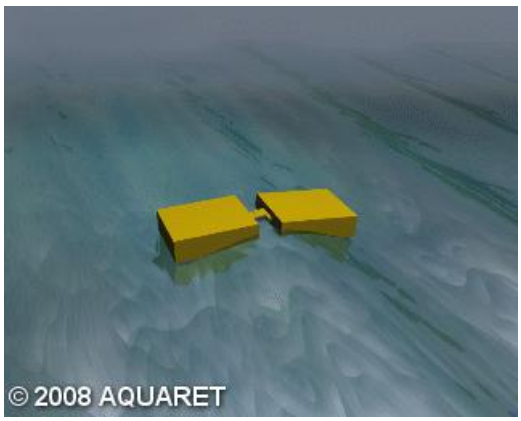

(e)

Figure 2.5: Example of principle of operations of some wave energy devices: a) OWC, b) overtopping device, c) point absorber, d) surging device, e) Self-reacting device. Pictures from EMEC website. http://www.emec.org.uk/marine-energy/wave-devices/

Table 2.1: Example of dimensions of MRE devices

	Device (*Company*)	Type	Shape	Length (m)	Height (m)	Weight (tonnes)	Draft hull (m)	Reference
Wave	Pelamis P2 (*Pelamis Wave Power*)	Self-reacting	Horizontal cylinders	180	4	1,350		Pelamis, 2014
	Ocean Energy Buoy (*Ocean Energy Ltd*)	OWC	Cuboid	24		1,800		Babarit, et al. 2012; Lavelle, 2011
	Bolt-2 LifeSaver (*Fred. Olsen*)	Point absorber	Square toroid	16	1	55		Sjolte, et al. 2013
	CETO (*Carnegie Wave Energy Limited*)	Point absorber	Vertical cylinder	11		200		Babarit, et al. 2012; Carnegie, 2014
	OPT Mark 3 (*Ocean Power Technologies*)	Point absorber	Vertical cylinders	11	43.5	180	32	OPT, 2014
	Penguin (*Wello Oy*)	Point absorber	Boat hull shape	30	9	1,600	7	EMEC, 2014
	Langlee (*Langlee Wave Power*)	Surging	Square frame and flaps			1,600		Babarit, et al. 2012
Floating wind	Hywind (*Statoil*)	Floating wind turbine	Vertical cylinder	6 at water line	165	5,300	100	Charles and Nuttall (2010)
	WindFloat (*Principle Power, Inc*)	Floating platform	Triangular frame				< 20	Principle, 2014
Floating tidal	BlueTEC (*Bluewater*)	Floating tidal turbine	Horizontal cross	24 x 40				EMEC, 2014

2.2.2 Wave energy resource

The incident wave power is particularly high on the western coast of Europe, especially in Scotland and Ireland, up to 75 kW/m in winter (The Department for Business, Enterprise and Regulatory Reform, 2008). The overall offshore wave energy resource in UK waters is of at least 50 TWh/year (Carbon Trust, 2006), which corresponds to the electricity demand of 11 million UK households (HM Government, 2010), or about one seventh of current UK electricity consumption (Carbon Trust, 2006). In addition to the offshore wave resource, the near-shore and shoreline wave energy resources have been estimated at 7.8 TWh/year and 0.2 TWh/year respectively (Carbon Trust, 2006).

However, there is a difference between the resource and the quantity of energy which can be harvested, obviously because the entire shore cannot be covered with wave energy devices, but also because of the physical limitations of a wave energy device, and because of the irregularity of the resource. Efficient control strategy could optimise the energy extracted from a wave. However, a wave energy device cannot extract all the energy from a regular wave even with an efficient control system as demonstrated by Falnes (2007). The control is even more difficult in a real sea state with irregular waves.

Wave energy is intermittent on different scales. On a seasonal scale, the natural seasonal variability is favourable to wave energy in the north hemisphere: wave energy resource is higher in winter, when the energy demand is also the highest making wave energy particularly suitable for the UK market. On a weekly scale, the wave power average can vary by a factor of 10 from one week to the next (Falnes and Løvseth, 1991). On a minute scale, the wave power between a wave group and during a wave group can vary by a factor of 50 (Falnes and Løvseth, 1991). The development of energy storage systems or the use of arrays of devices (Falnes, 1994) could smooth the power delivered to the grid (Falnes and Løvseth, 1991).

2.2.3 Political and economical framework

The development of wave energy technologies is highly depending on political support (Clement, et al. 2002), especially because these technologies are capital intensive.

In the UK, policies support low carbon technologies (renewable and nuclear) aiming to improve the security of energy supply, reduce greenhouse gas emissions which contributes to climate change, and create jobs and business (DECC, 2014). Several governments (for example the UK: Carbon Trust, 2006) prefer renewable energies to nuclear power. In order to facilitate the development of renewable energy, specific policies and regulatory frameworks have been established. For example, the French and British marine renewable energy policies have been detailed as part of the Merific project (2012). They consist of both financial and non-financial incentives.

The challenging target of the UK government is to produce 15% of energy using renewable sources by 2020 (HM Government, 2010). The place of wave energy into this renewable mix is highly depending on the commercial competitivity of wave energy relatively to other renewable and established technologies.

In order to compare the different wave energy technologies in terms of economical competitivity, and to compare them with other renewable energy technologies, levelised costs of energy (LCOE) are used. LCOE are the net costs to install an energy system divided by its expected life-time energy output. The short-term LCOE predictions (in 2020 or 2035) are more favourable to tidal energy but in 2050 they are expected to be lower for wave energy than for tidal energy (stream and range) (Ernst & Young, 2010). However, politicians and energy companies may be seeking immediate results rather than long-term results.

2.2.4 Wave energy gaps and barriers

Gaps can stop the development of a project. The gaps which need to be fulfilled in order to allow the development of wave energy are mainly financial: competitivity with non-renewable technologies and long-term funding.

Marine renewable technologies need to be competitive relatively to other technologies in order to secure public support and investments from the private sector (Carbon Trust, 2006).

It is difficult to ensure funding through a whole wave energy project, from early stage to venture capital investment (DECC, 2014). Several wave energy companies, such as Wavegen or Wavebob bankrupted. Pelamis, one of the leading wave energy projects, has also been significantly suffering from financial problem (Lynn, 2013).

Barriers can significantly slow a project. They can be non-technical or technical.
The most significant non-technical barriers will be discussed below, starting with the ones with the most severe consequences and finishing with the ones with the less severe consequences, as classified by Waveplam (2009): licencing, financing, infrastructure, conflicts of use, environment and public perception.

Obtaining a licence for deployment may be tedious, expensive and long and is absolutely necessary for a project. Some sites such as FaBTest are pre-licenced (FaBTest, 2014). This considerably simplifies the installation procedure.
Financing a wave energy project is critical. When financing is not interrupting a project, it is still a barrier at any stage of development. A sea trial project, even small, requires high initial funding which is not balanced by immediate revenues during the pre-commercial phase. During this phase, the technical and economic feasibility of the project should be demonstrated. This requires risky funding because the market potential has not been yet proven. Although at this stage funding is evolving from public to private investments (Murphy and Edwards, 2003). High initial funding is required because of a) the costs of installation, maintenance and operation, b) significant device and mooring capital costs due to high strength requirements to survive energetic sea states, and c) the diversity of wave energy devices, making each project one of a kind, which is not pushing the supply chain in terms of competitivity (SI Ocean, 2013).
The lack of appropriate infrastructures and logistics for building and testing may be a hurdle. As mentioned before, the supply chain needs to be developed, but this is difficult because of the diversity of wave energy devices. The use of similar equipment by different wave energy devices would facilitate the development of a specific and competitive supply chain (SI Ocean, 2013). Several test sites are available in the UK; however they need to be easily accessible, close to ports, with sufficient favourable weather windows for installation, maintenance and decommissioning. This last point may be one difficulty at the Wave Hub site which is 16 km offshore in an energetic location. In some cases (pre-commercial deployments), test sites additionally require a grid connection. Grid connection would be a more pressing issue at a later stage of development (Renewable UK, 2013).

A less pressing issue, but which still needs to be addressed, is the potential conflicts of use, and their socio-economic impacts. For example, in the South West of the UK, conflict can occur with other sea users: army, dredgers, fishermen, cargo ships or surfers (Garrad Hassan, 2008). Vandalism has not been reported at wave energy sites but for example, at the South West Mooring Test Facility (SWMTF), during mooring retrieval, an anchor was observed with a ROV out of its position, with the mooring line forming a loop on the seabed. When this anchor was retrieved, the chain was coiled around the anchor which suggests that a boat mooring in the vicinity of the buoy accidently pulled out the anchor when retrieving its own anchor. However, nothing was reported to the harbour master, which means that other sea users need to be informed and educated about wave energy devices.

Within the European Union, an Environmental Impact Assessment (EIA) must be carried out to obtain a licence (EMU, 2003). EIA addresses issues linked with fauna and flora, visual and noise disruption, and chemical contamination (South West of England Regional Development Agency, 2006). In particular, disturbance of the seabed by the mooring should be avoided. Entanglement of marine megafauna (large animals) in mooring has also recently been addressed by Harnois, et al. (In review).

Public perception is important, especially for receiving political support. Consumers may be worried about the cost of wave energy technology increasing their electricity bill. They should then be informed about benefits of such technology. Public may also have a negative perception of renewable energy, because of the widely reported failures (for example the mooring failure of Oceanlinx (Hasham, 2010) and Wave Dragon (Johanning, 2005)).

Technical barriers are those which can be solved by research activities. They may be global to all wave energy devices or device dependent. This section will only address general technical barriers, because of the great diversity of available wave energy devices and corresponding specific issues (IEA, 2006).

Reliability, survivability, performance, ease of deployment, maintenance and decommissioning should be improved while providing a cost-effective and low environmental impact solution. Wave energy devices are installed in energetic locations (IEA, 2006) and need to survive to harsh sea conditions. Available knowledge

from the oil and gas industry can be partially adapted to the wave energy devices. However, the wave energy sector cannot afford some expensive technologic solutions used by the oil and gas sector (SI Ocean, 2013), or cannot afford to follow the highly conservative standards. For oil and gas platforms, it is more cost effective to overdesign a mooring system than to repair or replace it (Ma, et al., 2013). This needs to be reconsidered for MRE devices because the ratio between the installation cost and the incomes is much lower for a MRE device than for an oil and gas platform.

In order to solve the technical barriers, specific research is required for WECs:

a) wave energy devices are more dynamic than large oil and gas platform and their dynamic behaviour should be better understood in order to design reliable and safe devices (IEA, 2006);

b) production of energy should be optimised. Power take-off (PTO) systems need in-depth research to improve performance. Near-shore wave resource should also be better measured and forecasted (IEA, 2006) in order to adapt the devices to a specific location.

c) the development of deployment/maintenance/decommissioning methods for all wave energy devices would reduce installation costs and increase confidence.

In order to address these technical barriers, specific standards and technologies should be developed for wave energy devices. Some of these standards and technologies may also be applicable to other MRE devices.

2.3 Mooring design

This section presents mooring design following the available mooring standards which have been extensively developed for the oil and gas industry. Design of a dynamic mooring system requires the understanding of the environmental loads, calculations taking into account the dynamic behaviour of the system and the application of safety factors on the results of these calculations. An additional fatigue analysis should be conducted. Further considerations need to be added to develop specific WEC moorings.

2.3.1 Mooring standards for the oil and gas industry

Standards are guides that should be followed during the design of a product to ensure that this product is safe, reliable, with a certain quality and considers environment. Standards also consider operation and maintenance. A product may have to be designed following a particular standard, for example for insurance purposes, or for the procurement of consents or licences.

Specific standards have been developed for the oil and gas industry. For example, DNV-OS-E301 (DNV, 2013), API RP 2SK (API, 2005) and BS6349-6 (BS, 1989) are mooring standards widely used by the industry. These guidelines and standards address the main issues of design and fatigue analysis, fabrication, installation and operation, maintenance and reliability. More specific texts, such as the NCEL report on anchors (1987), or IALA AISM guidelines (2001) for synthetic mooring lines or marking, are also available.

Designing a product to standards does not mean that failures will not occur. Offshore structures are designed for a very low probability of failure. However, some failure mechanisms may need further understanding. For example, Ma, et al. (2013) discussed the failures of permanent oil and gas mooring systems, all of them having been designed to standards. Standards need constant improvements to incorporate the state of the art of the understanding of failure mechanisms.

2.3.2 Environmental loads

Mooring design is aiming to estimate the maximum loads that the mooring lines will have to resist during their deployment. Mooring loads are mainly driven by the

motions of the floating structure, and these motions are themselves induced by environmental loads. Therefore it is important to accurately estimate environmental loads beforehand.

Environment is specific to a site and is characterised in the standards as an extreme combination of wave, current and wind conditions, each of them associated with a return period. This return period is the average period between occurrences of an event being exceeded and is associated with a failure probability.

The prediction and choice of waves for mooring design is discussed in detail below. Wind varies with time and with the height above the sea surface. The wind is represented in design calculations as the addition of the mean wind speed - calculated commonly for 1 hour, 10 minutes and 1 minute – and of a wind spectrum to consider the gusts. A current profile is generally used for design calculations, giving the current speed and direction through the water column.

2.3.2.1 Weibull distribution

Wave, current and wind return periods used for design by the different standards are detailed in Table 2.2 as well as their relative combination. For example, API RP 2A-WSD (API, 2010) recommends using the 100-year return period maximum individual wave, while API RP 2SK (API, 2005) recommends using either the 100-year return wave with its associated wind and current, or the 100-year wind with its associated wave and current. Standards (Table 2.2) recommend using a 10, 50 or 100 year return period wave. These results are not fundamentally different, especially because the difference between a 50-year return period wave and a 100-year return period wave is limited, the extremes following a Weibull distribution (Eq. (2.11)).

$$P[H_S < x] = 1 - \exp\left[-\left(\frac{x-A}{B}\right)^C\right] for\ H_S > A\ and\ C > 0 \qquad (2.11)$$

$$P[H_S < x] = 0\ for\ H_S \leq A$$

From Holthuijsen (2007), with *A* a location parameter, *B* a normalisation parameter and *C* a shape parameter (these parameters apply for this equation only)

For example, at Wave Hub, the 100-year return period significant wave height H_S is estimated at 13.7 m while the 50-year is estimated at 13.3 m and the 10-year at 12.2 m (JP Kenny, 2009).

2.3.2.2 Contour lines of the joint probability distribution

Contour lines are design curves which show points with the same probability of occurrence.

Design standard DNV-OS-E301 (DNV, 2013) requests design calculations to be performed for several sea states along a 100-year (H_S, T_P) contour line using an inverse First Order Reliability Method (FORM) based on Winterstein, et al. (1994).

The joint probability distribution of significant wave height H_S and peak wave period T_P at the site is required to draw the 100-year contour line. A method to calculate the joint probability distribution and predict contour lines has been developed by Haver (1987). Winterstein, et al. (1994) developed a methodology to directly obtain contour lines from probability of failures by introducing an inverse First Order Reliability Method (FORM).

Figure 2.6 is an example given by DNV-OS-E301 (DNV, 2013) of a 100-year contour line and of chosen (H_S, T_P) pairs for design calculations.

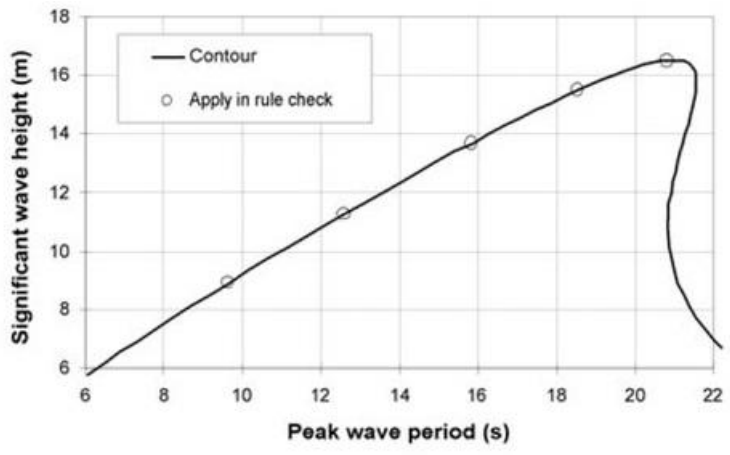

Figure 2.6: Example of sea states along a 100-year contour line from DNV-OS-E301 (DNV, 2013)

Table 2.2: Design parameters from different standards based on Barltrop (1998) and additional standards. This is a summary and the guidelines listed below provide considerably more details.

	Wave	**Current**	**Wind**	**Combination**
	Return-period (year) for H_S	*Return period (year)*	*Return-period (year)*	
HSE (1995)	50		50	
API RP 2A-WSD (2010)	100 maximum individual wave height		100	
API RP 2SK (1996)	100 year waves with associated wind and current or 100-year wind with associated wave and current			Most severe directional combination at the site
DNV-OS-E301 (2013)	Several points on the 100-year (H_S, T_P) contour (Figure 2.6)	10 (for UK and Norway)	100	In the same direction or directional if available
ISO 19901 – 1 (2005)	100 / reasonable period	100 / 10 (Norway) / reasonable period	100 / reasonable period	Selection of most appropriate directions or combination of directions
ISO 19901 – 7 (2013)	100	100	100	
BS 6349 – 1 (2013)	50 (quasi static) + range of wave periods and wave heights (dynamic)	> 50		
BS 6349 – 6 (1989)	> 50	> 50	> 50	

2.3.3 Dynamic response and loads of a mooring system

Once the design environmental conditions and associated loads have been identified, a prediction of the dynamic response of the floating structure due to environmental loadings is carried out in order to identify the maximum tension characteristics in the individual mooring lines of a mooring system.

Calculations can be conducted in the frequency or in the time domain. Calculations in the frequency domain are valid if the equations of motions are linear and non-linear effects such as viscous effects can be satisfactorily linearised. If these hypotheses are not valid then calculations should be conducted in the time domain. Brown and Mavrakos (1999) have compared the results from several time and frequency domain methodologies with experimental data. Differences in mooring damping estimation were observed.

2.3.4 Safety factors for survivability analysis

Mooring analyses are conducted for the survivability and the fatigue of the mooring system. DNV-OS-E301 (DNV, 2013) and API RP 2SK (API, 2005) standards provide safety factors to take into account inaccuracies during the mooring design.

$$S_C - T_{C\_mean.}\gamma_{mean} - T_{C\_dyn.}\gamma_{dyn} \geq 0 \quad (2.12)$$

for the DNV standard (partial safety factors), and

$$S_C - T_{C.}\gamma \geq 0 \quad (2.13)$$

for the API standard

With S_C the characteristic strength of the weakest element of the mooring system, T_C the maximum estimated tension and γ the safety factor. The subscripts mean and dyn refer to the mean or dynamic tension respectively. If statistics of the breaking strength of the component are not available, the characteristic strength S_C can be obtained from the MBL: $S_C = 0.95$ MBL.

These safety factors are provided:

a) for different limit states: Ultimate (ULS) when the device is intact, Accidental (ALS) after the failure of one mooring line and Fatigue (FLS) for cyclic loading;

b) for a quasi-static or a coupled dynamic analysis method. Quasi-static analysis method only includes steady and LF loads and therefore is not relevant for a highly dynamic floating structure.

c) DNV additionally defines two consequence classes: Class 1 when the failure is not likely to lead to unacceptable consequences ("loss of life, collision with an adjacent platform, uncontrolled outflow of oil or gas, capsize or sinking"), and Class 2 when it is likely.

Table 2.3 gives the value of the safety factors for DNV and API standards, for ULS and ALS.

The safety factors are comparable between the standards. An increase in the safety factor would not necessarily mean an increase in the design life: Ma, et al. (2013) noticed that an increase in design criteria would of course lead to stronger mooring lines and a higher design strength but this would not mean that these mooring lines will survive longer because of other effects which need to be considered for long term survivability: fatigue, corrosion, manufacturing quality or handling damage.

Table 2.3: Comparison of the factors of safety for dynamic analysis method provided by the offshore standards DNV-OS-E301 and API RP 2 SK

Design condition	**DNV Consequence class 1**		**DNV Consequence class 2**		**API**
	Mean tension	Dynamic tension	Mean tension	Dynamic tension	Dynamic
ULS/Intact	1.10	1.50	1.40	2.10	1.67
ALS/Damaged	1.00	1.10	1.00	1.25	1.25

2.3.5 Fatigue analysis

In addition to the survivability calculations (ALS and ULS), fatigue calculations (FLS) are conducted to ensure that the mooring system can resist to fatigue damage during its lifetime.

Fatigue damages are cumulative. For mooring design, the damage is evaluated by multiplying the number of stress cycles by the sum of "the probability density of the nominal magnitudes (peak-to-trough) of the stress cycles", and divided by the number of stress cycles for this amplitude which would lead to a failure (DNV-OS-E301 from

DNV, 2013). The number of stress cycles leading to a failure for a given load amplitude is usually described using S-N curves, as shown for example in Figure 2.7. In this example, an open link chain is expected to fail after $6x10^4$ cycles with an amplitude of 100 MPa. The highest the curve on this graph, the more cycles at a given stress range the material can resist before failure.

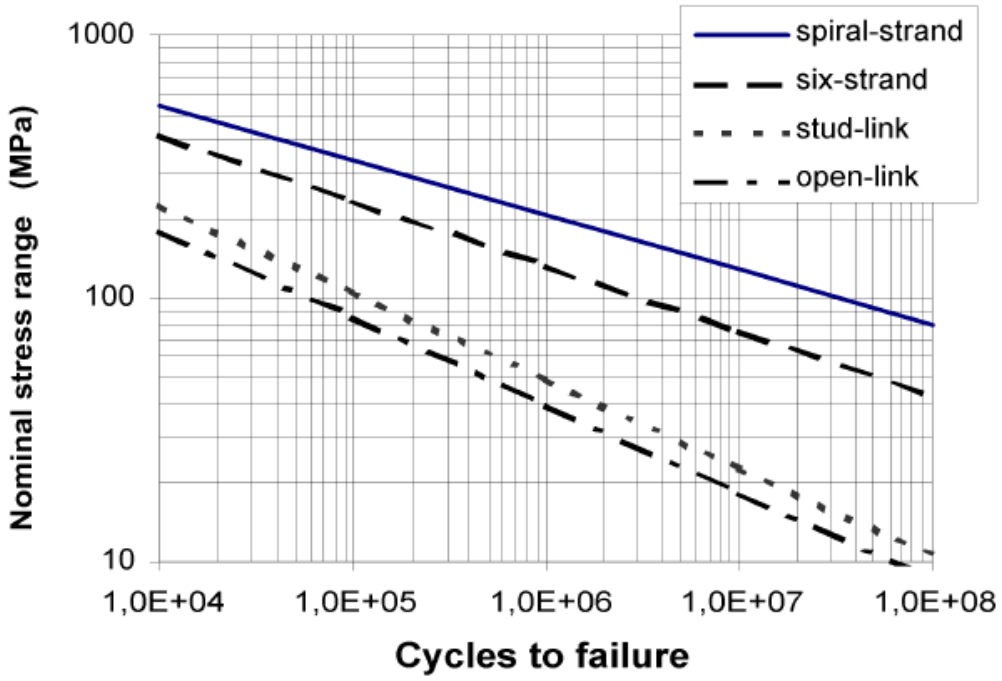

Figure 2.7: Example of S-N fatigue curves for different mooring components from DNV-OS-E301 (2013)

The stress is the load divided by the line cross-sectional area. Consequently the stress cannot be used to estimate fibre rope fatigue, because the rope section is reduced when the rope is extended. R-N curves are used instead, with *R* the relative tension: the tension divided by the Minimum Breaking Load (MBL). DNV-OS-E301 (DNV, 2013) does not provide low-tension R-N curves for Nylon ropes and advises to do testing. Figure 2.8 is an example of a R-N curve for a new type of Nylon rope developed by Tension Technology International.

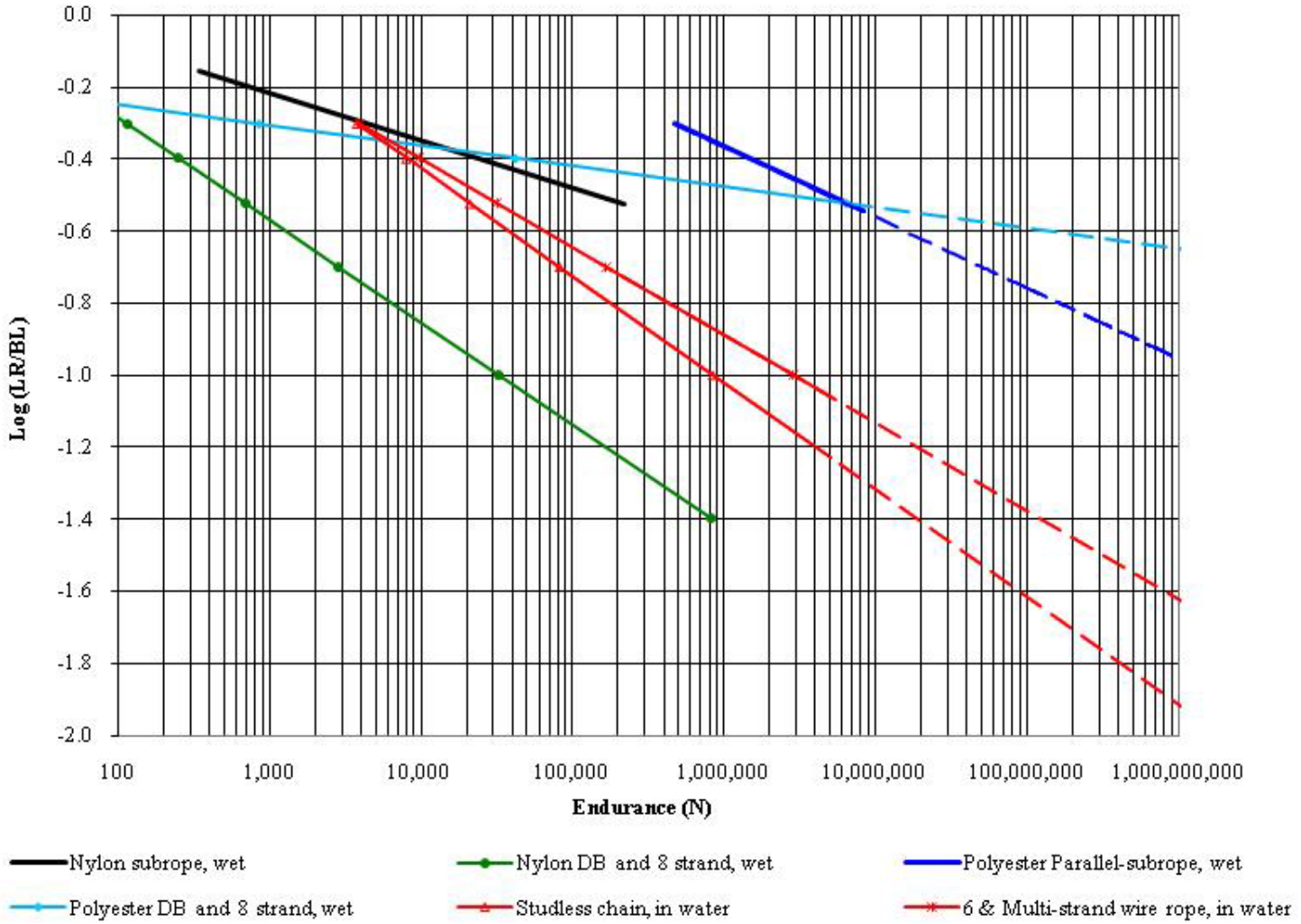

Log (LR/MBL)	LR = x% MBL:
-3.0	5 %
-2.3	10 %
-1.9	15 %
-1.1	33 % (safety factor of 3)
-0.5 (lower limit black curve)	61 %
-0.15 (higher limit black curve)	86 %

Figure 2.8: Example of Nylon R-N fatigue curves and comparison with other materials, from Ridge, Banfield and Mackay (2010). The black line is a new model of Nylon rope. LR: load range, BL: breaking load (same than the MBL)

2.3.6 Specific wave energy guidelines

Wave energy technologies are foremost floating moored structures. Therefore standards for other floating moored structures, such as offshore oil and gas structures can be used as a basis to develop specific wave energy standards.

A list of offshore guidelines, specific or general, has been compiled by Free Flow Energy Inc (2009) and their potential use for wave and current energy design has been highlighted. Nevertheless, offshore standards may be inappropriate for wave energy and more generally MRE technologies because of their specific requirements in terms of costs and behaviour.

In particular, the highly dynamic behaviour of wave energy devices needs to be considered (Johanning, Smith and Wolfram, 2005; Paredes, et al. 2013).

In addition, the low severity of a failure of a wave energy device mooring could be taken into account (Paredes, et al. 2013): wave energy devices are unmanned, potential leakages are small, and a shutdown has limited financial consequences. Consequently, Paredes, et al. (2013) suggested the addition of a new design class: Class 0.

However, this point is debatable. The most severe failure of a wave energy device is the loss of this device, potentially causing the loss of a whole array of wave energy devices. A large wave energy device adrift can cause significant damage to other sea users, leading to possible loss of human life. The commercial and political consequences of a failure should also be considered, especially in this early stage where failures would have a significant negative influence on public opinion, even though the financial and ecological consequences of a failure of a wave energy device are significantly less dramatic than a major outflow of oil or gas. Moreover, due to the lack of operational experience with wave energy devices, it is currently preferable to keep high factors of safety.

Currently, specific and precise guidelines for wave energy devices are not available. General documents, such as PCCI (2009) or EMEC (2009) reports present an overview of criteria to include in wave energy standards.

2.4 Mooring configurations and components

Mobile mooring systems have been developed for 2,500 years to moor boats (Bradney, 1987). Fish farms have been used for thousands of years in Asia, but have significantly been developed in the second half of the 20th century (Seaweb, 2004). Floating breakwaters have been used in Japan since 1930 (Peng, et al. 2013).

Permanent mooring systems for offshore applications started being developed in 1947 for oil and gas platforms (ABS, 2012). A permanent mooring system is a passive system which keeps in position a floating structure under varied environmental conditions for a long period of time. Keeping in position means keeping a floating structure under a restricted range of horizontal excursions (slow and large horizontal surge and sway motions), and also in some cases under a restricted range of heading (slow yaw motion).

Currently, moorings are being developed for wind turbine devices (Zhao, Zhang and Wu, 2012) and wave energy converters (Harris, Johanning and Wolfram, 2004; Johanning, Smith and Wolfram, 2005).

The most common mooring configurations and components are presented in this section. This chapter finishes by a presentation of the state of the art of wave energy moorings.

2.4.1 Mooring configurations and stiffness characteristics

A mooring system can be either a single point mooring or a spread mooring.

A single point mooring is made of one or several lines attached at one end to the seabed and at the other end to an intermediate buoy, and of a line connecting this intermediate buoy to the floating structure. This mooring system allows the floating structure to weathervane and can be particularly useful for a long and slender floating structure installed in environmental conditions coming from a wide range of directions.

A spread mooring is made of several lines attached at one end to the seabed and at the other end at different locations on the floating structure. This mooring system restricts the heading of the floating structure and limits the total excursion in surge and sway.

Mooring lines can be either slack or taut. Slack lines have a catenary shape if they are not buoyant. Catenary lines usually provide most of their restoring forces from the lift of heavy chains lying on the seabed. When the excursion of the device is increasing, tensions in the mooring lines opposing the direction of motion increase non-linearly, until the chains are fully lifted (Figure 2.9a from Johanning and Smith, 2008).

Taut mooring systems provide most of their restoring forces from the axial stiffness of the lines, with tensions in the mooring lines opposing the direction of motion increasing in a way depending directly of the line material stiffness. (Figure 2.9b from Johanning and Smith, 2008)

Compared to a catenary configuration, a taut mooring system usually occupies a smaller footprint area on the seabed and the excursion of the floating structure is smaller.

Accessory buoys or clump weights can be used in both configurations to locally modify the weight or buoyancy of the mooring limb and consequently the stiffness characteristics of the mooring system.

2.4.2 Mooring components

A mooring system uses a combination of components in its mooring lines. The list of components given below is not exhaustive, but the most commonly used components are described: mooring lines, anchors and connectors.

2.4.2.1 Mooring lines

The aim of a mooring line is to connect an anchor to a floating structure. The main requirements of mooring lines are:

- to be sufficiently strong to resist extreme environmental conditions,
- to provide restoring forces to avoid large excursion of the floating structure,
- to resist fatigue, corrosion and other long term marine effects,
- to be easy to transport and install,
- to be cost-effective.

Different materials can be chosen for a mooring line: for example chains, fibre ropes or wire ropes. The properties of each of those materials are detailed below, as well as the DNV standard relative to this mooring line material.

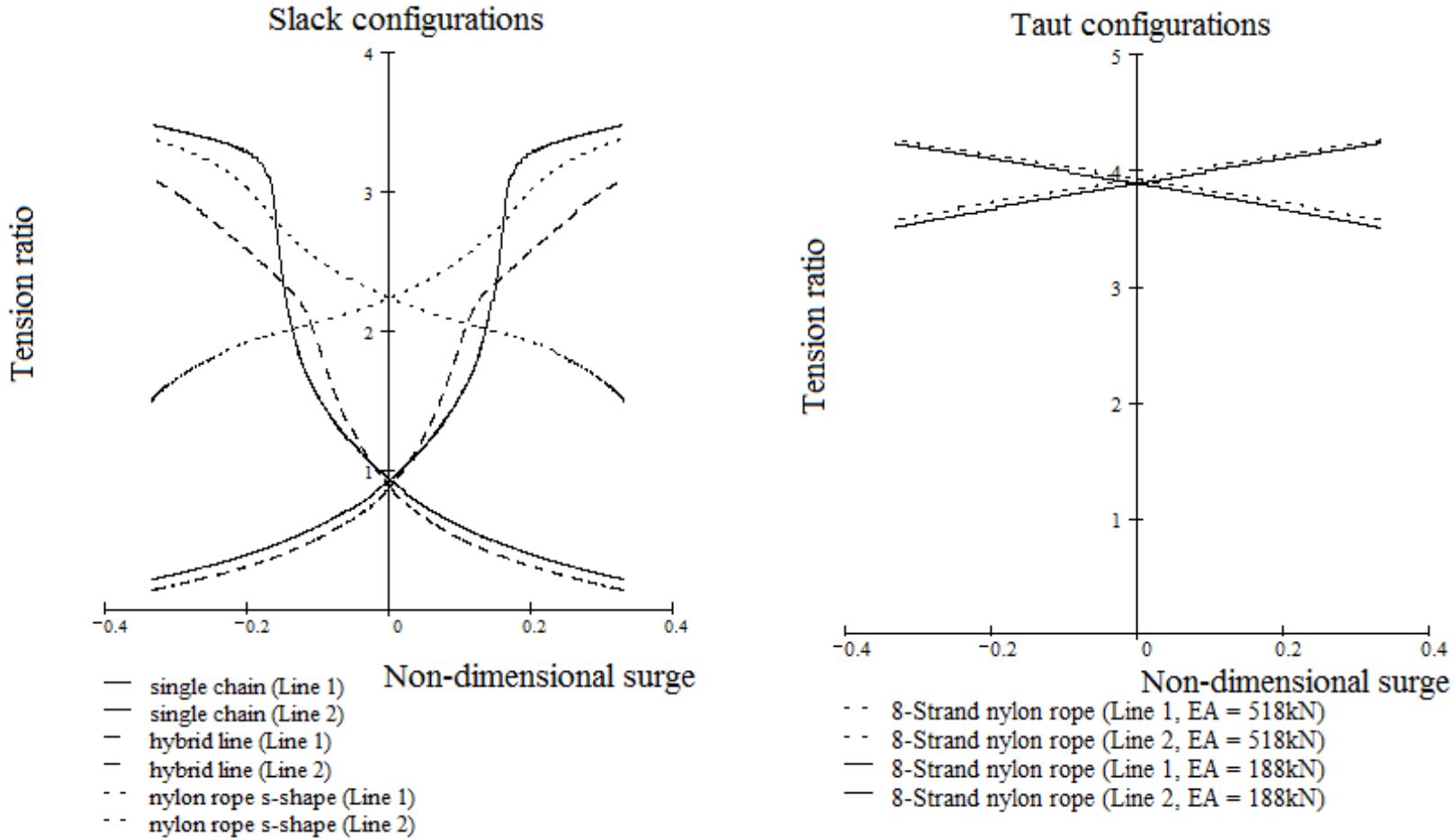

(a) **(b)**

Figure 2.9: Examples of tension characteristics for different a) slack and b) taut mooring configurations with two opposite lines (from Johanning and Smith, 2008). Tension ratio (the ratio of vertical to horizontal tensions T_H/T_V) in the mooring line is plotted against mooring motion (expressed as a non-dimensional surge parameter). Axial stiffness *EA* with *E* the Young's Modulus and *A* the sectional area of the rope

Cost analysis (Equimar, 2009) indicates that for a given strength, wire ropes tend to be more expensive than fibre ropes, which are themselves more expensive than chains. However, other parameters need to be taken into account than cost and strength. For example, the chains lying on the seabed are rather selected for the weight they provide than for their strength.

Properties of different mooring lines are presented in Table 2.4, although these properties will vary slightly depending on type, construction and manufacture.

Chains

(DNV-OS-E301, in DNV, 2013)

Chains have been used for a long time for mooring applications. Diameters of chain available for commercial use range approximately from 6 to 175 mm. Different grades are available, depending on the quality of steel used, providing different strengths: Grade R3, K3, R3S, R4 and R5 are commonly used for offshore applications. Chains can be studlink or studless. Studlink chains are heavier, have a higher drag coefficient and resist better to fatigue. Chains are used a) on the seabed section of a catenary mooring system, because of their weight which avoids excessive vertical loads on drag embedment anchors and because of their abrasion properties; b) in the water column, because of their bending properties, but their considerable weight may limit this application; c) near the water surface, in a highly dynamic zone, because of their bending properties. When using chains, corrosion needs to be considered.

Fibre ropes

(DNV-OS-E303, in DNV, 2010)

Fibre ropes are still in the development stage for offshore applications although their use is becoming more common. Fibre ropes available for commercial purposes range from 16 mm to 240 mm in diameter (Bridon, 2011), and are typically made of Nylon (polyamide), Polyester (polyethylene terephthalate), Aramid (para-aramid), or HMPE (High Modulus PolyEthylene). The common nomenclature of the fibre has been used in this thesis and their full correct chemical name has been stated in brackets.

Fibre ropes are significantly lighter than other materials and therefore can be used in the water column of a catenary or taut mooring system to reduce the weight of moorings on the floating structure. The elastic properties of fibre ropes are also of

interest to damp mooring loads and avoid snap loads. The stiffness of fibre rope is non-linear: small and linear for a small extension, and larger and non-linear for a larger extension, as shown in the example in Figure 2.10. Rope stiffness given in Table 2.4 corresponds to the linear stiffness for small extensions. Rope properties should be evaluated in sea water as sea water may reduce the strength of the material and its fatigue life. Lines elongate through time (creep) and hence they may need to be re-tensioned after a certain amount of time.

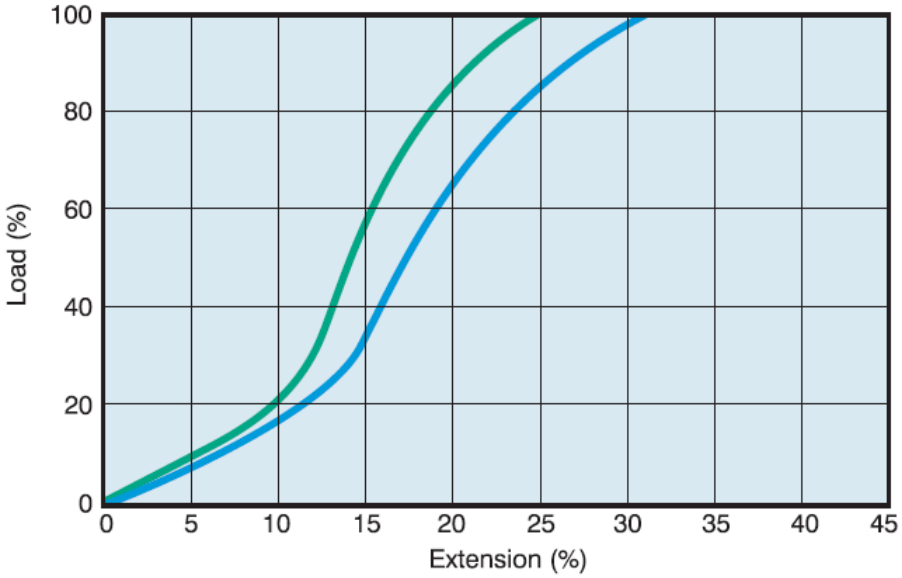

Figure 2.10: Example of fibre rope stiffness characteristics curve for a Nylon Superline rope from Bridon catalogue (2011)

Fibre ropes should avoid contact with the seabed because of the risk of damage through abrasion. They may also be damaged by fishbite, marine growth or UV if they are not protected with a jacket (Flory and Banfield, 2011).

The choice of fibre rope diameter depends on demands for both strength and elasticity: the stronger the rope, the less elastic it is, and the higher the mooring loads are. Because fibre ropes are a relatively new material for permanent moorings, and their fatigue properties still not completely understood (e.g. hysteretic heating), high safety factors are applied. For example, BV (2012) suggests increasing the safety factors of fibre ropes by 10% for polyester and 20% for other materials compared to the safety factors for the other elements of the moorings.

General guidance (DNV-OS-E301, in DNV, 2013) and specific standard (DNV-OS-E303, in DNV, 2010) about fibre ropes are available but, particularly for Nylon, require

clearer indications about the reduction in the strength of fibre ropes and the change in stiffness and other properties due to water absorption, eye splice (for some rope construction) and ageing or fatigue.

One of the main difficulties to develop standards for fibre ropes originates from the available range of rope construction (Figure 2.11) and from the changes in properties during the life of a fibre rope. In particular axial stiffness is a complex parameter which depends on load level, range, frequency and history (Barltrop, 1998).

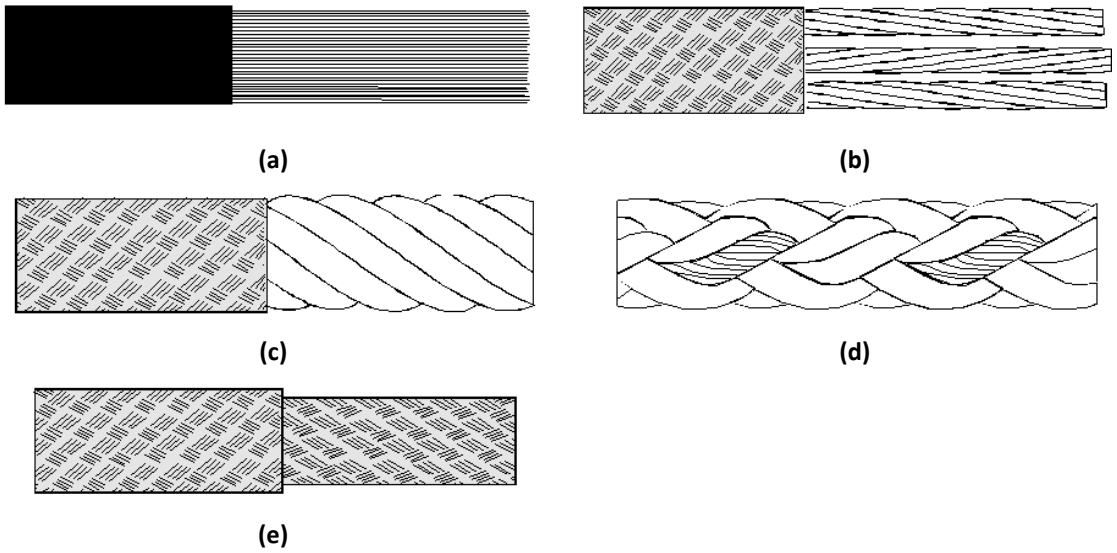

Figure 2.11: Example of different rope constructions a) parallel yarns, b) parallel strands, c) stranded (for wire ropes), d) plaited and e) braided, from Tension Technology International (2014)

Wire ropes

(DNV-OS-E304, in DNV, 2009)

Wire ropes have been used for tensioned mooring applications. Common wire rope constructions used for offshore applications are spiral strand and six strand, and different grades of steels are used in diameters up to 162 mm (Viking moorings, n.d.).

Wire ropes are used for tensioned mooring applications because of their relative limited weight and high strength, and because bending is limited for these applications – with wire ropes having limited bending properties. Wire ropes can be used in catenary or taut configurations (Ma, et al. 2013).

The choice of construction is a compromise between fatigue and abrasion resistance. High density polyethylene sheaths can be used to protect the wire ropes from abrasion as well as from corrosion.

Table 2.4: Indication of basic physical parameters of commonly used mooring materials. In this table only: *d* (mm) the rope diameter, *D* (mm) the bar diameter of the chain, and *C* a coefficient parameter depending of the chain material grade (equal to 22.3 for Grade 3). All technical data are from Barltrop (1998) except for the Nylon (Bridon, 2011) and for the masses (chain: Orcina, 2014, Nylon: Bridon, 2011, Polyester: Wichers, 2013, Aramid, HMPE: McKenna, 2004). Costs are from Harris, et al. (2004) Properties vary depending on exact type, construction and manufacture.

	Strength Minimum Breaking Load (MBL)	**Stiffness** Axial stiffness per unit length	**Mass in air** Per unit length	**Weight** Submerged weight	**Main properties**	**Use**	**Cost for a given strength**
Unit	N	N	kg/m	N/m			
Nylon (Superline)	228 d^2	~115 d^2	0.0005340 d^2	0.00050 d^2	Very compliant, very light, moderate strength	In the water column of a compliant mooring configuration	High
Polyester	250 d^2	5,000 d^2 to 1,3000 d^2	0.0007978 d^2	0.0067 d^2	Compliant, very light, moderate strength	In the water column	High
Aramid	450 d^2	15,000 d^2 to 52,000 d^2	0.0006521 d^2	0.00565 d^2	Stiff, very light, strong	In the water column	High
High Modulus PolyEthylene (HMPE)	575 d^2	15,000 d^2 to 52,000 d^2	0.0004415 d^2	0.0062 d^2	Very stiff, very light, strong	In the water column of a taut mooring configuration	High
Chain Grade 3	C x D^2 x (44 – 0.08 D)	90,000 D^2	0.0199 D^2 (studless) 0.0219 D^2 (studlink)	0.1875 D^2	Very strong, very heavy, very stiff	Catenary, in the water column or on the seabed	Medium
Wire spiral strand	900 d^2	90,000 d^2	0.0050 d^2	0.043 d^2	Strong, light, very stiff	In the water column, better for long term mooring	Low
Wire six strand	525 d^2 to 600 d^2	45,000 d^2	0.003611 d^2 (fibre core) 0.003990 d^2 (wire core)	0.034 d^2	Strong, light, moderately stiff	In the water column, better for mobile mooring	Low

2.4.2.2 Anchors

The role of an anchor is to keep a mooring line attached at a fixed point on the seabed. The main requirements for an anchor are to be able to resist high loads, horizontal and in some cases vertical, in a given seabed type (soft to hard), to be easy to install and to be cost-effective.

Different anchor designs are available: dead weight, drag embedment anchor, vertically loaded anchor, pile anchor and suction anchor. The properties of each type of anchor are detailed below, as well as the DNV standard relative to this type of anchor. The relative costs of anchor are summarised in Table 2.5.

Dead weight (DNV-OS-C101 Sec.11, in DNV, 2011)

Dead weight, also known as gravity anchor, is the simplest anchor. The holding capacity is provided by the weight in water of the anchor, and by the friction of the anchor on the seabed. This type of anchor is usually in steel or concrete (Vryhof anchors, 2010). However, this type of anchor is not very efficient, meaning that the anchor may need to be significantly large and heavy and consequently difficult to handle to provide a given holding power.

Drag embedment anchor (DNV-RP-E301, in DNV, 2000 and NCEL, 1987)

Drag embedment anchor, also known as fluke anchor, is the most popular anchor today. This type of anchor penetrates partly or fully in the seabed and the holding capacity is provided by the resistance of the soil in front of the anchor. This type of anchor can accommodate large horizontal loads, however, it can only accommodate limited vertical loads. These anchors are then often used with a catenary mooring system, with sufficiently long chains lying on the seabed to avoid vertical loads. This type of anchor requires a soft seabed (sand or mud) where it can penetrate, and has a higher holding power in sands and hard clays than in soft clays.

The holding power in mud and sand of different types and weight of drag embedment anchors can be found in NCEL (1987).

Vertically loaded anchor (DNV-RP-E302, in DNV, 2002)

Vertically loaded anchor (VLAs), also known as plate anchor is a new type of anchor, which is an improvement of the drag embedment anchor because it can accommodate larger vertical loads. It is installed much deeper than a traditional drag embedment anchor. These type of anchor can be used with a catenary mooring system and reduce significantly the footprint of the mooring system on the seabed by reducing the length of chains lying on the seabed.

Pile anchor (DNV-OS-C101 Sec.11., in DNV, 2011)

Pile anchor is a hollow steel pipe which is driven deeply into the seabed with a hammer or vibrator, using a designated (and expensive) installation methodology. The holding capacity is provided by the friction of the soil along the pile and by lateral soil resistance. This type of anchor can accommodate horizontal and vertical loads.

Suction anchor (DNV-OS-C101 Sec.11., in DNV, 2011)

Suction anchor is a variation of the pile anchor, with a larger diameter, which is installed in soft soils with a pump, using pressure difference.

Table 2.5: Relative anchor costs, adapted from EquiMar Deliverable 7.3.2. (2009)

Anchor	Costs (hardware and installation)
Dead weight	Low
Drag-embedment anchor	Medium
Special Vertical Load Anchor (VLA)	High
Pile anchor	High
Suction anchor	High

2.4.2.3 Connectors

The aim of connectors is to link the different elements of the mooring system and/or to avoid torsion in the mooring lines. The main challenge of connectors is to resist large loads and to resist fatigue, corrosion and other long term marine effects. Connectors are critical to the overall integrity of the mooring system.

Shackles (DNV-OS-E301, in DNV, 2013)

Shackles are a commonly used connector, made of a bow and a pin. Different types are available, depending on the application.

Swivels (DNV-OS-E301, in DNV, 2013)

Swivels are used to relieve the twist and torque that can build up in a mooring line, close to the anchor point, or between chains and a rope.

2.4.3 Wave energy mooring

In this section the specific needs of wave energy moorings are considered. Mooring configurations and materials which could be used for wave energy moorings are discussed. These mooring systems still require a better understanding which could be gained by a combination of numerical models, laboratory tests and field tests.

2.4.3.1 Specific needs of wave energy moorings

The primary function of a wave energy mooring is the same as the primary function of a conventional mooring: to keep a floating structure in position, and to resist to extreme environmental conditions, fatigue and other long-terms deteriorations.

In addition to this main function, most of the wave energy moorings ideally need to be designed to be motion-dependent and additionally to have their resonance frequency close to WF to produce energy (Harris et al., 2004). At least, the mooring design should not negatively influence the efficiency of the wave energy device. Zanuttigh, Angelelli and Kofoed (2013) compared the power production for the DEXA wave energy device for two types of mooring system: Catenary Anchor Leg Mooring (CALM) (single point mooring) and a catenary spread mooring. They observed that the CALM mooring leads to a larger power production. Cerveira, Fonseca and Pascoal (2013) also analysed two catenary spread moorings and found that the catenary lines had a negligible influence on the dynamics of the floating structure and on the power production. More globally Fitzgerald and Bergdahl (2008) presented an overall numerical method to quantify the influence of mooring lines on the performance of devices.

The other wave energy devices which do not need to be designed for resonance at WF may anyway have physical properties (e.g. length, mass) which do not allow their resonant frequency to be significantly different to WF.

The main changes in the dynamic response of a floating WEC compared to a traditional oil and gas structure is the addition of PTO damping B_{ij}^{PTO} (Eq. (2.14)):

$$\sum_{j=1}^{6}\begin{bmatrix} -\omega^2\left(M_{ij}^{Structure}+M_{ij}^{Mooring}\right) \\ -i\omega\left(B_{ij}^{Structure}+B_{ij}^{Mooring}+B_{ij}^{PTO}\right) \\ +\left(K_{ij}^{Structure}+K_{ij}^{Mooring}\right) \end{bmatrix}\xi_j = F_i \tag{2.14}$$

Wave energy devices usually export energy with a power cable. Tension, fatigue and tight bends should be avoided in this cable which means that the excursion of the floating structure should be restricted. This requirement is also useful in an array configuration, to avoid collision between the devices. Another requirement for an array configuration is to reduce the footprint (the occupied area) of the mooring on the seabed in order to pack as many devices as possible (or as economically viable, the first rows of the array potentially sheltering the next rows) in the area allocated to the wave energy farm.

Wave energy devices are usually installed in relatively shallow water depth, less than 100 m. At such water depths, the tidal range is large compared to the water depth and may be more difficult to accommodate In addition, the tidal flow can be significant at nearshore locations. The horizontal water particle velocity and motion is also large in shallow water. Table 2.6 shows the tidal range to water depth ratio at some nursery sites and full scale sites and found that tidal range may be more difficult to accommodate at nursery sites. Consequently the mooring solution for nursery sites may slightly differ from the full scale mooring solution.

Anchors requirements for WECs have been particularly investigated by Huang and Aggidis (2008). In particular, the accuracy of the WEC anchors positioning should be higher than the positioning of anchors for conventional moorings.

Table 2.6: Full scale and sheltered wave energy sites in the British Isles and their wave and tidal conditions

	Location	Scale	Nominal water depth (m)	Tidal range (m)	Tidal range/ Nominal water depth	Operational sea state		Extreme sea state	
						H_S (m)	T_Z (s)	H_S (m)	Return period (years)
Nursery site	SWMTF (hindcast results presented in this thesis)	1/3	27	5.4	20%	0-1	0-4	~4	~23
	FaBTest (FaBTest, 2012)	1	45 (15-55)	6	13%	0.75	2.25	8.2	25
	Galway Bay (SEAI, 2012)	1/4	22.5	4	18%				
Wave energy facility	Wave Hub (JP Kenny, 2009)	1	55 (50-60)	5.8	11%	0.8	/	12.2	10
	EMEC Billia Croo (Lawrence, Kofoed-Hansen and Chevalier, 2009)	1	~50	6	12%	2	/	~11-12	20

The number of mooring lines of a WEC mooring is limited in order to reduce the price of the mooring system and to avoid a reduction of the motion of the floating structure. Consequently, mooring lines and anchors should be highly reliable.

The cost of installation and operation of WEC moorings may be a barrier to finance sea trials. The development of cost-effective materials and innovative mooring configurations is required to lower these costs.

2.4.3.2 Wave energy mooring configurations and materials

Conventional mooring systems have been analysed in terms of suitability for wave energy application. Harris, et al. (2004) found that spread catenary and multi-catenary moorings, Catenary Anchor Leg Mooring (CALM) and Single Anchor Leg Mooring (SALM) are highly suitable for wave energy applications.

Fitzgerald and Bergdahl (2007) found that for a single catenary line, the excursion of the floating structure is quite large. A taut arrangement does not have this disadvantage and occupies a smaller footprint area on the seabed. However, this arrangement needs a high pre-tension and restrains the WF motions, does not accommodate tidal range well and requires anchors which accommodate vertical loads (Johanning and Smith, 2008).

The development of specific mooring designs, for example using an intermediate small buoy, with or without a clump weight in the mooring lines has been investigated by Fitzgerald and Bergdahl (2007):

- Intermediate buoys reduce the weight of the mooring line on the floating structure and the excitation of the catenary due to the motion of the floating structure, and consequently the snap loads. However, it requires the addition of a hawser connecting the intermediate buoy to the floating structure, and snap loads and fatigue may be significant in this hawser. However the hawser is easy to replace because close to the surface.
- Clump weights would additionally reduce the mooring footprint as well as the amplitude of the maximum mooring loads. However, this addition increases the weight of the cable.

Intermediate buoys with (Ricci, et al. 2012) or without (Gao and Moan, 2009) clump weights have also been investigated for array configurations but these studies are still at the feasibility stage and require further analysis.

Harris, et al. (2004) found that synthetic ropes are the most suitable material for mooring lines. In particular, Nylon fibre ropes with their high compliance and acceptable fatigue performances would be highly suitable for wave energy applications (Ridge, Banfield and Mackay 2010). Using fibre ropes in moorings instead of chains in the water column would additionally reduce the weight of moorings on the floating

structure. More sophisticated solutions are currently being developed by McEvoy (2012) and by Johanning and Parish (2012). Both are working towards a mooring tether which can extend to accommodate the tidal range, dampen the mooring loads and at the same time provide high strength in rough sea states.

Cost-effective anchors which can accommodate vertical loads in a wide range of seabed conditions (Fitzgerald and Bergdahl, 2007) would allow the development of new mooring systems for WECs. Available VLA anchors require a soft seabed and are difficult to install, clump weights are not highly efficient, and pile or suction anchors are expensive to install. Fitzgerald and Bergdahl (2007) suggested the investigation of torpedo anchors or explosively embedded anchors.

2.4.3.3 Experiments and numerical models for the development of wave energy moorings

Tank tests, numerical modelling, and sea trials should be used in combination to improve the understanding of the behaviour of the WECs. The outputs and limitations of tank tests, numerical model and sea trials are discussed below.

The aim of early stage tank tests is to validate concepts and to improve the performance of the PTO systems (Forestier, et al. 2007). In such tank tests, it is typical that the influence of the mooring system is ignored. Systems are represented in a simplified form which does not significantly influence the behaviour of the PTO system (Vicente, Falcão and Justino, 2011), and/or the limited water depth in the tank does not allow the moored model to be scaled correctly (Friis Madsen, Sørensen and Parmeggiani, 2012). However, it is crucial that the influence of the mooring system on PTO performance is taken into account at a more advanced stage.

Numerical models can be validated by tank tests and then be used with some confidence to conduct further investigations in a less expensive and time consuming manner.

OrcaFlex, a 3D time-domain finite element method (FEM) computer program, has been used for this thesis. The FEM divides each mooring line into segments with visco-elastic behaviour, connected by nodes with a given mass. The segments model the axial, torsional and bending properties of the line as well as their stiffness and damping

properties (Figure 2.11). The properties of each half-segment are lumped and assigned to the node at that end of the segment. OrcaFlex models are built using a combination of components such as buoys or lines. Environmental conditions (wave, wind or current) are input into the model. The floating structures can be modelled using the Morison equation or the potential radiation-diffraction theory.

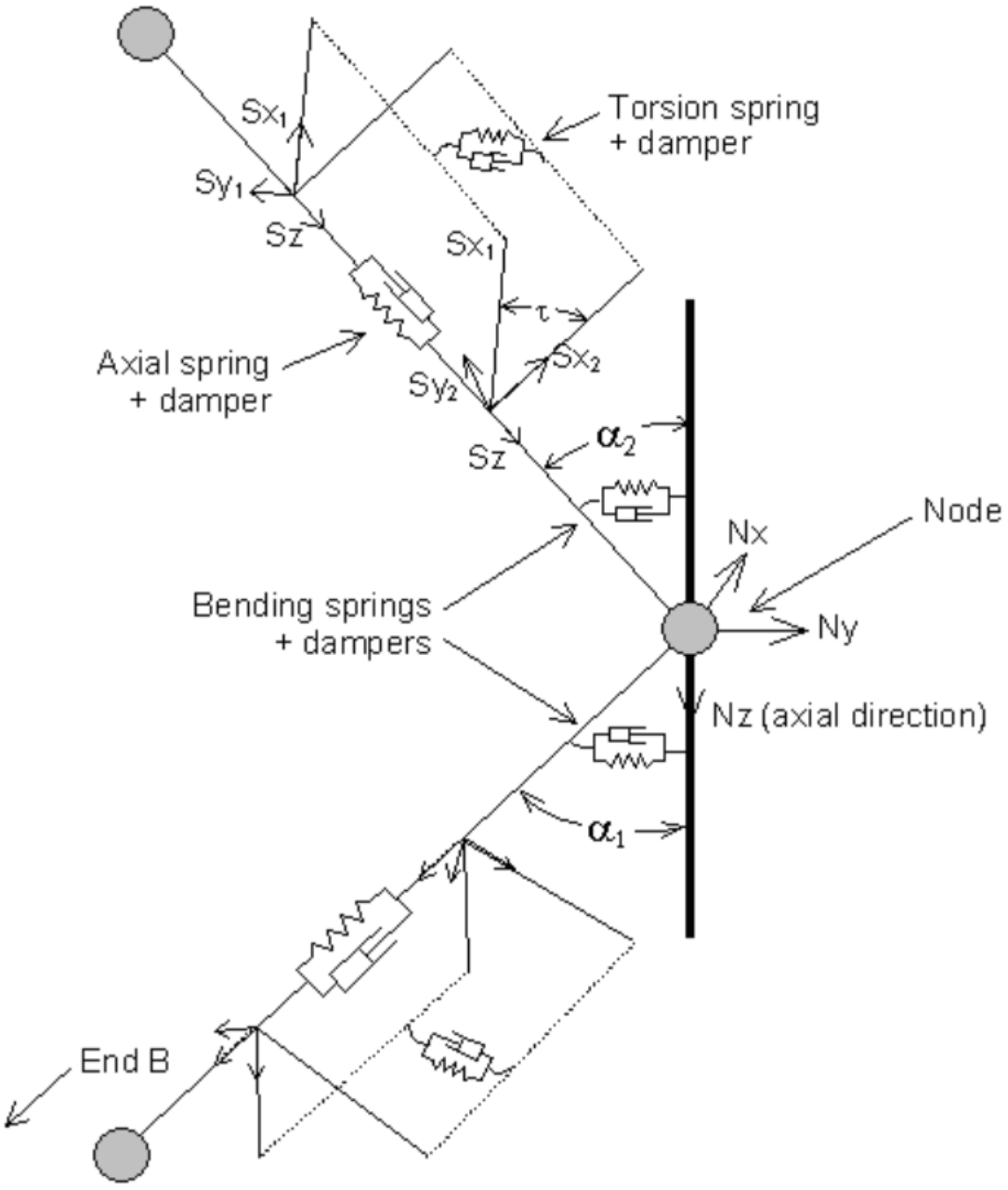

Figure 2.12: Detailed representation of OrcaFlex Line model, from Orcina (2014)

If the potential radiation-diffraction theory is used, frequency-dependent added mass and damping values need to be inputted into OrcaFlex. To implement these values in the time domain, OrcaFlex uses a method proposed by Cummins (1962) and implemented by Wichers (1979). At each calculation time *t*, the total added mass and damping load on the floating structure is given by the following convolution integral equation:

$$F(t) = -A(\infty)x''(t) - \int_0^\infty IRF(\tau)x'(t-\tau)d\tau \tag{2.15}$$

With x'' and x' the floating structure acceleration and velocity respectively, τ a time lag integration variable, $A(\infty)$ the infinite-frequency added mass matrix (instantaneous response to acceleration), *IRF* the Impulse Response Function.

The IRF characterises the response to past motion and is calculated as following:

$$IRF(\tau) = c(\tau)\int_0^\infty 4B(f)\cos(2\pi f t)df \tag{2.16}$$

With $c(\tau)$ a cutoff scaling function, $B(f)$ a damping matrix, f a frequency
The cutoff scaling function is introduced to avoid the calculation to be too long. The cutoff scaling function can be used because the Impulse Response Function decays to zero as the time lag τ goes to ∞.

OrcaFlex can use implicit or explicit method to calculate the system dynamic behaviour. Explicit method calculates the state of a system at time t+1 from the state of the system at the time t, while implicit method solves an equation using the state of the system at t and at t+1. The explicit scheme is robust but may be slow because it requires a very short time step, while the implicit scheme is faster but may produce inaccurate results.

OrcaFlex is one of the leading software packages for the dynamic analyses of mooring systems and is well validated for this purpose as shown for example by the comparison of its results with other software packages (Brown and Mavrakos, 1999). OrcaFlex has been widely used in the wave energy sector for example by Pelamis (Cruz, 2008; Orcina, 2010), Aquamarine (Orcina, 2010), or Ocean Power Technologies (Orcina, 2010). It has been used for research on specific wave energy moorings by Johanning

and Smith (2008) or by Fitzgerald and Bergdahl (2007). OrcaFlex also starts being used for floating wind turbines. A specific coupling module, FASTlink, has been developed to integrate the aerodynamic loads, the turbine control system and the flexure of the turbine in OrcaFlex numerical model (Masciola, et al., 2011).

The main limitations of the available codes are that the energy extraction may be complex to model (however it does not matter for survivability when the Power Take-Off are turned off), complex fluid-structure interactions such as green water loads or breaking waves cannot be modelled (Palm, Eskilsson and Paredes, 2013), devices with a small draft and a highly dynamic behaviour (large pitch or heave motions) cannot be represented accurately using the potential radiation-diffraction theory, and interactions between devices (e.g. waves created by the radiation of a device or shielding effect) was difficult to model until recently: their calculation has only been recently added in OrcaFlex (OrcaFlex 9.7). The use of viscous computational fluid dynamics (CFD) instead of potential radiation-diffraction codes could lead to more accurate results, but would require more computationally intensive calculations.

Sea trials allow testing at full scale or at least on a large scale, in a fully exposed site, such as Wave Hub, or more sheltered “nursery” site, such as FaBTest. An example of test sites in the UK is given in Table 2.6. These trials are conducted for a longer duration than tank tests, under a wide but uncontrolled range of environmental conditions. For example, the Fred Olsen device has been tested for more than 2 years at FaBTest. Sea trials provide information on key issues, identify new issues, and validate the performance of the device. One of the first issues of sea trials is also the logistics of managing a complex project. Thies, Johanning and Gordelier (2013) reported delays and difficulties for some offshore deployments of wave energy devices, and identified failures during sea trials leading to some elements being redesigned. In particular mooring failures have been observed for the Oceanlinx (Hasham, 2010) and the Wave Dragon devices (Christensen, Friis-Madsen and Kofoed 2005), in both cases after a large storm. For the Wave Dragon device, the measured mooring loads led to more work in reducing extreme mooring loads (Parmeggiani, Kofoed and Friis-Madsen, 2011) which included tank tests.

Sea trials, tank tests and numerical models are complementary in the development of a wave energy device.

Chapter 3. Sea trials

This chapter presents the field tests which have been providing data used for further analysis in this thesis. These data were gathered from two facilities: the South West Mooring Test Facility (SWMTF) and the Falmouth Bay test site (FaBTest). These two facilities are located in the South-West of the UK, less than three nautical miles (~ 5 km) apart on the South Cornish coast (Figure 3.1). At the SWMTF, an instrumented surface buoy, further referred as "instrumented buoy", is used to gather research data about mooring systems. At FaBTest, a wave energy device has been tested. The mooring of both floating structures is equipped with loadcells. Each facility has a wave measurement tool, an Acoustic Current Doppler Profiler (ADCP) for the SWMTF and a wave buoy at FaBTest.

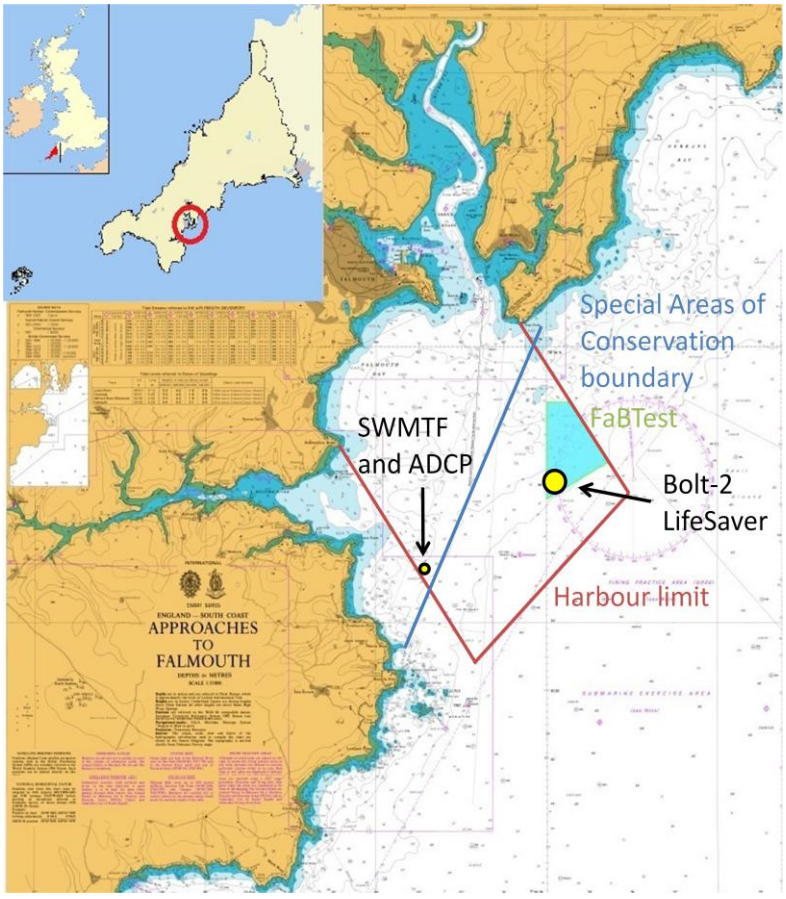

Figure 3.1: SWMTF and FaBTest indicative locations, adapted from UKHO admiralty chart. The device size is not representative.

This chapter describes the data collection and pre-processing. The different steps followed from the site location and instrumented buoy to the available data are presented in Figure 3.2.

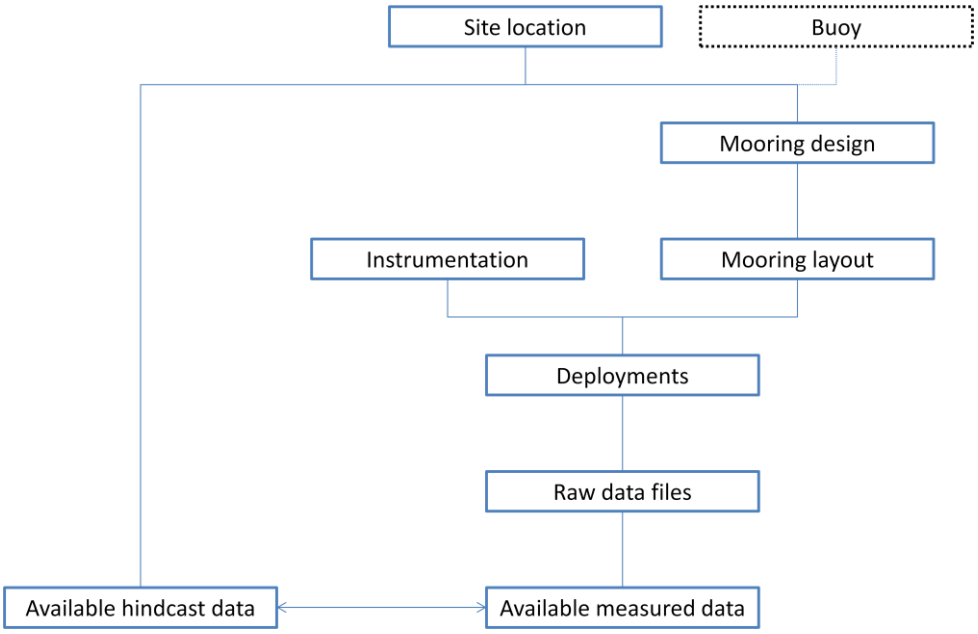

Figure 3.2: Different steps of the field test methodology

3.1 South West Mooring Test Facility (SWMTF)

The South West Mooring Test Facility (SWMTF) research is part of the mooring and hydrodynamic group at the University of Exeter, and has been funded through the Peninsula Research Institute for Marine Renewable Energy (PRIMaRE). This facility has been set up to conduct long term sea trials for moorings of Marine Renewable Energy (MRE) devices and has been previously described by Johanning, Spargo and Parish (2008) and by Harnois, Parish and Johanning (2012). The facility uses an instrumented buoy (Figure 3.3) and an ADCP to provide a wide range of data, including wave, current, water level and mooring load data. Measurements have been collected since end of 2010. The overall objective for carrying out field tests for moorings is to develop cost-effective and reliable MRE mooring solutions. Aspects under consideration are the improvement of the understanding and the reduction of uncertainties and risks of mooring operations, dynamics and fatigue, and the investigation of innovative solutions for MRE moorings, or for the wider offshore industry.

The SWMTF was already operational when the author started her PhD and joined University of Exeter. The location, instrumentation, file organisation, and mooring design for the first deployment had already been chosen. However, they will still be described and reasoned below, as they are inducing the results.

3.1.1 Choice of location

The location of the SWMTF was chosen based on its proximity to a port for an easy access, with a wave height approximately a third smaller than at the Wave Hub site, in a sheltered location but still with occasional energetic conditions. Four different locations have been considered for the SWMTF (Figure 3.4) using a wave model. The first location was West of the Lizard (the southernmost peninsula). This location is not shown on Figure 3.4: it was quickly discarded because the sea states were too energetic. More sheltered locations were then considered East of the Lizard. These locations were sheltered from the prevailing South-West swells but still exposed to energetic sea states coming from the East-South-East, due to the long fetch of the Channel. Location 3 (Figure 3.4) has the most relevant wave height, with approximately a 1:3 scale of the Wave Hub wave height and was consequently chosen to install the SWMTF. This location is also close to Falmouth Harbour which is convenient for maintenance.

Figure 3.3: SWMTF instrumented buoy; a) out of the water; b) on site; c) dimensions of the hull

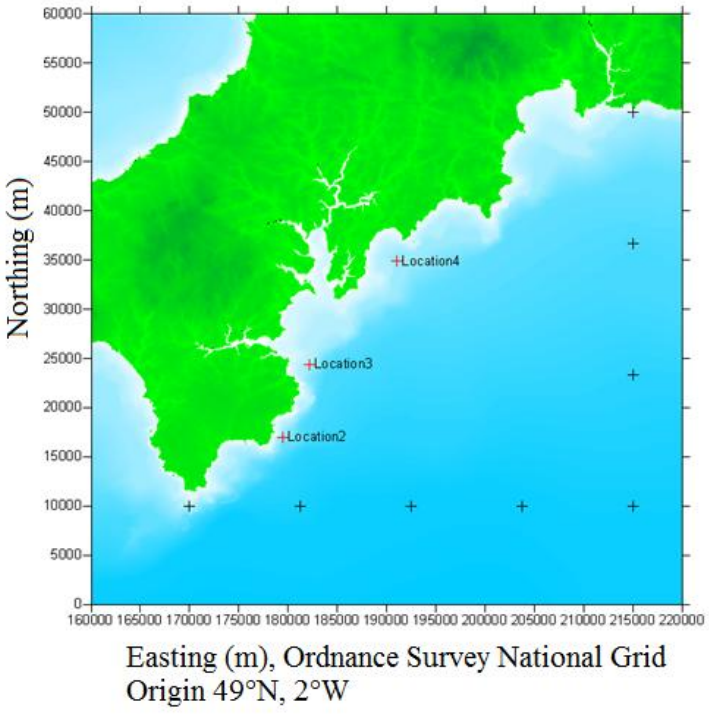

Figure 3.4: Locations considered for the SWMTF east of the Lizard (southern peninsula)

3.1.2 Instrumentation

An instrumented buoy of 3250 kg and 2.9 m float diameter (Figure 3.3) was equipped to record a whole range of data including mooring loads, instrumented buoy position, wave elevation, current and water level. Mooring loads and environmental data have been measured in order to understand which environmental conditions are leading to large mooring loads. Time series of mooring loads, instrumented buoy position and surface elevation have also been measured for further research aiming to understand the dynamic behaviour leading to extreme mooring loads. Consequently the instrument acquisition frequencies have to be sufficiently high to capture peak mooring loads. The suitability of the acquisition frequency is discussed in 7.1.1.1.
A summary of loadcells and ADCP properties can be found in Table 3.1.

Table 3.1: Properties of the loadcells and ADCP used at the SWMTF

Data	Measurement device	Location	Acquisition frequency (Hz)	Resolution	Range
In-line (axial) loads	3 axial loadcells: Elite 10062 (deployments 1-3)	Between a tri-axial loadcell and a limb	20	1 kgf	0-7 tonnef
Beam elevation and current	ADCP Teledyne RDI Workhorse Sentinel (600 kHz) ADCP	Seabed	2	Velocity: 0.01 m/s 0.5 m bins	Velocity: +/-5 m/s(default) 1.4-40.4 m depth

Conventional axial loadcells (Figure 3.5a, Table 3.1) recorded mooring load data at 20 Hz. The data were measured in Volts and were converted into kiloNewtons (kN). This conversion was based on the calibration of the loadcells which was conducted before deployment.
Tri-axial loadcells recorded mooring load data in three degrees of freedom (DOF) at 20 Hz. The axis orientation is shown in Figure 3.6. The data were measured in Volts and needed to be converted into kiloNewtons (kN). This conversion was based on the calibration of the loadcells which was conducted before the first deployment. Tri-axial loadcells were difficult to recalibrate between deployments because the instrumented buoy should be taken out of the water to remove the tri-axial loadcells for recalibration.

Tri-axial loadcells were trialled but proved to be difficult to use because of the coupling between the different motions and the absence of recalibration between tests.

A GPS was recording the instrumented buoy position at 10 Hz. The GPS was installed approximately 1.6 m above the centre of gravity of the buoy and 1.2 m laterally as shown in Figure 3.7. GPS data were measured in degrees and minutes for the latitude and longitude, and meters for the elevation. Consequently, the data needed to be converted in meters, taking the instrumented buoy target position as the reference (0,0,0) position. The instrumented buoy was also equipped with a compass, accelerometer and gyroscope. These instruments (GPS, compass, accelerometer and gyroscope) were pre-calibrated by the manufacturer and assumed to be reliable.

The orientation of these instruments is given in Figure 3.6 and the relative position of the GPS antenna and accelerometer/gyroscope in Figure 3.7. The compass position is not given as its measurements are compensated for pitch and roll. The z axis is pointing down. The aim of these instruments was to obtain a more accurate position of the instrumented buoy, in particular to improve the understanding of the excitation of the mooring lines at their top end. However these instruments proved to be difficult to use because they measured linear accelerations and angular velocities whose axes are moving with the buoy motion and which need to be integrated.

Other instruments were available, but were not used for this study, either because they were not working, or because the information they provide is not directly relevant for this study: anemometer (wind speed and direction), conductivity, temperature, density (CTD) and salinity sensor, strain gauges on the hull, current meter, instrumented buoy functioning (internal temperature and powers)

The data recorded by the instrumented buoy were all synchronised and continuously recorded and saved every 10 minutes. Data were sent to the shore using an aerial system.

A Workhorse Sentinel ADCP (Figure 3.5b, Table 3.1) was installed on the seabed 25 m towards the South-East direction in respect to the instrumented buoy target position as indicated in Figure 3.8. The ADCP was equipped with four inclined beams (20° inclination from the vertical, Figure 3.9a-b) to record wave and current data at 2 Hz. Current was evaluated using vertical bins (Figure 3.9b) with an height of s = 0.5 m, except for the first bin (near the seabed) which was 1 m high. Surface elevation and

wave parameters were calculated for these current measurements as explained in 3.1.3. A pressure sensor also measured the surface elevation vertically. The pressure sensor provides redundant measurements of water depth and wave height.

The ADCP needed to be recovered approximately every three months to change its battery and consequently was not redeployed at the exact same location. The ADCP may also have been slightly tilted, but its roll, pitch and heading sensors can be used for corrections once the ADCP is recovered (Figure 3.9c for the heading).

Data were saved in the memory card of the ADCP and were manually transferred when the ADCP was redeployed. It was consequently not possible to know if the ADCP was working properly before recovering it.

(a) (b)

Figure 3.5: a)Loadcells and b)ADCP used at the SWMTF

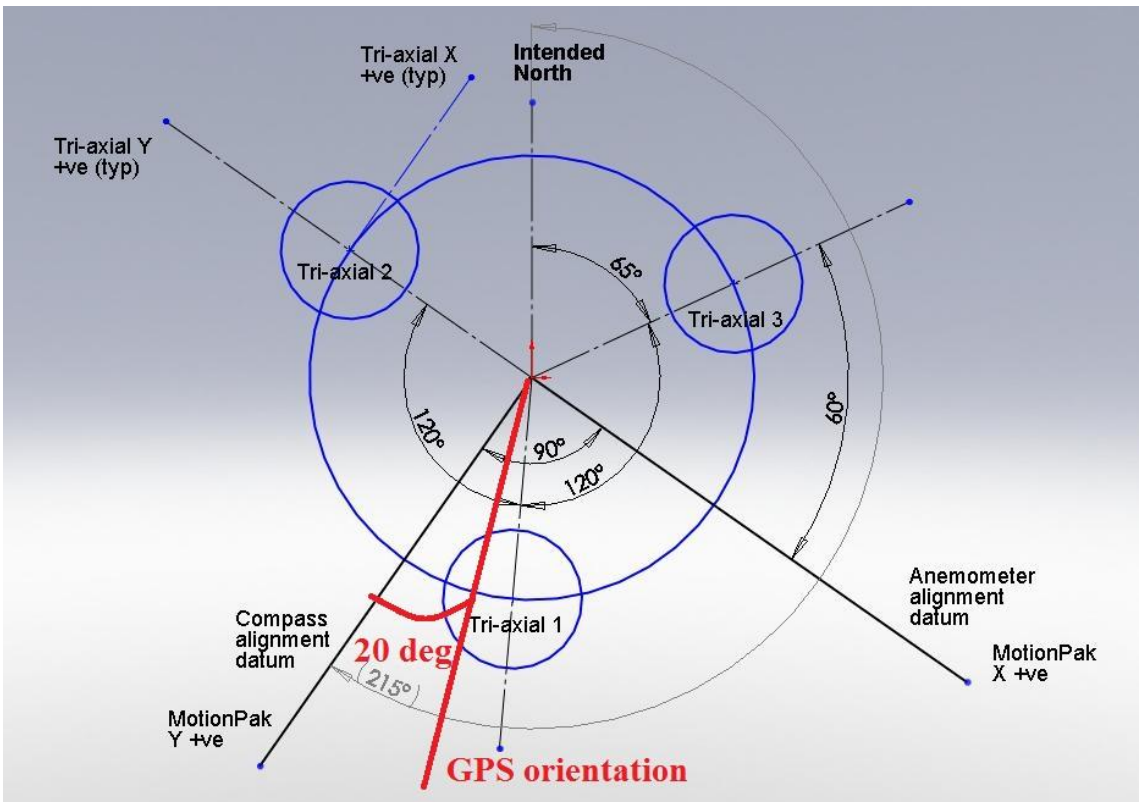

Figure 3.6: Orientation of the SWMTF instruments: accelerometer and gyroscope (MotionPak), Compass, GPS, tri-axial loadcells

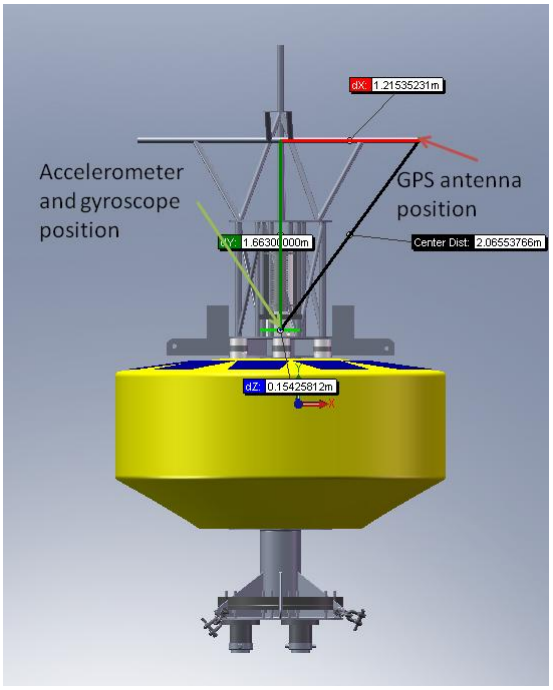

Figure 3.7: GPS, accelerometer and gyroscope position

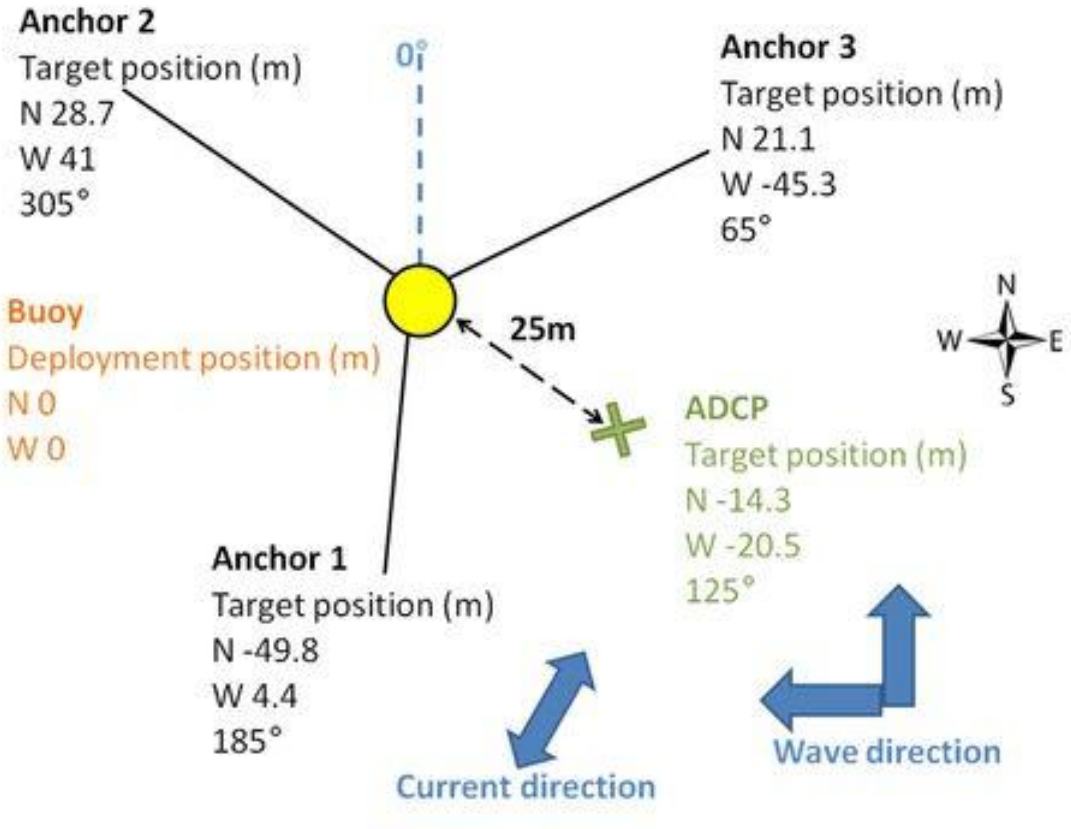

Figure 3.8: SWMTF mooring system layout, ADCP location and environmental load direction

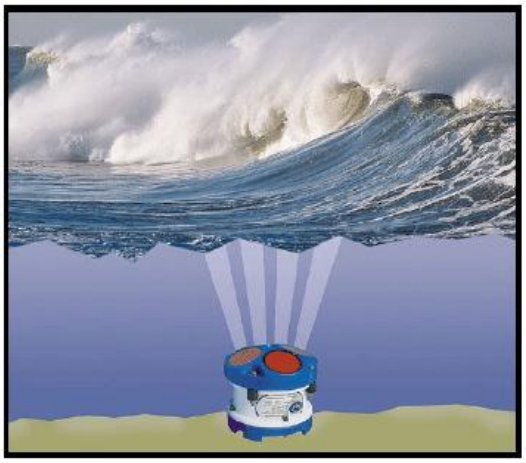

(a)

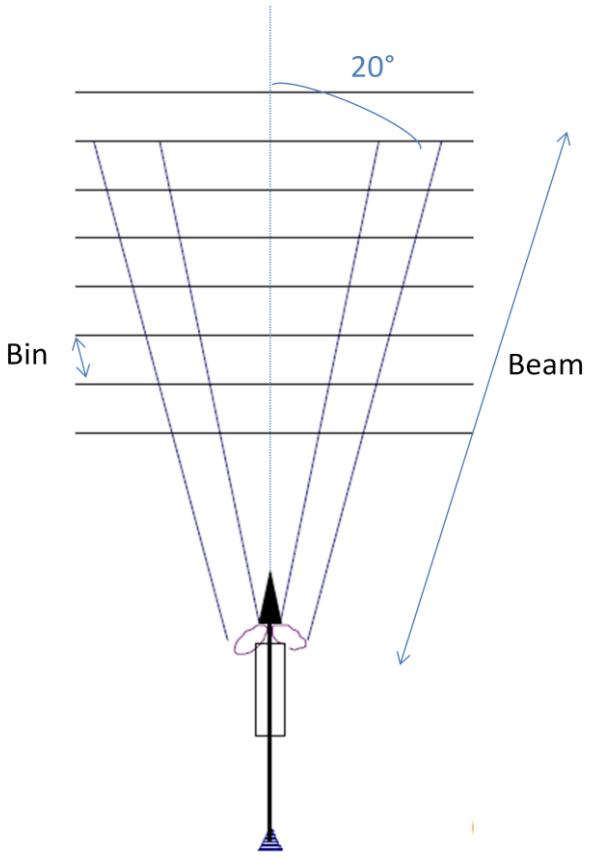

(b)

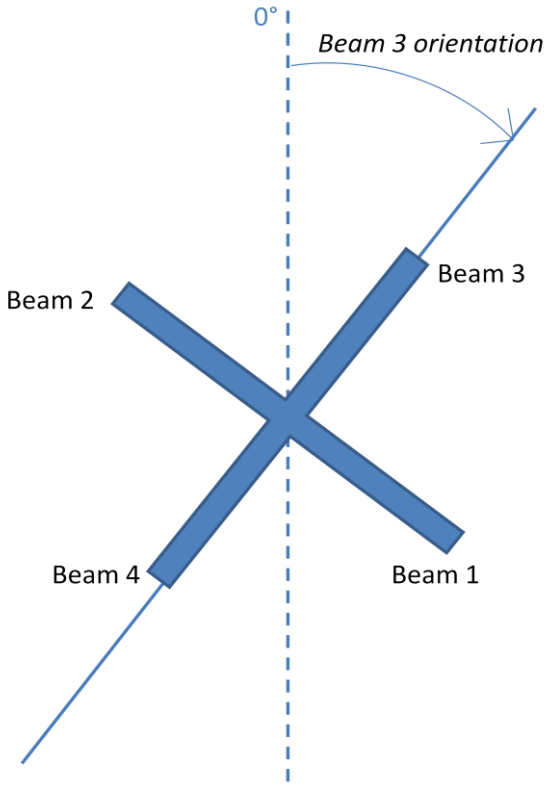

(c)

Figure 3.9: ADCP : a) four beams (RD Instruments, 2003), b) bin and beam (RD Instruments, 1996), c) orientation of the beams at SWMTF (view from the top)

3.1.3 Raw data files

The process followed by the files collected by the instrumented buoy from their collection to their conversion into readable data is summarised in Table 3.2 and described below. The data collected by the instrumented buoy were saved every 10 minutes in separated files, at rounded times (for example 20:50, 03:20…). Data were separated into different files depending on their acquisition frequency. The files were named by their date with the following format YYMMDDHHmmssm.ext with YY the year, MM the month, DD the day, HH the hour, mm the minute, ss the second, m the status (r if the file is open and being written to, m otherwise) and ext the extension of the files.

These files were compressed into a single zip named YYYY_MMDDHHmm.zip. These .zip files were transmitted to shore by aerial connection (radio link or 3G). Data were then stored in a directory indicating the date of the file YYYY/MM/DD. The files in the zip needed an initial decoding with the MtfConvert.jar program to convert them from a binary format to the ASCII CSV format. Final data files are summarised in Table 3.3.

Table 3.2: Summary of the operations on the data files from collection to readable data

Step of the data pre-processing	Data format
Initial file	YYMMDDHHmmssm.ext
Zip	YYYY_MMDDHHmm.zip
Data sent to shore	
Data stored	YYYY/MM/DD
Decoding	

Table 3.3: Summary of the data collected by the instrumented buoy at SWMTF

	Extension	Acquisition frequency	Number of columns	Data	Resolution	Range
Analog data	a20	20	19	Counter	N/A	N/A
				Axial load 1-3	1 kgf	0-7 tonnef
				Tri-axial load 1-3, x-z	1 kgf	0-7 tonnef (x-y), 0-14 tonnef (z)
				Linear acceleration x-z	0.001 g	+/-2 g (x-y), +/-3 g (z)
				Rotational velocity about x-z	0.01°/s	+/- 50°/s (roll, pitch), +/-30°/s (yaw)
	a04	4	6	Strain gauge 1-6	1 με	+/-100 με
	a01	1	7	Internal temperature	Temp.: +/- 0.1°C	Temp.: 10-90°C
				Compass heading	0.1°	0-360°
				Voltages	+/- 0.1 V	
Serial data	sgp	10	6	Counter	N/A	N/A
				Time	N/A	N/A
				Latitude, longitude, height	Lat., long.: +/- 1 cm Height: +/-2 cm	N/A
				Quality	fix not valid, GPS fix, DGPS fix, 3 fix, RTK fix (fixed-point integer), RTK fix (floating-point integer)	
	scr	5	4	Counter	N/A	N/A
				Water current x-y	0.001 m/s	+/- 3 m/s
				Water	0.1°C	+/-90°C
	ssa	0.5	5	Counter	N/A	N/A
				CTD: conductivity, temperature, density, salinity	Cond.: 0.01 mS/cm Temp.: 0.1°C Dens.: 0.01 kg/m^3 Salinity: 0.01 ppt	Cond.: 40-60 mS/cm Temp.: 0-20°C Dens.: 990-1030 kg/m^3 Salinity: 20-50 ppt
	swi	4	3	Counter	N/A	N/A
				Wind direction	1°	0-360°
				Wind speed	0.1 m/s	0-60 m/s

The steps to pre-processed the ADCP data is summarised in Table 3.4 and described below. The ADCP generated a raw data file with the extension .000 containing all the measurement data. This file was significantly large (typically containing three months' worth of measurements) and required the use of the ADCP firmware to open it. The data of the ADCP were initially continuously recorded and saved every 17.067 minutes (2048 points, a power of 2 being required to use fast Fourier transform (FFT) for spectral analysis). After problems with the ADCP firmware which was not able to handle faulty sets of data containing 2,049 or 2,050 points, data were recorded from the second SWMTF deployment for 17.067 minutes and saved every 20 minutes, meaning that there are 2.933 minutes which are not measured every 20 minutes.

Table 3.4: Summary of the WavesMon processing

Steps from raw files to pre-processed files	
Rawfile.000	
Processing with WavesMon	
Summary files LOG9.txt with statistical data	Time series and spectrum files

After each recovery of the ADCP, the wave and current statistical parameters were calculated using WavesMon (RD Instruments, 2011), the firmware provided by Teledyne RDI, the ADCP manufacturer. WavesMon processing is summarised in. WavesMon calculated for each 17.067 minute file statistical data such as the significant wave height H_S, the peak period T_P, time averaged (over the 17 minutes) current magnitudes for each bin in the vertical water column C_{Mag}, their corresponding directions C_{Dir}, and the average water depth h. After processing, the height of the ADCP, 0.4 m, was manually added to the water depth h.

The ADCP records three types of time series: range to surface for each beam (Surface track), pressure, and orbital velocities of the surface waves taken from three bins near the surface in each beam.

- The range to the surface along each beam is determined by quadratic interpolation using the bin having the maximum echo intensity plus its immediate neighbours at shorter and greater ranges. The time series of range to the surface are used for further qualitative investigations. However, these time series do not account for the tilt of the ADCP, which is due to the seabed not being perfectly flat.

- Water depth is estimated using the pressure time series. The mean value over a burst is the statistical value of water depth used for further investigations. Correction for depth-dependent attenuation based on linear wave theory is used.
- Orbital velocities are used to estimate directional spectrum. Currents are assumed to be uniform over a layer around a given water depth. Only three acoustic beams are required to measure current vectors. However, four beams are used: for each bin, each pair of opposite beams is used to calculate the current velocity at this depth along this axe, as well as the vertical velocity. The double measurement of the vertical velocity allows the validation of the assumption of current homogeneity at a given depth as well as the functioning of the equipment. Data are corrected from the ADCP referential to Earth referential to remove pitch, roll or heading of the ADCP: the correction of the ADCP attitude aims to calculate average velocity for beams at the same depth and calculate velocities for true east and north. This average velocity is used further as current velocity and current direction (RDI, 1996).

  Wave statistical parameters are obtained from the velocity time series. The velocity power spectrum is calculated (Terray, 1999). Surface height spectrum is obtained from the velocity spectrum using linear wave kinematics. Directional spectrum is obtained by considering each bin in each beam an independent sensor and by calculating a cross-spectrum between each sensor. This cross-spectrum is required to preserve phase information. The cross-spectrum is linearly related to the directional spectrum. Wave statistical parameters can then be calculated using the directional spectrum.

The ADCP used for the analyses carried out in this thesis is the model Workhorse Sentinel (600 kHz) developed by Teledyne RDI. It has 4 beams, and the bins were configured every 0.5 m, except for the first bin (closed to the seabed) which was 1 m high.

WavesMon corrected the data, calculated the statistical data for each burst and exported a summary in a chosen format. The format called LOG 9 was chosen because it provides a large range of data. The data available with this format and used for further analysis are given in Table 3.5. Additional parameters are available but have not been used for further analysis: T_{Psea} and T_{Pswell} and their associated directions

separate the sea states below or over a period chosen by the user. T_{max} is the wave period associated with H_{max}, and $H_{1/3}$, H_{mean}, $H_{1/10}$ and their associated period calculate different wave heights. These parameters have not been used as they are not commonly used in the literature.

Additionally to this summary file, WavesMon provided several time series and spectrum files for each 17 minute burst as detailed in Table 3.6. The name describing the type of the file was followed by the date and extension in the following format: YYMMDDHHmm.txt.

Table 3.5: Summary of some of the statistical data available in the LOG9 format of the processed ADCP data and used for further analysis, adapted from WavesMon manual (RD Instruments, 2011)

Name of the variable	Description	Method used to calculate this parameter
Burst	Burst number, number of the file during the deployment	/
YY, MM, DD, HH, mm, ss, cc	Date and time	/
H_S	Significant Wave Height (meters)	Spectral
T_P	Peak Wave Period (seconds)	Spectral
D_P	Peak Wave Direction (degrees)	Spectral
D_{mean}	Mean wave direction (degrees)	Spectral
h	Water level (from pressure sensor) (millimetres)	Average
H_{max}	Maximum wave height (meters)	Zero-crossing
bins	Number of bins (vertical data points)	/
depthlevel1Magnitude	Current magnitude at the first bin (m/s)	/
depthlevel1Direction	Current direction at the first bin(deg)	/
...	...	/
depthlevelNMagnitude	Current magnitude at the last bin(m/s)	/
depthlevelNDirection	Current direction at the last bin (deg)	/

Table 3.6: Processed time series and spectrums generated by WavesMon

Name	Number of columns	Number of lines	Data
DSpec	128 (frequencies)	90 (directions)	Directional spectrum (mm^2/Hz per cycle) calculated from the 4 beams
HPR	3 (heading, pitch, roll)	1,024/2,048 (2Hz)*	Time series of instrument orientation
Press	1	1,024/2,048 (2Hz)*	Time series of water depth as measured by the pressure sensor
PSpec	1	128 (frequencies)	Pressure derived surface spectrum (mm/sqrt (Hz))
SSpec	1	128 (frequencies)	Echo location surface spectrum (mm/sqrt (Hz))
Strk	4 (beams)	1,024/2,048 (2Hz)*	Surface track time series for 4 Beams in mm
Vel	12 (3 Bins, 4 Beams)	1,024/2,048 (2Hz)*	Velocity time series in mm/s
VSpec	1	128 (frequencies)	Orbital velocity derived surface spectrum (mm/sqrt (Hz))

*as mentioned before, WavesMon crashed when some of the files had a length of 2,049 or 2,050 data points because it could not use FFT. To avoid the crash, the first 1,024 data points were processed when the 2,048 points could not be processed.

3.1.4 Mooring design

In the absence of long term measurements, the mechanical elements of the system were designed based on an estimated extreme significant wave height H_S of 3.5 m (Johanning, 2008), 0.8 m/s current speed and 27 to 32.4 m water depth.

For each of the different deployments, a three leg catenary mooring (Figure 3.8) has been used with elastic lines in the water column, chains on the seabed, and drag embedment anchors. For example, Figure 3.10 and Table 3.7 show the layout of a mooring line during the first deployment. The number of mooring lines was kept low to limit the cost and avoid restraining the motion of the floating structure which could be prejudicial to energy production in a motion-dependent wave energy device. Elastic lines were chosen to reduce the mooring loads. Drag embedment anchors were chosen for their large holding power, cost effectiveness and simple installation. For all

deployments, the target deployment position of the instrumented buoy was 50°47.5'N 5°2.85'W. The mooring configuration of SWMTF was orientated to have the highest easterly H_S sea states between the mooring lines 1 and 3.

The mooring design was an iterative process which was rerun for the different deployments.

The same chains and anchors have been used throughout all of the deployments, because of their cost and durability and because they provided an appropriate Minimum Breaking Load (MBL) and weight (chains) or holding power (anchors).

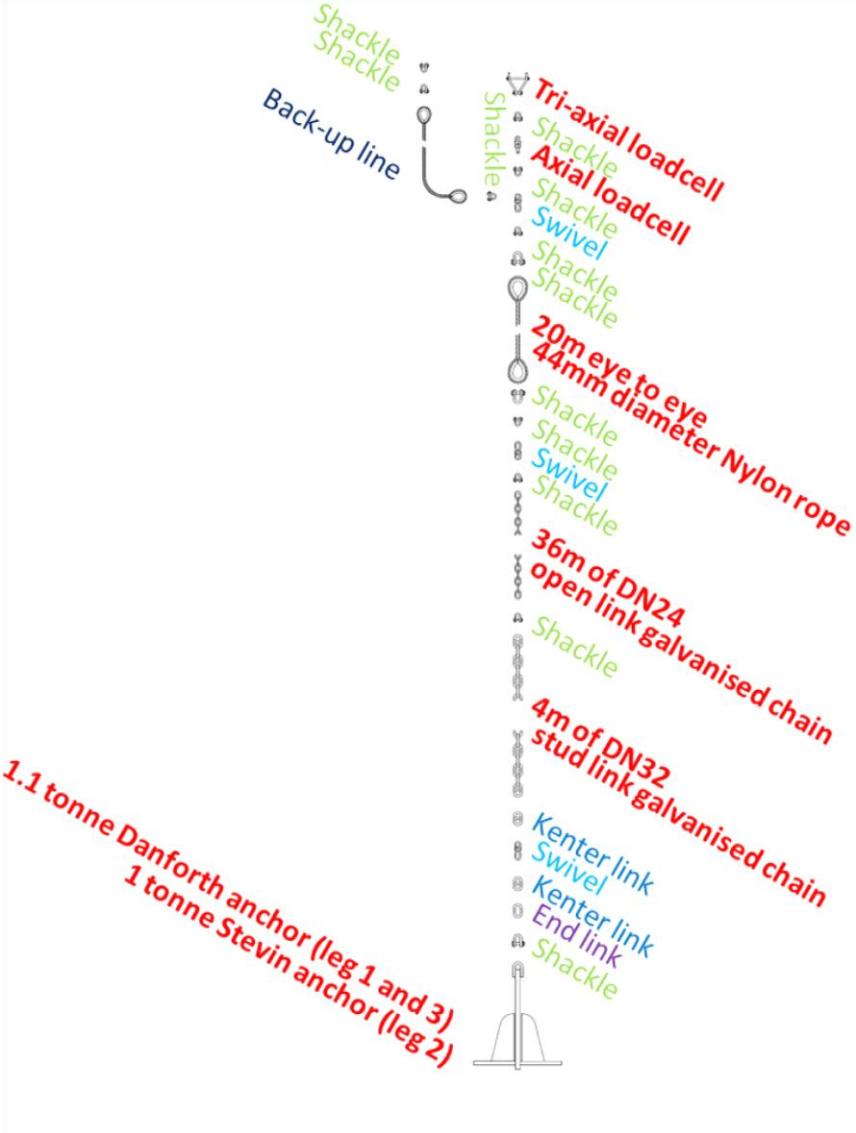

Figure 3.10: Mooring line layout for the SWMTF during its first deployment

Table 3.7: Mooring leg of the SWMTF instrumented buoy mooring (seabed to surface), without connectors. DN: nominal diameter

Mooring element	Properties
Type of legs	Catenary
Number of equally spread lines	3
Anchor distance to the floating structure	50 m
Anchor type	Drag embedment anchor (Figure 3.12)
Weight to avoid large excursion or vertical mooring load on the anchor (and if necessary length to avoid rocky seabed)	4 m DN32 stud link chain, grade and MBL unknown
No contact of the nylon rope with the seabed	36 m DN24 open link chain, grade 40 MBL ~ 385 kN
Nylon rope to provide compliance	20 m of nylon rope MBL: 461 kN, 44 mm Superline (first SWMTF deployment), MBL: 520 kN, 48 mm Braidline (second SWMTF deployment)
SWMTF instrumented buoy	3,250 kg buoy

3.1.4.1 First deployment: 14/03/2010-06/02/2012

For the first deployment, Nylon ropes were used in the water column. The aim of this test was to gain experience with the SWMTF and to start gathering research data with a compliant mooring.

After an iterative process with different rope diameters, a design load of 7 tonnef (69 kN) was derived from a fully dynamic analysis in OrcaFlex conducted by project manager David Parish at University of Exeter. Additionally, a target factor of safety of 3 was applied for the structural design to account for uncertainties. This relatively high factor of safety has been used because of uncertainties in the floating structure behaviour and because of the lack of experience for this kind of device. In addition, the reliability of the mooring was fundamental to obtain results and for the reputation of the wave energy company as well as of the test site. The cost-effectiveness of the mooring design was not the priority in this case but its survivability was.

This means that the elements of the mooring should have a MBL of 21 tonnef (206 kN). In other words, the manufacturer specifications of the elements of the moorings should indicate that the elements are able to resist loads up to 21 tonnef.

In order to choose a Nylon rope, the MBL of the rope was considered as reduced by 10% due to eye splice, 10% due to water absorption, and also reduced by an uncertain quantity due to ageing and fatigue (Parish, 2013). This led to the choice of a rope with a MBL of 41 tonnef. The closest available rope by the manufacturer Bridon with a Superline construction (Figure 3.11a) had a MBL of 47 tonnef (461 kN) and a diameter of 44 mm. Bridon has been chosen for convenience because it is a British manufacturer and it could provide an appropriate rope. The Superline construction has been chosen for its durability and strength, the loads been taken by the core, sparing the envelope while the envelope protects the core and compacts it. Considering the properties of this kind of rope, for the 7 tonnef design load, which is 15% of the MBL, the extension of the rope would be of 8% (Figure 3.11a). In this range of extension, the rope axial stiffness is constant and can be estimated at 858 kN as described in (3.1).

$$Axial\ stiffness = \frac{Design\ load\ (tonnes)\ x\ g}{Percentage\ of\ rope\ extension\ at\ design\ load} = \frac{7\ tonnes\ x\ g}{8\ \%} = 858\ kN \quad (3.1)$$

This estimation was validated by measurements. The axial stiffness (*EA* with *E* the Young's Modulus and *A* the sectional area of the rope) of the dry nylon rope used for this deployment was measured from tension-tension tests conducted using the Dynamic Marine Component (DMaC) facility at the University of Exeter (Weller, 2014). For a range of harmonic loading regimes with mean loads and amplitudes not exceeding 1.0% and 0.6% respectively of the MBL, the rope sample demonstrated axial stiffness values between 889-972 kN for oscillation periods ranging from 25 to 100 s.
This rope was changed for the next deployment because: a) its durability is limited, b) fatigue tests and other destructive analysis have been conducted on the aged rope, and c) other line materials were tested during the next deployments to investigate different dynamic behaviours.

The chains have been chosen for their strength, but also to provide a sufficient weight to avoid vertical loads on the drag embedment anchors. These chains will be kept for the next deployments because of their price and durability.

Anchors have been bought on the second hand market to reduce costs. Consequently, the availability of model and size was limited. Two 1.1 tonne Danfort Bruce anchors and one 1.0 tonne Stevin anchor (Figure 3.12) have been bought. The Danfort Bruce anchors have a slightly lower safety factor than the target one: their safety factor is 2.61 while the safety factor of the Stevin anchor is 3.17. However, the behaviour of this type of anchor is well known which allows the reduction of the safety factor.

Example of superline construction	Example of double braided construction
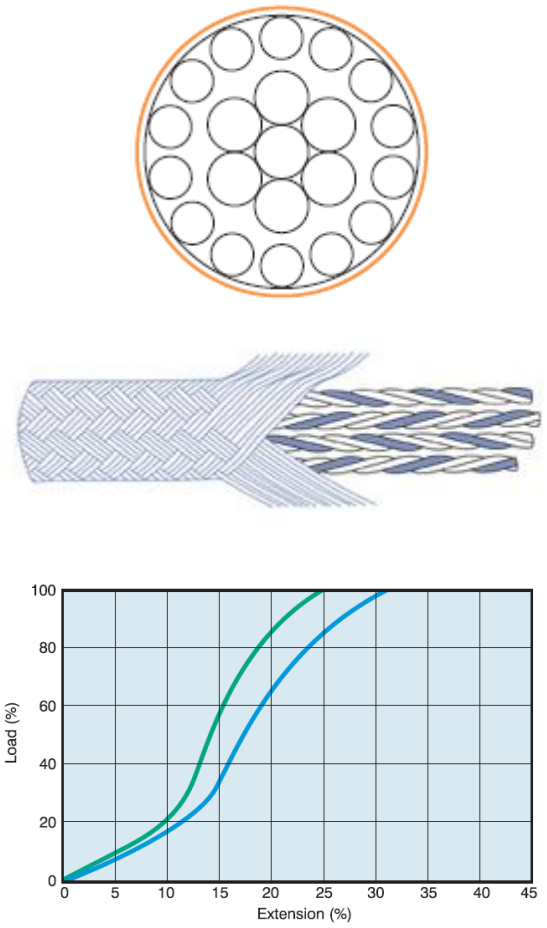	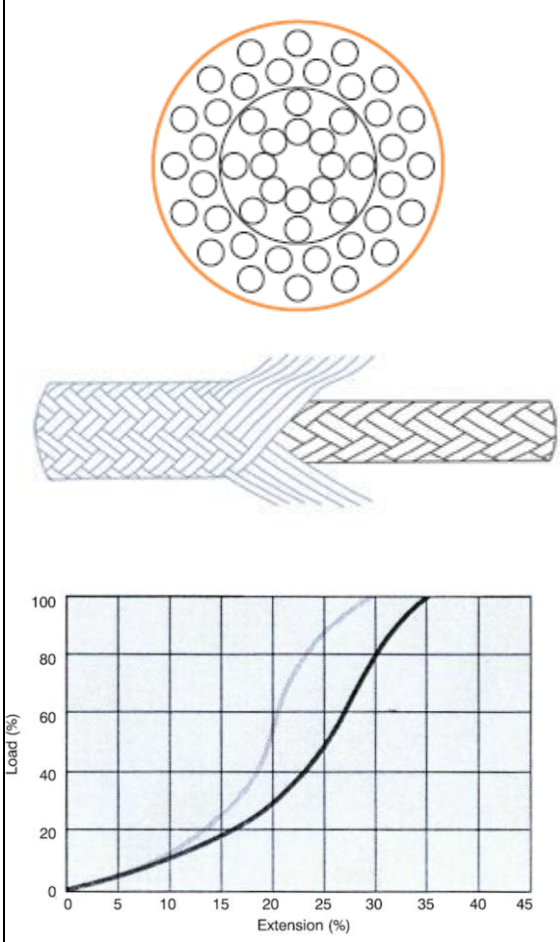
Diameter = 44 mm, MBL = 461 kN	Diameter = 48 mm, MBL = 520 kN
(a)	**(b)**

Figure 3.11: Nylon rope for the SWMTF: first deployment (left), second deployment(right). From top to bottom: rope construction (Bridon, 2011; Exsil n.v. - Koordenfabriek Van Houte n.v., 2014), rope stiffness (superline: Bridon, 2011; double braided: private communication with Lankhorst) (new rope: lower line, worked rope: higher line), rope size and strength

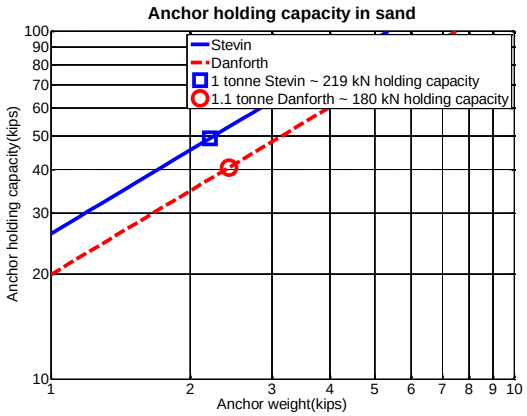

Anchors 1 and 3

1.1 tonne Danforth

180 kN holding capacity

Anchor 2

1 tonne Stevin

219 kN holding capacity

Figure 3.12: Holding capacity in sand of anchors used for the SWMTF as defined by NCEL (1987); 1kip ~ 454kgf ~ 4.45kN

3.1.4.2 Second deployment: 23/08/2012-03/06/2013

The aim of this test was to use Nylon ropes with a similar MBL to the one used during the first deployment, but with a higher compliance. This is achievable by using a different rope construction.

A 48 mm diameter rope (Figure 3.11b) was provided by Lankhorst with a double Braid construction and a MBL of 53 tonnef (520 kN). Double-braided ropes are composed of two concentric braided elements, each part contributing equally to the strength.

This rope was more elastic than the rope used during the first deployment: for a similar load, its extension will be higher. For the 7 tonnef design load, which is 13% of the MBL, the extension of the rope would be approximately 10% (Figure 3.11a). In this range of extension, the rope axial stiffness is constant and has been estimated as 7 tonnef x 9.81 $m.s^{-2}$/ 10% = 687 kN.

3.1.5 Deployments and data available

3.1.5.1 First deployment: 14/03/2010-06/02/2012

Operations during the first deployment are summarised in Figure 3.13.

The ADCP had to be retrieved to change its battery approximately every three months. It was immediately reinstalled on the seabed. This operation is further referred to as the “ADCP redeployment”. The ADCP worked well during its three first deployments. During the fourth ADCP redeployment (09/03/2011-15/06/2011), the ADCP failed and stopped providing data for a large period of time from the 03/06/2011. The ADCP was

accidentally deployed upside down for its last redeployment (15/06/2011-13/10/2011) and consequently did not provide data.

The orientation of the four beams of the ADCP was different during each deployment as shown in Table 3.8. In clockwise order, viewing from the top, the beams were organised as beam 3, 1, 4 and 2. The beams were perpendicular to each other and oriented as shown in Figure 3.9c.

Table 3.8: Summary of ADCP redeployment and beam 3 orientation during the first SWMTF deployment

Date installation	Date recovery	Beam 3 orientation
16/09/2010	18/10/2010	10.6°
18/10/2010	10/12/2010	264.5°
10/12/2010	09/03/2011	19.6°
09/03/2011	15/06/2011	37.6°
15/06/2011	13/10/2011	/ (not providing data)

The loadcells gave usable data for the whole deployment, except loadcell 3, which load drifted until saturation. Consequently data after the 05/02/2011 will not be considered for loadcell 3 for this deployment.

A jump in the load data was observed on the 27/01/2011. This jump was due to the drag of an anchor and will be explained in more details when the load data summary is presented. Data will be analysed separately before and after the anchor drag, because the mooring equilibrium was modified by this event: lower pre-tension, different sharing of the mooring loads between the three lines and different instrumented buoy equilibrium position.

3.1.5.2 Second deployment: 23/08/2012-03/06/2013

Operations during the second deployment are summarised in Figure 3.14.

The ADCP worked correctly for its two first deployments, but stopped working during its last redeployment, from March 2013. It was recovered on the 08/08/2013 after being located with a ROV. The beam orientation during this deployment is shown in Table 3.9.

Table 3.9: Summary of ADCP redeployment and beam 3 orientation during the second SWMTF deployment

Installation date	Recovery date	Beam 3 orientation
20/09/2012	18/12/2012	84.3°
18/12/2012	14/03/2013	112.9°
14/03/2013	08/08/2013	22.5°

The loadcells provide only a few usable data from the 23/08/2012 to the 17/09/2012. As a consequence, data collected during this period will not be used for further analysis. Furthermore, wave measurements were not available at this time. More loadcell data are available from November 2012 but loadcell 1 failed on the 20/01/2013 and loadcell 2 failed on the 15/02/2013.

3.1.5.3 Hindcast model

A 23 year hindcast SWAN model was available (Delft University of Technology, 2012; Van Nieuwkoop et al., 2012) from the 01/01/1989 to the 01/05/2012. This model can predict the wave climate on the whole Cornwall coast including the SWMTF site. This model has been validated with data from 6 wave buoys (Van Nieuwkoop et al., 2012) for the following parameters: the significant wave height H_S, the wave energy period T_{mm10} and the mean wave direction D_{mean}. Other parameters are provided by this hindcast model including T_P and T_Z but these parameters have not been compared with the wave buoy data.

Hindcast errors have been quantified for the validated parameters. The modelled significant wave heights H_S were generally underestimated by less than 4%, except for two wave buoys close to the shore were they were underestimated by 15% or overestimated by 6%. Detailed relative bias and scatter index (SI) are given in Table 3.10 for the significant wave height and the wave energy period as well as the absolute difference and root-mean-square error for the mean direction. The wave energy periods T_{mm10} were underestimated by 7 to 20%. The differences between the hindcast and measured mean wave direction D_{mean} were for most locations of approximately 20°.

The hindcast model will be used in the next chapter to indicate if the wave climates for the measured months were under or over the average compared to other years. The validated hindcast model will also be used to quality check the ADCP data. Hindcast

model are usually been validated by measurements, and not the other way round because hindcast model gives less accurate results. In this case, the hindcast model will indicate if the ADCP wave measurements are in the expected range of wave conditions.

Table 3.10: Wave buoy validation statistics from van Nieuwkoop, et al. (2012). The scatter index (SI) is a standard metric for wave model intercomparison.

Buoy name	***Number of data points***	H_{m0}		T_{mm10}		**Mean direction**	
		Relative bias	Scatter index	Relative bias	Scatter index	Absolute difference	Root-mean-square error
UoE 1	5006	-4%	17%	-18%	24%	23°	43°
UoE 2	7050	-3%	17%	-15%	20%	21°	38°
Perranporth	40003	-4%	19%	-20%	27%	19°	37°
Penzance	38562	-15%	32%	-17%	35%	23°	39°
Porthleven	363	-1%	19%	-7%	13%	5°	6°
Looe Bay	19159	6%	24%	-9%	28%	19°	35°

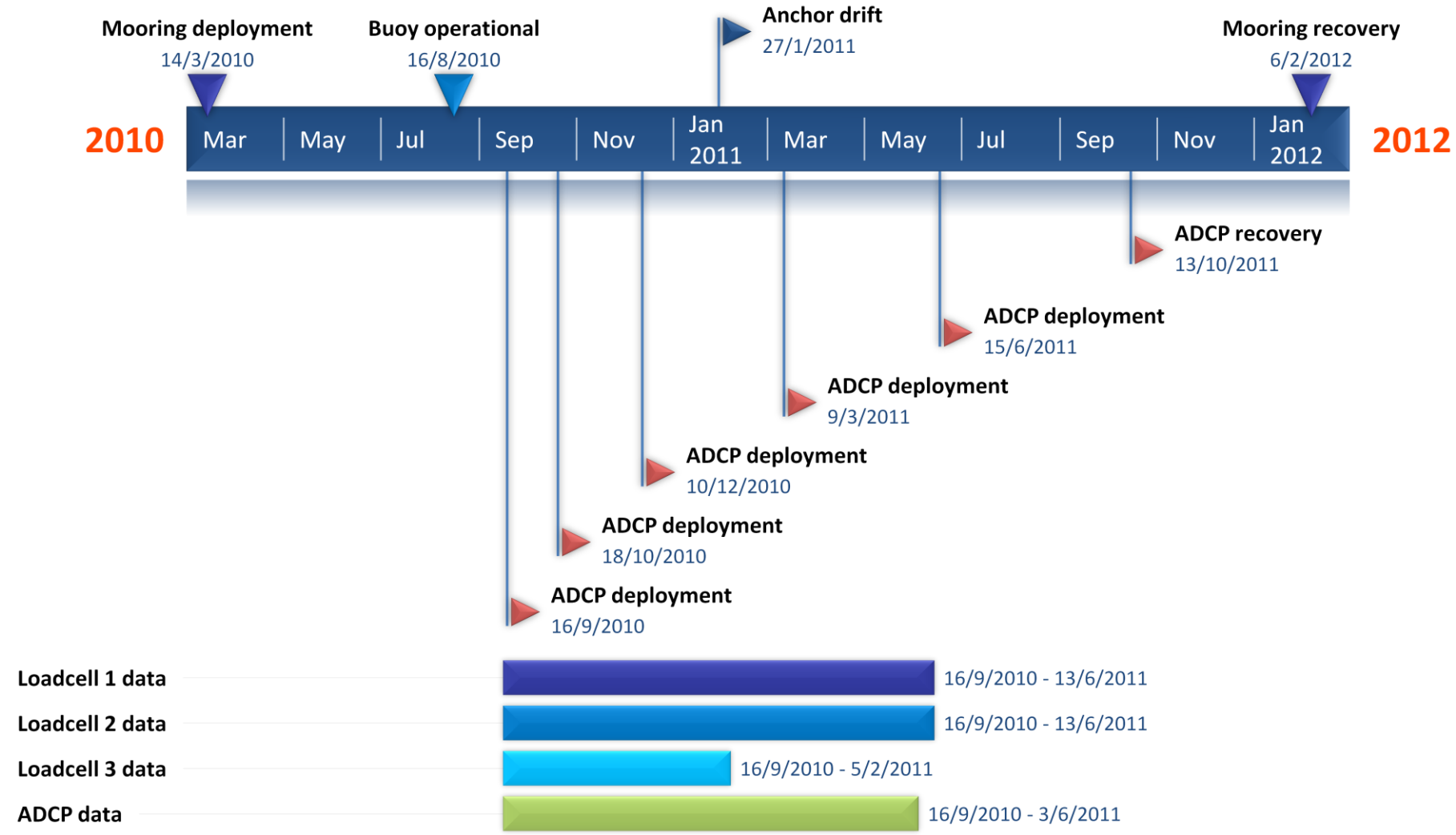

Figure 3.13: Summary of operations for the SWMTF during the first deployment

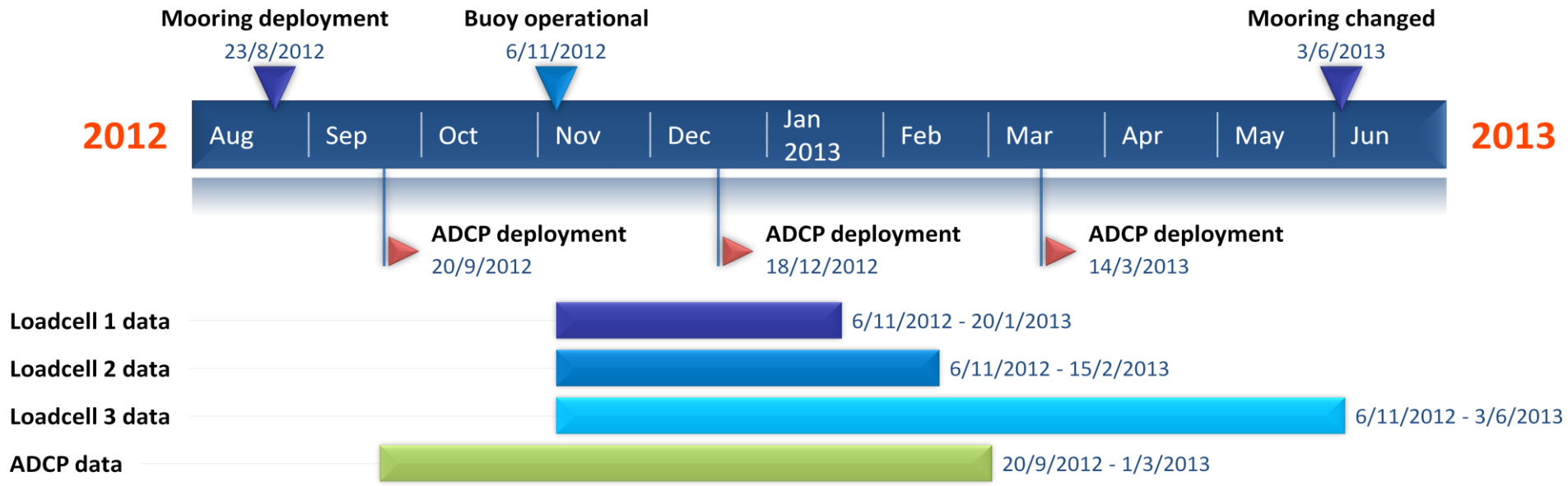

Figure 3.14: Summary of operations for the SWMTF during the second deployment

3.2 FaBTest: Bolt-2 LifeSaver device

The Falmouth Bay test site (FaBTest) is a demonstration facility that enables developers to test components, concepts or full scale devices in a moderate wave climate with excellent access to nearby port infrastructure.

As part of a collaborative Technology Strategy Board (TSB) project lead by Fred Olsen Ltd, the 'Bolt-2 LifeSaver' wave energy device (Hjetland et al., 2011) has been installed at the FaBTest site. The aim of the TSB project was to conduct sea trials at full scale, before a possible deployment in less sheltered conditions. These sea trials aimed to gain operational experience and investigate performances (Sjolte et al., 2013). In terms of research activity, the deployment of this prototype has been an opportunity to gather mooring load data from a working wave energy device.

3.2.1 Choice of location

The location of FaBTest test site was limited by several parameters which need to be taken into account for any renewable energy projects:

The water depth of the FaBTest site is within 20 to 50 m. FaBTest is located within the port limits which facilitate the procurement of the required planning consents. A special area of conservation is also located just outside of the port limits. Some historic wrecks are located South of the site. This explains why the site does not extend to the South limits of the port. A fairway for navigation is located West of the site. A fairway is a channel customarily navigated by vessels to enter the port. Also, ships are often anchored West of the site.

The 'Bolt-2 LifeSaver' was installed in the deepest part of the FaBTest site, in the South-West part of the site.

3.2.2 Instrumentation

The 'Bolt-2 LifeSaver' floating structure is an instrumented surface annulus buoy (Figure 3.15a) of 55 tonnes and 10 m inner diameter, 16 m outer diameter and 1 m height which was equipped to record a whole range of data. The data recorded on the floating structure were all synchronised. Data were recorded and saved in files containing a maximum of 20 minutes of data (240,000 data points for the load data

recorded at 200 Hz), not continuously but only when the sea state was sufficiently energetic, at the discretion of the wave energy developer.

The data provided by the wave energy developer were mooring loads: axial loadcells recorded mooring load data at 200 Hz (Figure 3.15b). The loadcells used for these measurements were Strainstall 5395 Underwater load shackles (Strainstall, 2014). The shackles had a rated load of 50 tonnef (491 kN), but were scaled for 0-30 tonnef (0-294 kN). The accuracy of these loadcells is claimed as better than 0.75% of the rated load, 0.375 tonnef (3.7 kN) in this case.

An integrated positioning system was installed on the wave energy device but did not always give accurate data due to poor performances of the GPS. The position data were recorded at 10 Hz.

A Seawatch mini II directional wave buoy (Figure 3.15c, Fugro, 2010, Sanmuganathan, 2009) belonging to the University of Exeter was used to record wave data at 2 Hz. The wave buoy was installed at a distance of 334 m South-West of the 'Bolt-2 LifeSaver' device (Figure 3.16).

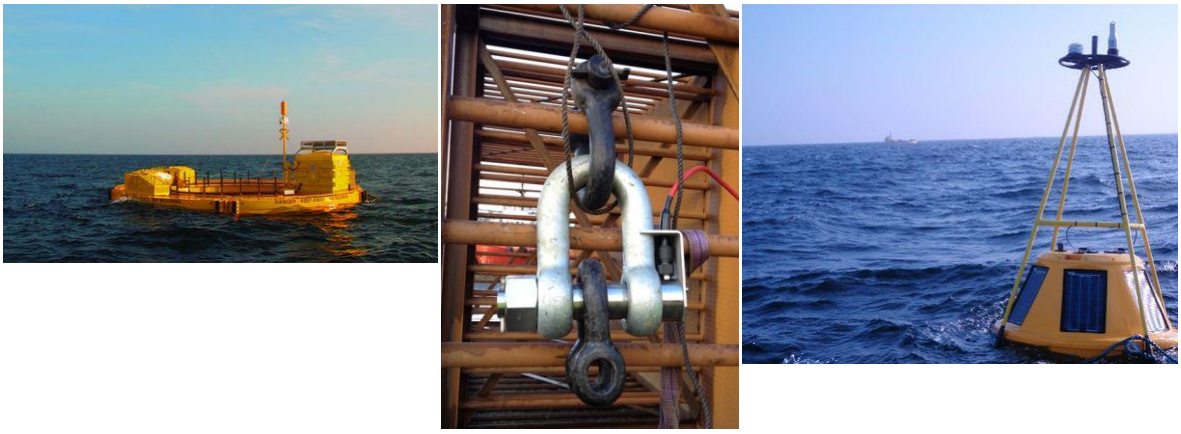

(a) **(b)** **(c)**

Figure 3.15: Wave energy device sea trials at FaBTest: a) Fred Olsen Bolt-2 LifeSaver floating structure, b) Mooring loadcell used by Fred Olsen; c) Wave buoy used at FaBTest

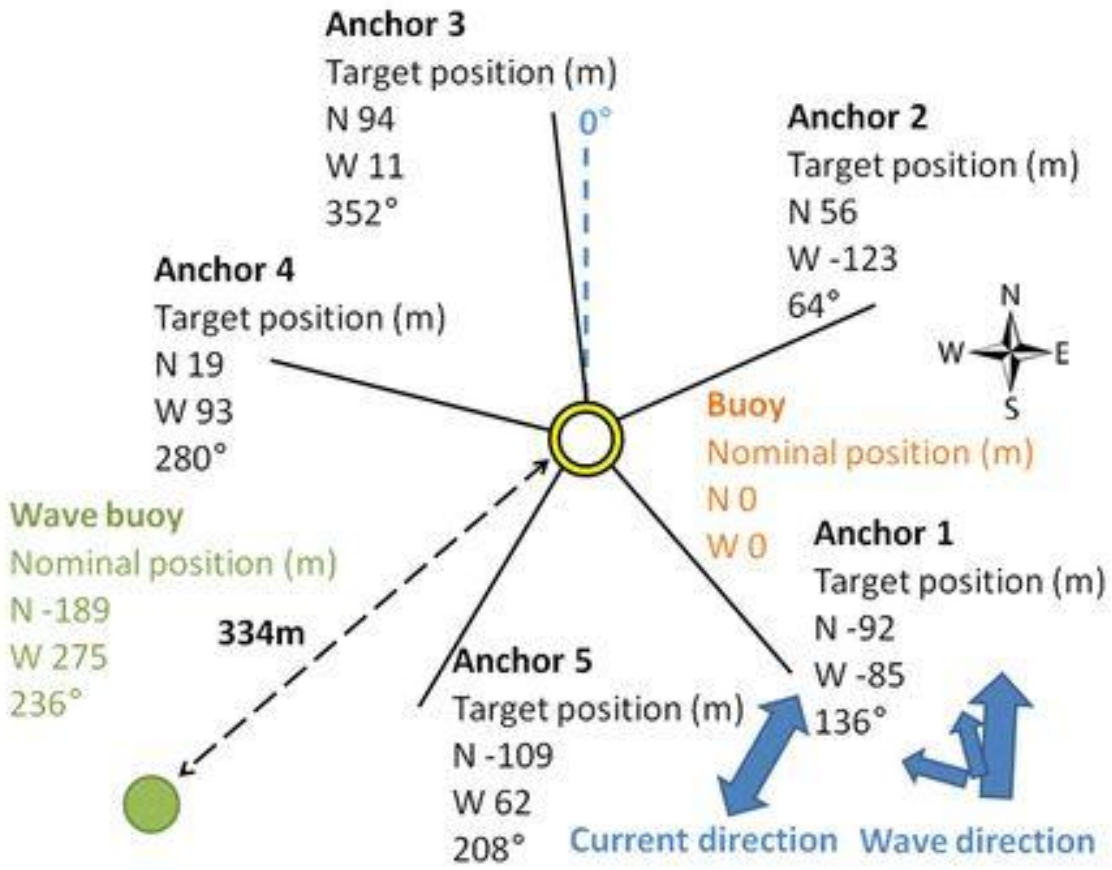

Figure 3.16: Bolt-2 LifeSaver secondary mooring system layout, wave buoy location and environmental load direction

3.2.3 Raw data files

Data were saved every 20 minutes or less when the floating structure was collecting data. The data were pre-processed by the wave energy developer. The data were separated into files for the mooring load and files for the wave energy device position. The files were named by their date with the following format: YYYYMMDD_HHmmss.csv.

The data from the wave buoy relevant to the present work have been provided by the University of Exeter wave buoy manager, Dr Ian Ashton, who used the wave buoy firmware to extract the parameters required for further analysis. Wave data were continuously recorded, then processed at the wave buoy every 30 minutes by the on-board firmware WaveSense. The following wave statistics were provided: H_S, H_{max}, D_{mean}, Q_P, T_Z, T_{mm10} and T_P. All parameters were calculated with spectrum analysis except H_{max}, which was calculated by zero-crossing analysis. The data were provided in a TAB delimited text file. Q_P and T_{mm10} have not been used in this thesis for further analysis.

3.2.4 Mooring design

As part of her Research Associate position, the author of this thesis contributed to the design of the Bolt-2 LifeSaver mooring system by designing, running and analysing mooring design calculations with OrcaFlex. The final choice of mooring system was taken by Fred Olsen and the mooring design externally validated.

The mooring for the Bolt-2 LifeSaver has been designed based on a primary and secondary storm and associated environmental conditions from two different directions as shown in Table 3.11. These storm conditions have been chosen based on a 2000-2008 SWAN hindcast model. The peak enhancement factor *γ* was automatically calculated by OrcaFlex following Isherwood (1987) formulae. Different values of the wave and wind directions were investigated.

Table 3.11: Primary and secondary storms used for Bolt-2 LifeSaver mooring design. T is the clockwise angle from the North

Parameter and unit	Primary storm	Secondary storm
H_S (m)	7.5	6.15
T_Z (s)	7.5	6.5
Spectrum	JONSWAP	JONSWAP
Peak enhancement factor γ	5.95	6.15
Cases of wave and wind direction	352T, 2T, 7T	275T, 285T, 316T
Wind speed (m/s)	30	30
Tide current speed (m/s)	0.5	0.5
Tide current direction	230T and 050T	230T and 050T
Water depth (m)	45 and 51	45 and 51

The device was moored with two sets of moorings: a primary and a secondary one. The primary mooring was made of three PTO winches connected underwater to fibre rope (Dyneema) lines kept taut with underwater buoys. The secondary mooring of this wave energy device, installed to ensure survivability, was equipped with conventional axial loadcells to record mooring load data for each mooring line. The secondary mooring was made of a five leg catenary mooring system installed as shown in Figure 3.16. Each of the mooring legs combines chains and nylon rope as described in Table 3.12. This table does not include connectors such as shackles and swivels. The deployment position of the Bolt-2 LifeSaver floating structure is 50° 6.0402’ N, 4° 59.6455’ W.

Table 3.12: Bolt-2 LifeSaver secondary mooring line layout (seabed to surface), without connectors

Property of the mooring line from the seabed to the floating structure	
Type of legs	Catenary
Number of equally spread lines	5
Anchor distance to the floating structure	Line 1 to 5 (m): 125/135/95/95/125
Anchor type	Drag embedment anchor
Weight to avoid large excursion or vertical mooring load on the anchor (and length to avoid rocky seabed)	40 to 80 m DN60 stud link chain, grade 1 (line 1 to 5 (m): 70/80/40/40/70) MBL = 1380 kN
No contact of the nylon rope with the seabed	38 m DN36 open link chain, grade 2 MBL = 672 kN
Nylon rope to provide compliance	32 m of 64 mm nylon Braidline rope MBL = 812 kN
Protection of the top end of the nylon rope	3 m DN36 open link chain, grade 2 MBL = 672 kN
Wave energy device	40 tonnes buoy

After an iterative process with different rope diameters, a design load of 217 kN was derived from a fully dynamic analysis in OrcaFlex. The simulations were run for 2000 s, and several analyses were run for different wave directions, for low and high tides, and for different significant wave heights. Analyses were run for an intact device, for a device with one, several or all PTOs broken, for each mooring line broken (each mooring line failure was investigated).

The phase angle was not varied in the wave field for the same sea state. The analyses were run without directional spread.

Additionally, a target factor of safety of 3 was applied for the mooring design to account for uncertainties. This means that the elements of the mooring have a minimum breaking load (MBL) of 651 kN. For the mooring synthetic rope, allowance is made for a 15% reduction in strength due to water absorption and a further 15% reduction in strength is made to allow for the eye splices. This led to the choice of a 64 mm Nylon Braidline rope manufactured by Lankhorst with an MBL of 1,124 kN (812 kN

after allowance for reduction in strength). The rope axial stiffness was estimated at 2,100 kN for small extensions.

The chains have been chosen to avoid vertical loads on the drag embedment anchors. The length of each chain was different to avoid the rocky area on the seabed to facilitate installation and ensure performances of the drag embedment anchors. The length of the different lines can be found in Table 3.12.

3.2.5 Deployment and data available

The floating structure was installed in March 2012 and recovered in June 2014. Load data have been collected from October 2012 to January 2014. Some data are missing because the monitoring system was turned off or because of a loadcell failure (likely to be due to a lightning).
The wave buoy provided data from the 19th of March 2012 to the 30th of June 2013.

The same hindcast model as the one used at SWMTF provided hindcast data for the FaBTest site.

Figure 3.17 summarises the main operations and the availability of measured data.

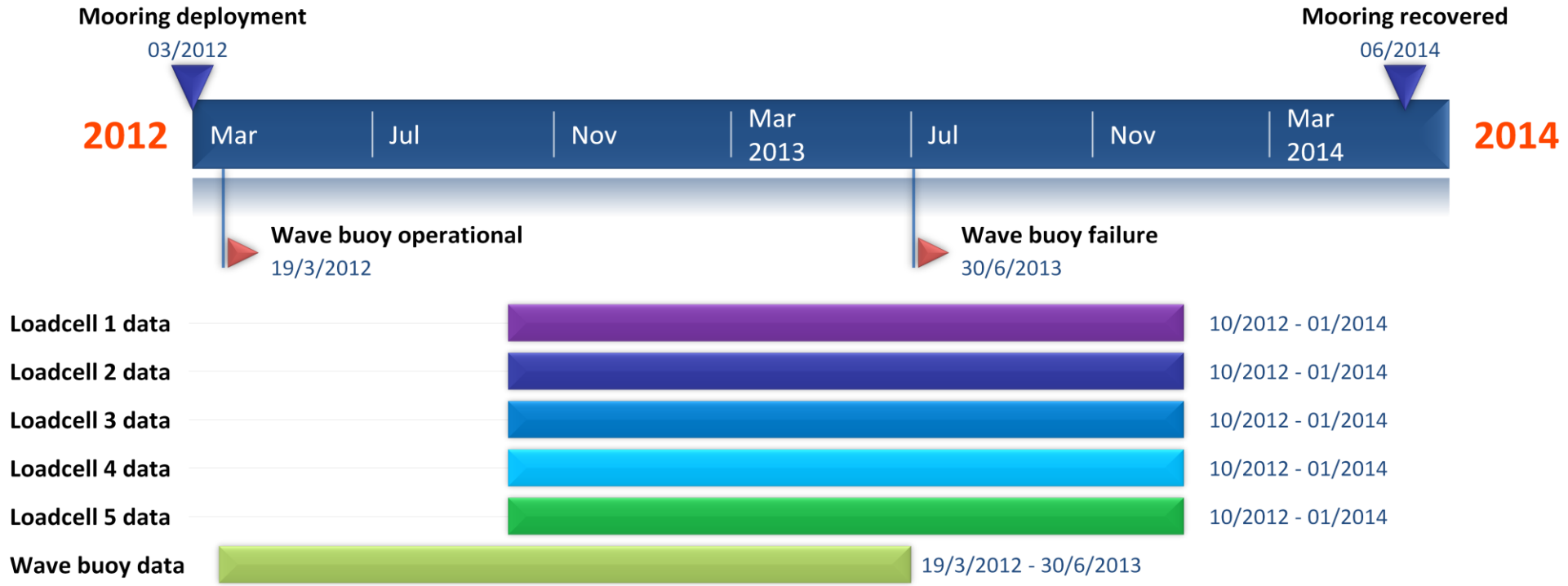

Figure 3.17: Summary of operations of Bolt-2 LifeSaver wave energy device

Chapter 4. Data analysis

The aim of this chapter is to present the statistical data which have been collected at the two facilities (presented in the previous chapter) and which will be used for further analysis (in the next chapter). These data are statistical wave and current data (significant wave height H_S, maximum wave height H_{max}, peak period T_P, zero-crossing period T_Z, peak direction D_P, mean wave direction D_{mean}, current magnitude C_{Mag} and direction C_{Dir}, and water level h) and statistical mooring load data (maximum, mean, standard deviation, standard score of the maximum (defined in (4.4)).

This chapter is divided in two parts, one for each facility (South West Mooring Test Facility and Bolt-2 LifeSaver device at FaBTest).
The structure of each part is similar:

- The data control and analysis methodology which have been followed to transform the raw time series of data into the processed, corrected and validated statistical data is presented.
- An example of time series of data is shown. Time series of data are not used in detail in this thesis. General trends need to be detected first by looking at the summary data. These time series of data are of high interest for further investigations of the dynamics of the mooring system. Furthermore, they are the data from which the statistical data are issued.
- Examples of summary data in different sea states are shown to indicate how statistical data are varying with the environment and to provide an order of magnitude of statistical data.
- The summary of the statistical data is presented: wave, current and water level (if available), and mooring load data.

4.1 South West Mooring Test Facility (SWMTF)

4.1.1 Data control and analysis methodology

Data were first pre-processed, then corrected and validated. The pre-processing aims to calibrate the data and calculate statistical parameters. The correction intends to correct or remove faulty data. The validation compares the data with other similar available data available from measurements (with a lower quality) or from validated numerical models.

4.1.1.1 Data pre-processing

Instrumented buoy

Mooring load data and GPS data needed initial calibration.

The mooring load data were converted from Volts (V) to kiloNewtons (kN) using calibration factors as shown for example in Table 4.1 for the axial loadcells. The calibration of the tri-axial loadcells was a complex process described by Ponomarev, Johanning and Parish (2010).

Table 4.1: Calibration factor (from Volts to kN) for the SWMTF axial loadcells for the period of analysis

	Loadcell 1	Loadcell 2	Loadcell 3
New ratio [kN/V]	40.6 x10^3	42.5 x10^3	43.0 x10^3
Offset [kN]	-1.51	-0.80	-0.15

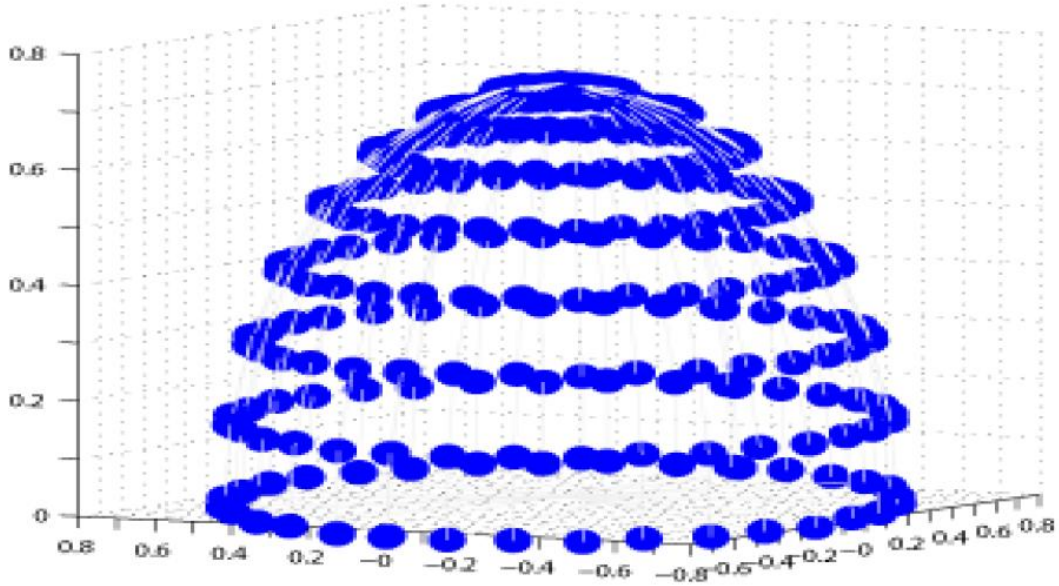

Figure 4.1: example of calibration curve (uncorrected) for the tri-axial loadcell (Ponomarev et al., 2010)

The GPS data were converted from degrees to meters. One degree does not represent the same distance in meters at different latitudes. For example, according to the Department of Army (1973), one degree at 0°N is equal to 111.32 km in longitude, and 110.57 km in latitude. At 50°N, one degree in longitude is equal to 71.70 km, and one degree in latitude to 111.23 km. The data have been converted with the instrumented buoy target deployment position (50°47.5'N 5°2.85'W) having the position (0 m, 0 m, 0 m). The 0 m upwards position corresponds to the low tide, at 27.8 m. Values are positive along the East and North axis. The difference in minutes between the instrumented buoy actual position and target position was multiplied by 1,194.93 in longitude and by 1,853.82 in latitude to obtain a position in meters.

Calibrated data are pre-processed as described in Table 4.2. Calibrated data were saved in files named YYMMDDHHmmssm***_out.csv, with *** the extension (a20, a04, swi...).

Statistical values for the minimum, mean, maximum and standard deviation were calculated for each parameter of each set of data. These statistical values were separately saved in the ASCII CSV format in files named YYMMDDHHmmssm***_out_summary.csv and in a MySQL database. A Matlab code was created to access the MySQL database.

All the files in the CSV format (calibrated data and statistical values) were compressed into a zip file named YYYY_MMDDHHmm.zip. These files were saved in a directory for processed data in a folder indicating the date of the file YYYY/MM/DD.

Table 4.2: Summary of the operations on the SWMTF data files from readable data to processed data

Step	Name of the output files
Calibration	YYMMDDHHmmssm***_out.csv
Calculation of statistical values	YYMMDDHHmmssm***_out_summary.csv + MySQL database
Compression of summary files	YYYY_MMDDHHmm.zip (YYMMDDHHmmssm***_out.csv + YYMMDDHHmmssm***_out_summary.csv)

Acoustic Doppler Current Profiler (ADCP)

As mentioned in the previous chapter, ADCP data were pre-processed with the instrument firmware WavesMon.

4.1.1.2 Data correction

The aim of the quality check and data correction is to identify and subsequently remove or correct erroneous data while valid data should not be affected. Quality control also aims to identify incidents such as the breaking of a mooring line, an anchor drag, or the entanglement of a marine animal in a mooring line.

Mooring load correction

The mean mooring loads were assessed. The mean loads should mainly be varying with the tide. An example of mean load data before correction is given in Figure 4.2.

In Figure 4.2a, a jump in the data occurred at end of January 2011. This is likely to be due to an anchor drag ("incident"). This incident will be discussed in details in 4.1.4.2.

In Figure 4.2b, the mean load is drifting which is likely to be due to the loadcell ("erroneous data"). This could have been due to moisture ingress, mishandling or component malfunction.

In this case, a correction needs to be implemented. A moving average using 1,000 points (1,000 x 10 minutes ~ 1 week) was calculated for the mean load. This moving average was removed to the minimum load, mean load and maximum load of the line. The mean of the mooring loads of the two other lines was added to the minimum load, mean load and maximum load of the line with the drifting loadcell (Figure 4.3).

The number of points for the moving average has been determined using a sensitivity study to determine the optimum window size (Figure 4.4), in order to remove the global drift of the signal but not the local variations due to tide or storm. After corrections, the data which could not be corrected were manually removed (for example after 02/2011 in Figure 4.3).

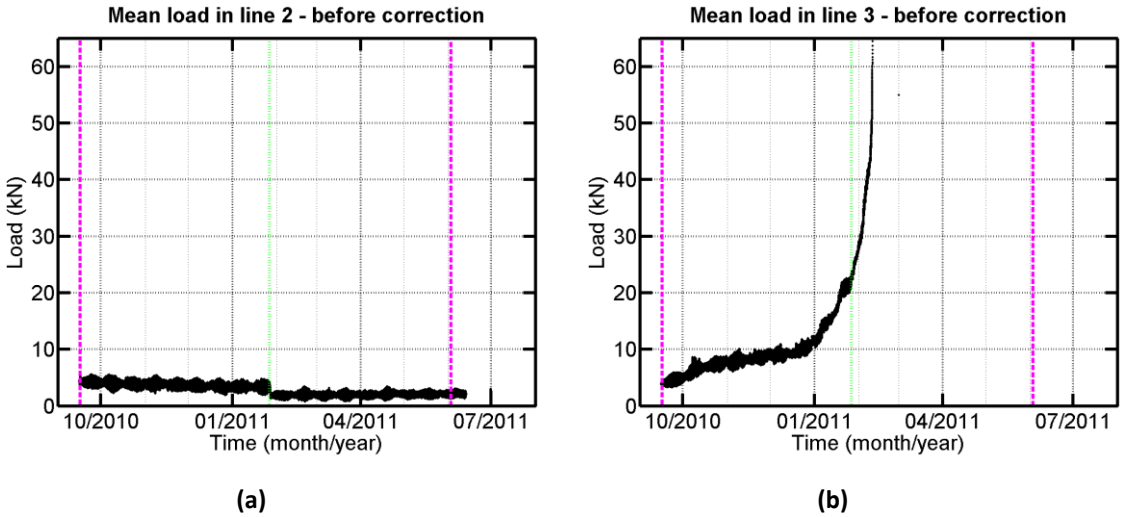

Figure 4.2: Example of SWMTF mean mooring load data before correction, during the first deployment before anchor drag in a) line 2, b) line 3. Green line: anchor drift, magenta lines: limit of the ADCP data availability

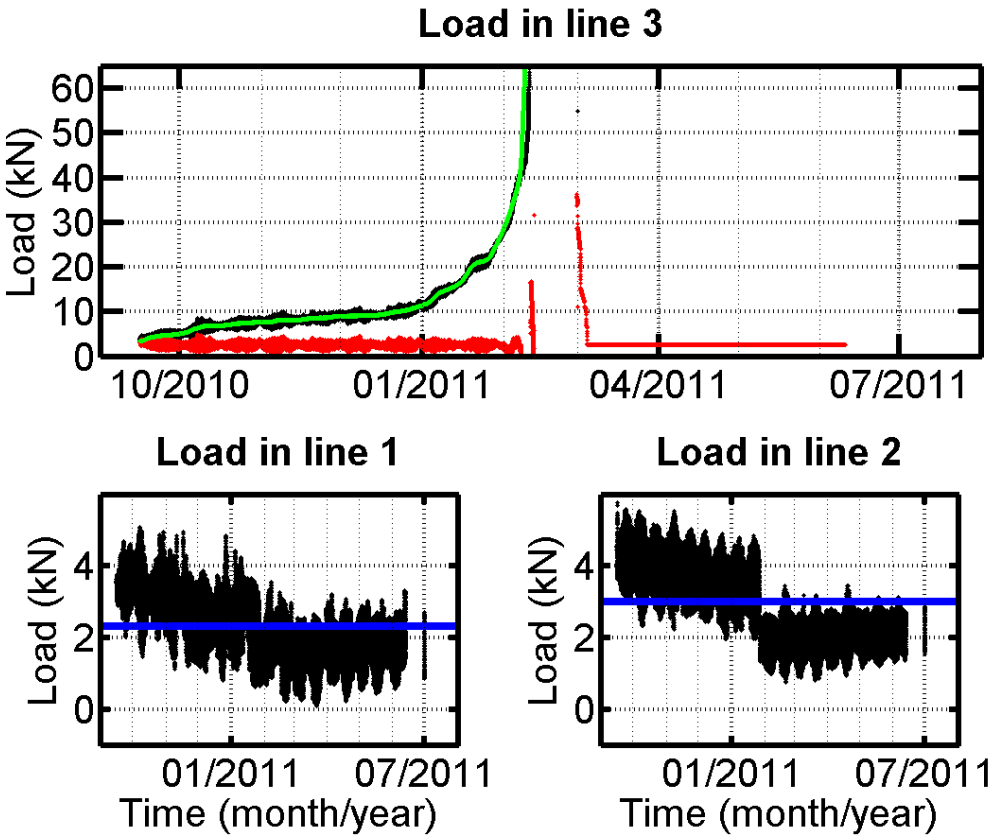

Figure 4.3: Example of correction of drift in the mooring load data for the SWMTF. Top: mean load data (black), moving average using 1,000 points (green) and corrected signal (red). Bottom: mean mooring loads on the two other lines for this period of analysis (black) and average of these mean loads (blue)

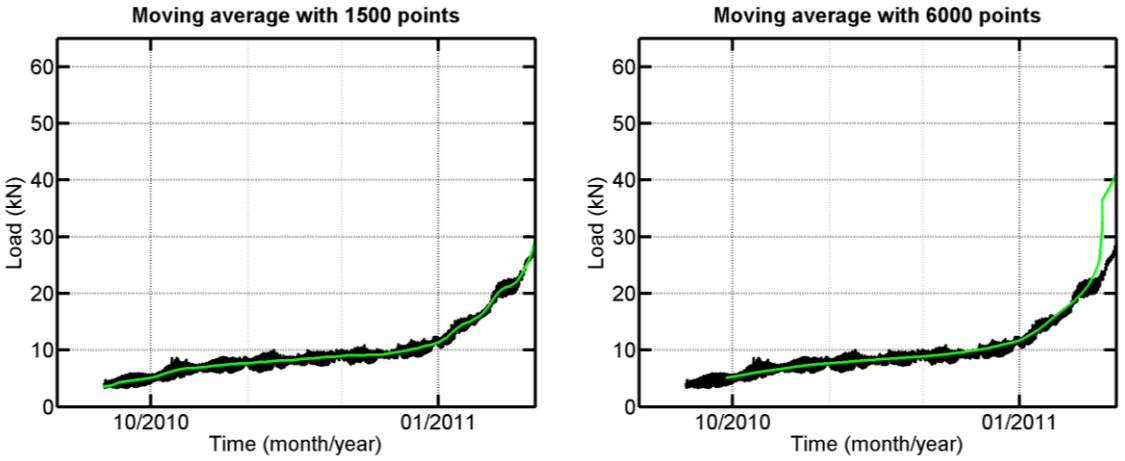

Figure 4.4: Comparison of moving averages used to correct drifting mooring loads for the SWMTF with a different number of points: a) 1,500 points, b) 6,000 points; black line: mean load, green line: moving average of this mean load

Correction of the wave parameters

Prior to detailed data analysis, some basic corrections (Table 4.3) were implemented to remove wave data which were obviously incorrect (not physically possible, or not expected at this location).

Table 4.3: Basic corrections applied to the SWMTF wave data

Check	Reason to remove data	Data removed
$D_P < 0°$	No physical meaning	Dataset (H_S, H_{max}, T_P, T_Z, D_P and D_{mean}) removed
$D_P > 360°$		
$D_{mean} < 0°$		
$D_{mean} > 360°$		
$H_S < 0$ m		
$T_P < 0$ s		
$T_Z < 0$ s		
$T_Z > 30$ s	Wind-generated gravity waves have lower periods	
$H_{max} < 0$ m	No physical meaning	H_{max} removed (only H_{max} because H_{max} was calculated using a zero-crossing method while the other parameters were calculated using a spectral method, see Table 3.5)
$H_{max} > 30$ m	Unlikely	

After applying these basic corrections, the wave statistical data (H_S, H_{max}, T_P, T_Z, D_P and D_{mean}) were plotted and assessed.

In particular, discrepancies were observed in the wave directions D_P and D_{mean}. The wave directions after basic corrections for the first SWMTF deployment were plotted in Figure 4.5. A difference in the mean of the wave direction between each ADCP re-deployment is observed. This may be due to the compass of the ADCP not being recalibrated every time the ADCP was redeployed. It was not feasible to recalibrate the ADCP on the boat and too time consuming to bring the ADCP back to the harbour to do it. The procedure for the calibration of the ADCP was changed for the second SWMTF deployment which may explain why this problem did not occur during the second SWMTF deployment.

For the first SWMTF deployment, the wave directions (D_P and D_{mean}) were adjusted as shown in Table 4.4. However, this only means that the relative direction of the waves is correct, but there may be a constant shift between the actual direction and the corrected direction.

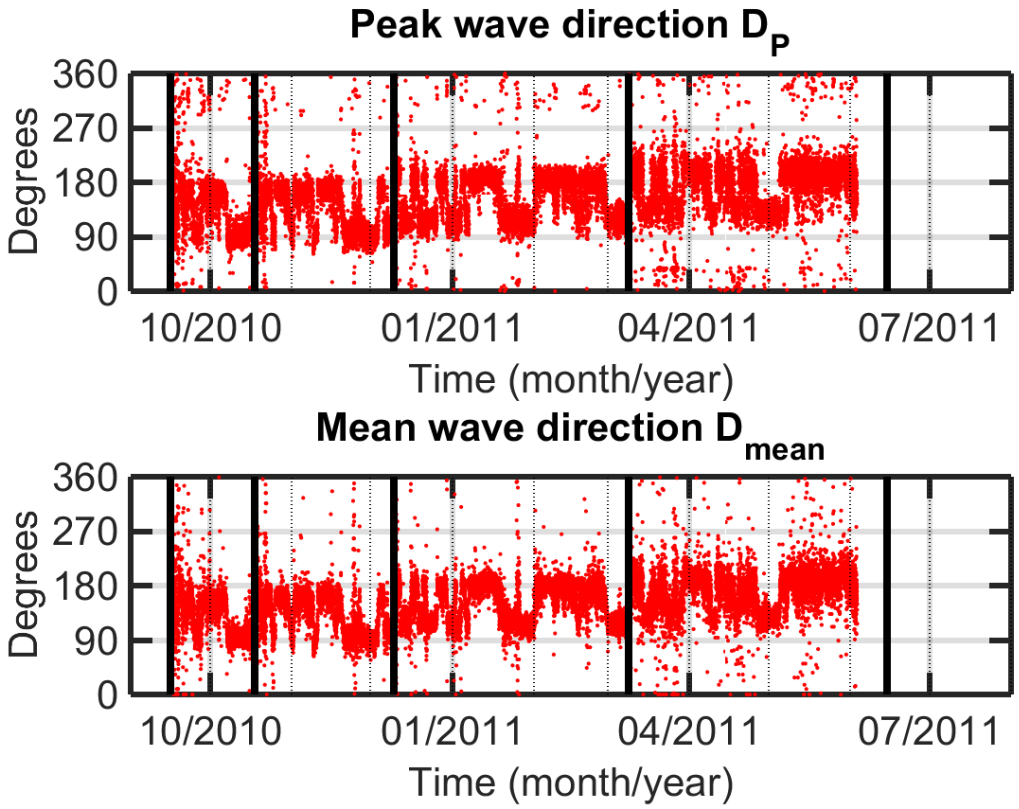

Figure 4.5: SWMTF wave direction measurements D_P and D_{mean} before correction during the first deployment. Vertical black lines: ADCP redeployment *(these are the directions from which the waves are coming which are opposite the direction of propagation used by DNV-RP-C205 (DNV, 2010)).*

Table 4.4: Corrections applied to SWMTF wave directions D_P and D_{mean}

ADCP deployment	Date	Correction
1	16/09/2010-18/10/2010	+19°
2	18/10/2010-10/12/2012	+16°
4	09/03/2011-15/06/2011	-23°

Correction of the water level

The height of the ADCP (0.4 m) was not taken into account during the processing and was added to the measured water depth.

Once this initial correction has been done, the water level data was plotted (for example in Figure 4.6). The water depth was varying with the tide, between 27 and 34 m. Any points outside of these values would have no physical meaning because large and fast variations (outlier points) in water level are not expected at this site. Consequently, water depth measurements below 27 m or over 34 m were removed (Table 4.5).

Figure 4.6 also indicates that the mean water depth value during the first ADCP deployment was higher than during the following deployments. This has no physical meaning. The water depth was adjusted to have the same mean depth over all deployments: the mean of the first ADCP deployment was removed and the mean over all other deployments was added.

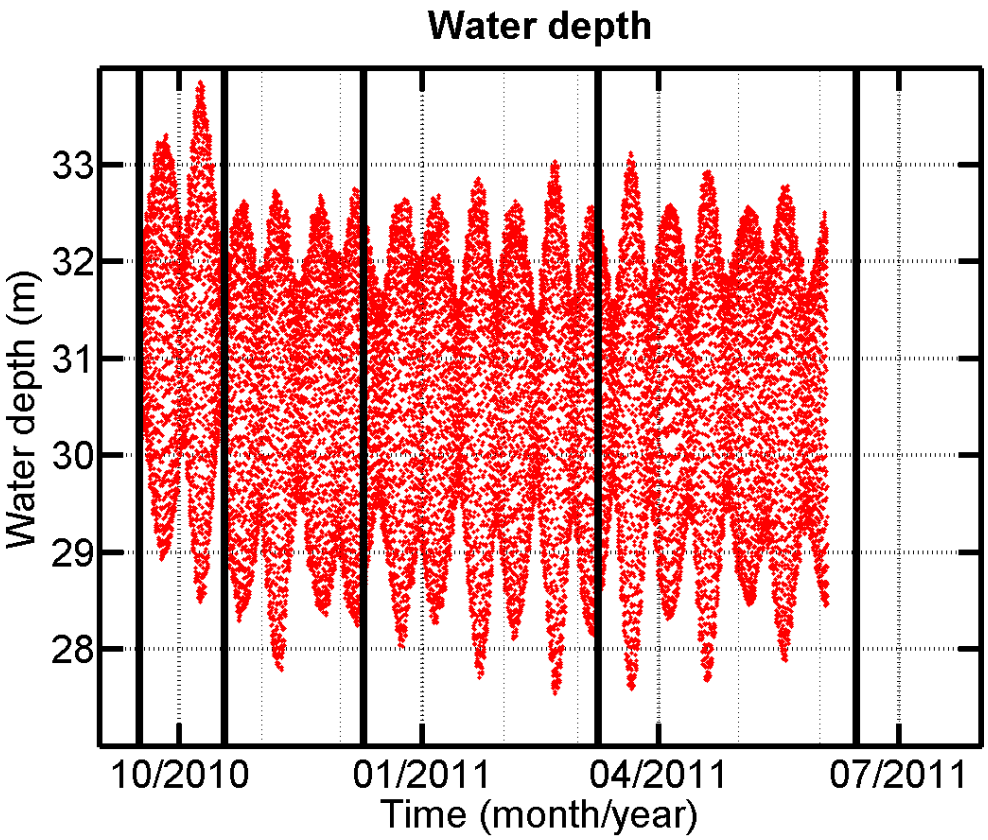

Figure 4.6: SWMTF water depth measurement before correction during the first deployment. Vertical black lines: ADCP redeployment

Correction of the current magnitude and direction

Basic and systematic corrections have been applied to the current magnitude and direction data to remove points without physical meaning. If the current direction was negative or over 360° or if the current magnitude was negative, these values of current direction or magnitude were removed (Table 4.5). This is because WavesMon, the ADCP software is providing data with positive current magnitude and angle between 0 and 360°. The values of current magnitude and current direction over the mean water level (depending on the tide) at a given time were also removed. In addition, current magnitude and direction were removed in a surface layer with a thickness of 5-15% of the total water column. In this surface layer, measurements are compromised by sidelobe reflections of the acoustic beams as discussed by RDI (1989), as shown in Figure 4.7.

The maximum current magnitude C_{Mag_max} and its associated direction C_{Dir_max} were evaluated in the bins below the surface layer, and over the seabed: the highest velocities should be in the middle of the water column.

C_{Mag_max} and C_{Dir_max} were the maximum current magnitude and associated direction between 7 and 15 m below the water surface. If the maximum current magnitude was zero, this value was removed as well as the associated current direction.

The current velocity *C* was introduced (Eq. (3.1)) to summarise the current magnitude and direction in a single variable because the tidal flow has two opposite directions. However, this variable does not isolate the tidal current from the current.

$$C = C_{Mag\_max} \times cos\left[C_{Dir\_max} - \overline{C_{Dir\_ebb}}\right] \quad (4.1)$$

with $\overline{C_{Dir\_ebb}}$ the mean ebb direction during the whole deployment. *C* is positive during ebb and negative during flood.

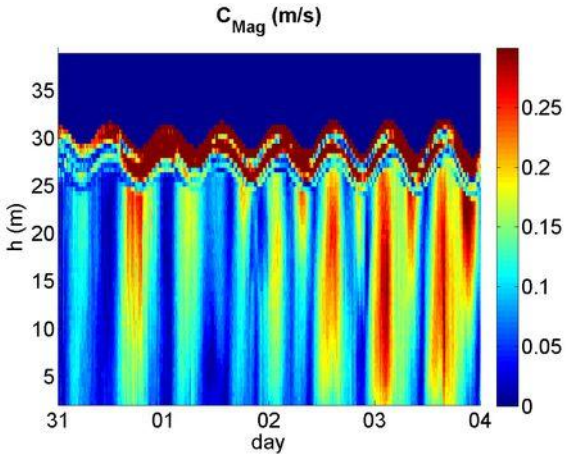

Figure 4.7: Example of SWMTF current magnitude measured between the 31/10/2010 and the 04/11/2010

Table 4.5: Basic corrections applied to the SWMTF measured water level *h* and current data C_{Dir_max} and C_{Mag_max}

Check	Reason to remove data
h < 27 m	Not expected at this location, outliers points
h > 34 m	
$C_{Dir\_max} < 0°$	No physical meaning
$C_{Dir\_max} > 360°$	
$C_{Mag\_max} < 0$ m/s	

4.1.1.3 Data validation

Measured data have been compared with other available set of data measuring or estimating the same quantity.

Validation of the wave data

Hindcast data have been compared with the wave measurements in order to assess the validity of the wave measurements. These hindcast data have been already validated and their inaccuracies assessed as explained in 3.1.5.3. This is why hindcast data are used in this case to validate wave measurements when the opposite is more common. They also indicate if the sea states were typical for the site at the time of year of the measurements: were the data recorded for an exceptionally calm or stormy year, or for an average year?

Recorded and hindcast wave data were both available for the first deployment of the SWMTF. Hindcast data were output every hour while measured data were output every 17 minutes (1,024 s) during the first SWMTF deployment. The parameters H_S, T_Z, T_P and D_{mean} were available from both the measured and hindcast data.

To start with, data are visually compared in Figure 4.8 (overall data) and Figure 4.9 (zoom). These figures indicate that ADCP data are more scattered than the hindcast data. This was to be expected as local conditions change faster than the model input.

The hindcast model tends to underestimate extreme H_S as observed for example in Figure 4.9 at end of January 2011 with an underestimation of 1 m. This underestimation has been explained by van Nieuwkoop et al. (2013) by the limited spatial and temporal resolution of the European Centre for Medium-Range Weather Forecasts (ECMWF) hindcast, which has been used as an input for this hindcast model.

T_Z is also consistently underestimated by the hindcast model by approximately 2 s. This is also due to the input of the hindcast model, and could be improved by recalibrating the hindcast model.

T_P and D_{mean} are fairly estimated. Van Nieuwkoop et al (2013) suggested that differences in D_{mean} could be due to the way that SWAN responds to an abrupt change in wind. It can be observed that the highest values of T_P are discrete. This is because the directional wave spectrum was calculated for 128 frequencies, in regular steps of 0.0078125 Hz. Consequently, the values of measured T_P are discrete and the higher values of T_P are more spaced than the smaller ones.

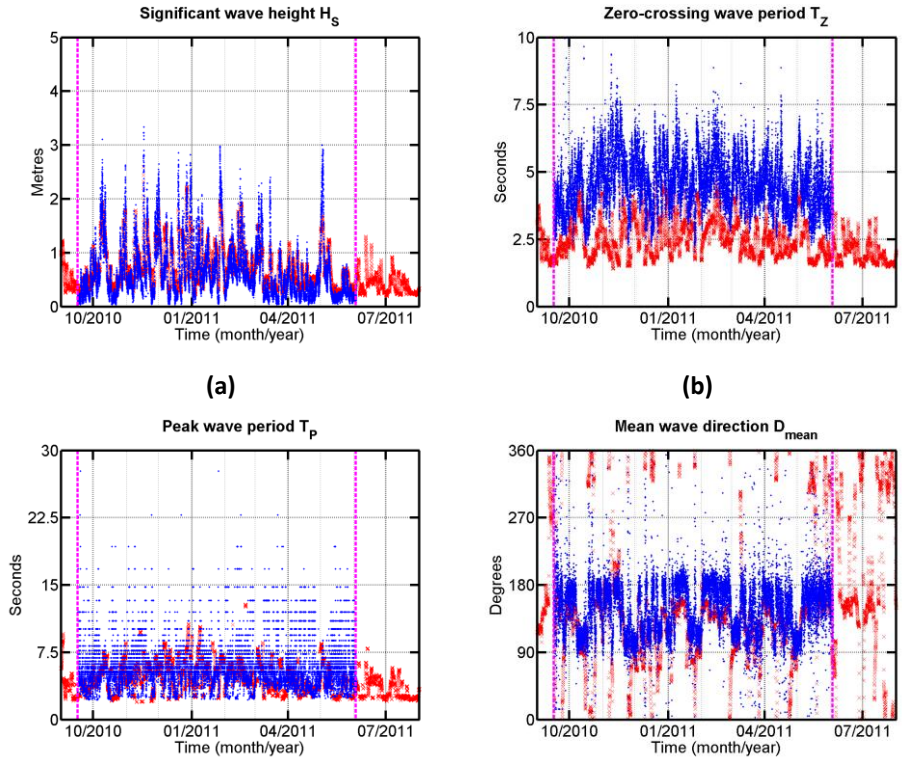

Figure 4.8: Comparison of the wave statistical data measured by the ADCP (blue dots) and calculated by the hindcast model (red crosses) during the first SWMTF deployment: a) H_S, b) T_Z, c) T_P, d) D_{mean}

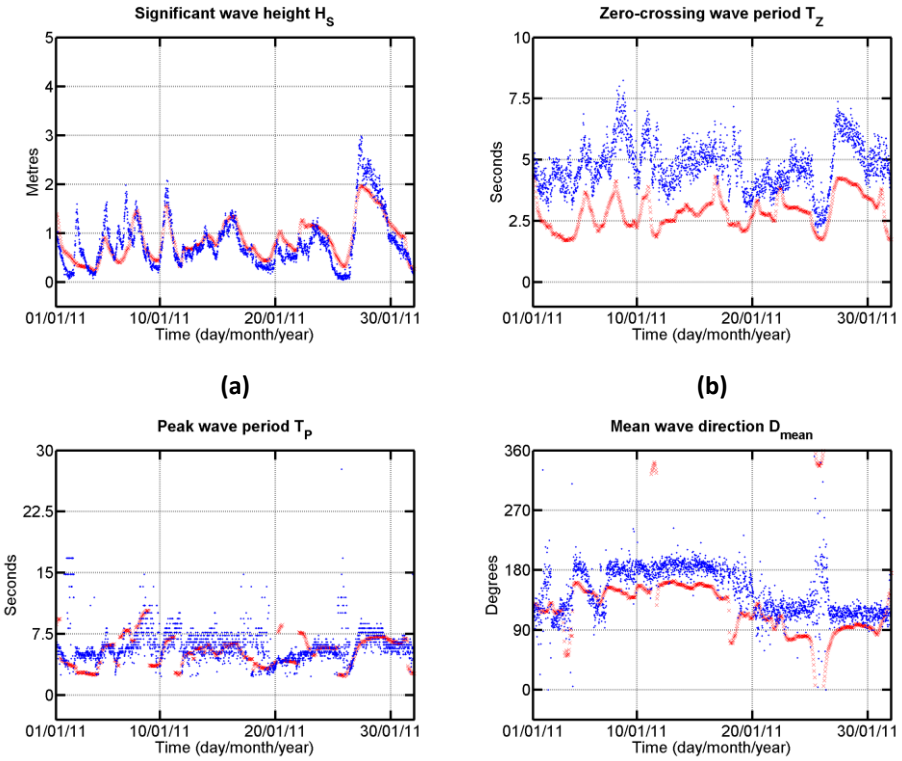

Figure 4.9: Comparison of the wave statistical data measured by the ADCP (blue dots) and calculated by the hindcast model (red crosses) during a short period (a month) of the first SWMTF deployment: a) H_S, b) T_Z, c) T_P, d) D_{mean}

Histograms (Figure 4.10) and scatter diagrams (Figure 4.11) have been used to compare the distributions of measured and hindcast wave statistical parameters. These diagrams summarise the results and identify the most frequent sea states. Results are presented for the first SWMTF deployment, when ADCP and hindcast data were available (16/09-2010-03/06/2011).

The histograms in Figure 4.10 confirm that the hindcast model estimates H_S well, but underestimates the number of occurrences of both the low (< 0.5 m) and the high values of H_S (2 m - 2.5 m). The model also overestimates the number of occurrences of the medium values of H_S (0.5 m - 1.5 m). The hindcast model underestimates T_Z by approximately 2 s. The model overestimates the number of occurrences of T_P below 6 s and underestimates it for the values over 6 s. The measured D_{mean} values are concentrated between 90 and 210° while the hindcast values are more spread.

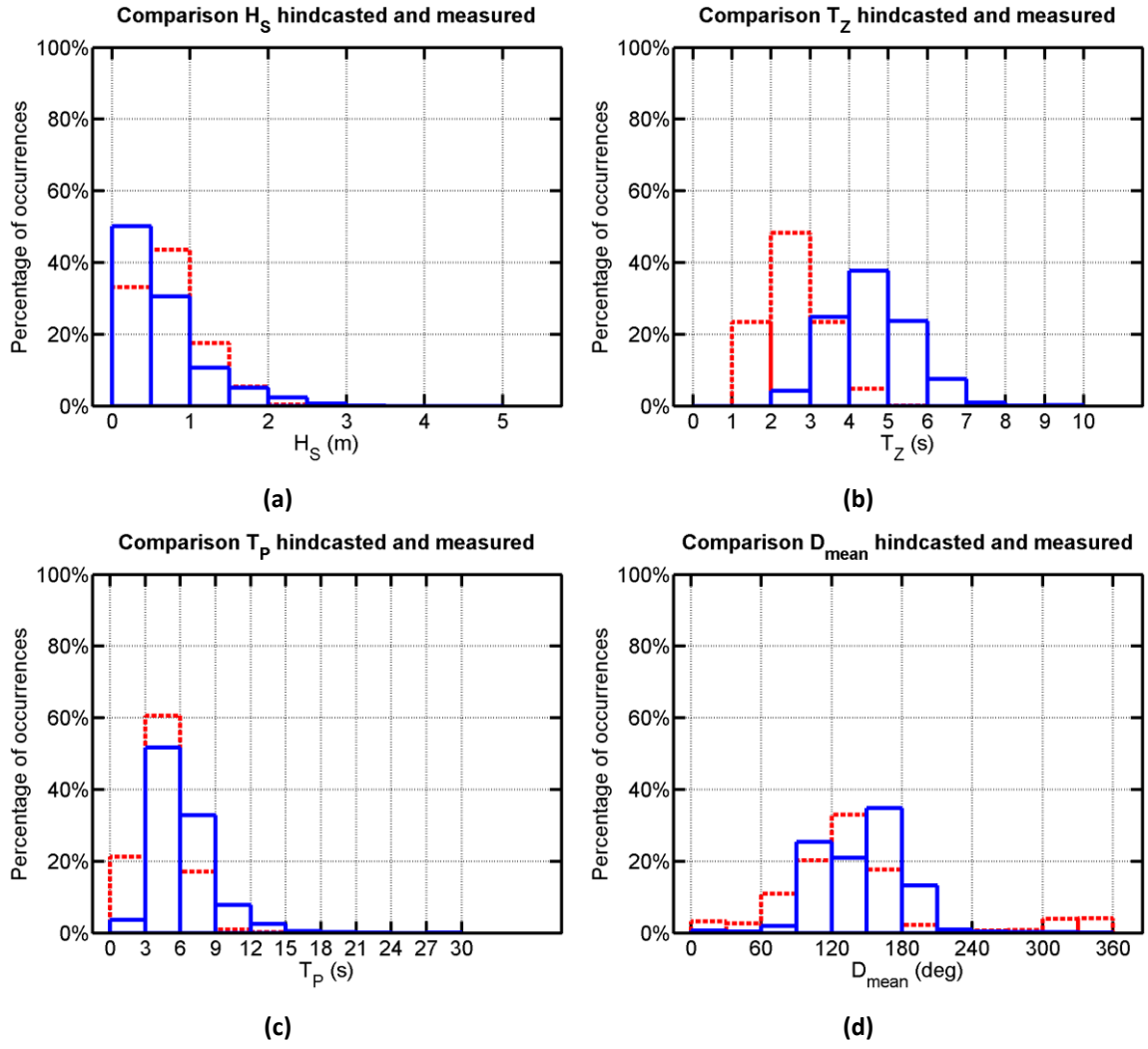

Figure 4.10: Comparison of the distribution of the wave statistical data measured by the ADCP (blue solid lines) and calculated by the hindcast model (red dotted lines) during the first SWMTF deployment: a) H_S, b) T_Z, c) T_P, d) D_{mean}

Scatter diagrams are commonly used for wave resource assessment. The H_S and T_P wave measurements from the SWMTF have been arranged in an 11x11 scatter diagram. This scatter diagram is transformed into a 13x13 scatter diagram by adding 2 initial rows and columns of zeros for interpolation purposes. Scatter diagrams count the number of occurrences of sea states in a particular range of H_S and T_P values (Eq. (4.2), Figure 4.11a). For all wave scatter diagrams presented in this document, the values of H_S between 0 and 5 m were considered, with bins of 0.5 m, and the values of T_P between 1.5 s and 16.5 s with bins of 1.5 s. H_S and T_P have been chosen for further investigations as they are the values that DNV-OS-E301 (DNV, 2013) uses for extreme waves for mooring design.

A matrix containing the joint percentage of occurrence (JPO) is calculated for each H_S and T_P pairs (Eq. (4.3) , Figure 4.11b).

$$SD(H_S,T_P)_{i,j} = \sum_{k=1}^{nb\_data} \left\langle \begin{array}{c} H_{S0} + (i-1)H_{Sbin} \le H_{Sk} < H_{S0} + iH_{Sbin} \\ and \\ T_{P0} + (j-1)T_{Pbin} \le T_{Pk} < T_{P0} + jT_{Pbin} \end{array} \right\rangle \tag{4.2}$$

$$JPO(H_S,T_P)_{i,j} = \frac{\sum_{k=1}^{nb\_data} \left\langle \begin{array}{c} H_{S0} + (i-1)H_{Sbin} \le H_{Sk} < H_{S0} + iH_{Sbin} \\ and \\ T_{P0} + (j-1)T_{Pbin} \le T_{Pk} < T_{P0} + jT_{Pbin} \end{array} \right\rangle}{nb\_data} \tag{4.3}$$

With $H_{S\,k}$ and $T_{P\,k}$ the wave conditions at a given time, $H_{S\,0}$ and $T_{P\,0}$ the minimum wave conditions considered, $H_{S\,bin}$ and $T_{P\,bin}$ the bin size

In order to get a visual representation of the joint percentage of occurrences, contour lines have been drawn (Figure 4.11c) and linear interpolation has been used to smooth the contour lines. The usage of multiple contour lines allows the separation of environmental conditions by percentage of occurrences.

The joint percentage of occurrences and the contour lines should not be confused with the conventional joint probability distributions and associated contour lines. The JPO only summarises measured data and is not used for predictions or probability. The contour lines used in this thesis indicate points with the same observed percentage of occurrences during a measurement.

For the first deployment, scatter plots of the measured data (Figure 4.12a) and of the hindcast data (Figure 4.12b) are plotted for comparison. For example, Figure 4.12a indicates that the measured sea states were occurring more than 7.5% of the time with H_S between 0.5 and 1 m and T_P between 4.5 and 6 s, and less than 1.5% of the time with H_S over 2.5 m. Some values were recorded over the average steepness values, for low values of H_S and T_P. These points may be erroneous values because measurements are more difficult in waves with a small wave height, or may be due to the definition of the average steepness value, which is an average value, which means it is possible to have values above this line.

The comparison of Figure 4.12a and Figure 4.12b confirms that the hindcast and the measured H_S and T_P are close. This gives confidence in the measured data.

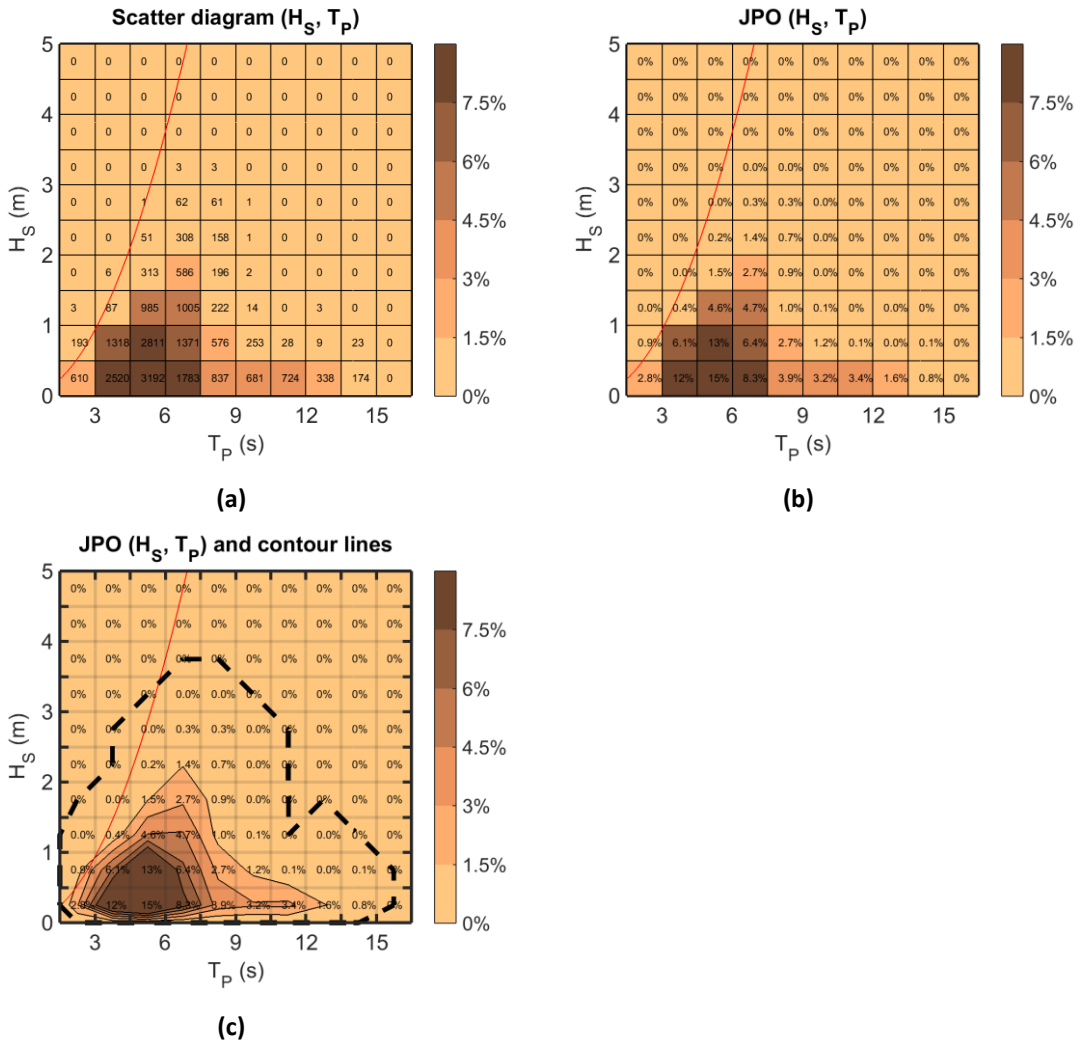

Figure 4.11: Scatter diagram: from number of occurrences to a graphic representation using contour lines. The red line shows the average wave steepness limit. Example of the first SWMTF deployment. a) Scatter diagram counting the number of occurrences of each sea state in a given range of H_S and T_P, b) Scatter diagram counting the percentage of occurrences of each state, c) graphic representation using linear interpolation of the percentage of occurrence of each sea state. Black dotted line: external contour line, no occurrences were recorded outside this line

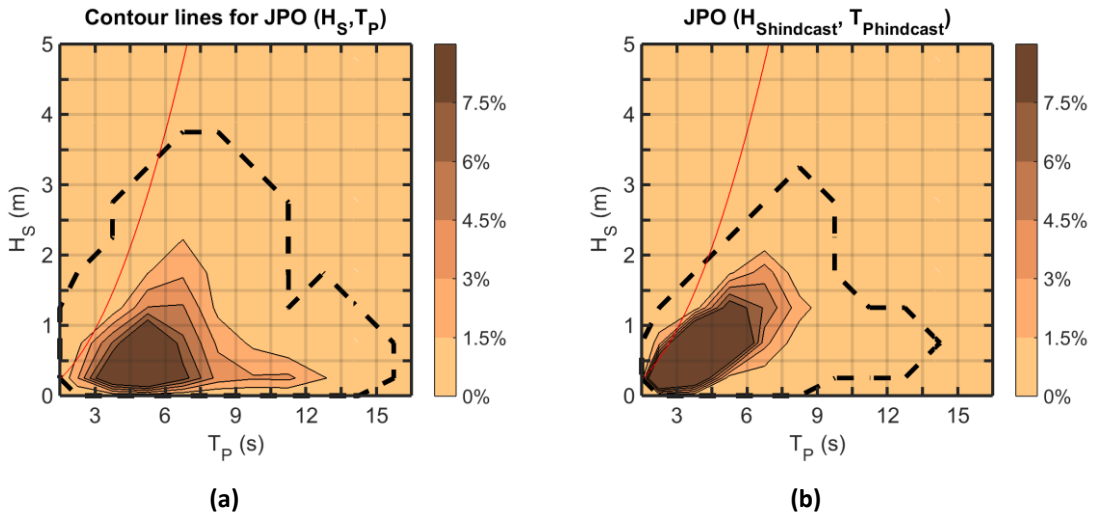

Figure 4.12: Measured and hindcast scatter plots a) of (H_S, T_P) measured by the ADCP and b) of ($H_{S\ hindcast}$, $T_{P\ hindcast}$) calculated by the hindcast model during the first SWMTF deployment. Black dotted line: external contour line, no occurrences were recorded outside this line. The red line shows the average wave steepness limit.

A scatter plot using the whole 23 years of hindcast data (Figure 4.13a) has been used to determine if the sea states during the first SWMTF deployment were exceptional or average compared to other years. This scatter plot is compared with the scatter plot for the hindcast data during the first SWMTF deployment (Figure 4.12b). The sea states occurring more than 3% of the time are associated with lower H_S and T_P for the 23 years hindcast data (Figure 4.13a) than for the first SWMTF deployment hindcast data (Figure 4.12b). This may be due to seasonal variations, because the data have been recorded during the winter, when the sea states are usually more energetic.

In order to remove the seasonal variations, a scatter plot shows the hindcast data from the 16th of September to 3rd of June from 1989 to 2012 (Figure 4.13b). This plot is compared with the hindcast scatter plot for the hindcast data during the first deployment (Figure 4.12b). The comparison indicates that the sea states during the first deployment were not exceptional but representative of the site average sea states at this time of year.

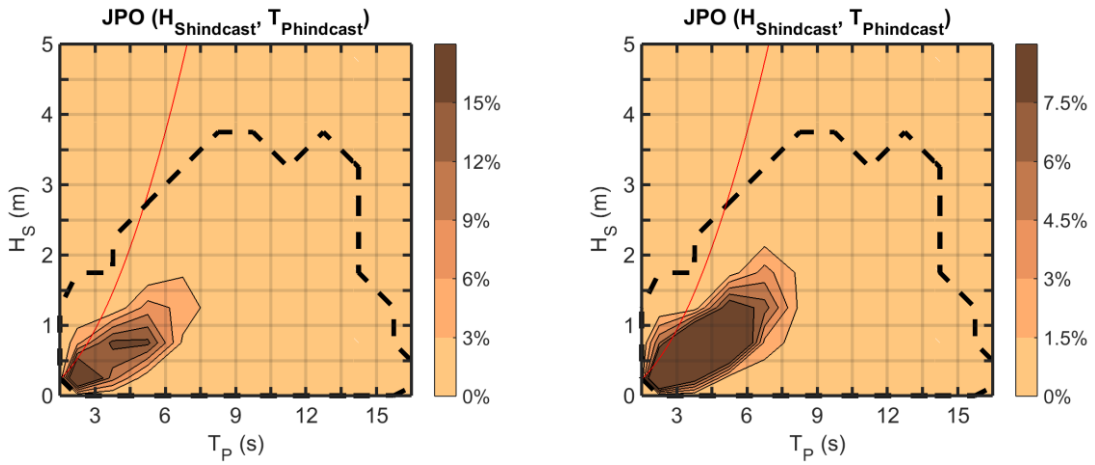

(a) **(b)**

Figure 4.13: Scatter plots a) for the 23 years of the wave hindcast, b) for the winters of the 23 years of the wave hindcast (16th of September to 3rd of June, every year from 1989 to 2012) at the SWMTF location. Black dotted line: external contour line, no occurrences were recorded outside this line. The red line shows the average wave steepness limit.

Validation of the load data

The mooring load data measured by the tri-axial loadcells on the mooring line axis have been compared with the data measured by the inline loadcells.

The mean (Figure 4.13) and maximum (Figure 4.15) loads have been compared. Measurements were in the same order of magnitude. The mean loads measured by the tri-axial loadcells are lower on line 1 and higher on line 2 and 3 compared to the loads measured by the inline loadcells. The maximum loads are lower on all mooring lines with the tri-axial measurements than with the inline measurements.

Differences between the measurements can be explained by the fact that: a) only the axial load is considered for the tri-axial loadcells. The root square of the sum of the load on the x, y and z axes should have been calculated to compare the data, but the values on the other axes were drifting or offset as shown for example in Figure 4.16. This trend was observed in most of the tri-axial loadcells for the x and z directions; b) there may be differences due to the calibration of the axial and tri-axial loadcells.

The comparison between the axial and tri-axial loadcells (Figure 4.13) gives confidence in the results from the axial loadcells. However, the data from the tri-axial loadcells do not allow a complete validation of the axial mean load values: a small offset in the magnitude of mean load data may have been possible but the order of magnitude has been confirmed by the numerical model.

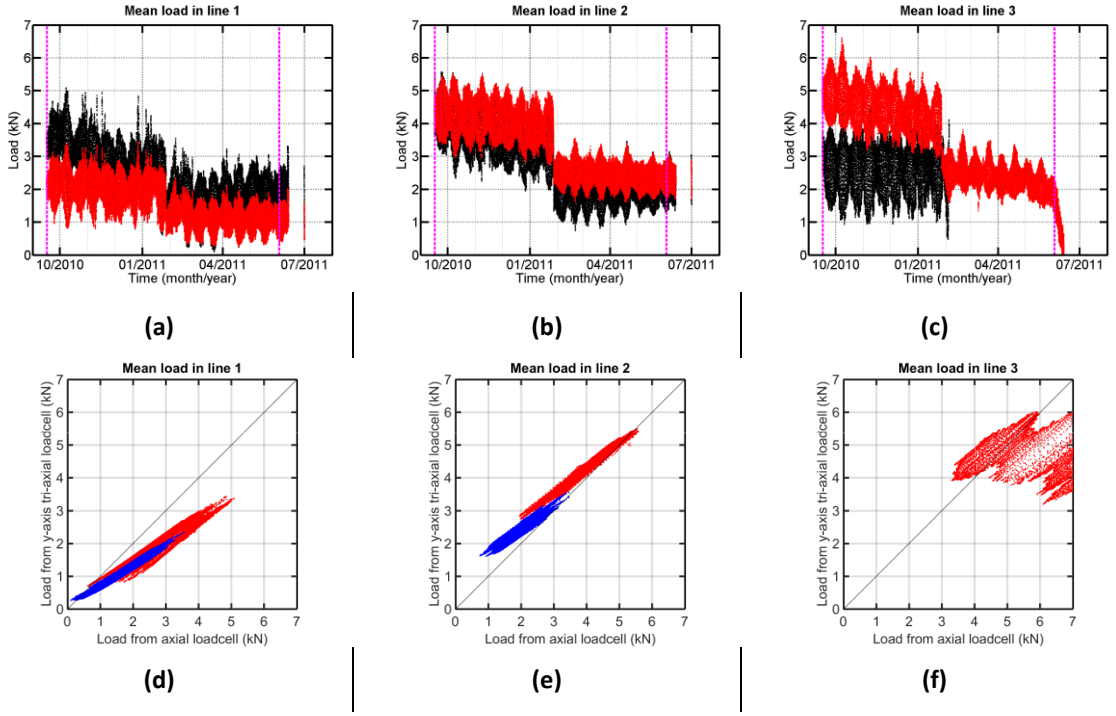

Figure 4.14: (a-c) Comparison of the variations over time of the SWMTF mean loads measured by the inline loadcells after correction (black dots) and measured by the tri-axial loadcells (red dots) on their y axis (along the mooring line), (d-f) measured before (red dots) and after (blue dots) anchor drag. From left to right: loadcells 1 to 3

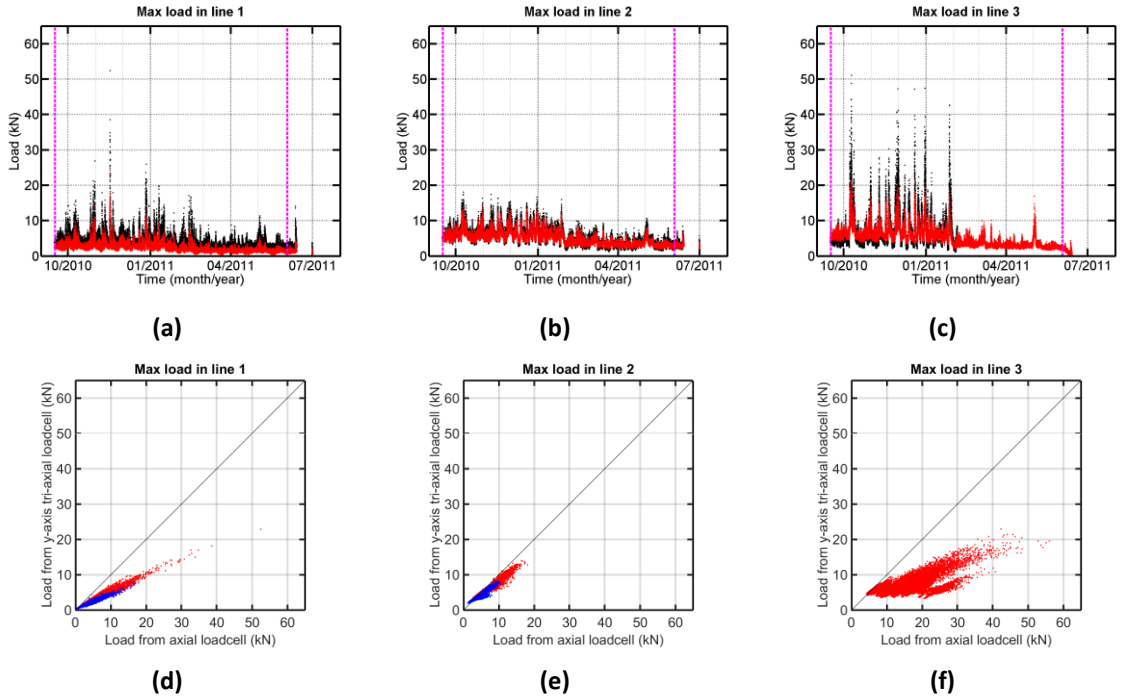

Figure 4.15: Comparison of the SWMTF maximum loads (a-c) measured by the inline loadcells after correction (black dots) and by the tri-axial loadcells (red dots) on their y axis (along the mooring line), (d-f) measured before (red dots) and after (blue dots) anchor drag. From left to right: loadcells 1 to 3

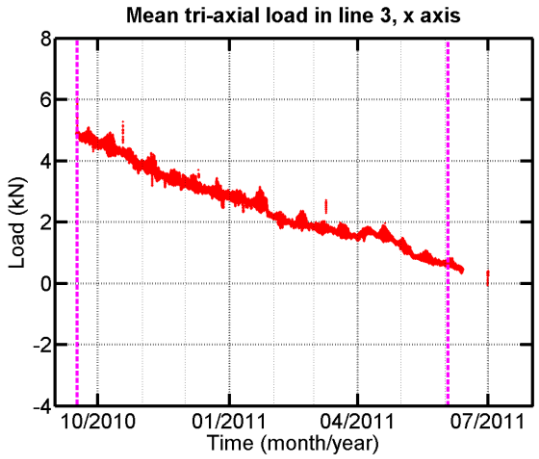

Figure 4.16: Example of measurement of mean load on the x axis of tri-axial loadcell 3 at SWMTF

Validation of the motion data

Figure 4.17 shows the summary of the GPS data for the first SWMTF deployment. A non-physical jump was observed in the longitude and latitude dataset at the end of March 2011 (4.10^5 and 6.10^6 m respectively). This erroneous motion has been identified as the result of the incorrect processing of the statistical GPS data. The error originates from the conversion of latitude and longitude to meters and requires the reprocessing of all motion data.

The height plot also shows that data are missing in February 2011 and from end of April 2011. A jump (~15 m) in the longitude and latitude data is observed at the beginning of October 2010 and in March 2011. The first jump cannot be explained based on a physical phenomenon, while the second jump may be due to an observed anchor drag.

The quality of the available GPS data limits any further investigations. Consequently, the motion data provide insufficient information that would allow the implementation of a detailed analysis on the correlation between response characteristics and mooring line tensions. Motion data from the GPS system are only applied for qualitative observations of time series within this study and not for any quantitative analysis.

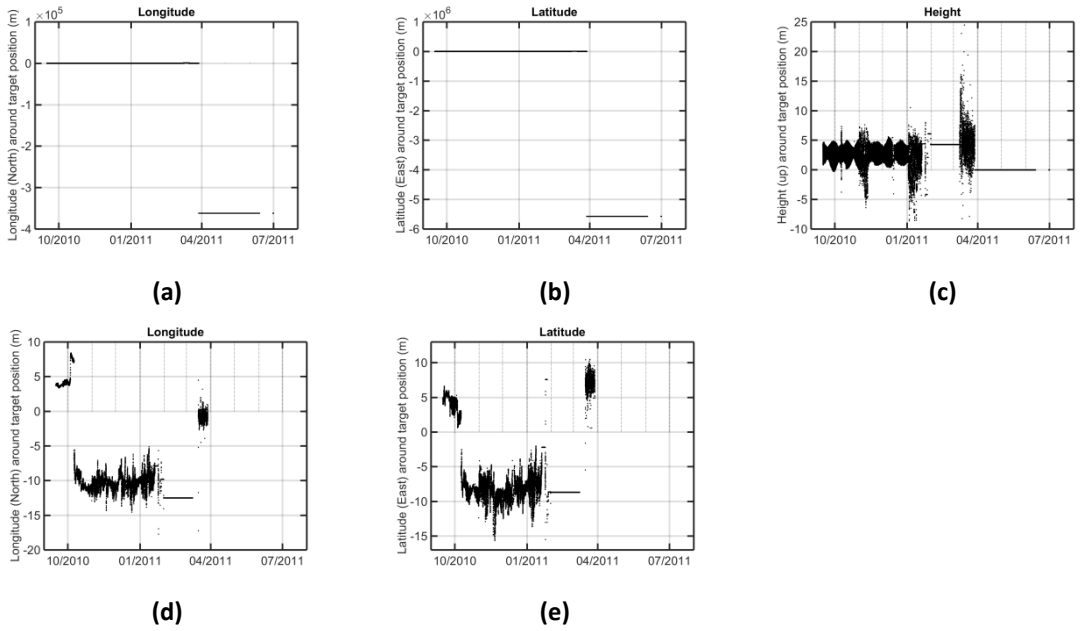

Figure 4.17: Mean GPS motion for the first SWMTF deployment as stored in the MySQL database and usable for further research: a) longitude motion and d) zoom; b) latitude motion and e) zoom, c) height motion

4.1.2 Example of time series of data

An example of time series of data is shown in this section. This example aimed to indicate the dynamics of the system and the quality of the original data (e.g. if there is a lot of noise in the data).

Data are shown for a 10 minute dataset (Figure 4.18a for the ADCP data, Figure 4.19a-c for the inline loadcell data, Figure 4.20a-c and Figure 4.19 for the GPS data, Figure 4.22a-f for the accelerometer and gyroscope data).
The dataset chosen for this example was recorded the 17/11/2010 between 02:00 and 02:10, during a storm. This sea state was chosen because its shows the dynamic behaviour of the mooring system under rough sea conditions. It was also chosen because it was recorded at the beginning of the deployment, when the instrumentation was still working well (in particular the loadcells).

The surface elevation (Figure 4.18a, range to surface from Surface track) was shown as measured by the acoustic beam 3, without correcting the tilt of the ADCP. Beam 3 was chosen because it was the closest to the SWMTF instrumented buoy. This plot shows wave with a zero-crossing period around 7 s.

The data on mooring line 3 (Figure 4.19c) were shown as recorded, and no correction was applied on the mean load but the loadcell already started drifting.
The position is the position at the GPS, and not the position of the centre of buoyancy or gravity of the buoy (Figure 4.20a-c and Figure 4.19). Similarly, the accelerations and rotational velocities are given at the position of the MotionPak sensor (Figure 4.22a-f). These data would need to be mathematically integrated and translated to obtain the position of the centre of gravity or buoyancy of the buoy at a given time. It would also be interesting to observe the motion at the mooring line attachment point.

The instrumented buoy data were not exactly starting at 02:00 (Figure 4.19). The instrumented buoy recording time was accurate because given by the GPS, synchronised with satellites. The time of acquisition slowly drifted, but was accurately known. This was not the case for the ADCP clock, which was manually synchronised with the GPS clock during deployment, but only relied on its internal clock during deployment.
The 10 minute graphs are difficult to read because of the high number of data and a visual inspection of these graphs only indicates the approximate mean, minimum, maximum and standard deviation values.
Zooms on 1 minute (Figure 4.18b for the waves, Figure 4.19d-f for the mooring loads, Figure 4.20d-f for the buoy motion, Figure 4.22g-l for the linear accelerations and rotational velocities) show more clearly the dynamic mooring behaviour when a peak load occurred.
These zoom pictures indicate that the quality of the data seems satisfactory, because a) the acquisition frequency is significantly higher than the observed phenomenon, b) the resolution of the instruments is small enough to avoid jumps or steps in the data and c) there is no noise.

As explained previously, ADCP data may be not well synchronised with the instrumented SWMTF buoy data which may explain why no large waves were observed in the zoom on the wave data (Figure 4.18b). Also, the wave data are given as measured by beam 3, at a position different from the SWMTF buoy.
The distance between the ADCP target position and the buoy target position was 25 m. For a wave period of 5 s and for regular waves, using the deep water theory, the wave

phase velocity is equal to $\frac{gT}{2\pi} = \frac{9.81 m.s^{-2} \times 5s}{2\pi} = 7.8\, m.s^{-1}$, and the peaks and troughs take approximately 3.2 s to be at the buoy target position, and the wave groups take 6.4 s to be at the buoy target position. For a wave period of 25 s, the peak and troughs take 0.6 s to be at the buoy target position, and the wave groups 1.2 s.

The elevation measured by beam 4 is also shown in Figure 4.18c. Beam 3 and 4 are opposed, the angle between the beams and the vertical is 20° and the water depth for this example was approximately 32 m, which means that the distance between the two points near the surface observed by beam 3 and 4 is equal to 2 x 32 m x tan 20° ≈ 23 m.

The comparison between the surface elevation measured by beam 3 (Figure 4.18b) and beam 4 (Figure 4.18c) shows that the wave shape significantly changed.

A short and large mooring load was observed in loadcell 1 with an amplitude over 50 kN, and four smaller peaky loads (> 10 kN) were observed before the large peak (Figure 4.19d). During the same period of time, the mooring loads stayed low in loadcell 2, below 15 kN (Figure 4.19e), and were moderate in loadcell 3 (Figure 4.19f), up to 25 kN.

Simultaneously, the instrumented buoy had a large motion to the North, of approximately 6 m amplitude (Figure 4.20e) and upward, of approximately 4.5 m amplitude (Figure 4.20f), immediately followed by a motion to the South, of approximately 6 m amplitude and down, of approximately 6 m amplitude. This can also be shown in the 3D plot in Figure 4.21.

These motions can be related to the RAOs of the moored system which are presented in Figure 6.13 (model scale). For a wave period of 7 s (full scale), which corresponds to a model scale frequency of $5^{0.5}/7$ = 0.3 Hz, the RAOs indicate that the buoy follows the waves with RAOs close to 1 in surge and heave and 0 in pitch. The surge and heave motion observed in Figure 4.20 are in the same order of magnitude than the surface elevation (Figure 4.18) which indicates that the large motions were likely to be due to a large wave.

Assuming that the buoy follows the wave, the largest heave motion (Figure 4.20c and f), with an amplitude of aproximately 6 m, indicates that the maximum wave steepness was equal to $\frac{buoy\_heave\_motion\_amplitude}{\lambda} = \frac{6m}{g(7s)^2/2\pi} = 0.08$

This means that the high mooring load and large motions were due to a steep but not exceptionally steep wave. However, it should also be considered that the heave motion may be lower than the wave height, and that the wave steepness was actually higher in this case and closer to the breaking limit.

The large mooring load was also preceded by a large positive surge acceleration, followed by a large negative surge acceleration (Figure 4.22g). The pitch velocity was highly varying after the peaky load (Figure 4.22k).

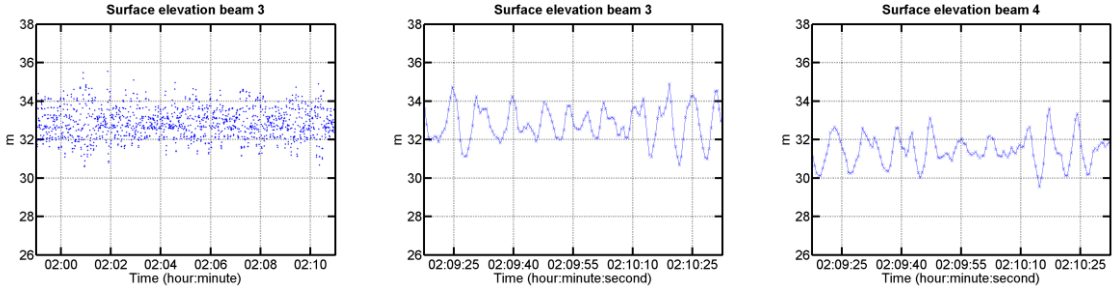

Figure 4.18: Example of times series of wave elevation measured the 17/11/2010 between 02:00 and 02:10 at beam 3 of the ADCP for the SWMTF a) during 10 minutes and b) zoom on 1 minute, c) zoom on 1 minute at beam 4

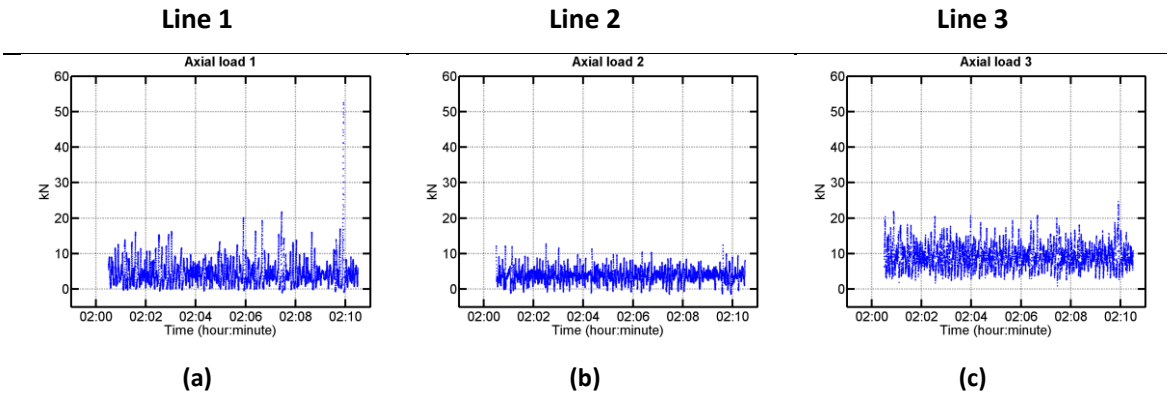

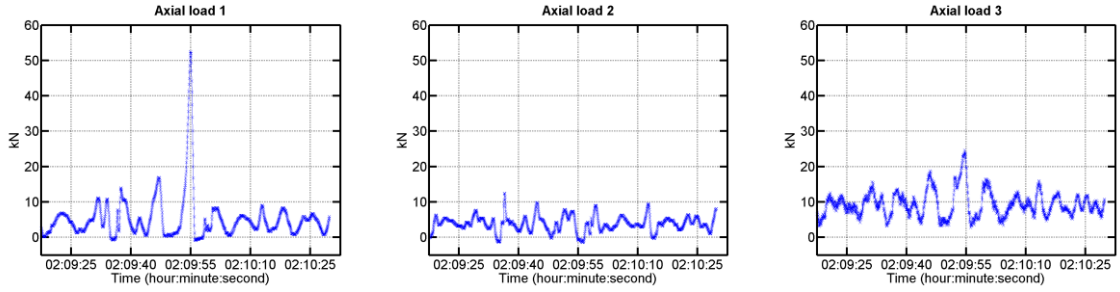

(d) **(e)** **(f)**

Figure 4.19: Example of time series of mooring loads measured the 17/11/2010 between 02:00 and 02:10 by the three SWMTF axial loadcells; (a-c) whole 10 minute time series, (d-f) zoom on 1 minute

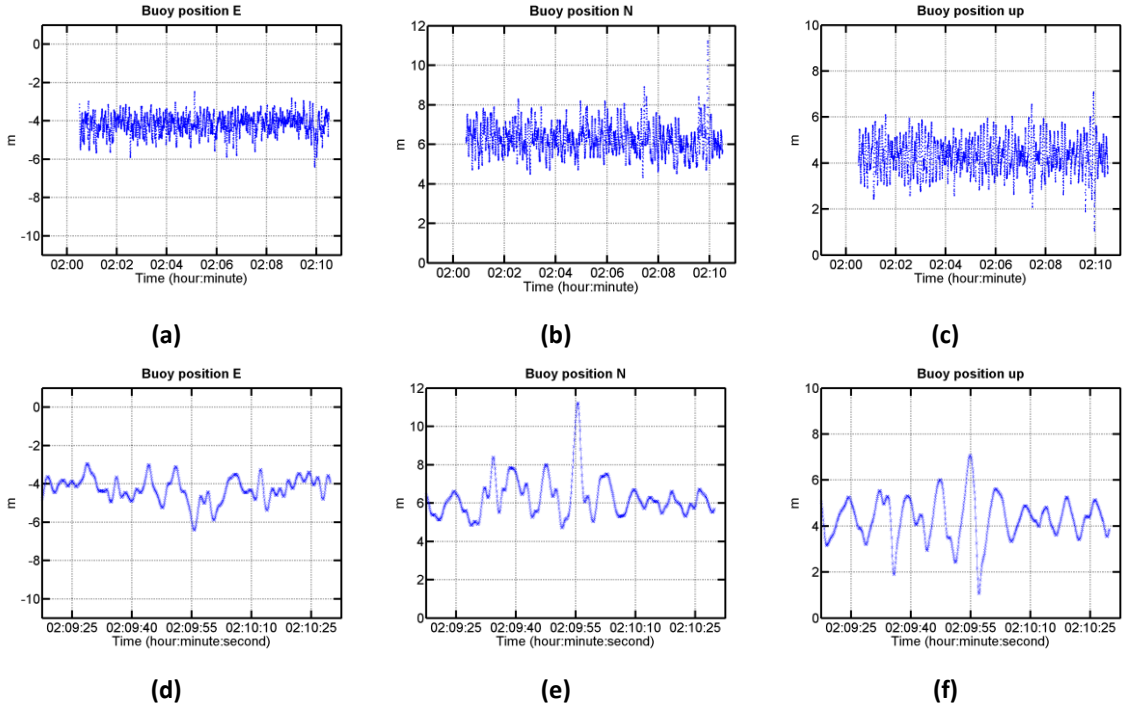

Figure 4.20: Example of SWMTF buoy motion in the three translation DOF measured the 17/11/2010 between 02:00 and 02:10; (a-c) whole 10 minute time series, (d-f) zoom on 1 minute, E: East, N: North

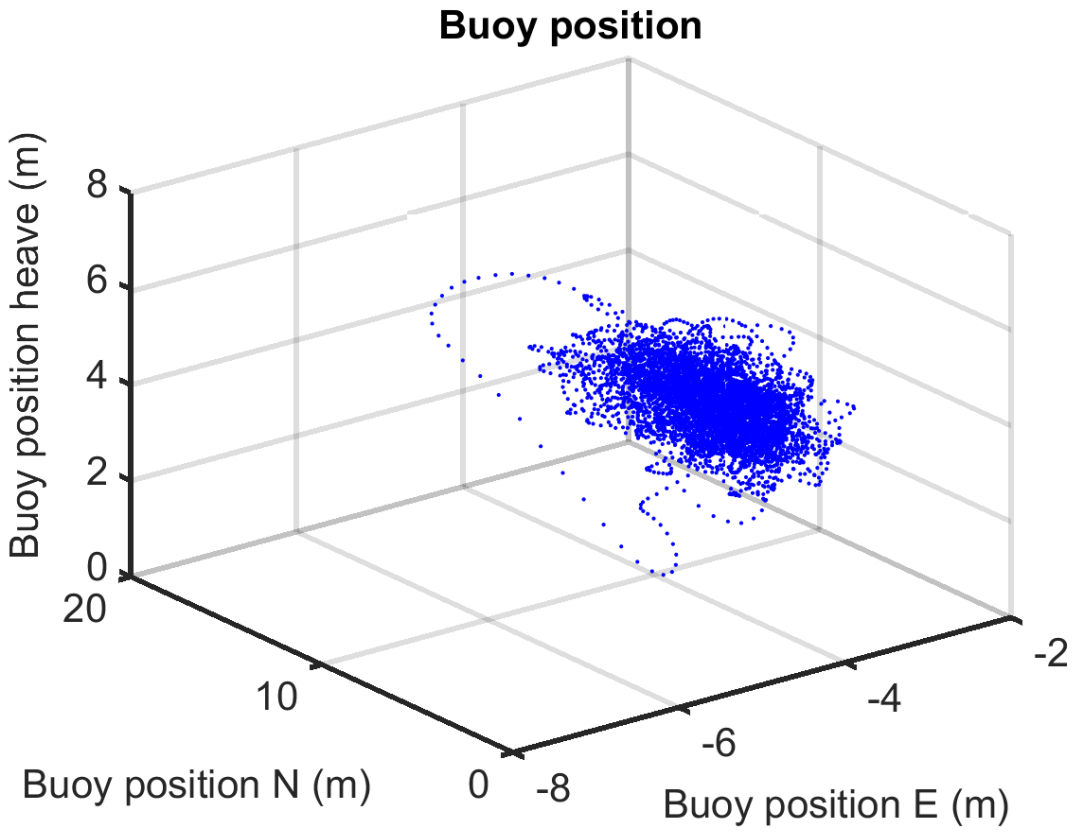

Figure 4.21: Example of SWMTF buoy motion in the 3 DOF in translation during 10 minutes on the 17/11/2010 between 02:00 and 02:10

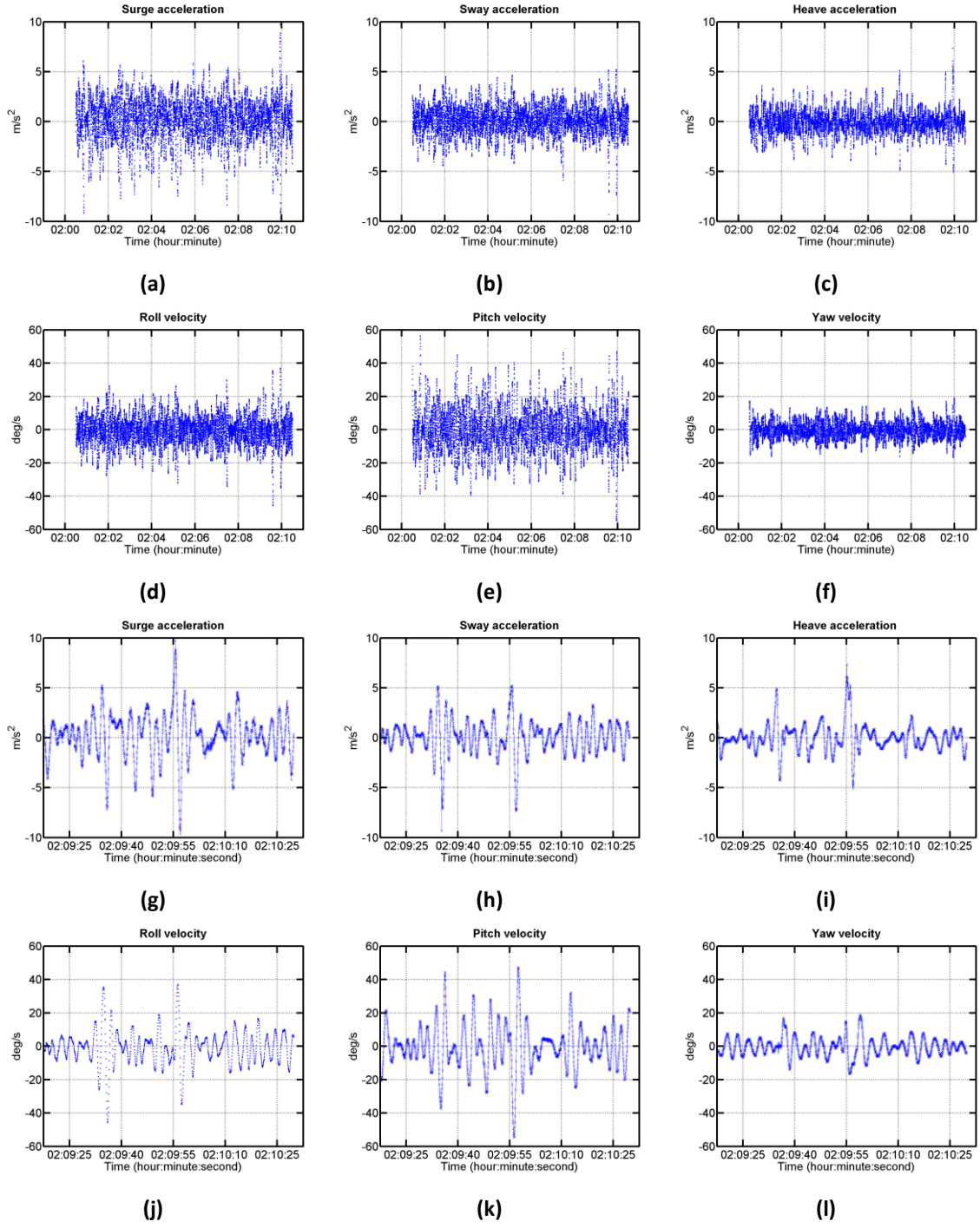

Figure 4.22: Example of measurements of the SWMTF buoy linear accelerations (a-c) and angular velocities (d-f) during 10 minutes and zoom on 1 minute (accelerations: g-i, velocities: j-l), the 17/11/2010 between 02:00 and 02:10

4.1.3 Example of summary data

In this section, the environmental and mooring load data summaries are presented in order to assess the environmental conditions at the test site, and to evaluate the range of mooring loads. Summary data are the data which have been used for further analysis in this thesis. The next step, developed in the next chapter, will be to detect peak mooring loads and analyse the associated environmental conditions.

The mean, maximum, standard deviation and standard score of the maximum of the mooring loads have been calculated for each 10 minute dataset.

The mean, maximum and standard deviation are parameters which are commonly used for statistical analysis. The mean load gives an indication of the mooring pre-tension (but overestimate the pre-tension because mean environmental loads and dynamic loads are included in the mean load), the maximum load of the amplitude of the highest dynamic load, the standard deviation of the spreading of the mooring loads. The standard score of the maximum load has been additionally introduced in order to detect datasets containing dynamic mooring loads with a large amplitude per units of standard deviations.

The standard score of the maximum (4.4) is defined as the difference between the maximum and the mean per unit standard deviation and allows the comparison of i) the dynamic part of the load (the amplitude of the maximum mooring load minus the mean mooring load), and ii) of the spreading of the mooring loads in the selected dataset.

$$S_{\max}(x) = \frac{\max(x) - mean(x)}{std(x)} \tag{4.4}$$

x is the dataset of mooring load and S_{max} the standard score of the maximum

S_{max} assesses the non-linearity of mooring loads. If the mooring loads were following a Gaussian distribution, 99.865% of the S_{max} values would be below 3, or in other words, S_{max} values over 3 would occur in 1/741 files, which is every 741 x 10 minutes = 5.1 days. Using the normcdf function in Matlab, return period has been estimated following Eq. (4.5) for a range of values of S_{max} in Table 4.6. Results indicate that values over 5.5 are unlikely (return period over 1,000 years) if the mooring load distribution is Gaussian.

$$return\ period = \frac{10\ minutes}{60minutes \times 24h \times (1 - normcdf(value\ of\ S_{max})} \quad (4.5)$$

Table 4.6: Return period of high values of S_{max} if the load distribution was Gaussian

Value of S_{max}	Return period for a Gaussian distribution
3	5 days
4	219 days
5	2,423 days = 6.6 years
5.5	1,002 years
6	19,285 years
7	14,865,532 years

The days shown in this section were chosen in October or November 2010 to limit the discrepancies due to instrumentation or changes in the mooring system. The data used in these sections are data after corrections. Two storms (Southerly and Easterly), an average day (based on the scatter diagram), and a calm day are shown below.
Table 4.7 summarises the choice of the datasets used in this section.

Table 4.7: Selection of sea states representative of the wave conditions for SWMTF

Wave conditions	Selection
Easterly storm	Highest mooring load on line 3
Southerly storm	Highest mooring load on line 1
Average day	H_S < 1 m and 3 s < T_P < 7.5 s
Calm day	H_S < 0.1 m

The values for the surface elevation are taken for beam 3 which is the closest to the SWMTF instrumented buoy, and the averaged elevation value has been removed because the ADCP may have been slightly tilted and the surface elevation data were not corrected for tilt.
Table 4.8a indicates that in the case of a Southerly storm, moorings loads are high (> 50 kN) on mooring line 1 (facing the waves) and the instrumented buoy is significantly moving in the North direction.

In the case of an Easterly storm (Table 4.8b), the highest mooring loads are observed on mooring line 3 (> 50 kN) and the instrumented buoy is significantly moving to the West.

In both cases negative mooring loads have been recorded. They may be the results of an incorrect calibration of the loadcells or of the mooring line becoming slack and being compressed, its bending stiffness not allowing the line to buckle out instantaneously. Standard deviation (up to 5) and standard scores (up to 12.15) of mooring loads are high for the mooring lines facing the waves.

For a moderate swell (Table 4.8c), mooring loads stay below 8 kN. The instrumented buoy motion amplitude is reduced and stays below 1 m. The standard deviations of mooring loads do not exceed 0.51 kN and their standard score of the maximum 5.48.

The same trend is observed for the calm day (Table 4.8d). The minimum wave elevation is an incorrect point likely to be due to noise.

The high values of S_{max} indicate that the load distribution is non-Gaussian. This could be due to the mooring line non-linear behaviour or to the loading non-linearity.

The mooring line non-linear behaviours have already being discussed in 2.1.2.2 and can be: geometric non-linearity, non-linear stretching of synthetic ropes, non-linear seabed friction or non-linear viscous damping of the mooring line. Section 7.2.4 discusses which mooring line behaviour is likely to be dominant.

Considering waves as the main cause of loading, the loading non-linearity can in this case be slamming, green water, impact loads or rogue waves. The example showed in 4.1.2 presents a case with a large S_{max} but without an exceptionally large wave, so rogue waves can be dismissed. Slamming, green water and impact loads require further investigations in order to assess their contribution to the non-linearity of mooring loads.

Table 4.8: Example of summary wave elevation, mooring load, and buoy motion data for different representative sea states for SWMTF

a) Stormy day: Southerly storm			**17/11/2010**			**02:00-02:10**	
h (m)	31.91	H_S (m)	2.62	D_P (°)	174	T_P (s)	7.7
			Min	Mean	Max	Std	S_{max}
Elevation 3 (m)			-2.27	0.00	2.69	0.78	3.43
Load 1 (kN)			-1.01	4.75	52.48	3.93	12.15
Load 2 (kN)			-1.42	3.89	12.81	2.04	4.39
Load 3 (kN)			-4.73	3.62	19.04	3.33	4.63
Buoy E (m)			-6.41	-4.19	-2.47	0.53	3.27
Buoy N (m)			4.33	6.26	11.22	0.76	6.54
Buoy up (m)			1.05	4.34	7.09	0.74	3.70

b) Stormy day: Easterly storm			**09/10/2010**			**09:30-09:40**	
h (m)	30.24	H_S (m)	2.48	D_P (°)	97	T_P (s)	6.5
			Min	Mean	Max	Std	S_{max}
Elevation 3 (m)			-2.25	0.00	2.11	0.66	3.19
Load 1 (kN)			0.08	2.38	8.03	0.85	6.64
Load 2 (kN)			-1.06	4.41	15.74	2.13	5.32
Load 3 (kN)			-4.26	3.65	51.12	5.00	9.50
Buoy E (m)			-9.29	-4.50	-2.57	0.83	2.33
Buoy N (m)			1.03	2.85	4.65	0.49	3.67
Buoy up (m)			0.54	2.54	4.35	0.59	3.07

c) Average day: Southerly swell			**02/10/2010**			**01:10-01:20**	
h (m)	30.67	H_S (m)	0.55	D_P (°)	193	T_P (s)	5.43
			Min	Mean	Max	Std	S_{max}
Elevation 3 (m)			-0.63	0.00	0.43	0.19	2.31
Load 1 (kN)			2.35	3.60	5.27	0.31	5.48
Load 2 (kN)			2.24	4.23	6.26	0.46	4.45
Load 3 (kN)			2.94	5.21	7.35	0.51	4.22
Buoy E (m)			-3.83	-3.46	-3.16	0.10	2.96
Buoy N (m)			4.51	4.94	5.40	0.15	3.09
Buoy up (m)			2.46	2.95	3.51	0.16	3.53

d) Calm day: virtually no waves			**22/10/2010**			**13:40-13:50**	
h (m)	29.70	H_S (m)	0.04	D_P (°)	103	T_P (s)	12
			Min	Mean	Max	Std	S_{max}
Elevation 3 (m)			~~-7.25~~	0.00	0.49	0.35	1.39
Load 1 (kN)			2.43	3.40	4.42	0.24	4.35
Load 2 (kN)			2.24	3.98	5.45	0.38	3.91
Load 3 (kN)			1.20	2.69	4.51	0.41	4.45
Buoy E (m)			-3.91	-3.67	-3.46	0.07	3.09
Buoy N (m)			4.60	4.94	5.49	0.12	4.44
Buoy up (m)			2.61	3.06	3.41	0.10	3.45

4.1.4 Data summary

This section presents the summaries of the measured environmental and mooring load data. The original and corrected data through time are presented, highlighting the available data for further analyses. The environmental data (based on 17 or 20 minute dataset) are interpolated to match each mooring load dataset (taken every 10 minutes). Figure 4.23 shows an example of linear interpolation of the wave data. This method is acceptable because of the 3- hour stationarity of sea states.

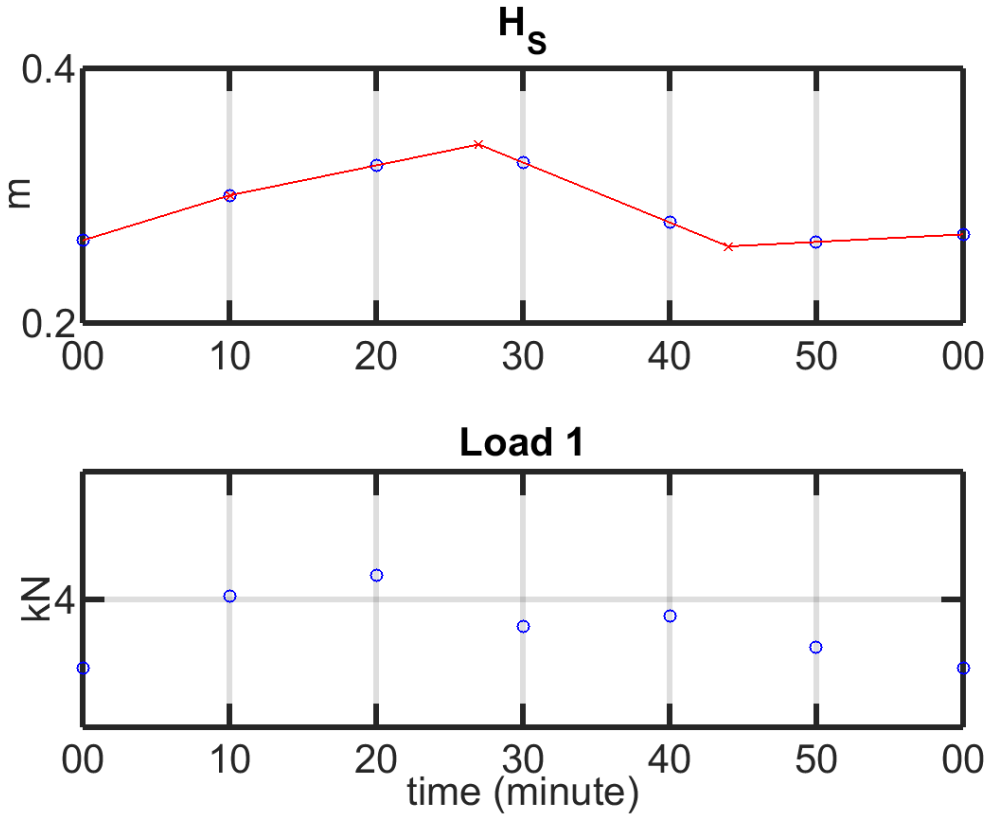

Figure 4.23: Interpolation of the wave data; top: original (red crosses) and linearly interpolated (blue circle) Hs data; bottom: example of original load data which provide the time for interpolation

The interpolated environmental data and mooring load data are plotted through time and their distributions are output to identify a) any frequent amplitude of environmental conditions or mooring loads, b) the variations in amplitude. The plots also aim to compare the environmental conditions and mooring loads during the different periods of deployments.

The data for the SWMTF have been separated in different periods of analysis corresponding to different mooring configurations (Table 4.9).

Table 4.9: Periods used for further analysis of the SWMTF data

First deployment		**Second deployment**
Before anchor drag	After anchor drag	New mooring line
16/09/2010-27/01/2011	27/01/2011-03/06/2011	06/11/2012-20/01/2013
133 days	127 days	75 days

4.1.4.1 Environment

Wave

A summary of the statistical wave data measured during the two first SWMTF deployments is plotted in Figure 4.24. These statistical data were extracted of a 1,024 s dataset. The variations of the H_S and H_{max} parameters indicate the storms and calm periods (Figure 4.24a-d). The wave periods T_Z and T_P stayed in a narrow range (Figure 4.24e-h), mostly between 2.5 and 7.5 s. Two clear wave directions can be identified (Figure 4.24i-l): South and East (origin of the waves). Waves coming from the South seem to be more frequent but the number of occurrences needs to be counted.

Table 4.10 summarises the number of available points (before interpolation) and equivalent duration of the periods of analysis, the number of storms with H_S over 3 m, the minimum, mean, maximum and standard deviation values measured for H_S, H_{max}, T_Z and T_P, and the number of bins populated in the scatter diagram. The length of wave data gathered after the anchor drag is similar to the length of data gathered before. The length of wave data gathered during the second SWMTF deployment is approximately half of the length of the data gathered during the first SWMTF deployment before the anchor drag or after the anchor drag.

The maximum H_S and H_{max} are in the same order of magnitude for the different deployments.

The statistical wave data – calculated every 17 or 20 minutes using 1,024 s datasets (so containing approximately 230 to 270 waves according to the mean wave period at this site)- are interpolated to provide environmental data for each mooring load dataset – recorded every 10 minutes. If wave data were unavailable for more than 3 hours, for example during the redeployment of the ADCP, then the interpolated data were removed for this period of time. A summary of the interpolated wave data is available

in Table 4.11. This table indicates that the interpolated data are similar to the measured data, meaning that most of the measured data are used and only a few measured data are missing for interpolation. Interpolated wave data are the data which are used for further investigations.

The number of occurrences of H_S, T_P and D_P during each period of analysis is shown in Figure 4.25a-i. The aim of these figures is to assess the number of storms, moderate swell and calm periods and their direction relatively to the mooring line directions. Figure 4.25a-c indicates that the number of occurrences of low values of H_S (< 0.5 m) is higher during the first SWMTF deployment after the anchor drag than before. The number of occurrences of sea states with H_S between 1 and 2 s is similar for all period of analysis. In all cases, the number of occurrences of H_S over 2 m is small and most of the T_P are between 3 and 9 s. The number of occurrences of D_P (Figure 4.25d-f) has been summarised with rose plots. These rose plots are showing the number of occurrences of sea states with a given direction. The waves are almost equally coming from the South and from the East during the first deployment before anchor drag, while they are more frequently coming from the South during the first deployment after anchor drag and only occasionally coming from the East during the second deployment.

The interactions between the different wave parameters are assessed: H_S/D_P, T_P/D_P and H_S/T_P respectively.

Plots showing which interpolated wave direction was associated with interpolated H_S and T_P have been drawn (Figure 4.25j-l and m-o respectively): for each data point, the vector H_{Svec} *and* T_{Pvec} (red dots) with an amplitude equal to H_S or T_P and a direction equal to the peak direction D_P was plotted. The waves have been plotted from their direction of origin, to directly compare them with the directions of the mooring lines. That is why the three mooring lines are also drawn (blue lines). These figures indicate that two main wave climates are occurring for the SWMTF: one with waves coming from the East, with large associated H_S, the other with waves coming from the South, with smaller associated H_S. However, some waves were also observed coming from the North West, with low wave amplitudes, resulting from local North West wind seas. T_P were not particularly associated with a wave direction, as shown by their massive spread.

The plots are generally similar for the different sets of data, but the waves coming from the South have lower H_S during the first deployment after anchor drag. The waves coming from the East also have lower H_S (> 3 m) in the second SWMTF deployment.

The correlation between H_S and T_P has been highlighted by the use of scatter plots. (H_S,T_P) scatter plots are available for the different sets of data (Figure 4.25j-l). The most frequent sea states were for H_S below 1 m and T_P between 3 and 7.5 s. This reflects the sheltered nature of the site. The sea states with the largest H_S had T_P between 6 and 7.5 s. The waves during the first deployment after the anchor drag had more frequent sea states with low H_S and high T_P than before the anchor drag.

Table 4.10: Summary and variations of wave and current data measurements during SWMTF deployments before interpolation

	First deployment								**Second deployment**			
	Before anchor drag				After anchor drag							
Number wave data points	11,046				10,536				4,896			
Equivalent time (days)	11,046 x 1,024 s = 131 days				10,536 x 1,024 s = 125 days				4,896 x 20 minutes = 68 days			
Total time deployment (days)	132 days				126 days				74 days			
Number of bins populated on the wave scatter diagram	38				34				32			
Number of bins populated on the current scatter diagram	50				67				46			
Number of data points with H_S > 3 m	6				0				10			
Number of storms with H_S > 3 m	2				0				1			
	Min	Mean	Max	Std	Min	Mean	Max	Std	Min	Mean	Max	Std
H_S (m)	0.04	0.72	3.34	0.53	0.04	0.55	3.00	0.46	0.04	0.69	3.44	0.49
H_{max} (m)	0.08	1.21	4.98	0.81	0.08	0.93	4.79	0.68	0.27	1.70	5.44	0.80
T_Z (s)	2.05	4.67	25.97	1.20	2.29	4.54	18.41	0.93	2.11	4.22	29.13	1.54
T_P (s)	2.10	6.17	27.70	2.20	2.20	6.33	22.80	2.75	2.50	6.56	25.00	2.46
C (m/s)	-0.25	0.07	0.50	0.13	-0.40	0.04	0.54	0.18	-0.20	0.07	0.44	0.13
h (m)	27.73	30.62	33.24	1.29	27.56	30.60	33.13	1.31	27.75	30.62	33.03	1.30

Table 4.11: Summary and variations of wave and current data measurements during SWMTF deployments after interpolation

	First deployment								**Second deployment**			
	Before anchor drag				After anchor drag							
Number wave data points	18,837				17,958				9,697			
Equivalent time (days)	18,837 x 10 minutes = 131 days				17,958 x 10 minutes = 125 days				9,697 x 10 minutes = 67 days			
Total time deployment (days)	132 days				126 days				74 days			
Number of bins populated on the wave scatter diagram	41				37				37			
Number of bins populated on the current scatter diagram	50				67				49			
Number of data points with $H_S > 3$ m	7				0				20			
	Min	Mean	Max	Std	Min	Mean	Max	Std	Min	Mean	Max	Std
H_S (m)	0.04	0.72	3.30	0.51	0.04	0.57	2.95	0.48	0.04	0.70	3.41	0.49
H_{max} (m)	0.09	1.19	4.76	0.77	0.09	0.96	4.53	0.70	0.44	1.94	5.23	0.82
T_Z (s)	2.10	4.66	24.87	1.12	2.32	4.56	13.65	0.89	2.11	4.22	29.13	1.41
T_P (s)	2.30	6.14	24.66	1.99	2.30	6.33	22.80	2.43	2.50	6.57	20.28	2.26
C (m/s)	-0.28	0.08	0.50	0.14	-0.40	0.05	0.53	0.18	-0.29	0.08	0.44	0.13
h (m)	27.74	30.62	33.24	1.29	27.57	30.60	33.12	1.30	27.75	30.62	33.03	1.29

First SWMTF deployment

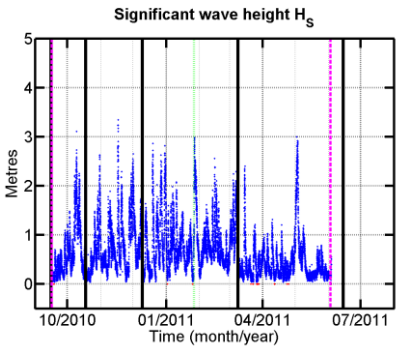

(a)

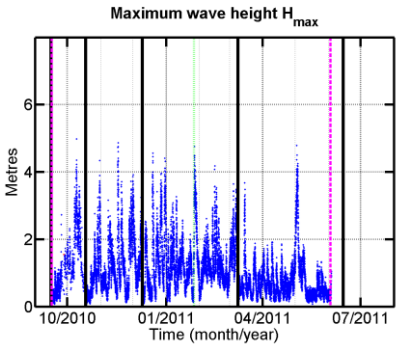

(c)

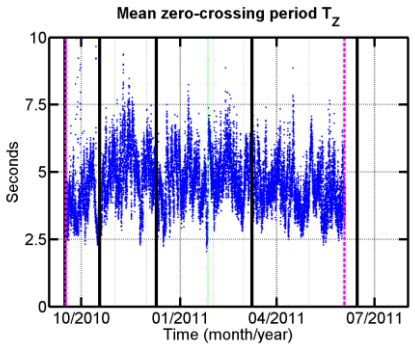

(e)

Second SWMTF deployment

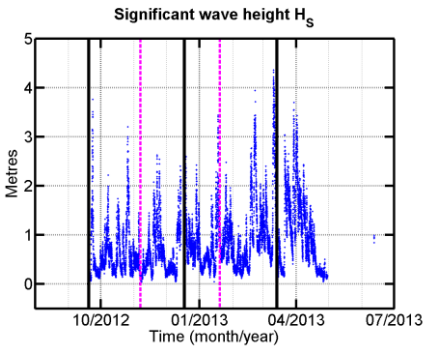

(b)

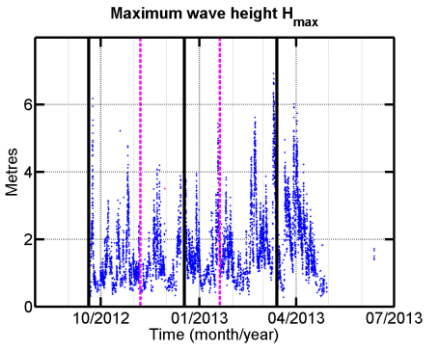

(d)

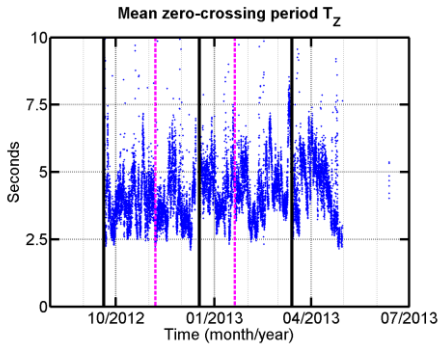

(f)

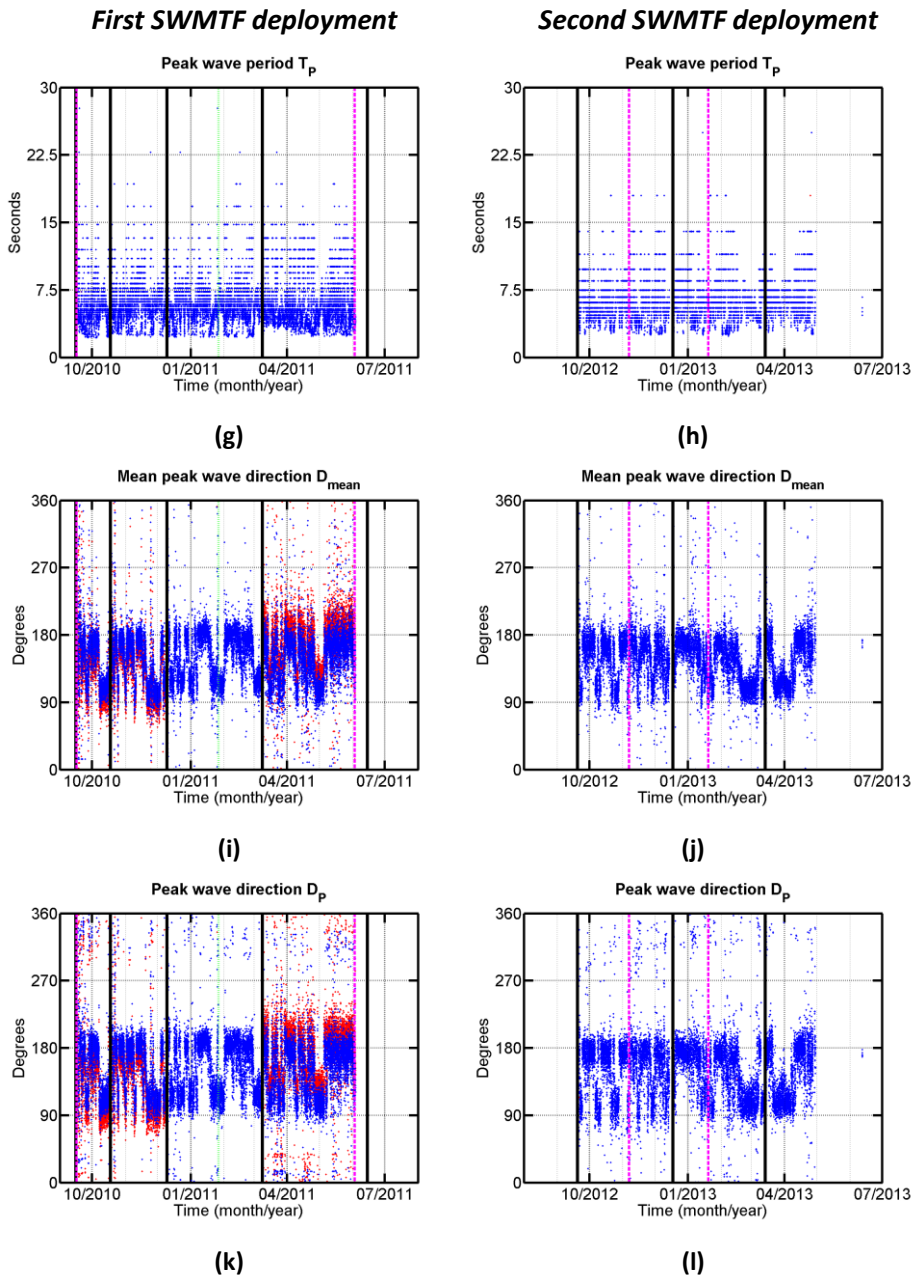

Figure 4.24: Summary of the wave statistical data recorded by the ADCP at SWMTF during the first (left column) and second (right column) deployment: (a-b) H_S, (c-d) H_{max}, (e-f) T_Z, (g-h) T_P, (i-j) D_{mean}, (k-l) D_P. Data before (red dots) and after correction (blue). Vertical black lines: ADCP redeployment, vertical dashed magenta lines: limit of data used for further analysis, vertical dotted green line: anchor drag

First deployment **Second deployment**

Before anchor drag After anchor drag

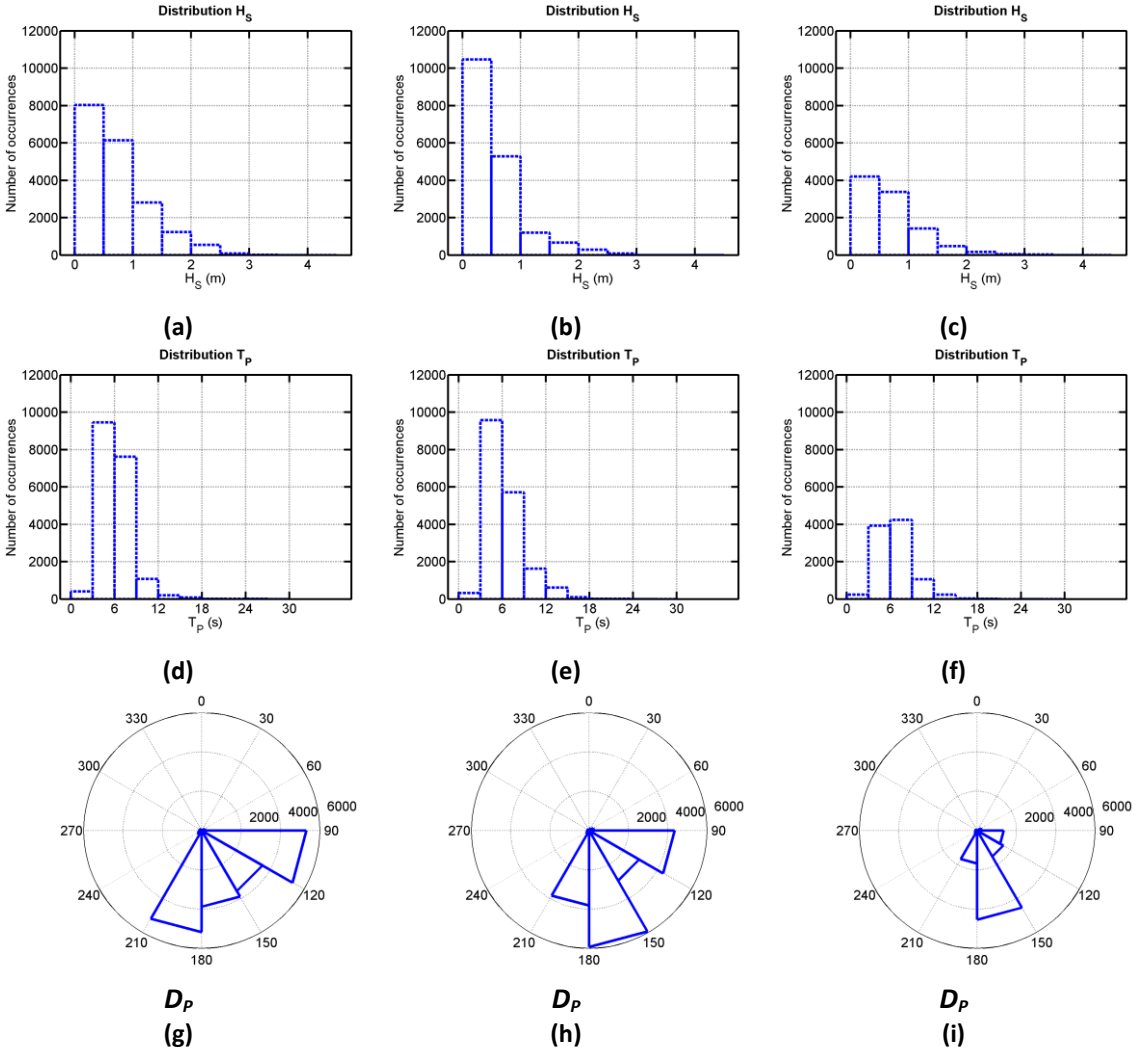

First deployment **Second deployment**

Before anchor drag After anchor drag

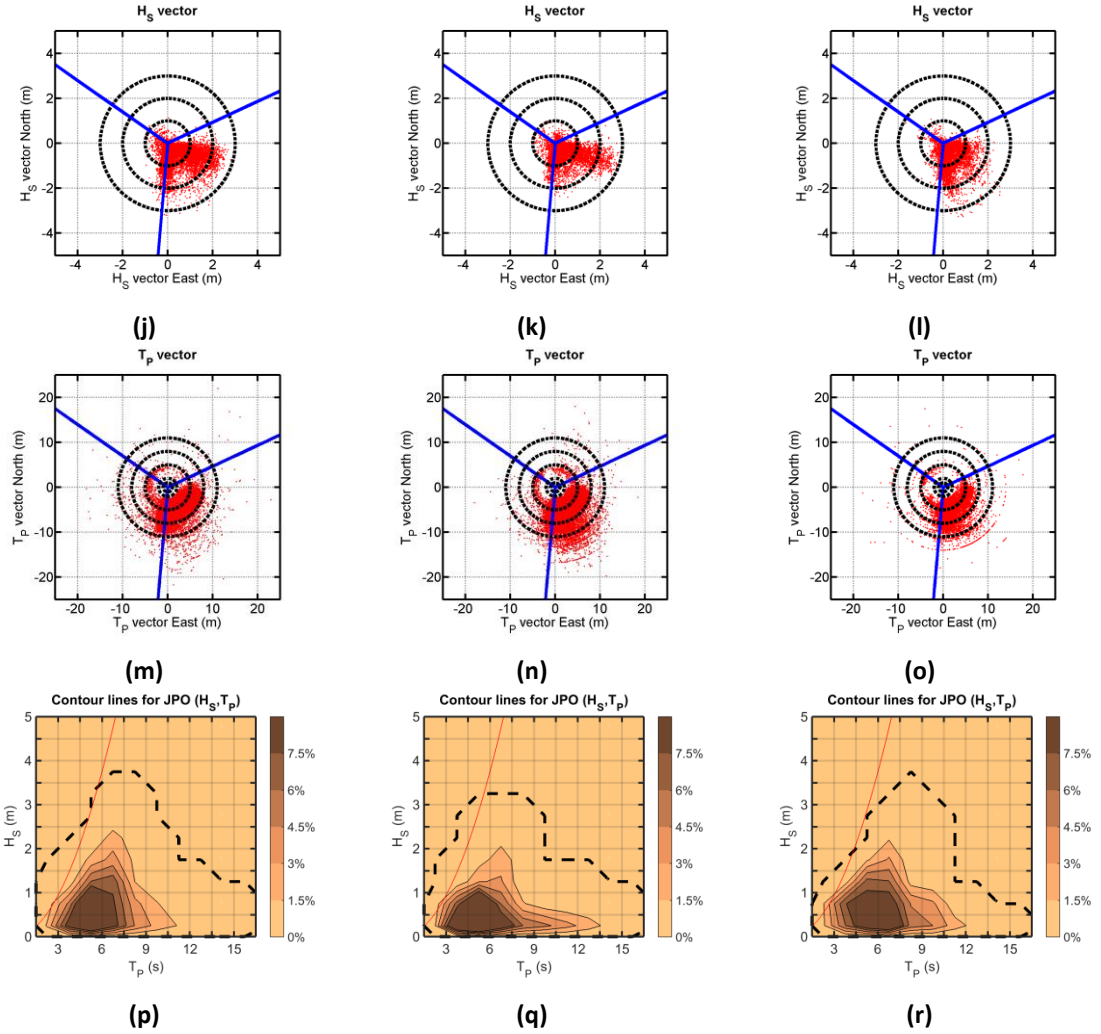

Figure 4.25: Presentation of the distributions of SWMTF interpolated wave data: (a-c) H_S, (d-f) T_P, (g-i) D_P, and correlations between wave parameters: (j-l) D_P and H_S, (m-o) D_P and T_P, (p-r) H_S and T_P. In j-o: Blue lines indicate the mooring line orientation; In p-r: Black dotted line: external contour line, no occurrences were recorded outside this line; the red line shows the average wave steepness limit. The wave direction is the direction from which the waves are coming.

Tidal current and water level

A summary of the current speed and water level data recorded during the two first SWMTF deployments has been plotted in Figure 4.26. Current velocity and water level were approximately the same every 14 days and were varying in a regular way. The current velocity and water level were also changing on a smaller time scale (semidiurnal). Two clear current directions can be identified: South and North.

Table 4.10 summarises the minimum, mean, maximum and standard deviation values measured for *C* and *h* and the number of bins populated in the tidal scatter diagram.

The tidal scatter diagram has been calculated following a similar methodology than for the wave scatter diagram as shown in Eq. (4.6):

$$SD(C,h)_{i,j} = \sum_{k=1}^{nb\_data} \begin{bmatrix} C_0 + (i-1)C_{bin} \le C_k < C_0 + iC_{bin} \\ and \\ h_0 + (j-1)h_{bin} \le h_k < h_0 + jh_{bin} \end{bmatrix} \quad (4.6)$$

With h_k and C_k the tidal conditions at a given time, h_0 and C_0 the minimum considered tidal conditions, h_{bin} and C_{bin} the bin size. For all tidal diagrams considered in this document, the values of *C* between -0.6 and 0.6 m/s were considered, with bins of 0.12 m/s, and the values of *h* between 27 m and 34 s with bins of 0.7 m.

The statistical values of *C* and *h* are similar for the different set of data (Table 4.10).

Figure 4.27 shows an example of water depth and current velocity variations over 1 day. The current velocity increases with the water depth (flood) until it reaches a step while the water depth reaches its maximum. Then the current velocity stays high while the water depth decreases (ebb). When the water depth reaches its minimum, the current velocity starts decreasing. Slack water (null current velocity) occurred near high tide (before) and low tide (after). This phenomenon is site dependent so it is important to check it for the particular site. It can be observed that current velocity is not sinusoidal. This could be due to surface currents caused by winds (the measured current is the maximum current in the water column), to the shape of the coastline or to the local bathymetry.

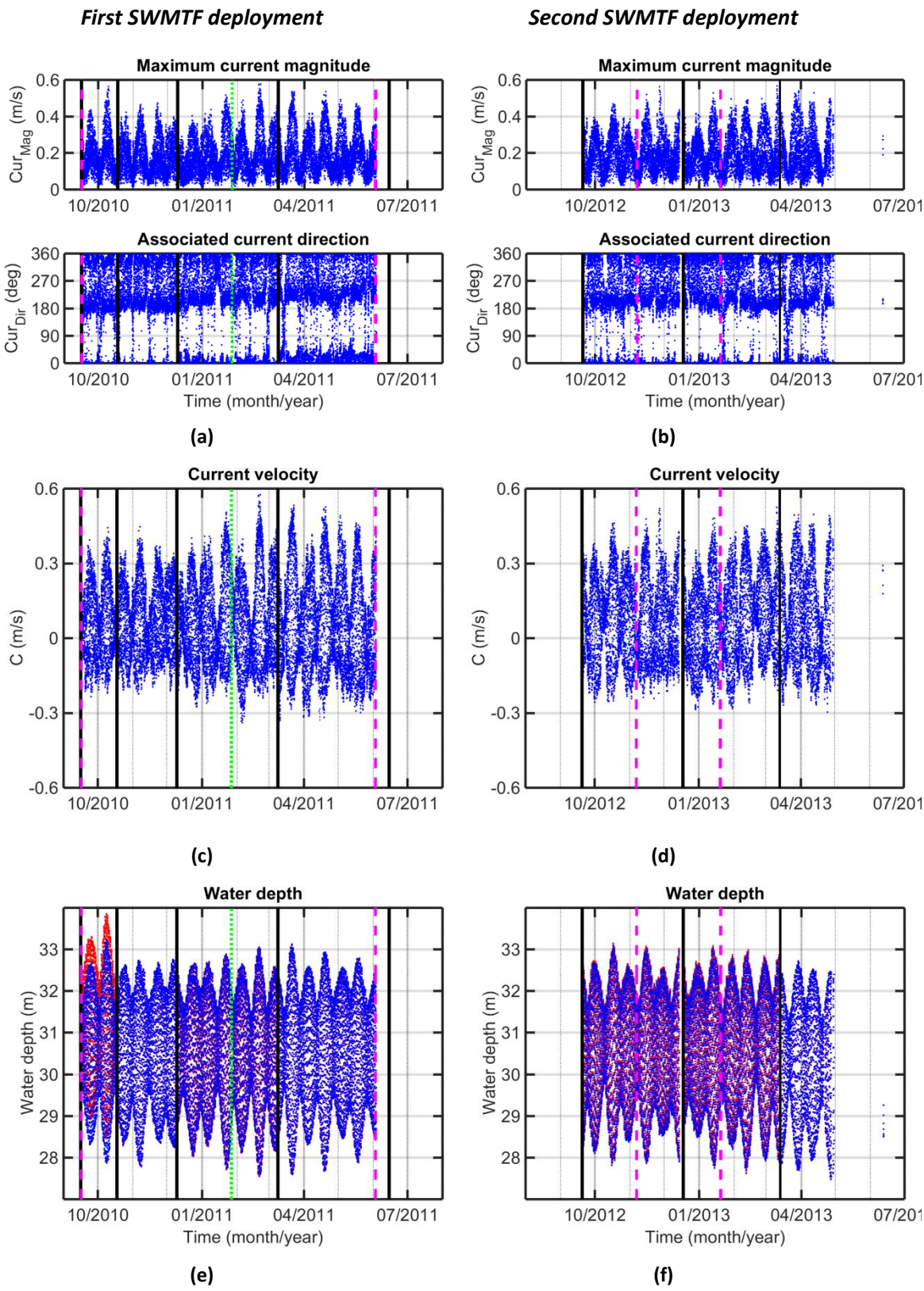

Figure 4.26: Summary of tidal variations recorded by the ADCP at SWMTF during the first (left column) and second (right column) deployment: (a-b) C_{Mag_max} and C_{Dir_max}, the current direction is the direction where the current goes (c-d) *C*, (e-f) *h*. Data before (red dots) and after correction (blue). Vertical black lines: ADCP redeployment, vertical dashed magenta lines: limit of data used for further analysis, vertical dotted green line: anchor drag

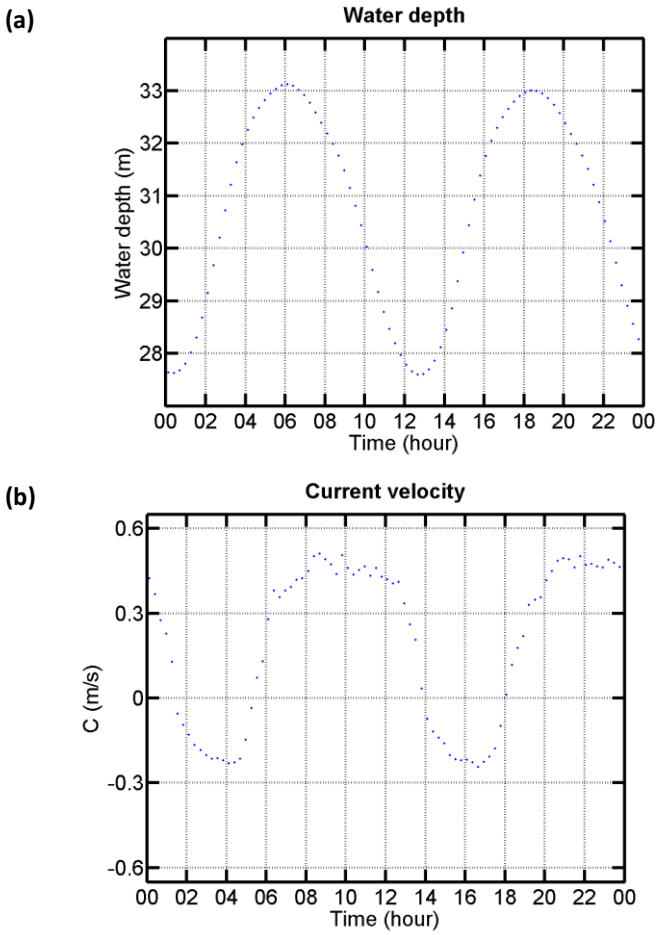

Figure 4.27: Example of daily tidal variations at SWMTF: example measured the 21/03/2011 by the ADCP of a) water depth *h* and b) current velocity *C*

The distribution of the tidal parameters *C* and *h* is similar for the different deployments, the number of occurrences depending of the duration of the deployment. Current was coming from the South South West (180 to 220°) or the North (330 to 10°). The current was most frequently heading to the South West (Figure 4.28a-c). The orientation of the current is different between the deployments but this may be due to the calibration of the ADCP. Figure 4.28d-f indicates that the most frequent values of *C* were between -0.1 and 0.3 m/s. Figure 4.28g-i shows that the water depth is frequent around 29.5 and around 32 m.

Summary plots (Figure 4.28j-l) indicate the relationship between C_{mag_max} and $C_{Dir\_max.}$. Currents coming from the South South West had the highest amplitude.

The (*h*,*C*) scatter plots in Figure 4.28m-o indicate that the most frequent tidal conditions (> 6% of the time) are for a water depth between 31.2 and 32.6 m and a current speed between -0.12 and +0.06 m/s.

First deployment

Second deployment

Before anchor drag

After anchor drag

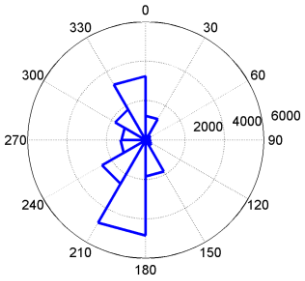

C_{Dir}

(a)

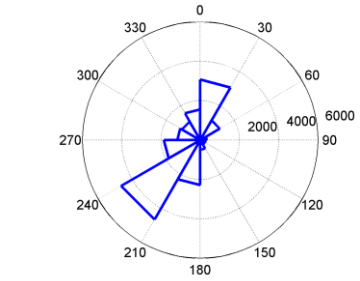

C_{Dir}

(b)

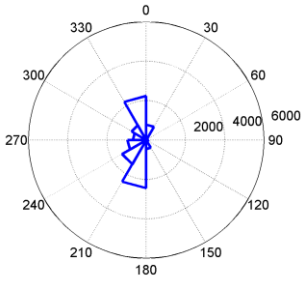

C_{Dir}

(c)

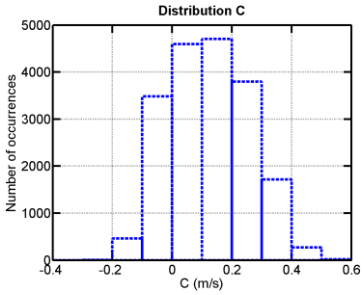

(d)

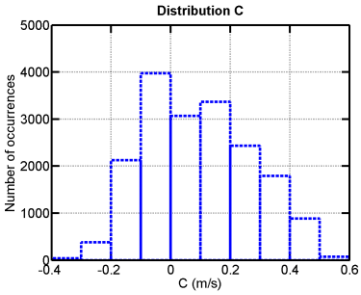

(e)

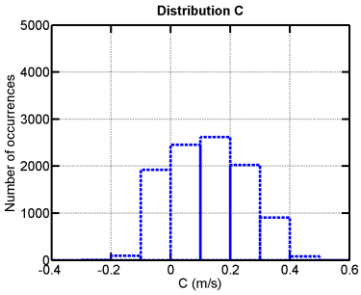

(f)

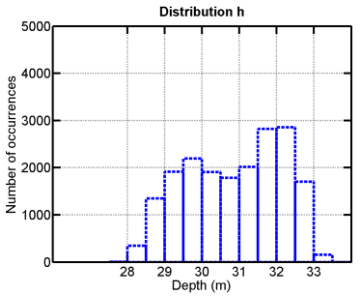

(g)

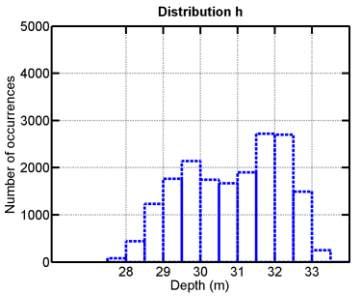

(h)

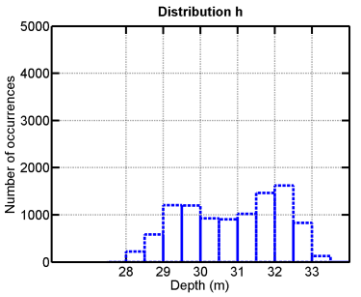

(i)

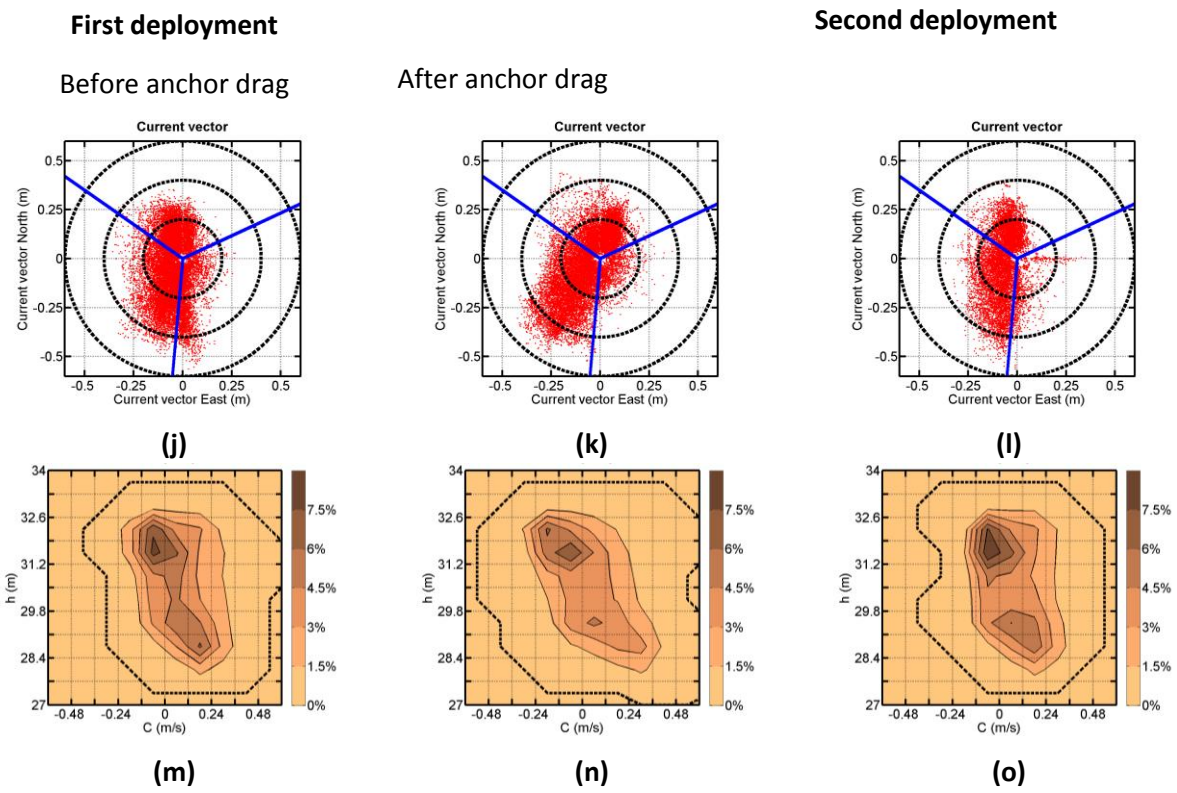

Figure 4.28: Distributions of SWMTF interpolated current data: (a-c) C_{Dir_max} , (d-f) *C*, (g-i) *h*, and correlations between current parameters: (j-l) C_{Dir_max} and C_{Mag_max}, the current direction is the direction where the current goes and (m-o) *C* and *h;* j-l: Blue lines indicate the mooring line orientation; p-r: Black dotted line: external contour line, no occurrences were recorded outside this line. The current direction is the direction from which the current is coming.

4.1.4.2 Mooring loads

Summaries of the maximum (Figure 4.29), mean (Figure 4.30, and zoom in Figure 4.31) standard deviation (Figure 4.32) and standard score of the maximum (Figure 4.33) mooring loads are plotted for each loadcell and for each period of analysis. Original and corrected data are plotted.

A drift in the mean and maximum original values of loads in line 3 can be observed (Figure 4.29e, Figure 4.30e) but was removed by the correction. Measurements from loadcells 1 and 2 also drifted during the second SWMTF deployment, but after the period of interest for this study delimited by the magenta dotted lines.
A sudden decrease in the mean load of line 1 and 2 (Figure 4.30a-b) can be observed at the end of January 2011. This decrease is not observed in mooring line 3 because of the failure of this loadcell. This sudden decrease is due to the unexpected drag of an anchor during a moderate storm. Harnois, Parish and Johanning (2012) analysed this event in more details. This drag event occurred during a storm of medium amplitude, heading in a North West direction. This is the first storm of this kind of amplitude since three storms with similar amplitude at the end of December 2010.
Similarly, at the beginning of October 2012, a jump in the loadcell data can be observed. It was the unwanted result of pulling tests. These data were not included in further analysis because of the lack of wave data at this time.

The maximum loads were in the same order of magnitude in mooring line 1 and 3 and lower in line 2 (Figure 4.29), which could be expected because line 1 and 3 are facing the predominant waves.
The mean loads were relatively similar in the different mooring lines (Figure 4.30-29). This similarity is expected for a well balanced mooring system. The mean load in mooring line 1 and 3 should be slightly higher than in mooring line 2 because of the mean wave drift. Because of the calibration of the loadcells and of possible offsets, this was not observed. The mean load was mainly varying with the tidal elevation. The slow and small decrease in the mean load before the anchor drag event and slow increase after it is difficult to interpret, and can be due either to the instrumentation, or to the

synthetic lines changing properties for example due to marine growth or mooring lines becoming longer.

The standard deviation shows a large number of peaks with significant amplitude in mooring line 3 during the first deployment before anchor drag (Figure 4.9). During this deployment, the number of occurrences of waves coming from the East was higher than during the other period of analysis, and the amplitude of the waves was significant as shown in Figure 4.25 which may explain this result.

The standard deviations of the mooring loads (Figure 4.32) was lower during the second (< 2 kN) than during the first deployment (< 6 kN). Values were the highest in line 3 during the first deployment, and in line 1 during the second deployment.

The standard scores of the maximum load (Figure 4.33) are generally small (< 6) and in a narrow range (3-6) in all mooring lines but with some outlier points.

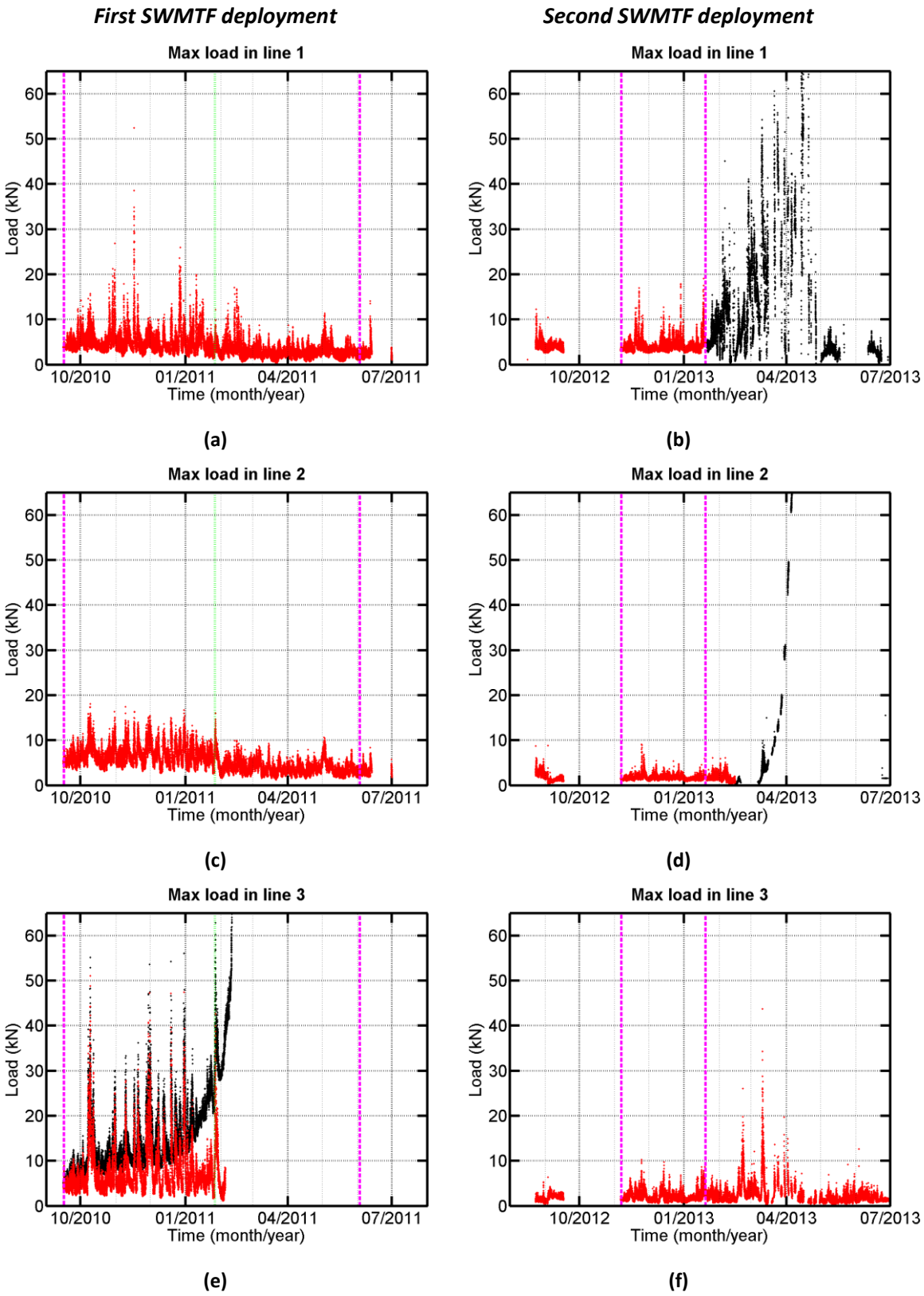

Figure 4.29: Maximum mooring loads for the SWMTF before (black) and after correction (red) measured in the three loadcells (top to bottom) during the first (left) and second (right) deployments. Vertical black lines: ADCP redeployment, vertical dashed magenta lines: limit of data used for further analysis, vertical dotted green line: anchor drag

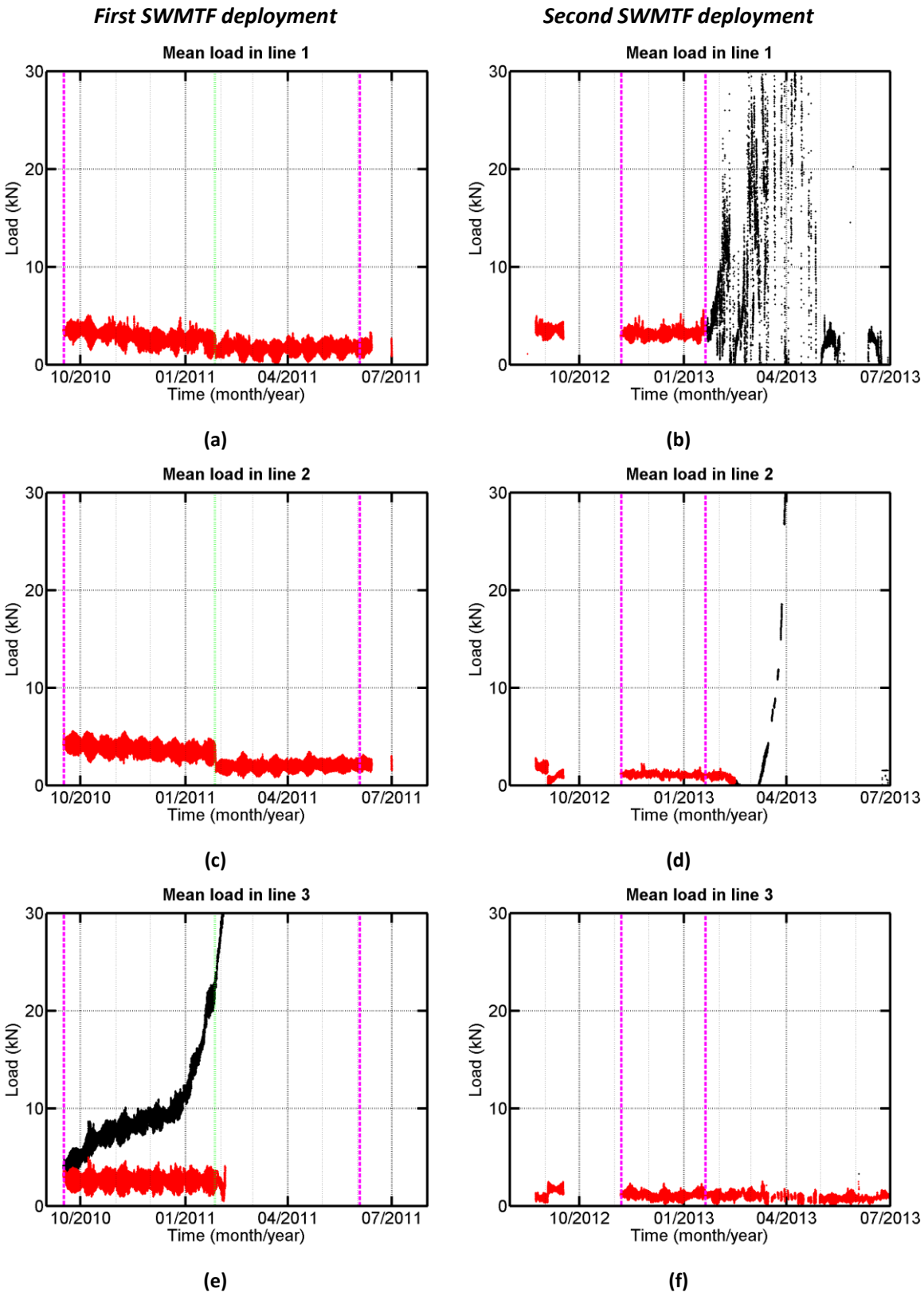

Figure 4.30: Mean mooring loads before (black) and after correction (red) measured in the three loadcells (top to bottom) during the first (left) and second (right) SWMTF deployments. Vertical black lines: ADCP redeployment, vertical dashed magenta lines: limit of data used for further analysis, vertical dotted green line: anchor drag

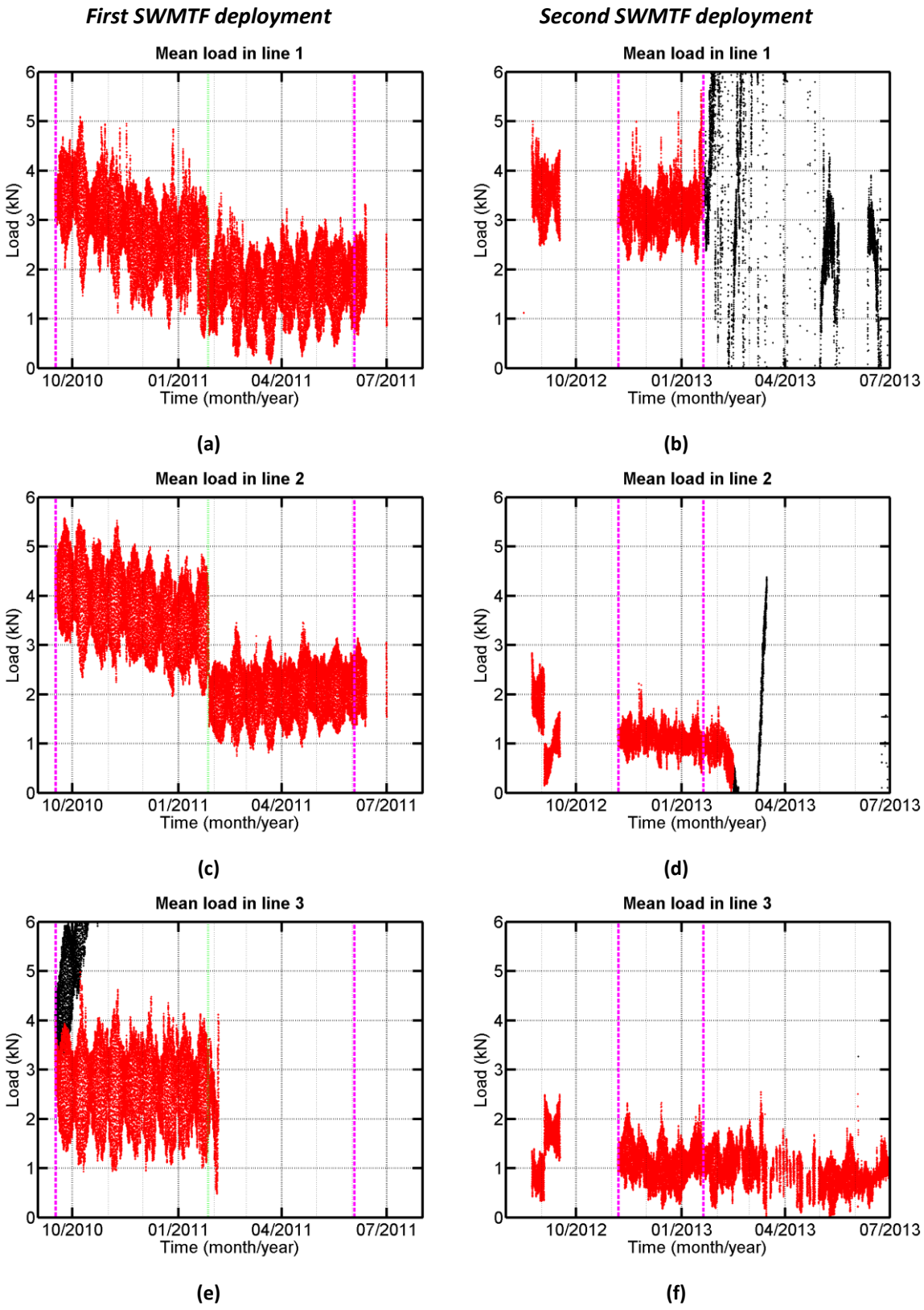

Figure 4.31: Zoom on the mean mooring loads before (black) and after correction (red) measured in the three loadcells (top to bottom) during the first (left) and second (right) SWMTF deployments. Vertical black lines: ADCP redeployment, vertical dashed magenta lines: limit of data used for further analysis, vertical dotted green line: anchor drag

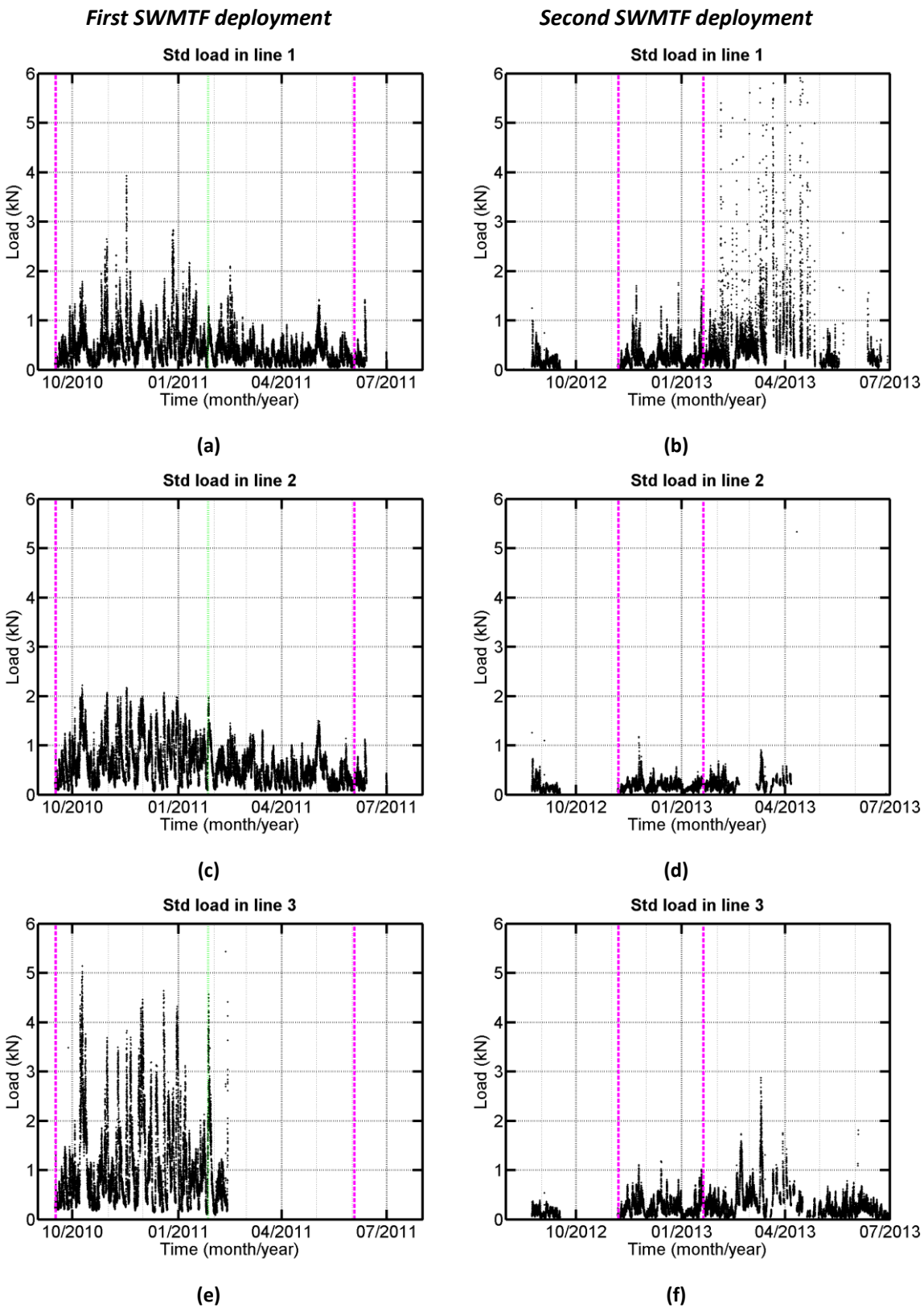

Figure 4.32: Standard deviations of mooring loads before (black) and after correction (red) measured in the three loadcells (top to bottom) during the first (left) and second (right) SWMTF deployments. Vertical black lines: ADCP redeployment, vertical dashed magenta lines: limit of data used for further analysis, vertical dotted green line: anchor drag

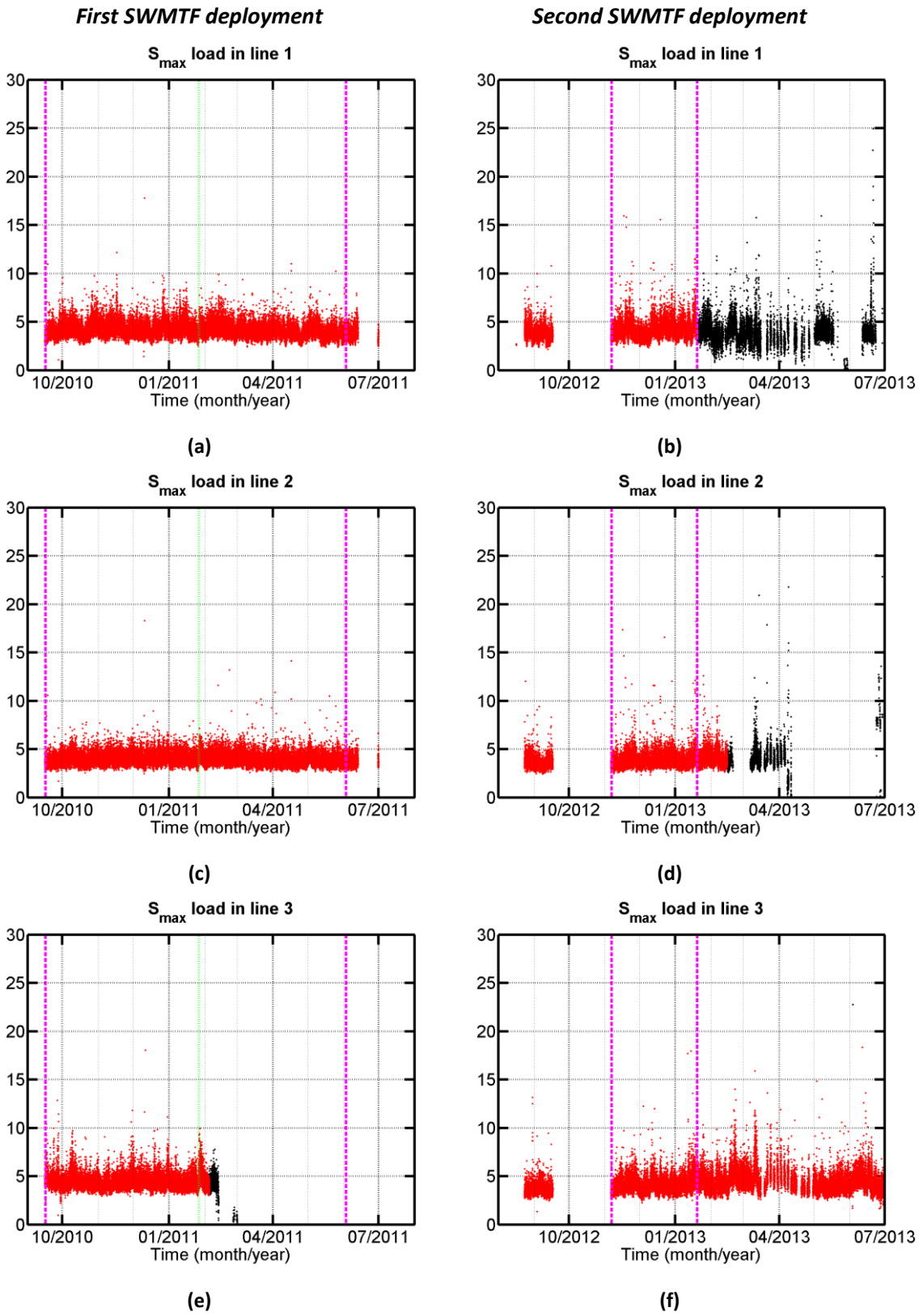

Figure 4.33: Standard score of the maximum mooring load before (black) and after correction (red) measured in the three loadcells (top to bottom) during the first (left) and second (right) SWMTF deployments. Vertical black lines: ADCP redeployment, vertical dashed magenta lines: limit of data used for further analysis, vertical dotted green line: anchor drag

Table 4.12 summarises the range of mean mooring loads in each loadcell. The mean mooring load in all mooring lines is lower after the anchor drag than before. The mean mooring load in mooring line 1 is higher during the second SWMTF deployment and lower in line 2 and 3 than during the first SWMTF deployment.

Table 4.12: Variations of the mean mooring load measured at SWMTF in the three mooring lines (after correction)

		Line	Min (kN)	Mean (kN)	Max (kN)	Std (kN)
First deployment	Before anchor drag	1	0.61	2.82	5.10	0.81
		2	1.96	3.76	5.58	0.73
		3	0.94	2.66	4.98	0.75
	After anchor drag	1	0.10	1.69	3.55	0.61
		2	0.75	2.08	3.46	0.49
		3		/ no data because of loadcell failure		
Second deployment		1	2.10	3.24	5.62	0.51
		2	0.41	1.14	2.22	0.24
		3	0.18	1.13	2.33	0.37

Table 4.13 summarises the events associated with the maximum mooring loads in each loadcell. The amplitude of the maximum mooring loads was higher during the first deployment before the anchor drag, when the mooring was the less compliant.

For a given mooring line and for the different set of data, the maximum mooring loads occurred for similar wave directions: waves coming from the South for line 1, and from the East for line 2 and 3. The highest amplitudes of mooring loads did not occur for the highest amplitude of H_S (Table 4.10).

The amplitude of the maximum mooring loads was compared with the MBL of the rope: 461 kN during the first deployment and 520 kN during the second deployment. These loads were not endangering the survivability of the mooring system as they were significantly below the MBL.

Table 4.13: Variations of the maximum mooring load measured at SWMTF in the three mooring lines (after correction)

		Line	Amplitude (kN)/%MBL	Date	Time	H_S (m)	T_P (s)	D_P (°)
First deployment	Before anchor drag	1	52.5/11%	17/11/2010	02:00-02:10	2.62	7.7	174
		2	18.1/4%	09/10/2010	09:40-09:50	2.55	6.4	97
		3	51.1/11%	09/10/2010	09:30-09:40	2.48	6.6	97
	After anchor drag	1	17.1/4%	13/02/2011	00:30-00:40	1.35	5.8	165
		2	10.7/2%	02/05/2011	07:40-07:50	2.01	6.1	93
		3	/ no data					
Second deployment		1	19.1/4%	18/01/2013	07:20- 07:30	3.31	8.5	165
		2	9.2/2%	24/11/2012	20:50- 21:00	2.09	7.1	101
		3	10.3/2%	24/11/2012	17:40- 17:50	2.26	6.7	89

In order to summarise the mooring tension variations, the distributions of mean (Figure 4.34-Figure 4.35), maximum (Figure 4.36-Figure 4.37), standard deviations (Figure 4.38) and standard scores of the maximum (Figure 4.39) mooring loads have been plotted.

The distributions of the mean loads (Figure 4.34) are varying depending on the mooring loadcells and on the set of data. The calibration of the loadcell and the corrections applied to the mooring loads may bias these results. Most of the maximum mooring loads (Figure 4.36) are below 10 kN, with a large number of maximum loads between 0 and 5 kN. The maximum percentage of occurrences of the standard deviations of the mooring loads occurred for the values between 0 and 1 kN. All distributions of the standard score of the maximum load (Figure 4.39) are centred between 3 and 4.

Zooms on the highest values of the mean (Figure 4.35) and maximum (Figure 4.37) mooring loads have been plotted in order to observe the tails of the distributions: are the distributions regularly decreasing – as they would for example in a Gaussian distribution? The mean loads are all decreasing in the tail of the distribution. All the distribution of maximum loads except one are also decreasing: on mooring line 1 during the first SWMTF deployment before anchor drag, a mooring load with an amplitude over 50 kN occurred while there were no occurrences between 40 and 50 kN.

First SWMTF deployment ***Second SWMTF deployment***

Before anchor drag After anchor drag

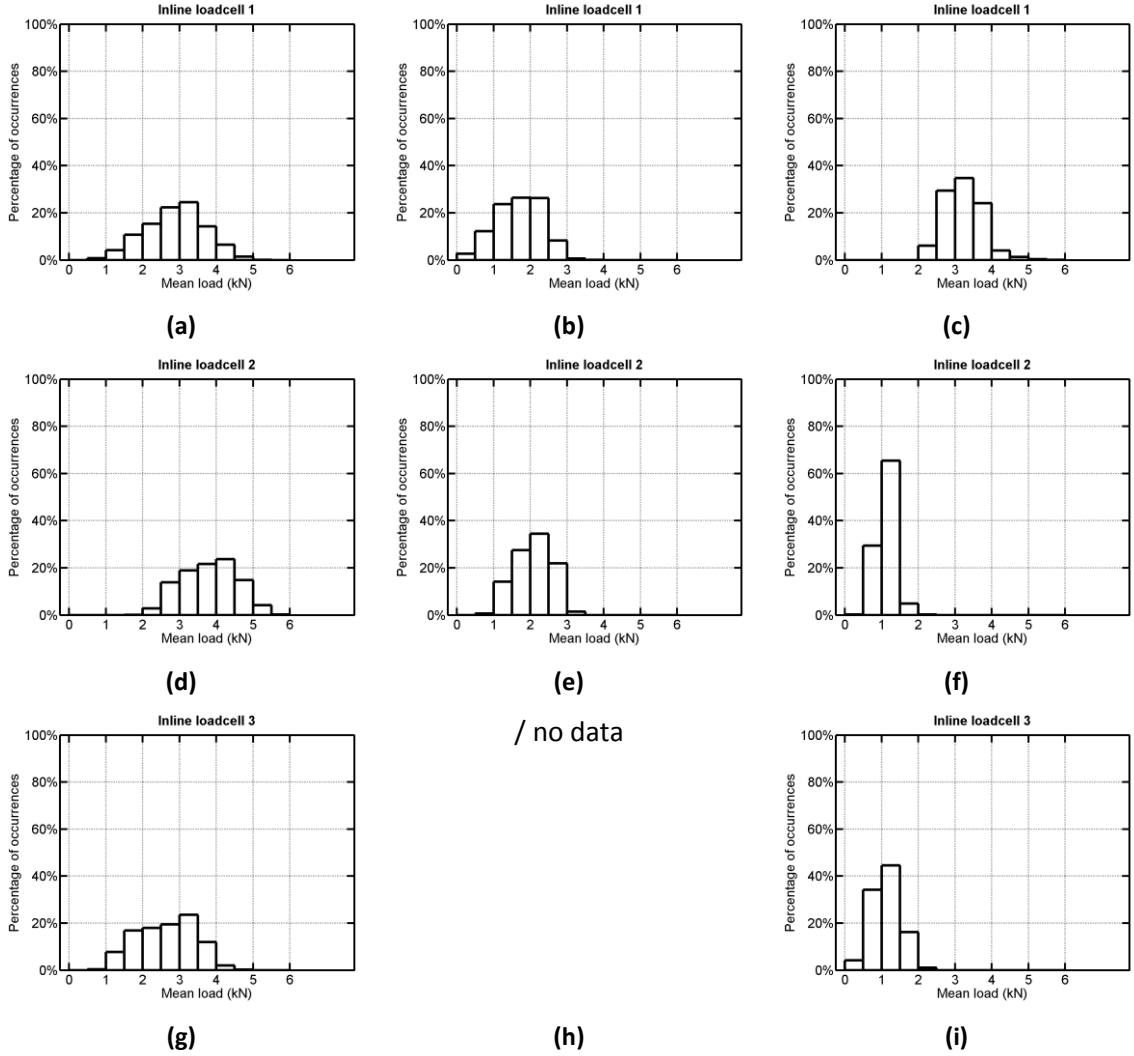

Figure 4.34: Distribution of corrected mean mooring loads in the three lines (top to bottom) during the SWMTF deployments

First SWMTF deployment		*Second SWMTF deployment*
Before anchor drag	After anchor drag	
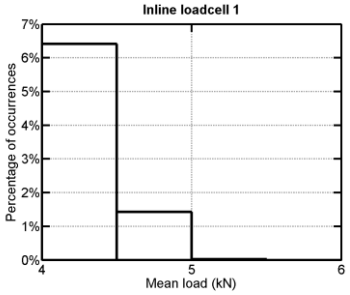	no occurrences in this range of values	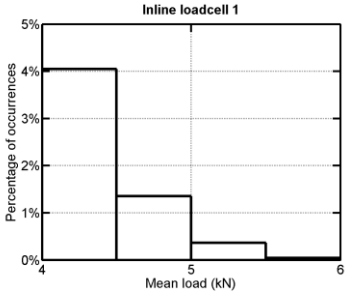
(a)	**(b)**	**(c)**
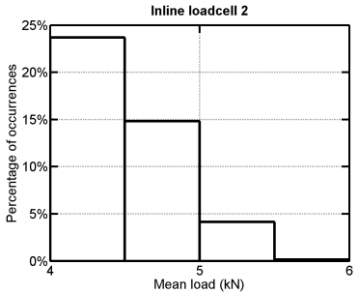	no occurrences in this range of values	no occurrences in this range of values
(d)	**(e)**	**(f)**
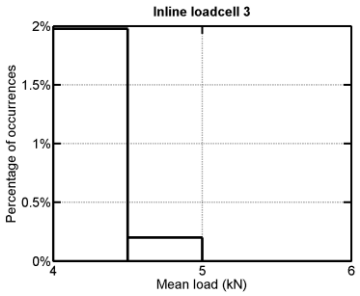	/ no data	no occurrences in this range of values
(g)	**(h)**	**(i)**

Figure 4.35: Distribution of corrected mean loads in the three lines (top to bottom) during the SWMTF deployments: zoom on the large mean mooring forces (> 4 kN). The vertical scale is different for each plot.

First SWMTF deployment ***Second SWMTF deployment***

Before anchor drag After anchor drag

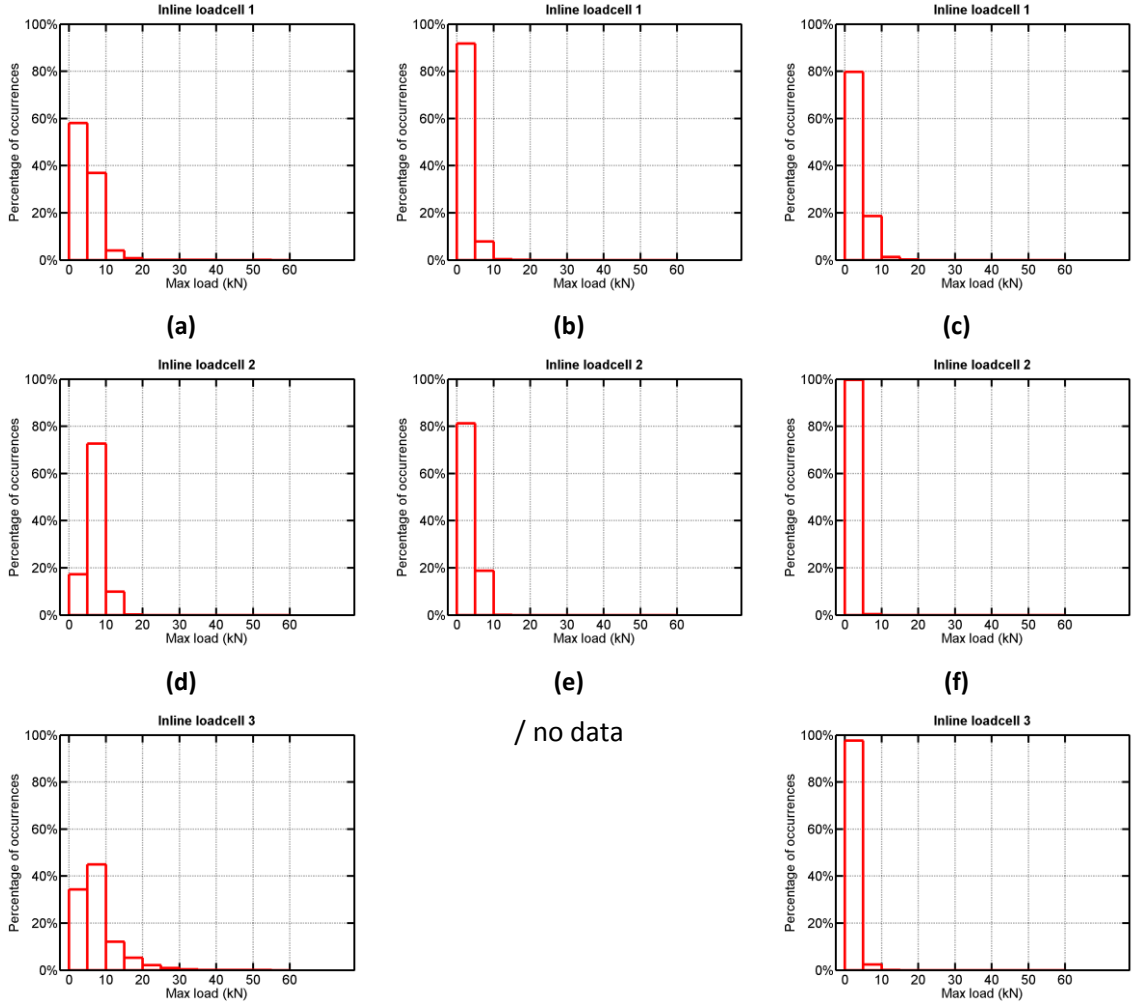

/ no data

Figure 4.36: Distribution of corrected maximum loads in the three lines (top to bottom) during the SWMTF deployments

First SWMTF deployment ***Second SWMTF deployment***

Before anchor drag After anchor drag

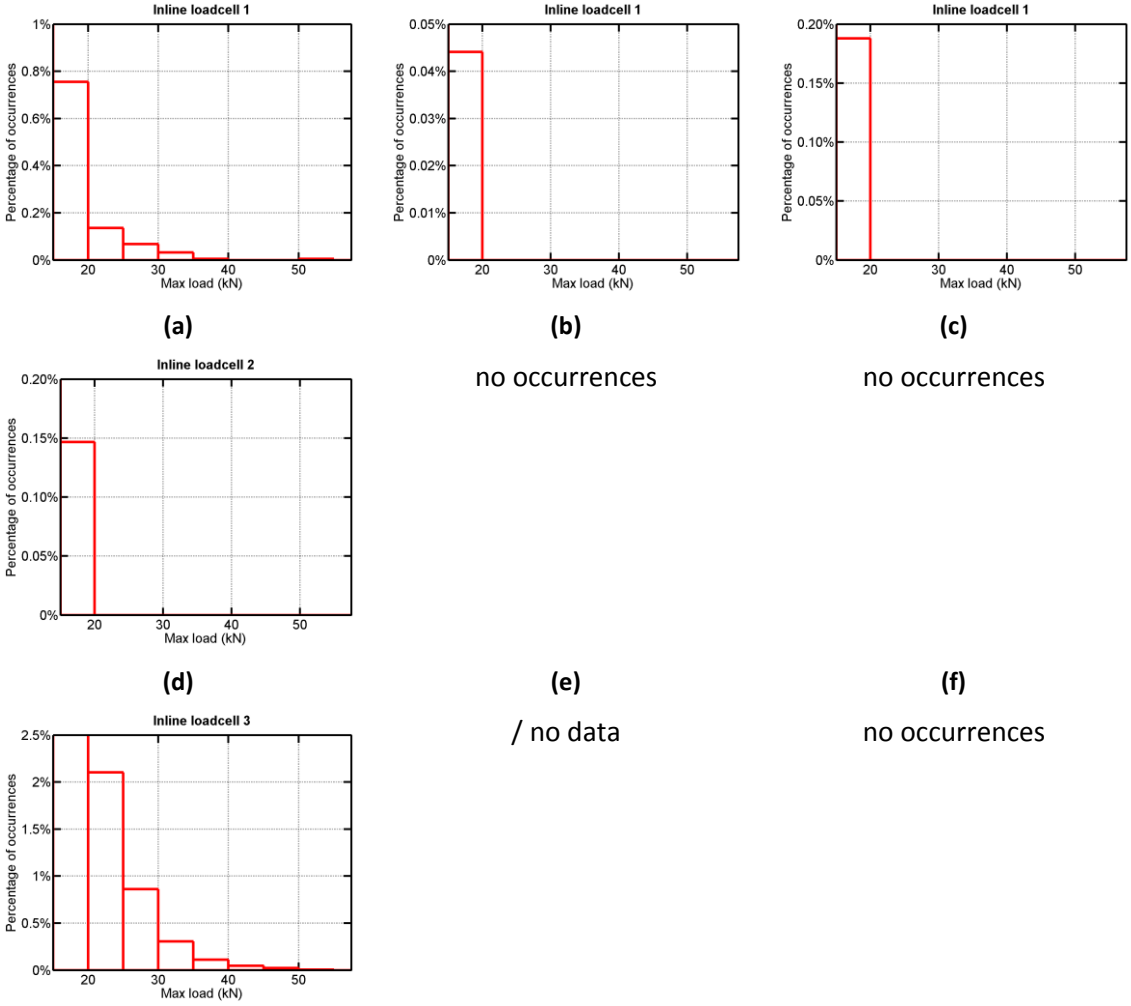

Figure 4.37: Distribution of corrected maximum loads in the three lines (top to bottom) during the SWMTF deployments: zoom on the large mooring forces (>15 kN). The vertical scale is different for each plot.

First SWMTF deployment ***Second SWMTF deployment***

Before anchor drag After anchor drag

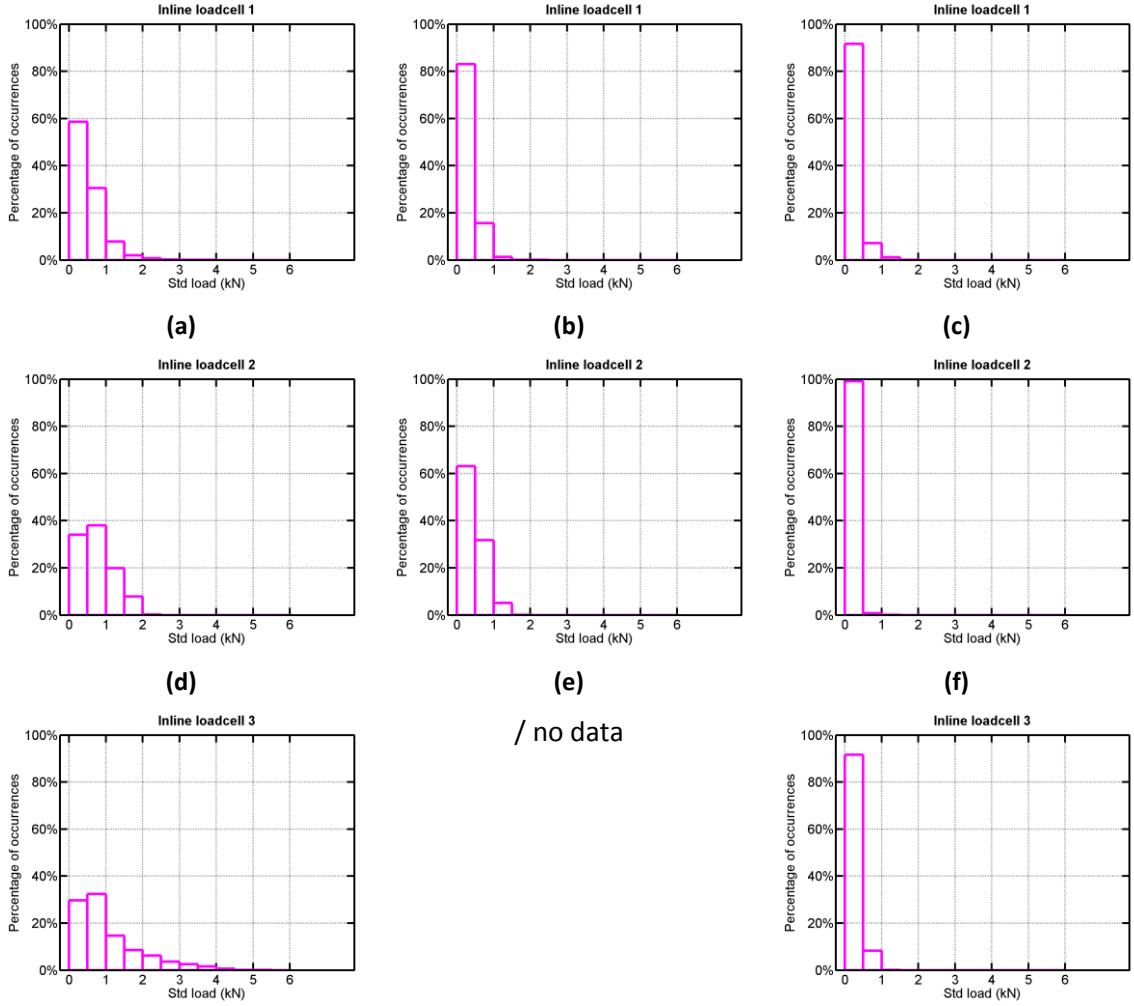

Figure 4.38: Distribution of measured standard deviation of mooring loads in the three lines (top to bottom) during the SWMTF deployments

First SWMTF deployment ***Second SWMTF deployment***

Before anchor drag After anchor drag

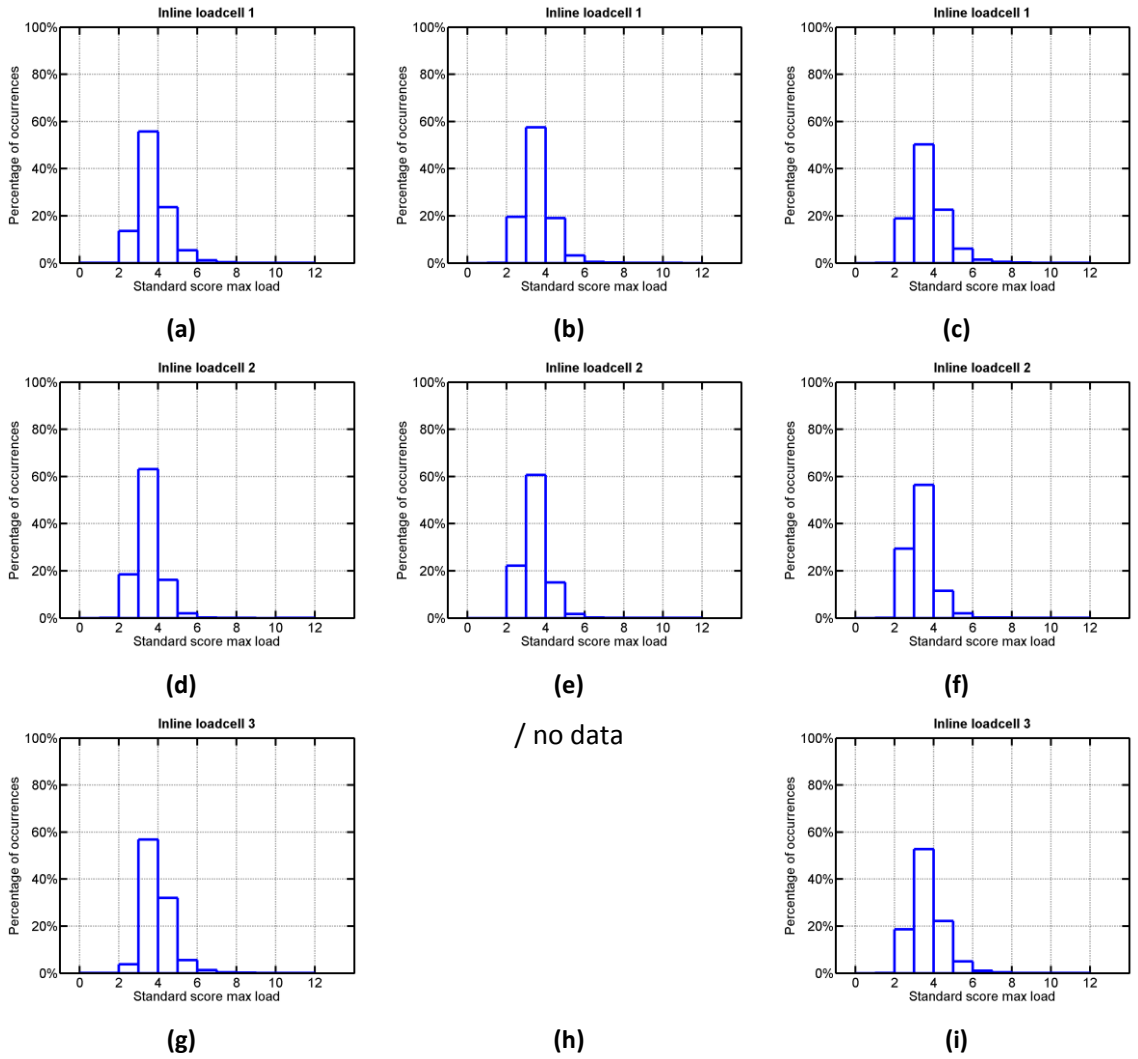

Figure 4.39: Distribution of measured standard score of the maximum mooring loads in the three lines (top to bottom) during the SWMTF deployments

For each set of data, the amplitude of the maximum mooring load for each loadcell and for each available sea state has been plotted in Figure 4.40. The scale is different for loadcell 2 because the amplitude of the mooring loads is significantly lower.

The significant reduction in the amplitude of mooring loads after anchor drag and during the second SWMTF deployment is clearly visible on these graphs.

First SWMTF deployment ***Second SWMTF deployment***

Before anchor drag After anchor drag

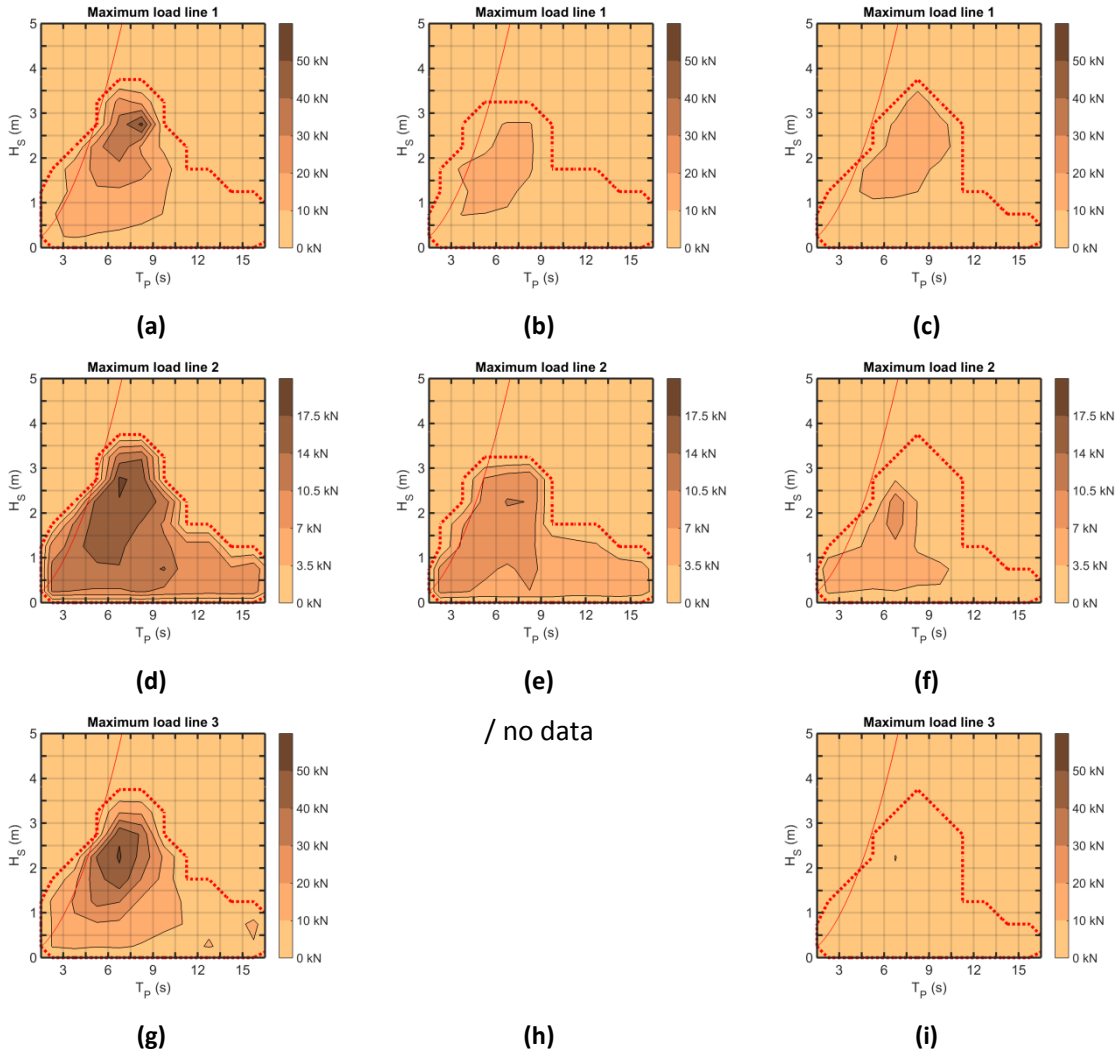

/ no data

Figure 4.40: Maximum mooring loads for each range of sea states loads in the three lines (top to bottom) during the SWMTF deployments. The red solid line shows the average wave steepness limit. Red dotted line: external contour line, no occurrences were recorded outside this line.

The action of waves and current on mean and dynamic loads has been investigated. Second order wave motions and current are expected to modify the mooring mean load.

Figure 4.41 shows the amplitude of the maximum mooring loads and their associated wave direction. Figure 4.42 shows the mean mooring loads and associated wave direction. Figure 4.43 shows the maximum mooring loads and associated current direction. Figure 4.44 shows the mean mooring loads and associated current directions.

In Figure 4.41, on mooring line 1 and 3, the amplitude of maximum mooring loads is associated with wave directions being close to the mooring line direction. This means that for a given mooring configuration, the maximum tension is mainly driven by the waves.

A wide range of mean load is observed on all mooring lines for the two main wave directions (Figure 4.42) and anywhere on and between the two main wave directions. This means that the mean load is not driven by the wave direction.

Figure 4.43 indicates that maximum mooring loads occurred for all current directions.

Similarly Figure 4.44 indicates that a wide range of mean load is associated with the two tidal current directions.

The values of mean load could vary because of the vertical or horizontal offset of the floating structure generated by the tidal range or tidal current respectively. During a calm period, Figure 4.45 indicates that the increase in water depth is leading the increase in the mean mooring load. The maximum mean load on mooring line 2 occurs simultaneously with the maximum water level, while the maximum mean load on mooring line 1 occurs one hour before the maximum water level. Investigating the buoy position and relating it to the mean and peak mooring loads would give more insight into the mooring behaviour. The statistical data for motions are incorrect at the moment and need a major update. The error originates from the conversion of latitude and longitude from degrees to meters and requires the reprocessing of all motion data.

First SWMTF deployment ***Second SWMTF deployment***

Before anchor drag After anchor drag

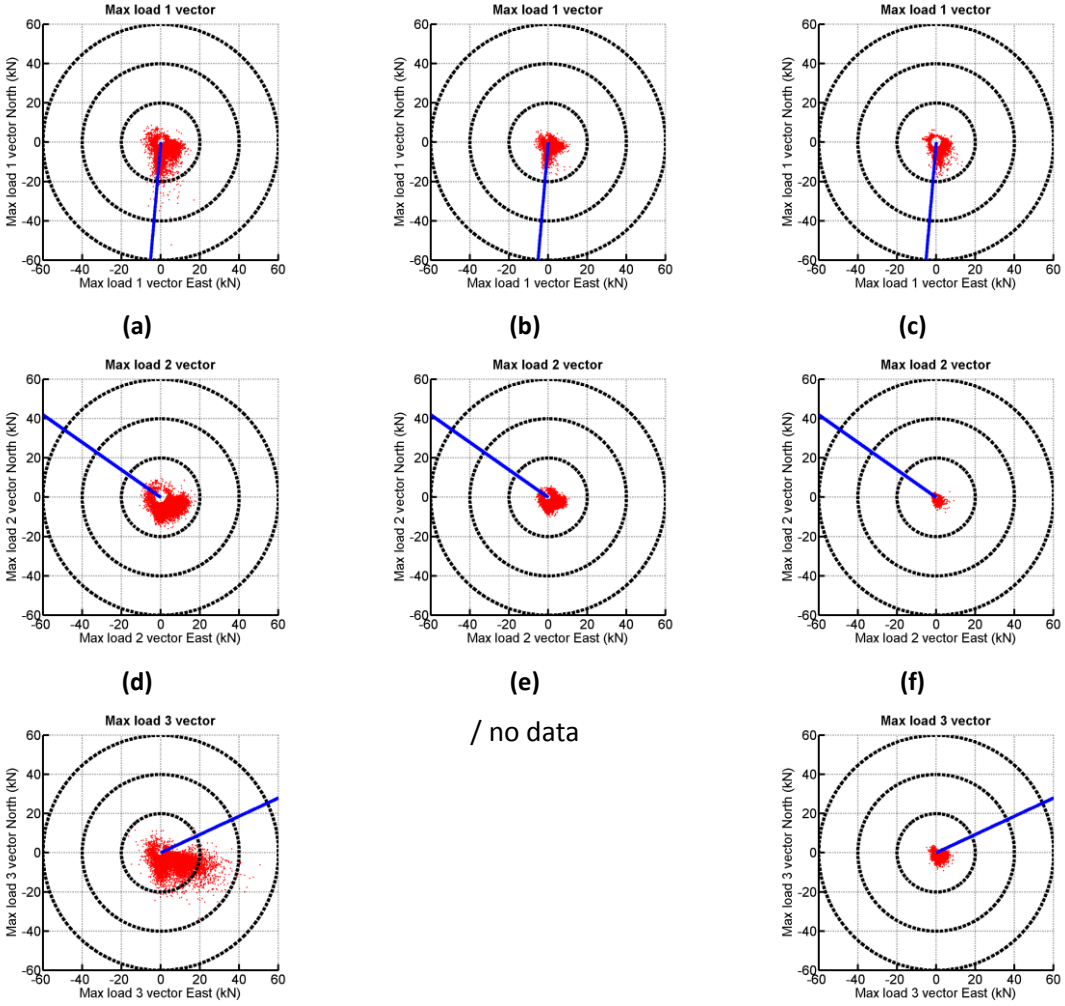

/ no data

Figure 4.41: Maximum mooring loads and associated wave directions D_P for the different mooring lines and for the different periods of analysis during the SWMTF deployments. The wave direction is the direction from which the waves are coming.

First SWMTF deployment ***Second SWMTF deployment***

Before anchor drag After anchor drag

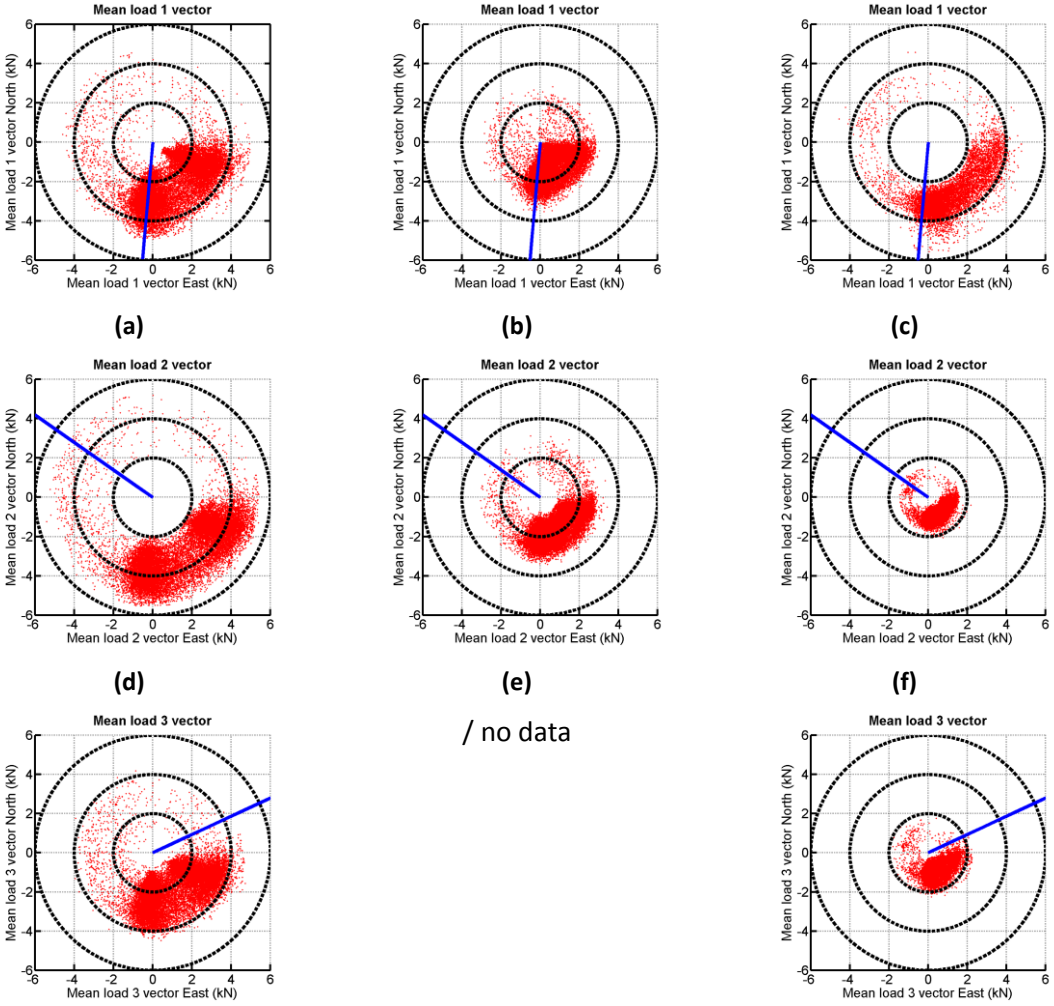

Figure 4.42: Mean mooring loads and associated wave directions D_P for the different mooring lines and for the different periods of analysis during the SWMTF deployments. The wave direction is the direction from which the waves are coming.

First SWMTF deployment ***Second SWMTF deployment***

Before anchor drag After anchor drag

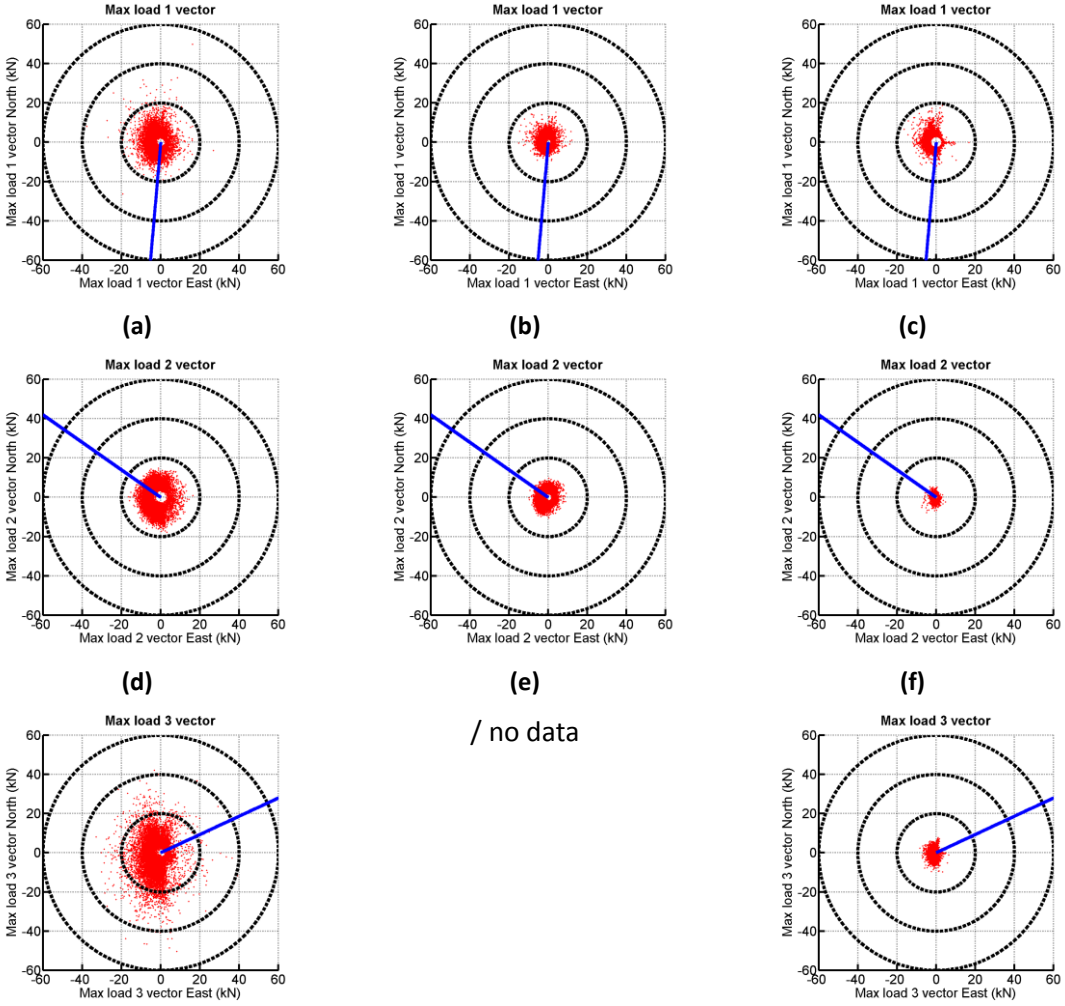

Figure 4.43: Maximum mooring loads and associated current directions C_{Dir} for the different mooring lines and for the different periods of analysis during the SWMTF deployments. The current direction is the direction from which the current is coming.

First SWMTF deployment ***Second SWMTF deployment***

Before anchor drag After anchor drag

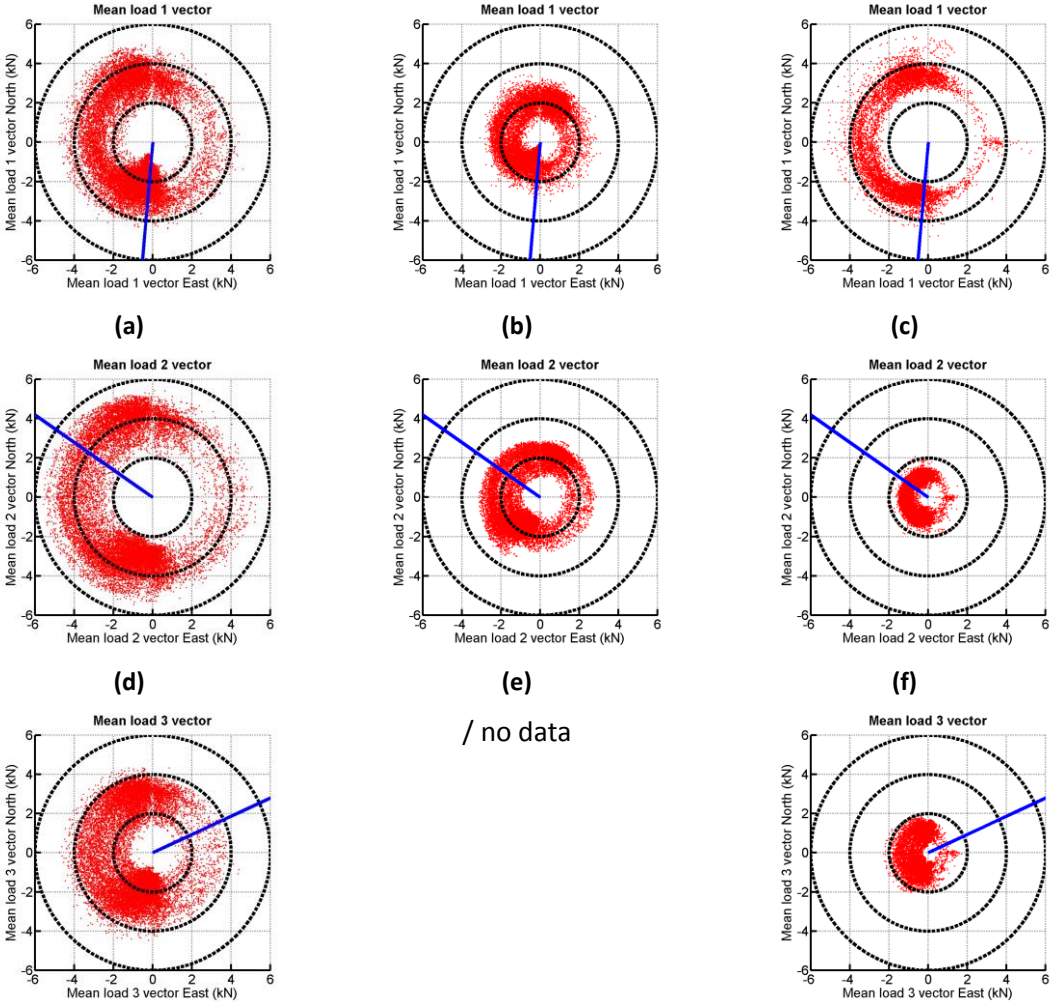

Figure 4.44: Mean mooring loads and associated current directions C_{Dir} for the different mooring lines and for the different periods of analysis during the SWMTF deployments. The current direction is the direction from which the current is coming.

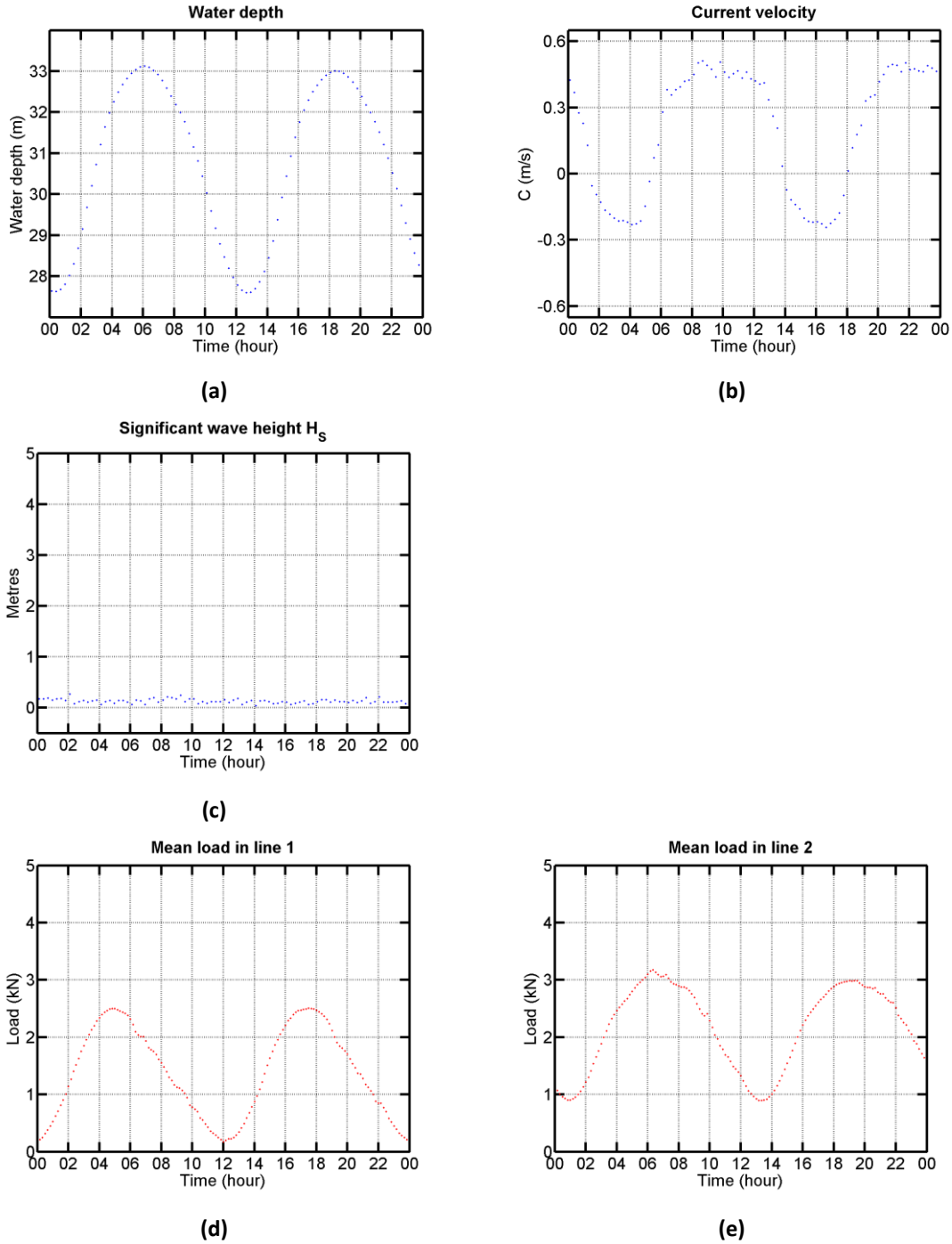

Figure 4.45: Example of daily tidal variations and associated mooring load variations in the absence of waves at SWMTF on the 21/03/2011: a) *h*, b) *C*, c) H_S, d) mean load in line 1, e) mean load in line 2. Mean load in line 3 was not available at this time (Loadcell failure).

For each period of analysis, the relationship between the water depth and the pre-tension when H_S was below 0.1 m has been plotted in Figure 4.46. A linear fit has been calculated for each mooring line and each period of analysis. The parameters of this linear fit are summarised in Table 4.14. The anchor drag decreased the pre-tension. Except for line 1, the mean load was generally lower on the mooring during the second SWMTF deployment than during the first SWMTF deployment.

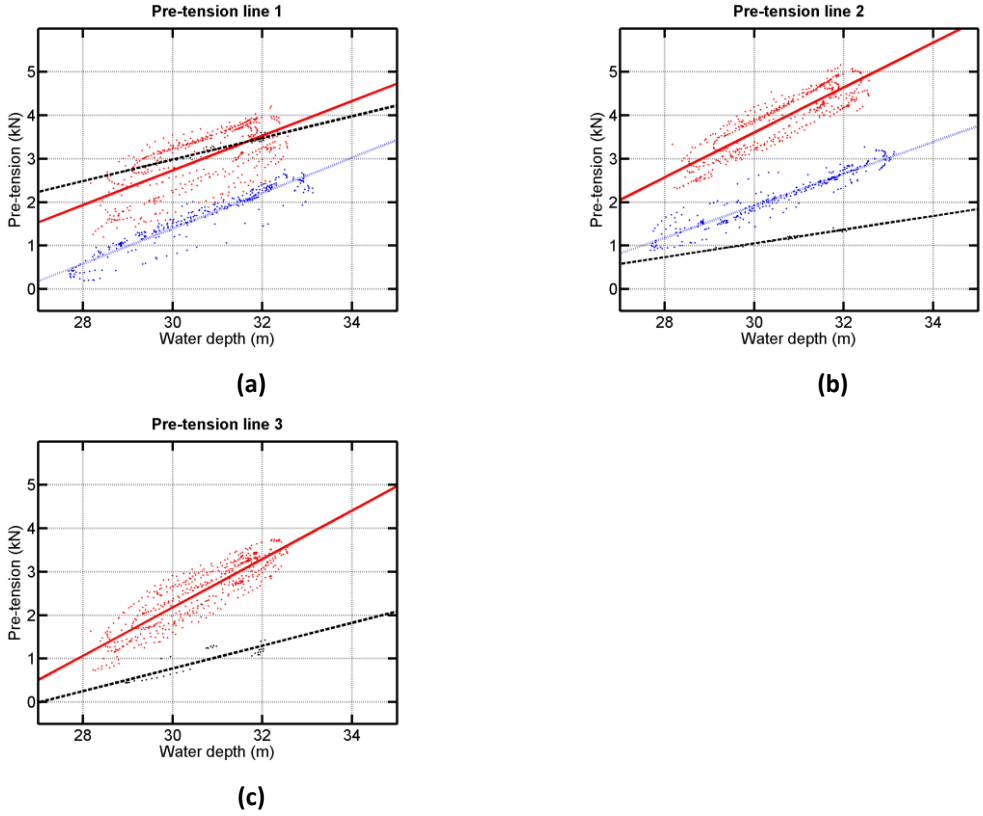

Figure 4.46: Relationship between mooring line pre-tension and water depth in the absence of waves for the different mooring lines for the SWMTF. a) line 1, b) line 2, c) line 3. Red and solid line is for data before anchor drag, blue and dotted line for data after anchor drag, and black and dashed line for the second SWMTF deployment

Table 4.14: Linear fit of the relationship between the pre-tension and static current load and the water depth for the different mooring lines and the different periods of analysis for SWMTF

	First SWMTF deployment				**Second SWMTF**	
linear fit ax+b	Before anchor drag		After anchor drag		**deployment**	
Line	a	b	a	b	a	b
1	0.40	-9.23	0.41	-10.81	0.25	-4.49
2	0.52	-11.91	0.37	-9.10	0.16	-3.69
3	0.56	-14.55	/ no data		0.26	-7.10

A comparison of the mean loads between mooring lines during the same period of analysis would indicate if the mooring system was well balanced and if the loadcells had any offset (Figure 4.47). For the first SWMTF deployment before anchor drag, the mean load was higher in line 2, by approximately 2 kN more than in line 3 and by 0.5 to 1 kN than in line 1. During the first deployment after anchor drag, the mean load was still higher by 0.5 kN in line 2 compared to line 1. During the second deployment, the mean load was similar in line 2 and 3, and significantly higher in line 1, by over 2 kN. The offset could be due to a small mooring imbalance or loadcell calibration.

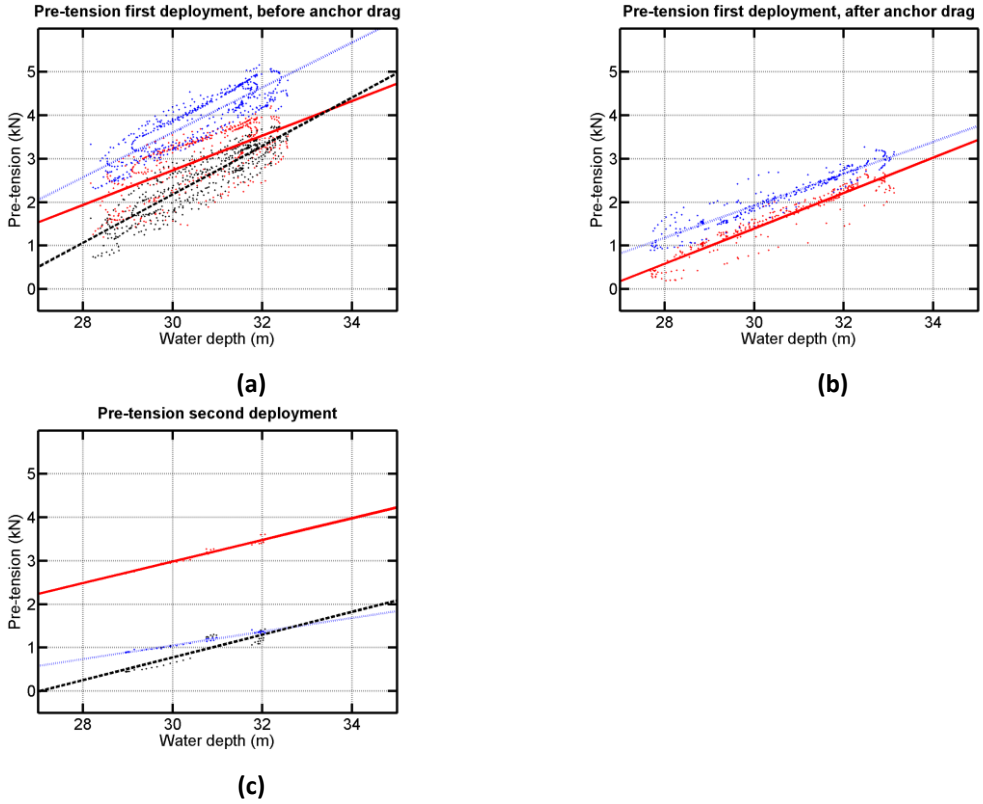

Figure 4.47: Relationship between i) mooring line pre-tension and ii) water depth in the absence of waves for the different period of analysis for the SWMTF. a) first deployment, before anchor drag, b) first deployment, after anchor drag, second deployment. Red and solid line is for data for line 1, blue and dotted line for data for line 2, and black and dashed line for data for line 3

4.2 FaBTest: Bolt-2 LifeSaver device

4.2.1 Data control and analysis methodology

4.2.1.1 Data pre-processing

Mooring load data were provided and pre-processed by Fred Olsen Ltd.

Fred Olsen Ltd provided files in two folders: one for the mooring load data at 200 Hz, one for the position data at 10 Hz. The data were already calibrated by the wave energy company.

The mooring load files contain the time in Matlab format in the first column and the mooring loads in tonnef in the 5 loadcells in the 5 following columns. The mooring load data were converted from tons to kN by multiplying them by a factor of 9.81 kN/tonnef.

A processing routine to calculate summary load data has been developed. For each file, the minimum, mean, maximum and standard deviation of all data were calculated. The length of the data was also saved, because the files were from different durations. The summary data were saved in a Matlab file.

The wave buoy data have been processed with the buoy firmware by the wave buoy manager. The data were saved in a TAB delimited .txt file, with a column for: time at the format DD/MM/YYYY HH:mm, the significant wave height H_S, the maximum wave height H_{max}, the mean wave direction D_{mean}, the spectral peakedness parameter Q_p, the average wave period T_{mean}, the zero-crossing period T_Z, the energy period T_{mm10} and the peak period T_P.

4.2.1.2 Data correction

Mooring load correction

Data were not continuously recorded but only when the monitoring system was turned on. 12,734 datasets have been collected. The length of the datasets was not always the same, but could have been any length below 20 minutes. The measurements being at 200 Hz, the data files have a length equal or below 240,000 points. The distribution of the length of the data files has been plotted in Figure 4.48.

This plot indicates that more than 50 % of the files (6758 files) contain more than 225,000 points. A minority of files (872 files) contains between 25,000 and 225,000 data points. Based on these results, datasets were only considered for further investigations when the length of the data files was over 225,000 points (1,125 s, or 18 minutes 45 seconds). This avoids the comparison of statistical data from files which are 10 times shorter. The statistical data (mean, max, standard deviation, S_{max}) are calculated for the files with a sufficient number of data points.

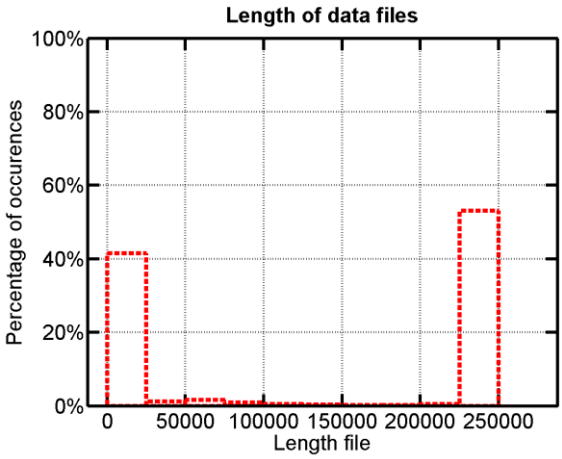

Figure 4.48: Distribution of the length of the Bolt-2 LifeSaver mooring load data files

The original (all datasets) and the selected (sufficiently long) mean load data were plotted. .

Several points had a mean load of 0 kN or below. An outlier point between 10/2012 and 01/2013 had a mean load around 4 kN. After investigating all mooring line mean loads, the following correction was applied: if a mean load was below 5 kN (outlier points), the corresponding statistical load data (mean, max and standard deviation) were removed.

The original and selected maximum loads were plotted in Figure 4.50. Figure 4.50 indicates that most of the outlier points occurred in files considered too short for further analysis.

On mooring lines 3 and 5, a single outlier point was detected on the 12/12/2013 at 21:26 with an amplitude of 243 and 176 kN respectively. On mooring line 2, a single outlier point was detected on the 31/07/2013 at 02:30 with an amplitude of 320 kN These points are not shown in Figure 4.50 for clarity reasons. These points occurred in files containing a sufficient number of points (240,000) for further investigations.

Because these points are isolated, they are not likely to be an extreme mooring load because other high mooring loads would have been observed during the same storm, in the file before or after. The sea states on these days were not known because the wave buoy stopped recording data at end of June 2013. The time series of the dataset containing these mooring loads were individually investigated (Figure 4.51). These investigations concluded that these points did not have any physical meaning and resulted from the temporary malfunctioning of the instrumentation.

These outlier points were removed by applying the following correction: if the maximum load was over 175 kN, the corresponding load data were removed.

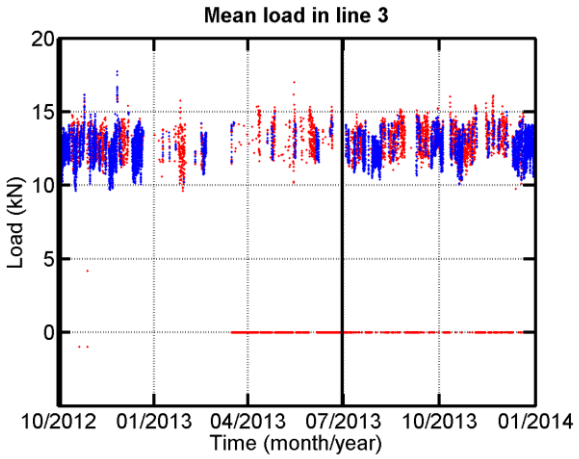

Figure 4.49: Example of summary of mean mooring load data on mooring line 3 at Bolt-2 LifeSaver device(red: all files, blue: files with sufficient number of data points)

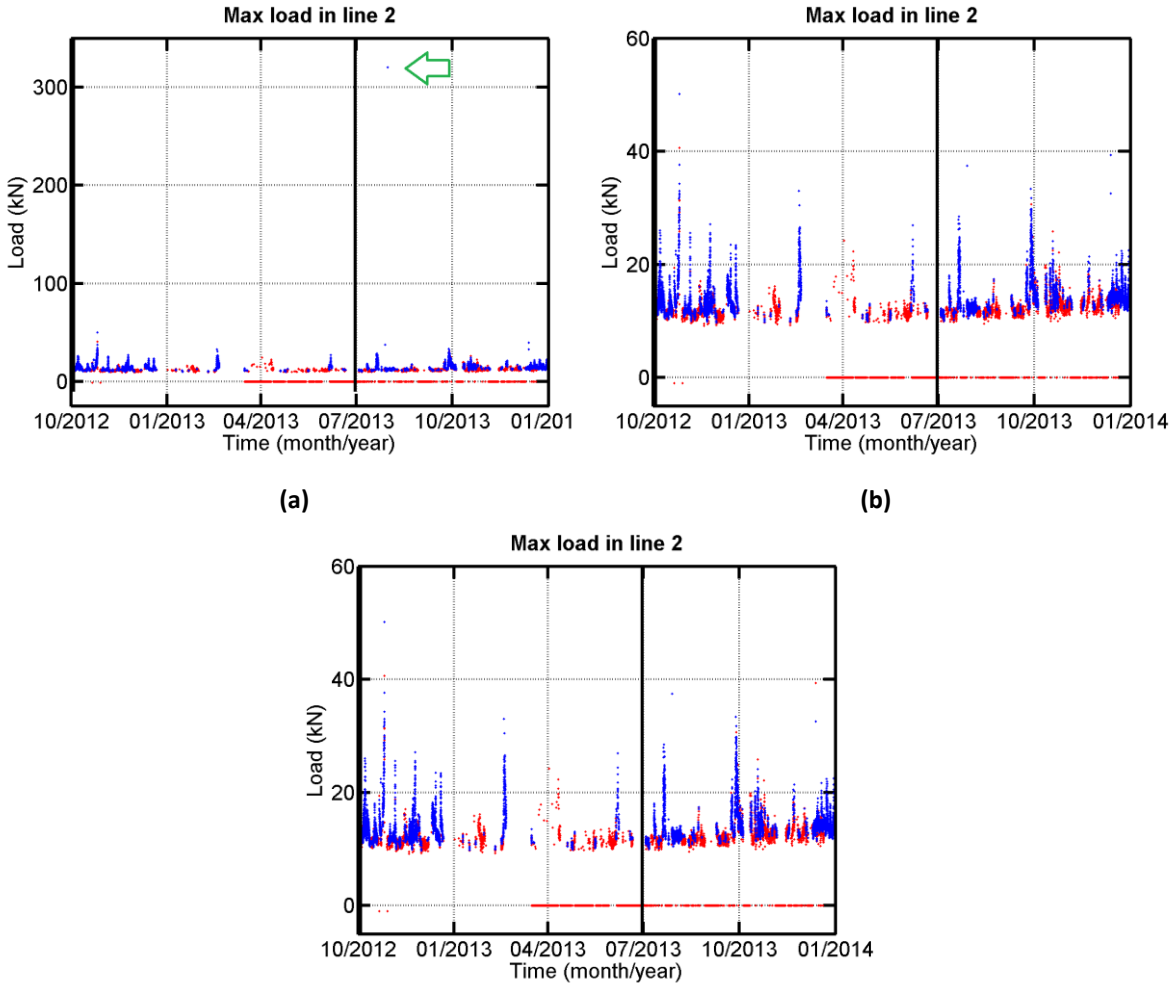

Figure 4.50: Example of a) summary of measured maximum mooring load with a sufficient number of data points on line 2 at Bolt-2 LifeSaver device; b) zoom on these data before (red: all files, blue files with sufficient number of data points) and c) after correction (red: all files, blue: results after correction)

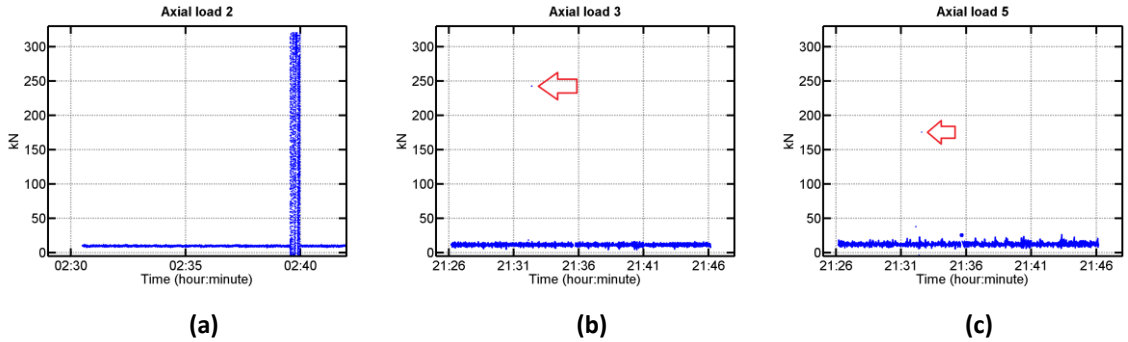

Figure 4.51: Time series of mooring load at Bolt-2 LifeSaver device with outlier points in mooring lines a) 2, b) 3 and c) 5

Wave buoy correction

A basic quality check was applied to the wave buoy data to remove data which have no physical meaning. If H_S was below 0 m, if D_{mean} was below 0° or over 360°, if T_P was below 0 s, or if T_Z was below 0 s, this set of data (H_S, H_{max}, T_P, T_Z, D_P and D_{mean}) was removed.

If H_{max} was negative, this value of H_{max} was removed. Other points were not removed because they were calculated using a spectral method while H_{max} was calculated using a zero-crossing method.

The measured H_S data are plotted in Figure 4.52. One outlier point needed to be removed. If H_S was over 5 m, if H_{max} was over 8 meters, if T_Z was over 10 s, if T_P was over 15 s, the set of data (H_S, H_{max}, T_P, T_Z, D_P and D_{mean}) was removed.

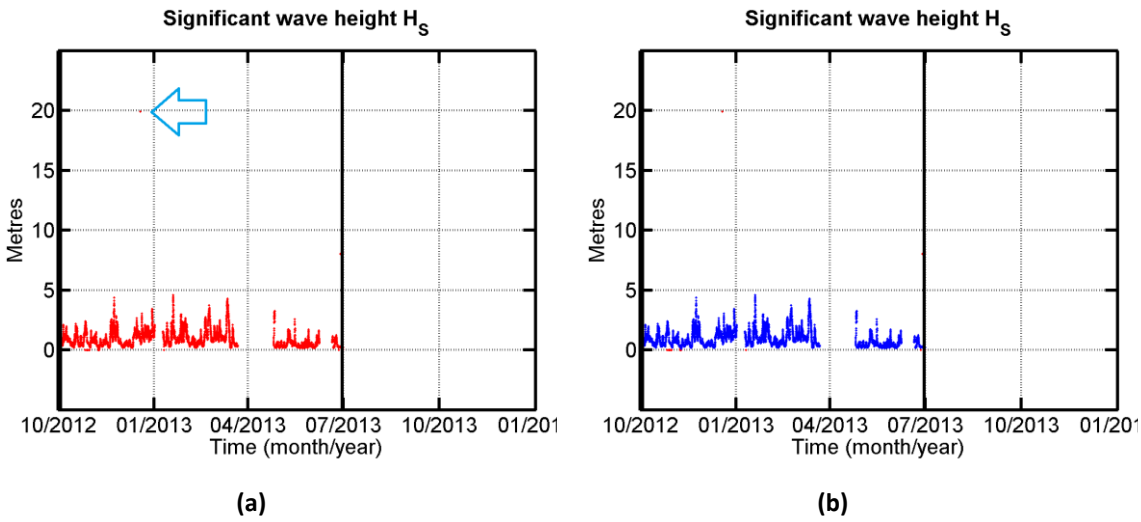

Figure 4.52: H_S measured at FaBTest before a) and after b) correction (blue points: points after correction, red points: points before correction)

4.2.2 Example of time series of data

An example of time series is shown for a 17 minute (1,024 s) dataset for the waves (Figure 4.53a) and 20 minute dataset for the mooring loads (Figure 4.54) and position data (Figure 4.55).

A zoom on all data has been done when a large load occurred to give an example of dynamic behaviour. The wave buoy was more than 300 meters away from the wave energy device so it is difficult to directly relate the wave elevation with the instrumented buoy position because the waves will break or recombine between the wave buoy and the wave energy device.

The quality of the data is at first glance satisfying, for the same reason as for the SWMTF data.

In this example, a peaky load was observed in loadcell 5, and a smaller peak can be observed before the large peak (Figure 4.54). The mooring loads stayed low in loadcells 2 to 4 and were moderate in loadcell 1. The peak load occurred during a large motion to the South-East (Figure 4.55) and upward, and during a large yaw rotation.

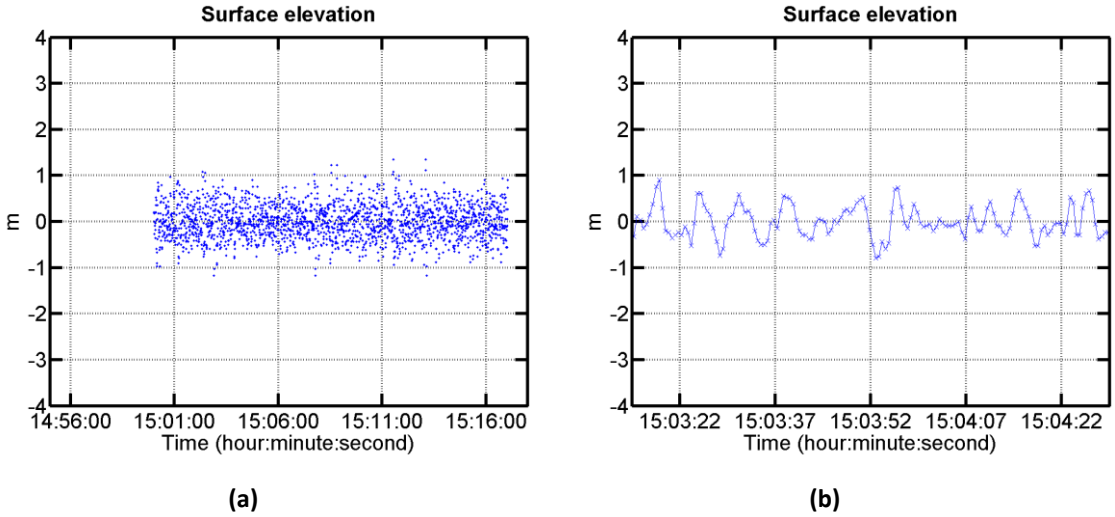

Figure 4.53: Example of a) dataset of wave elevation at the wave buoy and b) 1 minute zoom at FaBTest

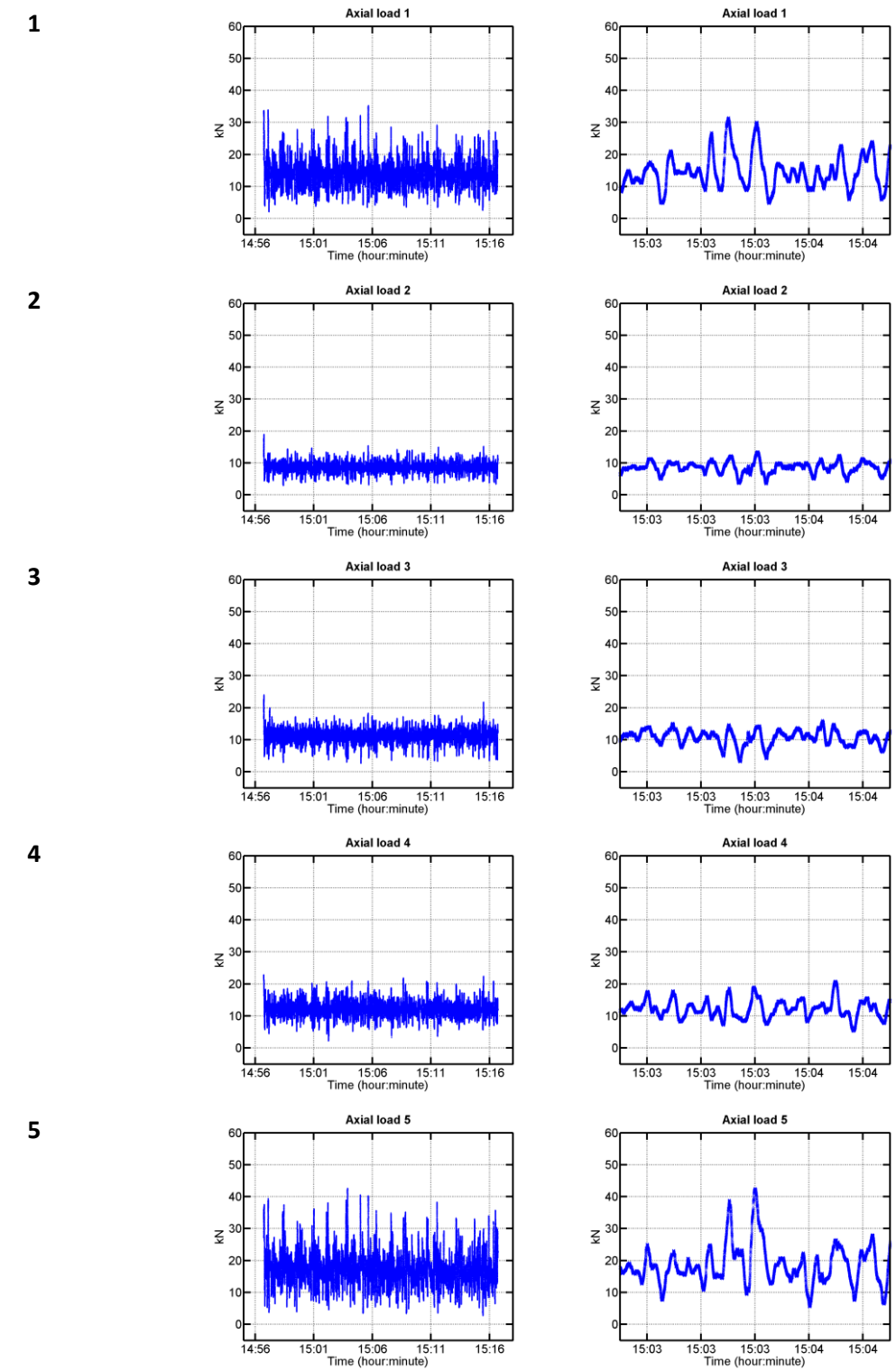

Figure 4.54: Example of dataset of mooring loads in axial loadcells (left) and 1 minute zoom (right) at Bolt-2 LifeSaver device

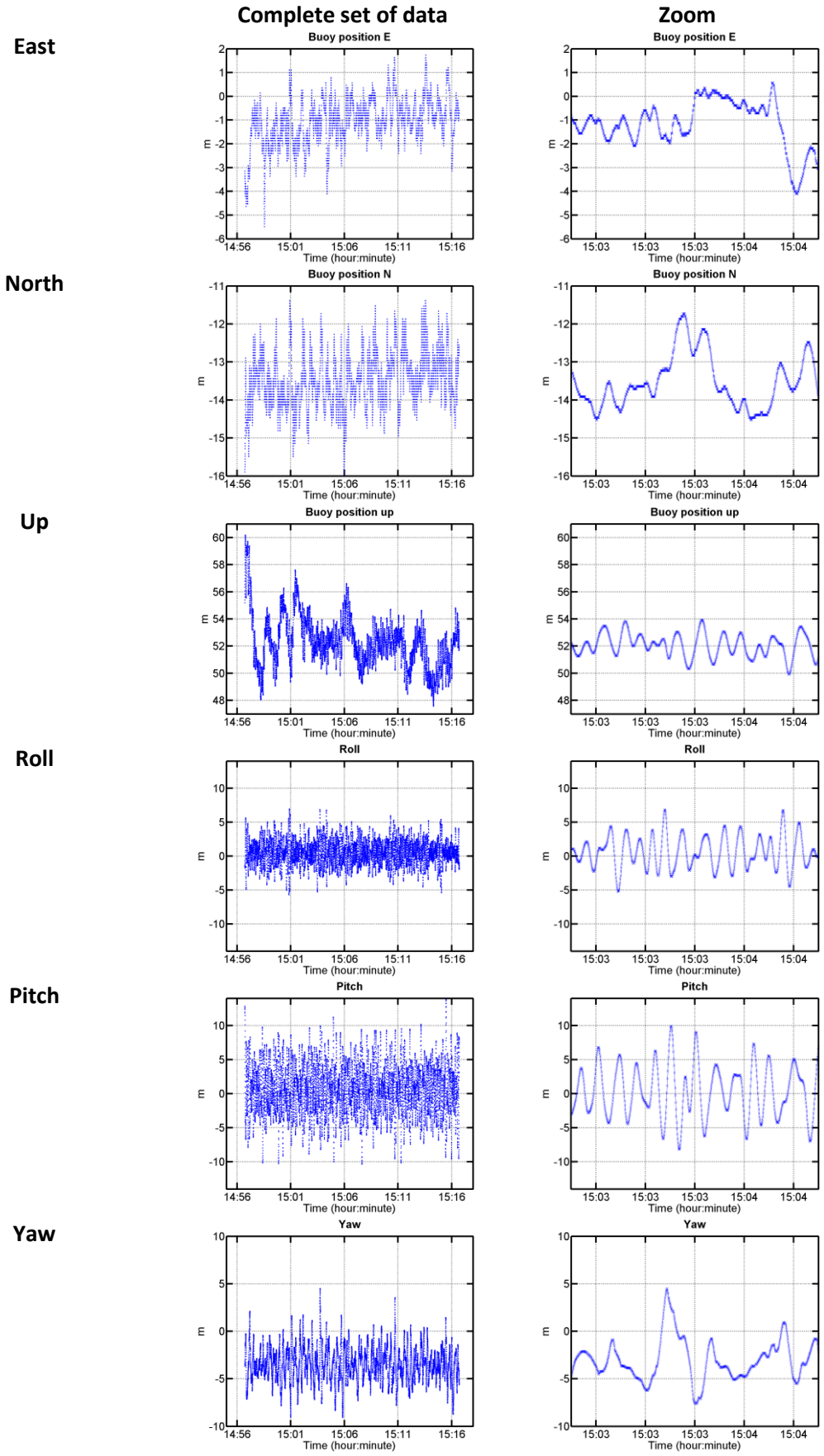

Figure 4.55: Example of a) dataset of Bolt-2 LifeSaver device motion and b) 1 minute zoom

4.2.3 Example of summary data

The summary of the wave conditions and of the mooring data for four representative sea states (Table 4.15) are shown: two storms (Southerly and Easterly), an average day (based on the site scatter diagram), and a calm day.

Table 4.15: Selection of sea states representative of the wave conditions for FaBTest

Wave conditions	Selection
South-Easterly storm	Higher H_S for a South-Easterly storm (D_P < 140°)
Southerly storm	Higher H_S for a Southerly storm (D_P ~ 180°)
Average day	0.5 m < H_S < 1.5 m and 4.5 s < T_P < 6 s
Calm day	Smallest H_S with a sufficient number of mooring load data

Statistical values for the mooring loads and environmental conditions are shown for these four cases in Table 4.16. During the Southerly storm, the amplitude of the maximum mooring loads was the highest in mooring line 5 (42.65 kN), and also high in mooring line 1 (35.34 kN), because both mooring lines are oriented to the South. The standard score of the maximum load is over 4.1 for all mooring lines.

For the Easterly storm, the amplitude of mooring loads was moderately high (< 20 kN) in mooring lines 1 to 3 which are facing the North to the South-East. The standard score of the maximum was high in mooring line 2 (7.27), which is the line facing the waves during this storm.

Data gathered during the moderate swell indicate that the amplitude of the maximum mooring load was relatively high in mooring line 1 (34 kN). The amplitude of this maximum mooring load is actually higher than the amplitude of the maximum mooring load measured for the Easterly storm, with an higher H_S. Standard score of the maximum load was over 7 in mooring line 1.

During the calm day, mooring loads were similar in all mooring lines, with a maximum load in line 1 and 3 (13.1 kN) and standards scores of the maximum between 3.17 and 4.97.

Table 4.16: Example of summary mooring load data for different representative sea states at Bolt-2 LifeSaver device

Stormy day: Southerly storm		**22/11/2012 14:56:43-15:16:43**				
	H_S (m)	4.35	D_P (°)	185	T_P (s)	9.6
		Min	Mean	Max	Std	S_{max}
Load 1 (kN)		2.10	14.15	35.34	4.49	4.72
Load 2 (kN)		2.93	8.68	18.96	1.72	5.96
Load 3 (kN)		2.66	11.10	24.07	2.39	5.43
Load 4 (kN)		2.22	12.19	22.84	2.60	4.10
Load 5 (kN)		2.76	17.45	42.65	5.58	4.52
Length data		240,000				

Average day: moderate swell		**24/11/2012 12:27:19-12:47:19**				
	H_S (m)	1.48	D_P (°)	140	T_P (s)	5.5
		Min	Mean	Max	Std	S_{max}
Load 1 (kN)		7.80	16.25	34.48	2.58	7.08
Load 2 (kN)		5.92	10.83	16.01	1.02	5.07
Load 3 (kN)		6.95	12.84	17.47	1.47	3.14
Load 4 (kN)		5.27	10.87	15.81	1.10	4.49
Load 5 (kN)		6.22	13.27	21.23	1.87	4.26
Length data		240,000				

Stormy day: Easterly storm		**24/11/2012 20:27:33-20:47:33**				
	H_S (m)	2.81	D_P (°)	132	T_P (s)	6.9
		Min	Mean	Max	Std	S_{max}
Load 1 (kN)		3.88	11.38	24.04	2.30	5.49
Load 2 (kN)		3.57	10.52	24.65	1.94	7.27
Load 3 (kN)		4.74	13.06	22.86	2.10	4.67
Load 4 (kN)		1.33	8.76	16.40	1.49	5.13
Load 5 (kN)		2.33	8.63	16.16	1.62	4.66
Length data		240,000				

Calm day		**20/06/2013 15:05:35 -15:25:35**				
	H_S (m)	0.16	D_P (°)	160	T_P (s)	5.7
		Min	Mean	Max	Std	S_{max}
Load 1 (kN)		13.11	14.13	15.20	0.34	3.17
Load 2 (kN)		9.86	10.78	12.12	0.27	4.97
Load 3 (kN)		13.10	14.20	15.57	0.36	3.86
Load 4 (kN)		10.78	11.59	12.56	0.26	3.80
Load 5 (kN)		11.40	13.11	14.57	0.43	3.35
Length data		240,000				

4.2.4 Data summary

The wave and mooring load data presented in this section are the data recorded between the 03/10/2012 and the 30/06/2013 because wave and load data were simultaneously available during most of this period.

These data are used for further analysis in the next chapter and the conditions to select data are summarised in Table 4.17.

Table 4.17: Data used for further analysis of the Fred Olsen Bolt-2 Lifesaver device data

Conditions
03/10/2012 - 30/06/2013
Wave data available
Mooring load data available
Length of mooring load dataset > 225,000 points

4.2.4.1 Environment

A summary of the statistical wave data gathered during the Bolt-2 LifeSaver deployment is plotted in Figure 4.56. Figure 4.57 shows the interpolated wave data when mooring load data were simultaneously available because mooring data were not continuously available.

In both graphs, data before October 2012 are not shown because no mooring load data were available at all. Some wave data are missing from end of March 2013 to middle of April 2013 due to wave buoy faults. If wave data were not available for more than 3 hours, then the interpolated data were removed.

Storms and calm periods can be identified as shown by the H_S and H_{max} parameters (Figure 4.56a-b). T_Z and T_P stay in narrow ranges, with the T_P data being more scattered (Figure 4.56c-d). Two clear wave directions can be identified (Figure 4.56e): waves coming from the East (90-120°), and coming from the South (180-210°). During the period of analysis, waves were more often coming from the South.

Table 4.18 summarises the length of interpolated wave data, the number of storms with H_S over 4 m, the minimum, mean, maximum and standard deviation values measured for H_S, H_{max}, T_Z and T_P and the number of bins populated in the scatter diagram.

Plots showing the wave direction associated with H_S (Figure 4.58a) highlight the two main storm directions, but also show that some sea states with a low H_S were also coming from the North-West, because of locally generated North-West wind sea, in the absence of swell. The waves coming from the South were aligned with mooring line 5. Figure 4.58b indicates that T_P does not seem to be associated with the wave directions. Figure 4.58c shows the number of occurrences of D_{mean} in a given range of direction and confirms that sea states coming from the South were more frequent. Figure 4.58d is a (H_S, T_P) scatter plot and indicates that the most frequent wave conditions were for H_S between 0.5 and 0.75 m and T_P between 6 and 7 s.

Table 4.18: Summary of interpolated wave data from the 03/10/2012 to the 30/06/2013 at FaBTest when mooring load data are available and the datasets have a sufficient length

Properties			**Value**	
Number wave data points			4878	
Equivalent time (days)			45	
Number of bins populated on the scatter diagram			44	
Number of storms with H_S > 4 m			1	
Number of data points with H_S > 4 m			4	
	Minimum	Mean	Maximum	Std
H_S (m)	0.1562	1.0105	4.3493	0.6164
H_{max} (m)	0.3125	1.6196	6.9961	0.9369
T_Z (s)	2.4435	4.5275	7.3822	0.8651
T_P (s)	1.9550	6.6185	12.5900	1.9523

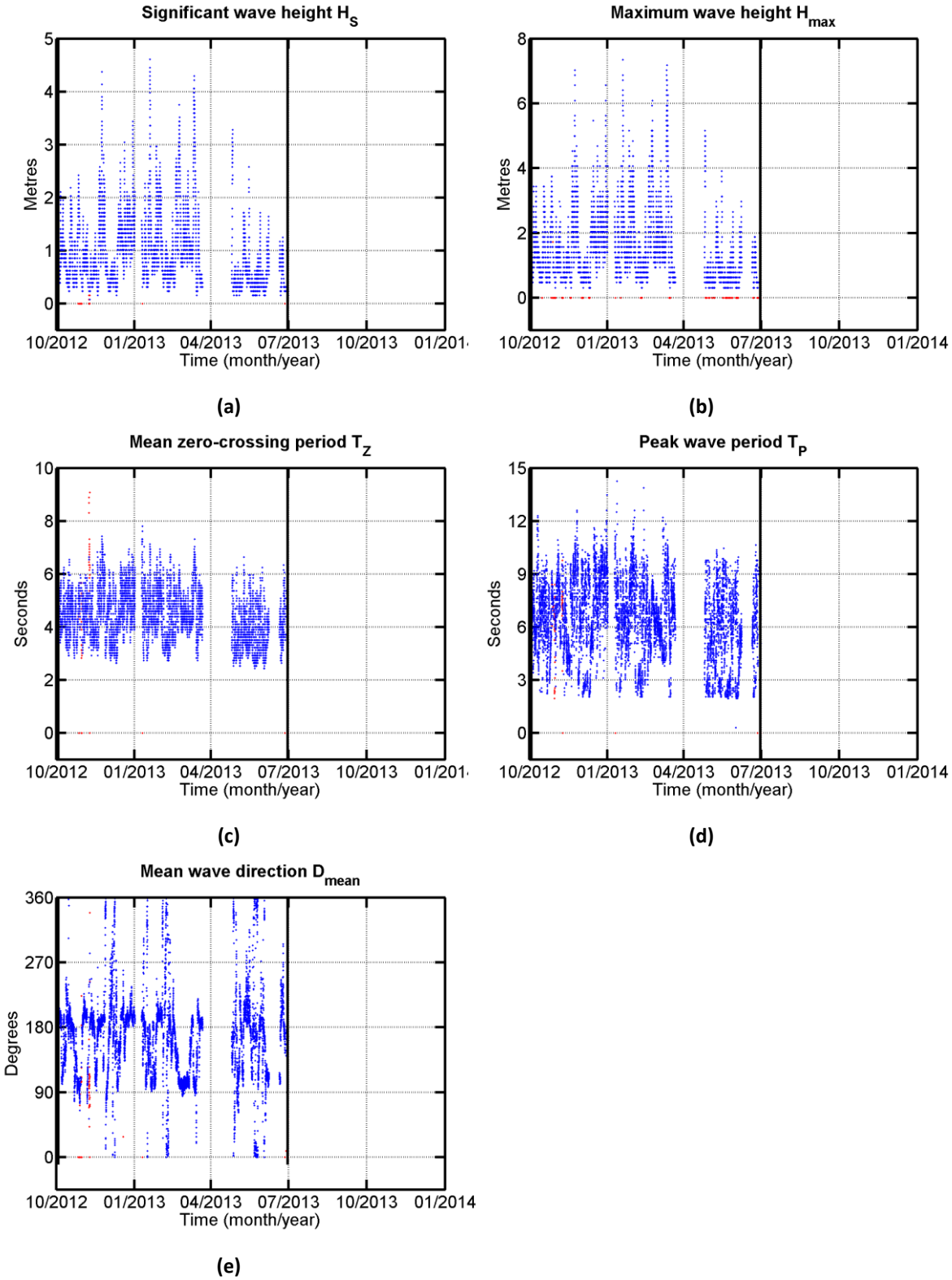

Figure 4.56: Summary of the wave data recorded by the FaBTest wave buoy after correction from the 03/10/2012 to the 30/06/2013 (red dots indicate points which have been removed during the correction). Black vertical line: end of wave data availability

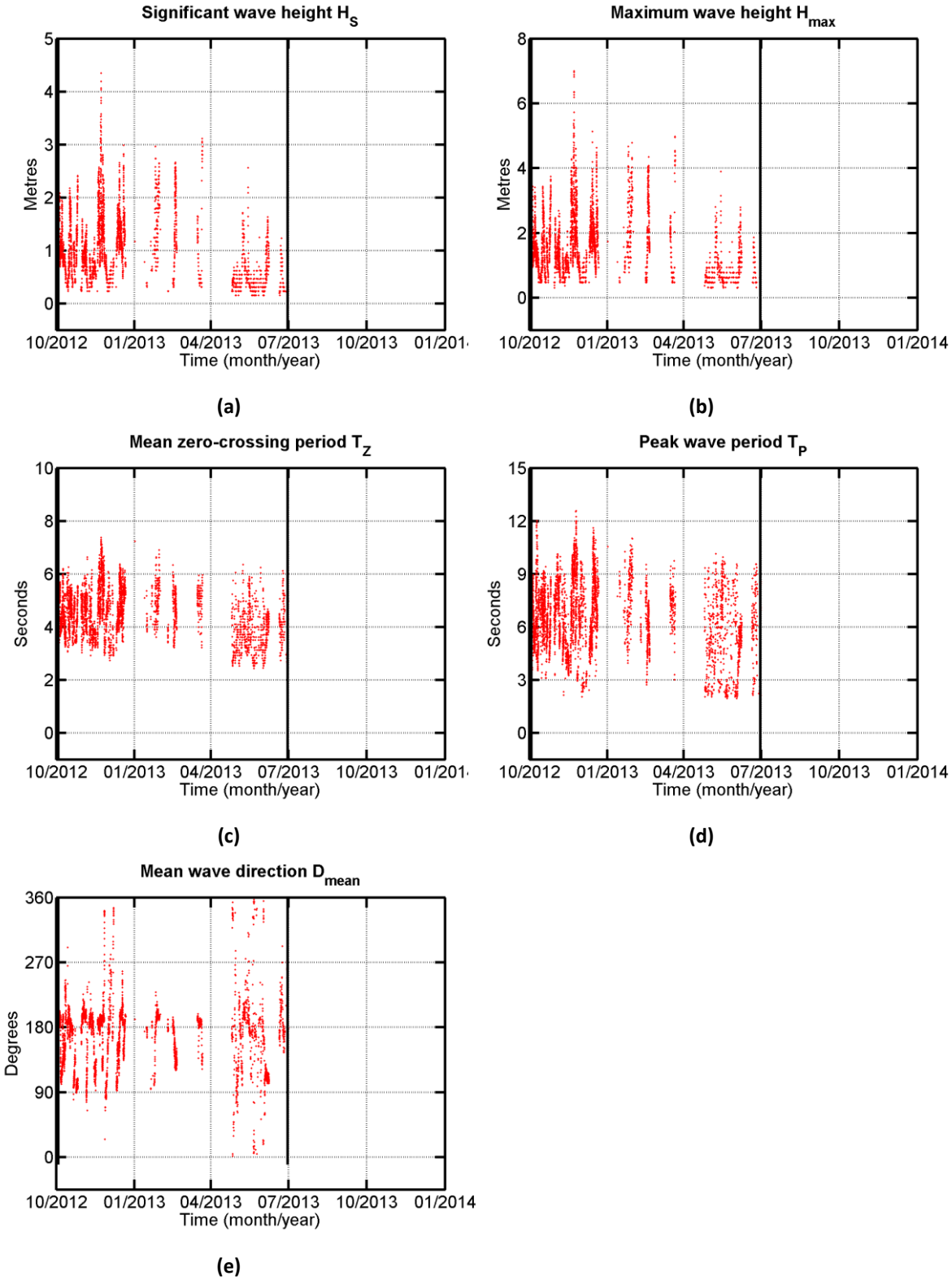

Figure 4.57: Summary of the interpolated wave data at FaBTest after correction. Black vertical line: end of wave data availability

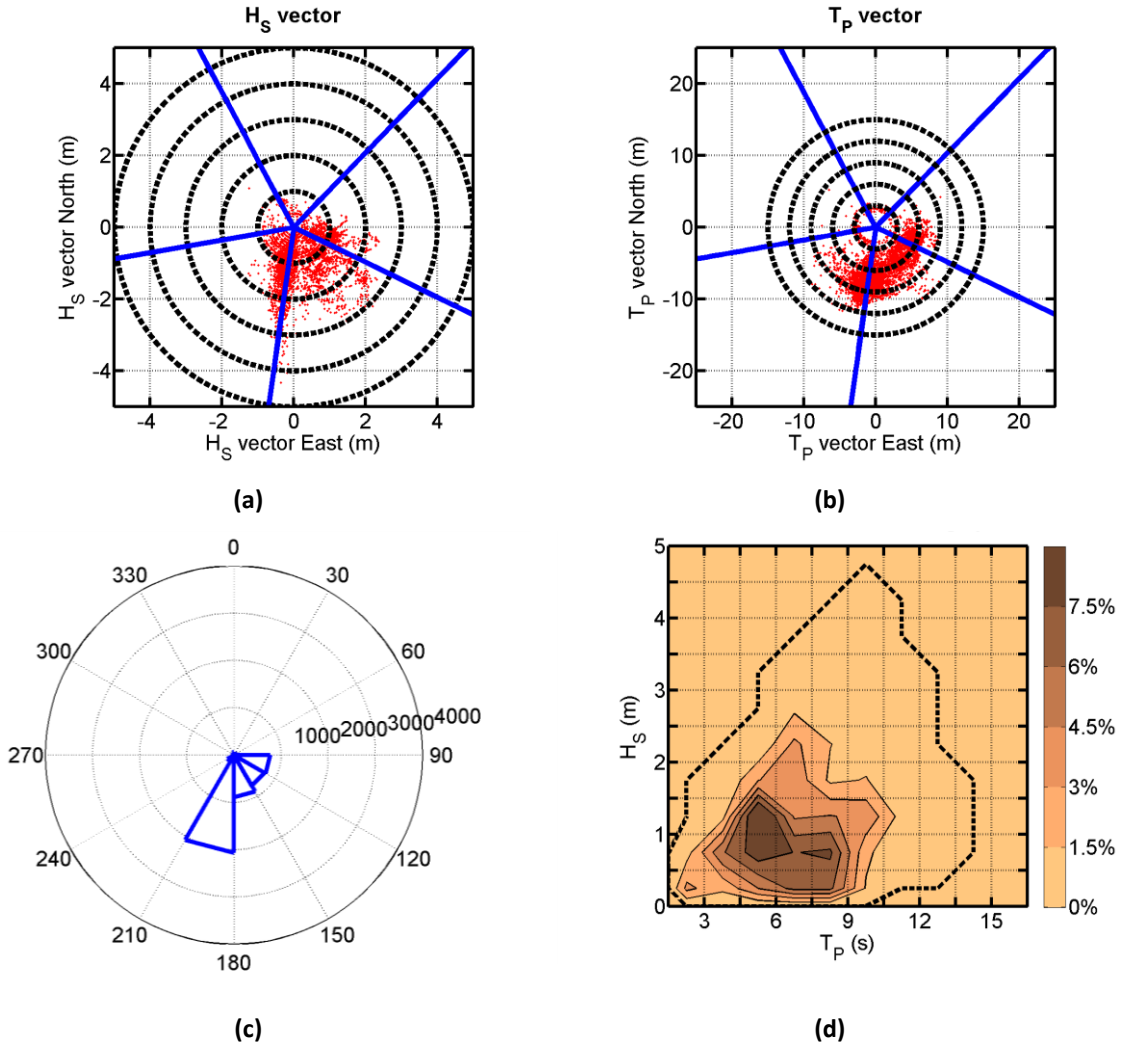

Figure 4.58: Presentation of the FaBTest correlation between interpolated wave parameters: a) D_{mean} and H_S, b) D_{mean} and T_P, c) distribution of D_{mean}, d) H_S and T_P; in a-b: Blue lines indicate the mooring line orientation. In d: Black dotted line: external contour line, no occurrences were recorded outside this line. The wave direction is the direction from which the waves are coming.

4.2.4.2 Mooring load data

Summaries of the maximum (Figure 4.59), mean (Figure 4.60), standard deviations (Figure 4.61) and standard score of the maximum (Figure 4.62) loads have been plotted for each loadcell.

Line 1 and 5 are experiencing the highest mooring load (up to 90 kN) because they are facing the waves. The minimum breaking load (MBL) of the mooring is 672 kN, so the maximum mooring loads are safely (7.4 times) below the breaking limit of the mooring line. The mean loads were in the same order of magnitude in the different mooring lines, mainly varying with the water level. The standard scores of the maximum load were small (< 10) except for some outlier points.

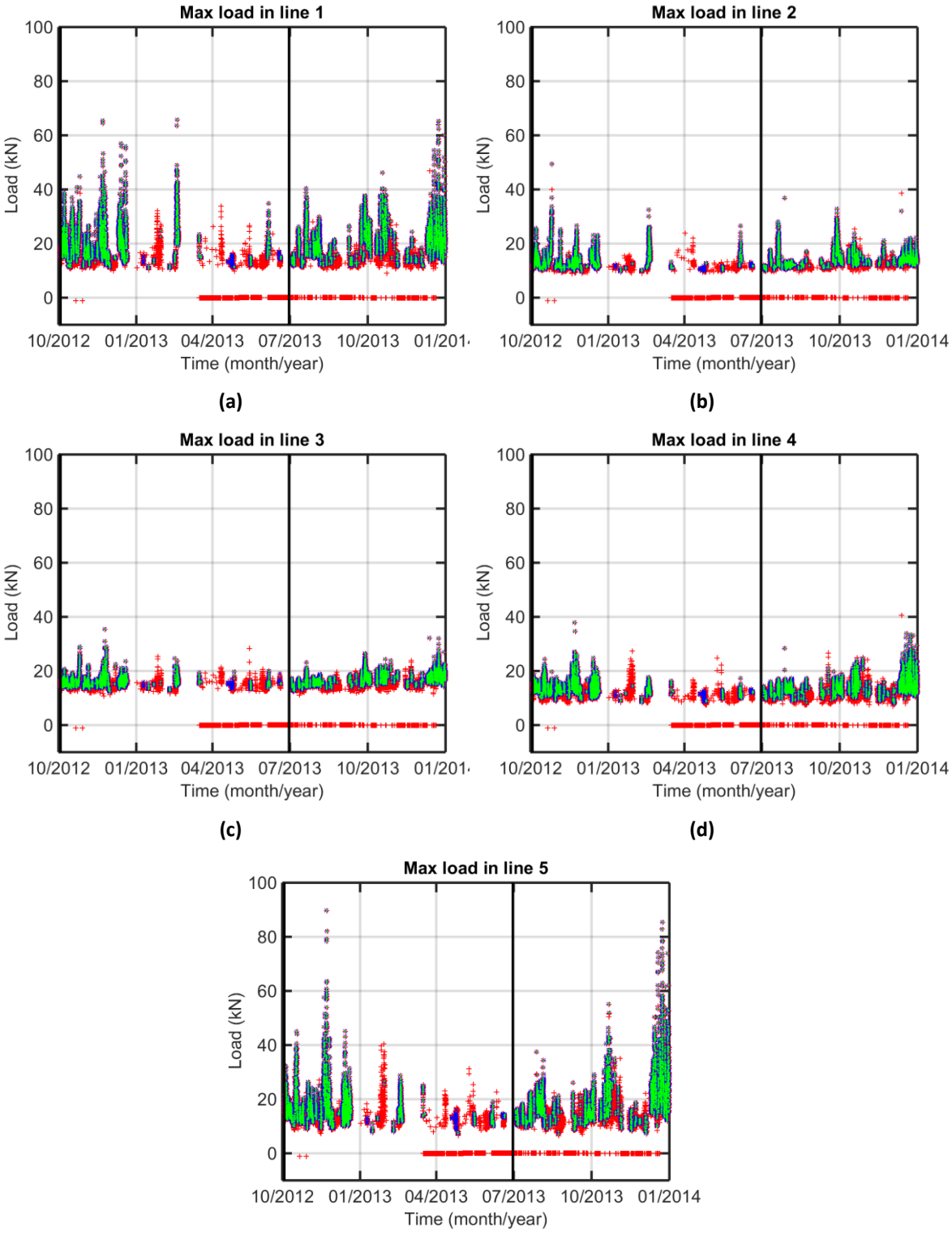

Figure 4.59: Maximum loads measured by the five inline loadcells (a-e) of Bolt-2 LifeSaver device. Black vertical line: end of wave data availability. Red points: all data points, blue data points: files with a sufficient length, green data points: files with a sufficient length and with wave data available

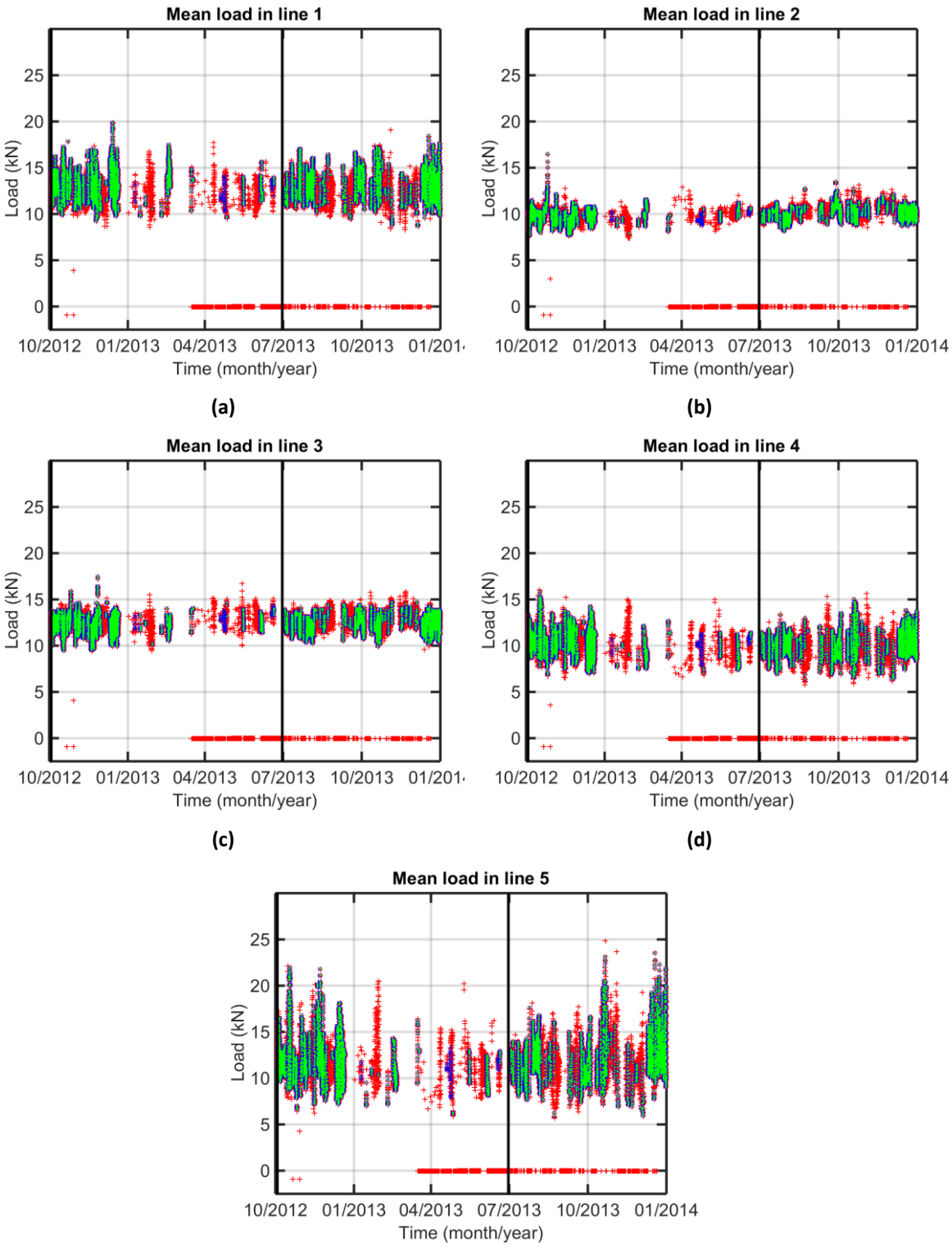

Figure 4.60: Mean loads measured by the five inline loadcells (a-e) of Bolt-2 LifeSaver device. Black vertical line: end of wave data availability. Red points: all data points, blue data points: files with a sufficient length, green data points: files with a sufficient length and with wave data available

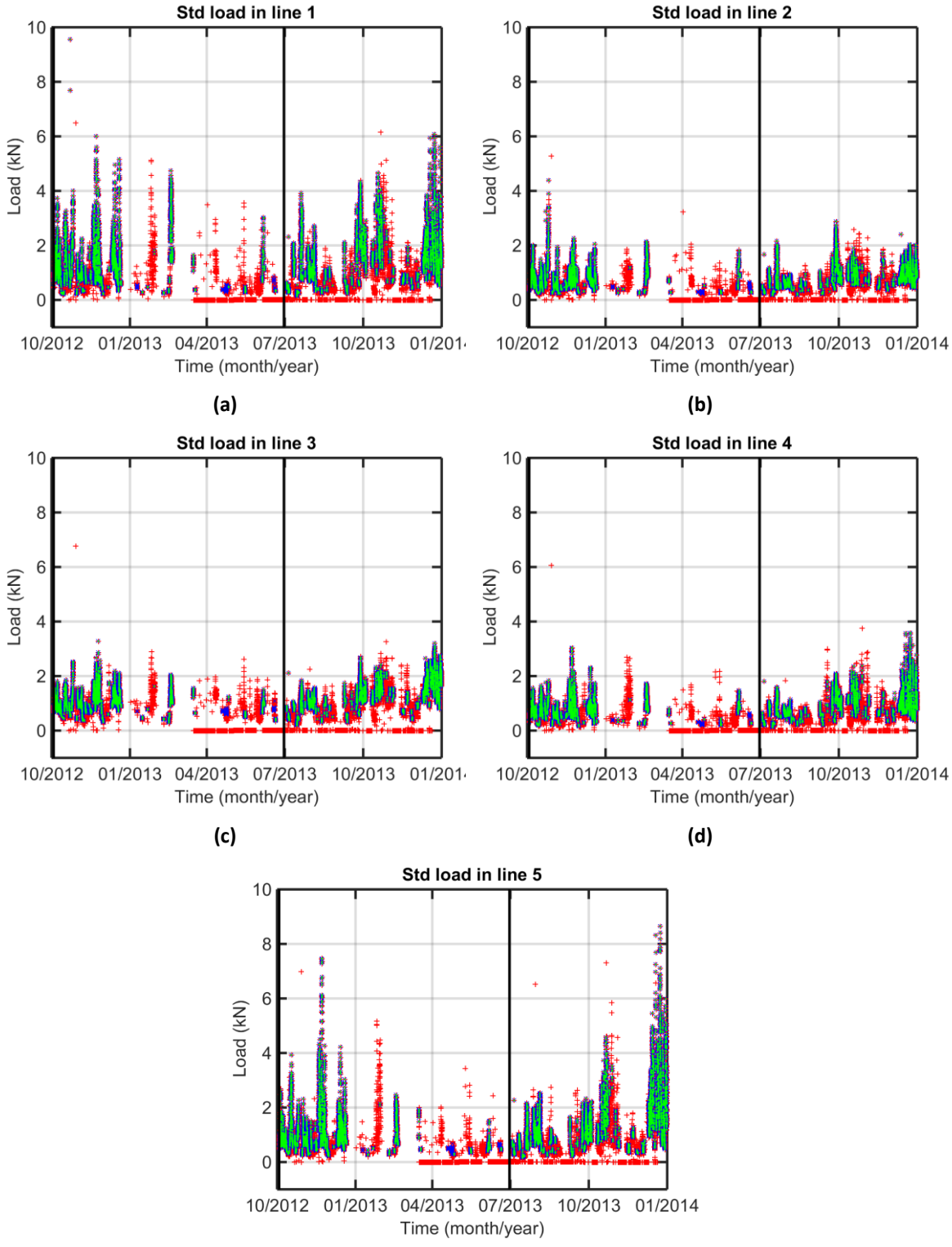

Figure 4.61: Standard deviations of the mooring loads measured by the five inline loadcells (a-e) of Bolt-2 LifeSaver device. Black vertical line: end of wave data availability. Red points: all data points, blue data points: files with a sufficient length, green data points: files with a sufficient length and with wave data available

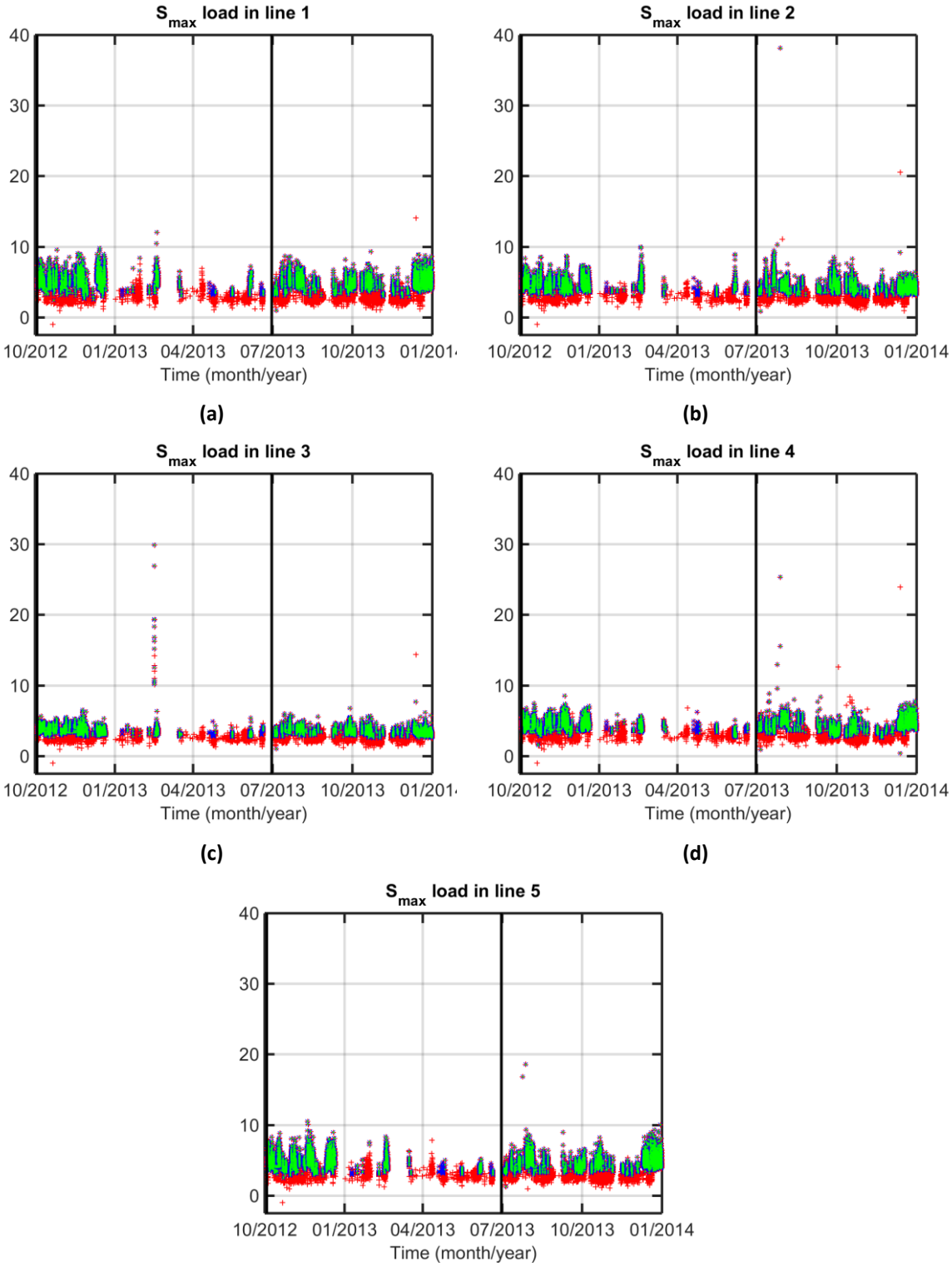

Figure 4.62: Standard scores of the maximum mooring loads measured by the five inline loadcells (a-e) of Bolt-2 LifeSaver device. Black vertical line: end of wave data availability. Red points: all data points, blue data points: files with a sufficient length, green data points: files with a sufficient length and with wave data available

The mean load variations are summarised in Table 4.19. The variations are similar in all mooring lines, with slightly higher maximum values in line 1 and 5, due to the variations caused by storm events.

The maximum load event in each mooring line has been identified in Table 4.20. The dates of occurrence of these events, as well as the corresponding sea states, are also summarised. The highest mooring load was observed on mooring line 5, followed by mooring 1 and then 2. The maximum mooring loads in line 1 to 3 occurred for storms with H_S below 3 m with waves coming from the East or South-East. The maximum loads in line 4 and 5 occurred during the same storm with H_S over 3 m and waves coming from the South.

Table 4.19: Variations of the mean mooring load in the five mooring lines at Bolt-2 LifeSaver device

Line	Min (kN)	Mean (kN)	Max (kN)	Std (kN)
1	9.4	13.5	20.2	1.7
2	7.8	10.0	16.7	0.9
3	9.6	12.4	17.7	1.0
4	7.0	10.6	16.1	1.5
5	6.2	12.2	22.3	2.5

Table 4.20: Maximum measured mooring load in the five mooring lines at Bolt-2 LifeSaver device

Line	Amplitude (kN) / % of MBL	Date	Time beginning dataset	H_S (m)	T_P (s)	D_{mean}(°)
1	66.8/10%	18/02/2013	05:18:23	2.39	7.3	126
2	50.2/7%	26/10/2012	08:39:35	2.20	8.3	107
3	36.0/5%	24/11/2012	20:47:34	2.72	7.2	139
4	38.6/6%	22/11/2012	11:56:47	3.37	9.3	188
5	91.2/14%	22/11/2012	11:56:47	3.37	9.3	188

The distributions of mean, maximum, standard deviations and standard scores of the maximum loads are plotted in Figure 4.63 and Figure 4.64. The distributions of the mean loads are centred between 10 and 12.5 kN for line 2, 4 and 5 and between 12.5 and 15 kN for mooring lines 1 and 3. In mooring lines 2 to 4, most of the maximum mooring loads are below 20 kN, while in mooring line 1 and 5 approximately 35% and 25% respectively of the maximum mooring loads are over 20 kN. For all loadcells, the standard score of the maximum is usually below 10 and distributions are centred between 4 and 5 for line 1 and 5, and between 3 and 4 for line 2 to 4.

The amplitude of the maximum mooring load for each loadcell and for each range of sea state has been plotted in Figure 4.65. The highest values of mooring loads have been measured in line 1 and 5, for the highest H_S and for an intermediate value of H_S (1.5 - 2.5 m) with T_P between 3 and 6 s. In mooring lines 2 and 3, the highest mooring loads were measured for similar combination of H_S/T_P. In line 4, the highest mooring loads were measured for T_P between 7.5 and 9 s and H_S over 2.5 m.

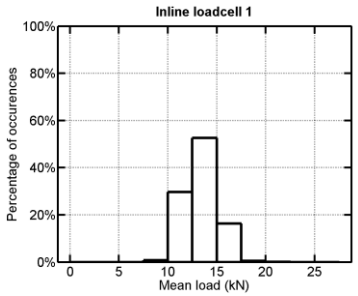
Inline loadcell 1
Percentage of occurences
100%
80%
60%
40%
20%
0%
0
5
10
15
20
25
Mean load (kN)

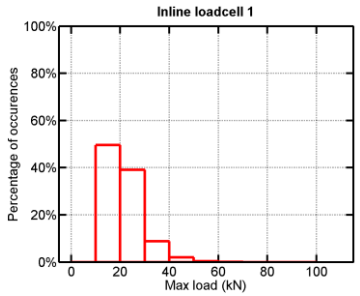
Inline loadcell 1
Percentage of occurences
100%
80%
60%
40%
20%
0%
0
20
40
60
80
100
Max load (kN)

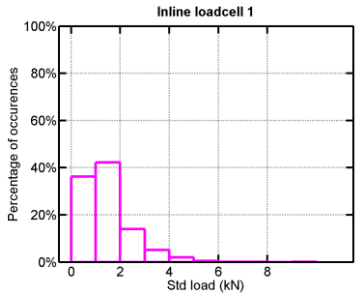
Inline loadcell 1
Percentage of occurences
100%
80%
60%
40%
20%
0%
0
2
4
6
8
Std load (kN)

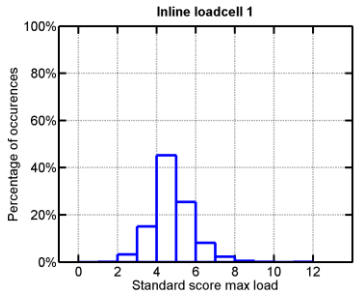
Inline loadcell 1
Percentage of occurences
100%
80%
60%
40%
20%
0%
0
2
4
6
8
10
12
Standard score max load

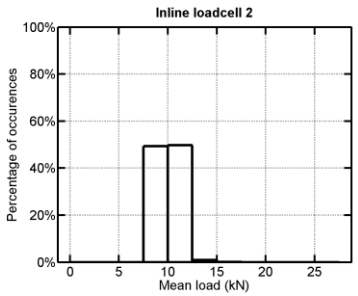
Inline loadcell 2
Percentage of occurences
100%
80%
60%
40%
20%
0%
0
5
10
15
20
25
Mean load (kN)

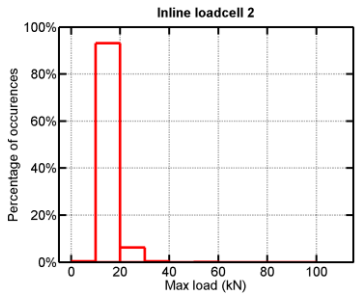
Inline loadcell 2
Percentage of occurences
100%
80%
60%
40%
20%
0%
0
20
40
60
80
100
Max load (kN)

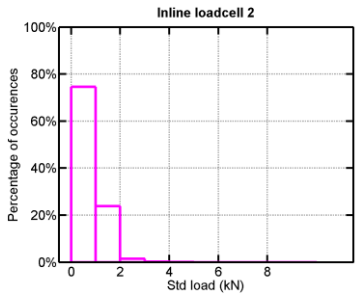
Inline loadcell 2
Percentage of occurences
100%
80%
60%
40%
20%
0%
0
2
4
6
8
Std load (kN)

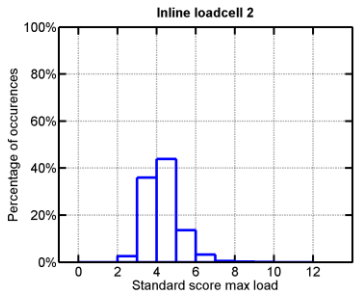
Inline loadcell 2
Percentage of occurences
100%
80%
60%
40%
20%
0%
0
2
4
6
8
10
12
Standard score max load

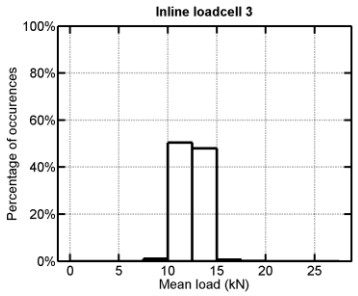
Inline loadcell 3
Percentage of occurences
100%
80%
60%
40%
20%
0%
0
5
10
15
20
25
Mean load (kN)

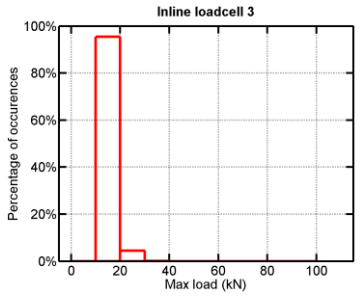
Inline loadcell 3
Percentage of occurences
100%
80%
60%
40%
20%
0%
0
20
40
60
80
100
Max load (kN)

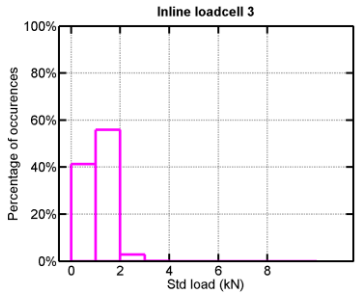
Inline loadcell 3
Percentage of occurences
100%
80%
60%
40%
20%
0%
0
2
4
6
8
Std load (kN)

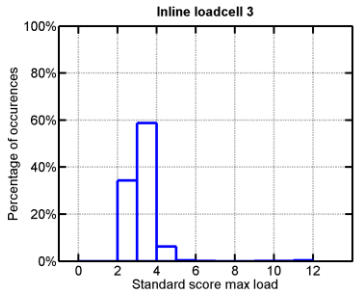
Inline loadcell 3
Percentage of occurences
100%
80%
60%
40%
20%
0%
0
2
4
6
8
10
12
Standard score max load

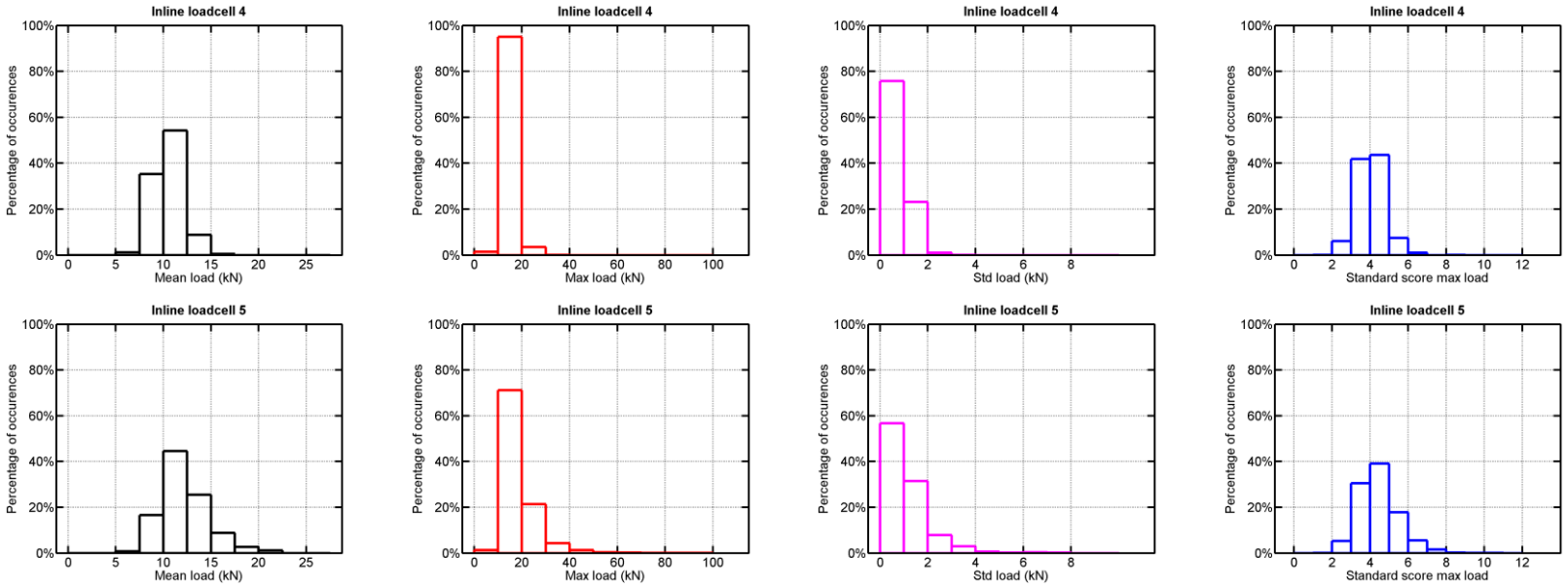

Figure 4.63: Distribution of mean (left), maximum (middle left), standard deviation (middle right) and standard score of the maximum mooring loads (right) in the five loadcells (top to bottom) of Bolt-2 LifeSaver device.

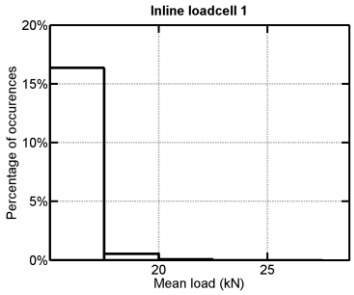

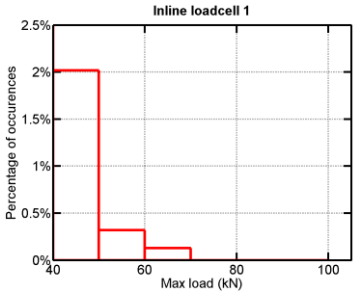

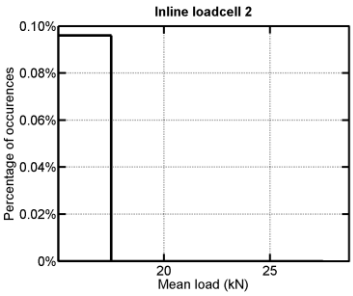

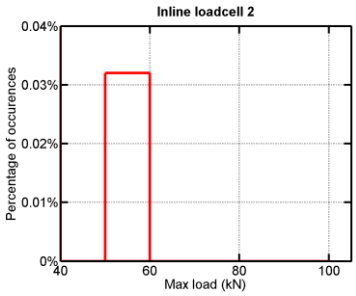

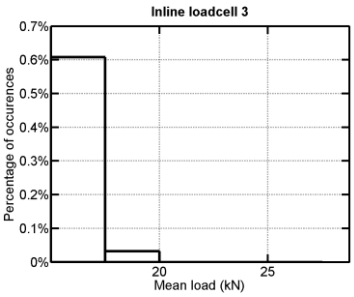

/ no data over 40 kN

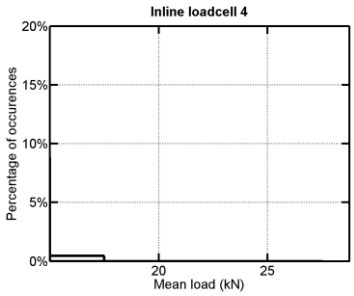

/ no data over 40 kN

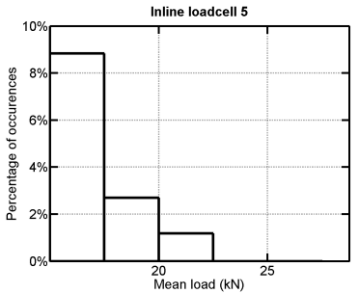

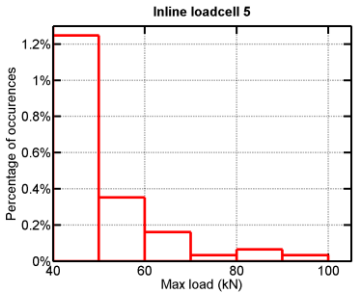

Figure 4.64: Zoom on the highest values (> 15 kN and > 40 kN respectively) for the distributions of mean (left) and maximum mooring load (right) in the five loadcells (top to bottom) of Bolt-2 LifeSaver device.

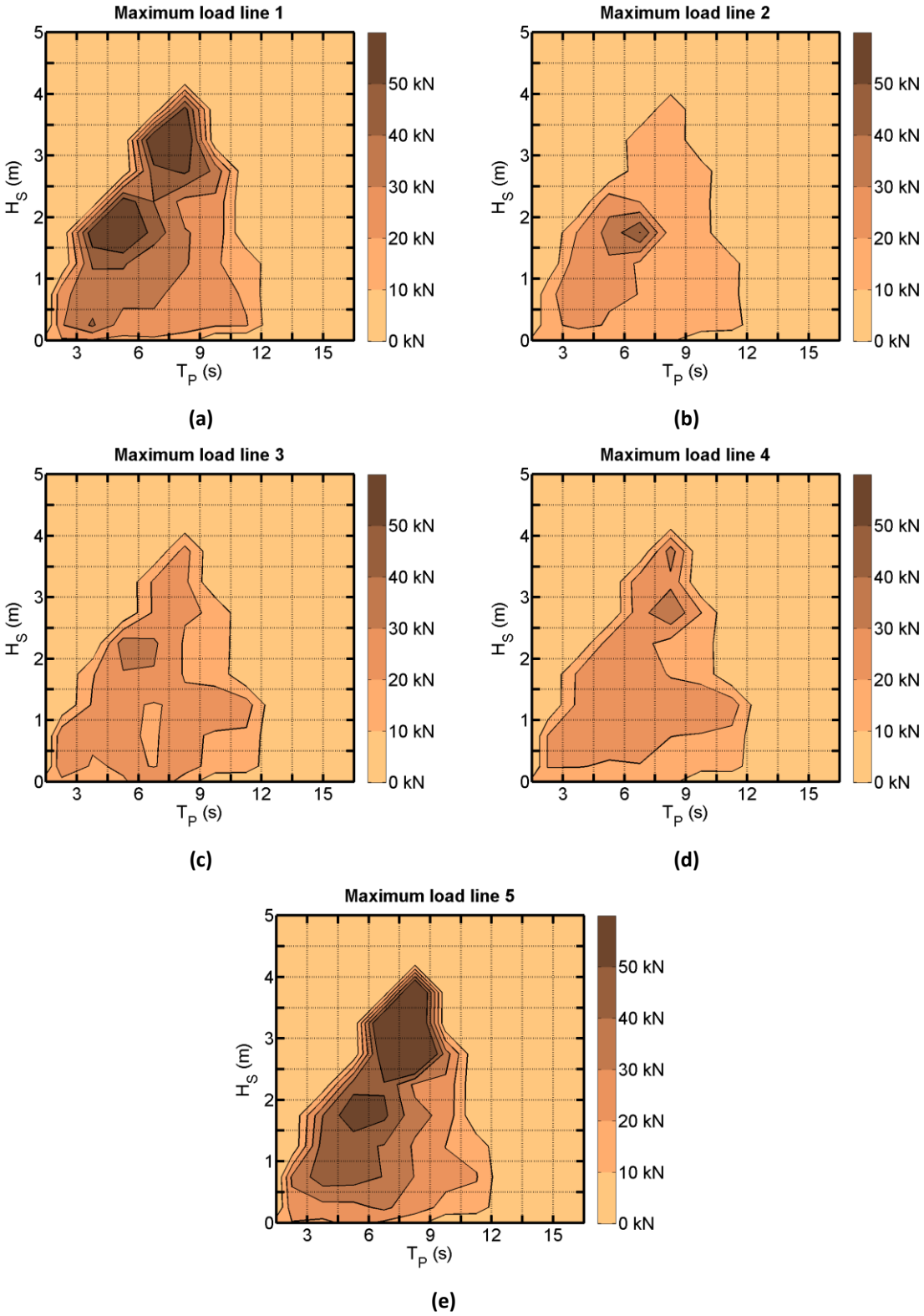

Figure 4.65: Maximum mooring loads and associated wave climate (H_S, T_P) for Bolt-2 LifeSaver device for the different mooring lines (a-e).

Chapter 5. Detection of peak mooring loads and analysis of associated environmental conditions

In this chapter, the data which have been collected at both facilities and presented in the previous chapter are used to assess which environmental conditions are more frequently associated with peak mooring loads. The considered environmental conditions are the significant wave height H_S, the peak period T_P, the peak direction D_P, the current speed C (which incorporates the tidal current and is calculated depending on tidal direction) and the water level h.

The environmental conditions have been assessed in the previous chapter and will be used as a reference. These conditions will be further referred to as the "general environmental conditions".

In this chapter, peak mooring loads are identified; their corresponding environmental conditions are recorded; the environmental conditions associated with peak mooring loads are compared with the general environmental conditions.

The joint percentage of occurrences of the wave conditions associated with peak mooring loads $H_{S\ peak}$ and $T_{P\ peak}$ is compared with the joint percentage of occurrences of the general wave conditions H_S and T_P. The direction D_P of the general wave conditions is also compared with the direction of the waves associated with peak mooring loads $D_{P\ peak}$, and with the mooring line orientation.

In addition, when available, the joint percentage of occurrences of the tidal conditions associated with peak mooring loads C_{peak} and h_{peak} is compared with the joint percentage of occurrences of the general tidal conditions C (current velocity) and h (water depth). Similarly, the directionality and amplitude of the general tidal conditions is compared with the directionality of the tidal conditions associated with peak mooring loads.

For each sea state, the largest amplitude of the peak mooring loads is assessed. The value of the mean load when a peak load occurs is also examined in combination with the associated wave and current directions. The distribution of the peak mooring load and of their mean load is assessed.

5.1 Detection of peak mooring loads

The time series presented in the previous chapter indicate that some mooring loads are sudden and their amplitude is large compared to the other mooring loads at this time.

In order to determine if a dataset contains peak mooring loads, a systematic statistical approach is used rather than a long and computer-intensive investigation of time series. Two factors were introduced:

- The minimum tension threshold τ is used to validate that these mooring loads have sufficiently large amplitudes to be potentially harmful either to the survivability or to the fatigue.
- In addition, the peak mooring load factor *K* is introduced to isolate datasets containing mooring loads which are significantly higher than other mooring loads in the same period of time. This parameter checks that the peak load is the result of a dynamic behaviour, and not from an increase in load due to slow second order motion. In addition, this parameter assesses the non-linearity of the peak mooring load.

Sudden and large mooring loads are characteristics of snap loads. However, before snap loads, the mooring line becomes slack. This methodology does not check the line slackness. That is why the author chooses the terminology “peak mooring loads” instead of “snap loads”. It is actually difficult to check that the mooring line becomes slack because of offsets in the mooring loadcells.

The peak mooring loads are also not called “extreme mooring loads”, as extreme mooring loads are expected to be associated with extreme sea states, such as a 10-year return period sea state. Because of the short duration of the sea trials, it was unlikely to observe the behaviour of the mooring system under extreme conditions.

For each mooring line and each dataset, *K* is compared to the standard score S_{max} of the mooring load (defined in Eq. 4.4) while τ is compared to the maximum mooring load. An example of comparison of *K* and τ is shown in Figure 5.1 for different time series datasets in different sea conditions for mooring line 1 (the same datasets were used in the previous chapter in 4.1.3. to show statistical data for different typical sea states). In this example and following the methodology described above, a peak mooring load was detected only in Figure 5.1a.

a) Stormy day: Southerly storm

17/11/2010 02:00-02:10

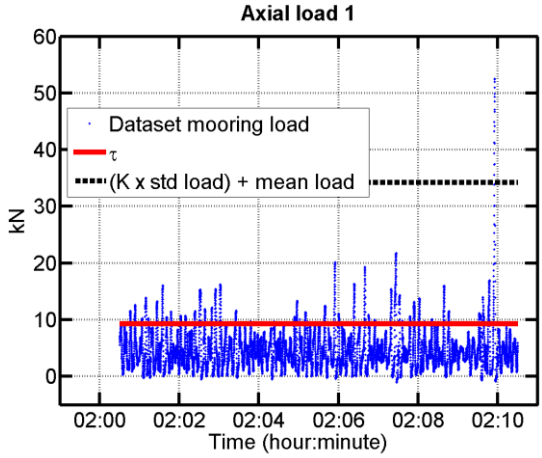

c) Average day: Southerly swell

02/10/2010 01:10-01:20

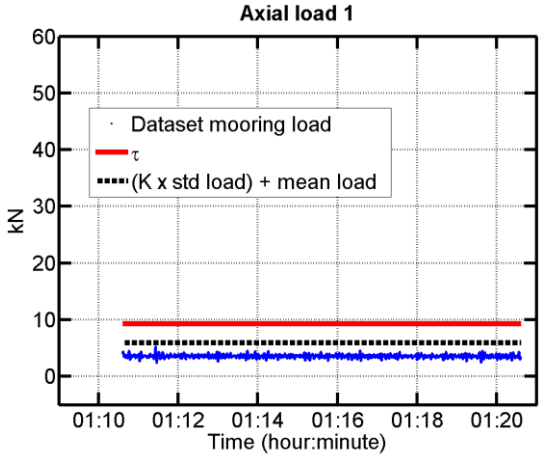

b) Stormy day: Easterly storm

09/10/2010 09:30-09:40

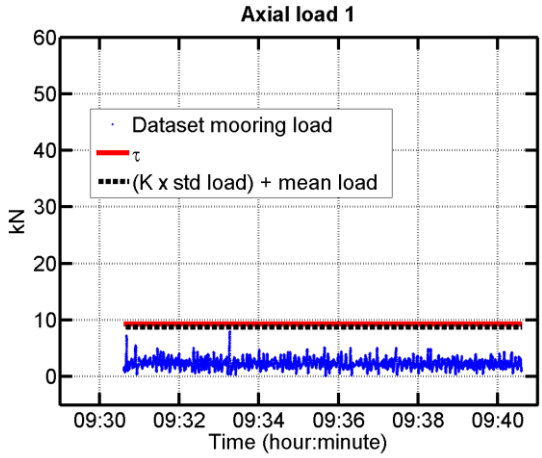

d) Calm day: virtually no waves

22/10/2010 13:40-13:50

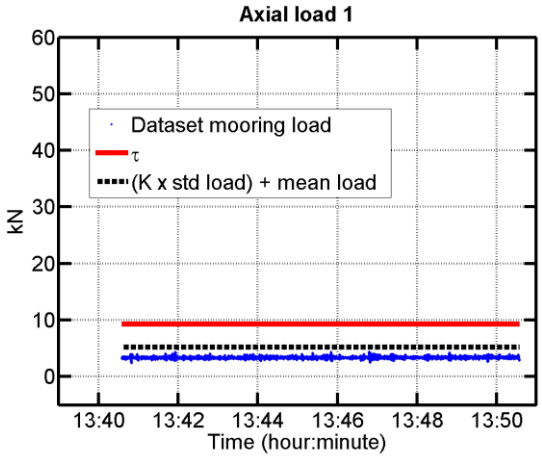

Figure 5.1: Example of detection of peak mooring loads at SWMTF on mooring line 1 for four different datasets representative of four different sea states: comparison of *K* and τ with the maximum load and the standard score of the maximum load respectively

The choice of K and τ changes the number of datasets considered as containing peak mooring loads. In Table 5.1, the number of datasets considered as containing peak mooring loads was calculated for different values of K and τ. The larger the K and τ values, the less datasets of mooring loads are identified as containing peak mooring loads. On the contrary, if τ is set to 0 kN and K to 0, this means that all datasets are defined as containing peak mooring loads. Each factor individually allows a drastic reduction of the number of datasets of interest.

For this study and based on this table τ and K values were chosen at τ equal to three times the average of the mean loads on all mooring lines during the period of interest and K equal to 7.5. The aim was to select the peakiest events, and to remove the peaky

events which are not due to the environment. Consequently *K* was the leading factor to detect peak mooring loads, and τ has been used only to remove events which are not relevant for this study.

τ and *K* were similarly defined for the different period of analysis at both facilities, as they allow to directly compare the results and to select a sufficient but restrain number of datasets.

An example of an event not relevant for this study is shown in Figure 5.2. In this example, a sudden increase in tension is observed between 13:28 and 13:30. However, this increase seems sudden and large only because the standard deviation of mooring load was low for this dataset. The maximum mooring load is below τ. The minimum tension threshold τ was removing such events in a calm sea state which are not relevant for this study. This event may have been due to ship wake or instrumentation faults.

Table 5.1: Example of percentage of occurrences of datasets considered as containing peak mooring loads for different values of τ and *K*. Example based on the mooring load data measured on line 1 during the first SWMTF deployment before anchor drag.

τ\K	**0**	**2.5**	**5**	**7.5**	**10**
0 kN	100.00%	99.99%	14.86%	0.39%	0.01%
10 kN	5.01%	5.01%	3.40%	0.28%	0.00%
20 kN	0.21%	0.21%	0.21%	0.06%	0.00%
30 kN	0.04%	0.04%	0.04%	0.02%	0.00%
40 kN	0.00%	0.00%	0.00%	0.00%	0.00%
50 kN	0.00%	0.00%	0.00%	0.00%	0.00%

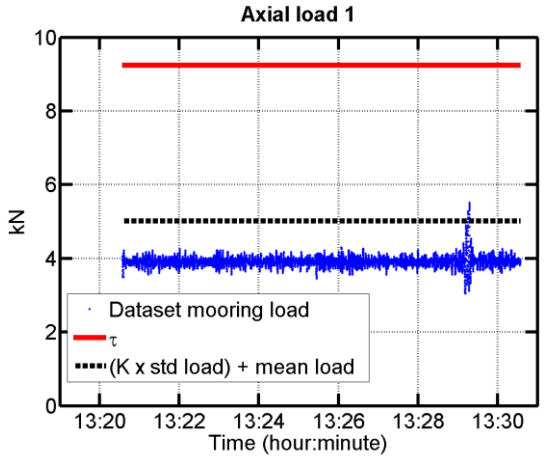

Figure 5.2: Example of a dataset showing a sudden but small increase in mooring load, measured on mooring line 1 at SWTMF on the 18/09/2010 at 13:20

For each dataset of time series of mooring load the standard score is calculated and the maximum mooring load is considered. Figure 5.3 shows an example of detection of peak mooring loads for the SWMTF on mooring line 1 over several days. This example shows mooring loads statistical values (maximum load and S_{max}) and associated summary environmental conditions (H_S, T_P, C, h). If the standard score and the maximum value were higher than K and τ respectively, then a peak mooring load was detected and indicated by a red circle. The environmental parameters $H_{S\ peak}$, $T_{P\ peak}$, h_{peak} and C_{peak} occurring at this time were recorded. This methodology is repeated on all mooring lines and for the whole duration of the periods of interest.

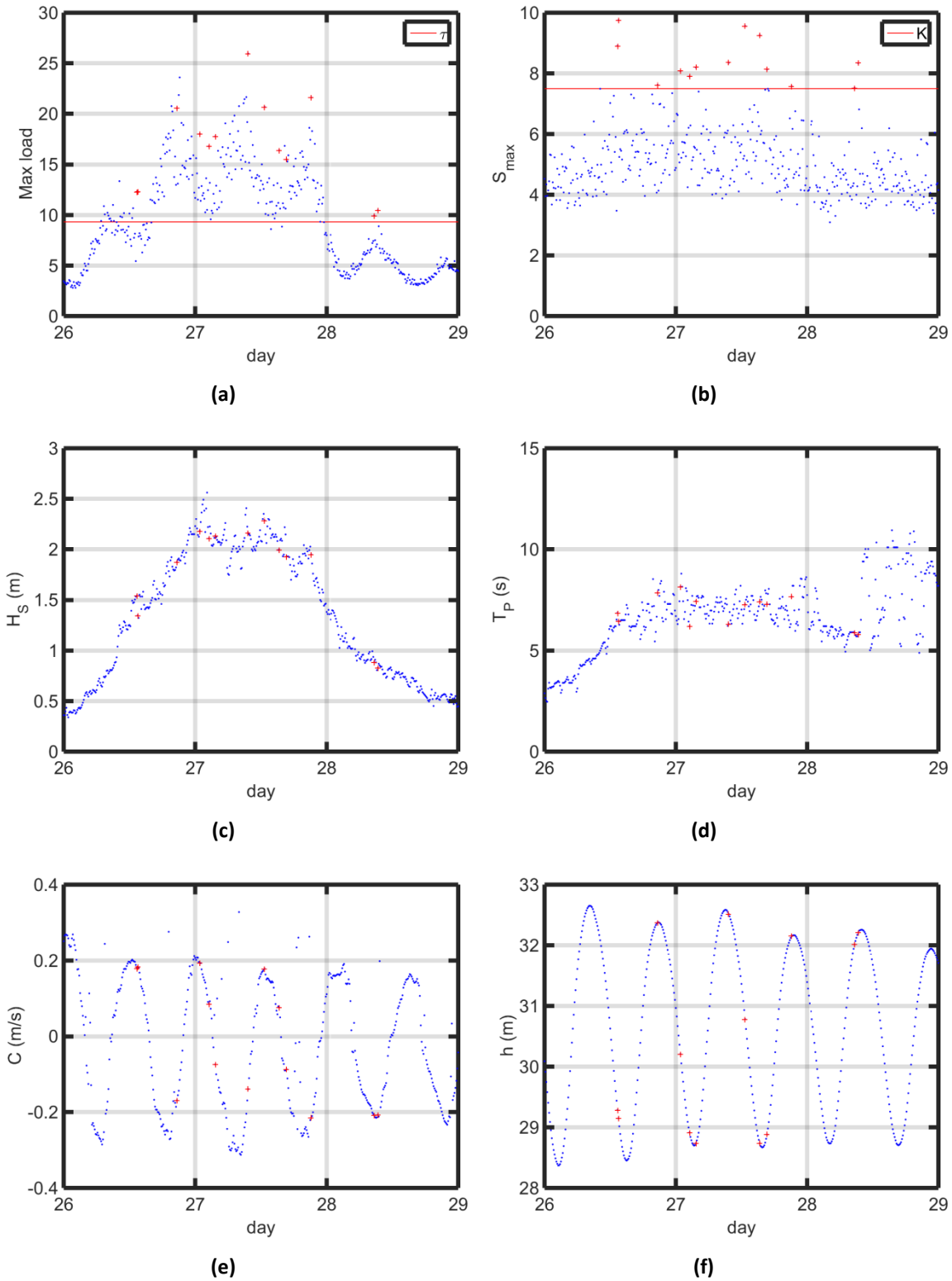

Figure 5.3: Example of (a-b) detection of peak mooring loads on mooring line 1 at SWMTF over several days and (c-f) observation of the corresponding environmental conditions between the 25/12/2010 and the 02/02/2011; a) maximum load, b) S_{max}, c) H_S, d) T_P, e) C, f) h. *Some peaks occurred very closely and one of the data point may be sheltered.*

5.2 Analysis of selected peak mooring loads and corresponding environmental conditions

The joint percentage of occurrences of environmental conditions associated with peak mooring loads JPO($H_{S\,peak}$, $T_{P\,peak}$) and JPO(C_{peak} , h_{peak}) are calculated following Eq.(5.1) and Eq.(5.2) respectively.

$$JPO(H_{S\,peak},T_{P\,peak_{i,j}} = \frac{\sum_{peak=1}^{nb\_peak} \left\langle \begin{array}{c} H_{S0} + (i-1)H_{S\,bin} \le H_{S\,peak_k} < H_{S0} + iH_{S\,bin} \\ and \\ T_{P0} + (j-1)T_{P\,bin} \le T_{P\,peak_k} < T_{P0} + jT_{P\,bin} \end{array} \right\rangle}{nb\_peak} \quad (5.1)$$

With $H_{S\,peak\ k}$ and $T_{P\,peak\ k}$ the wave conditions associated with peak mooring loads at a given time, and *nb_peak* the total number of detected peak mooring loads

$$JPO(h_{peak},C_{peak})_{i,j} = \frac{\sum_{peak=1}^{nb\_peak} \left\langle \begin{array}{c} h_0 + (i-1)h_{bin} \le h_{peak_k} < h_0 + ih_{bin} \\ and \\ C_0 + (j-1)C_{bin} \le C_{peak_k} < C_0 + jC_{bin} \end{array} \right\rangle}{nb\_peak} \quad (5.2)$$

With $h_{peak\ k}$ and C_k the tidal conditions associated with peak mooring loads at a given time, and *nb_peak* the total number of detected peak mooring loads

Scatter plots are drawn to summarise the results. These plots need to be compared with the scatter plots of the joint percentage of occurrences of general environmental conditions JPO(H_S, T_P) presented in the previous chapter in 4.1.4.1 and 4.2.4.1. For this purpose, the external contour line (black external dashed line) of the H_S and T_P, or C and h scatter plot is added to the plot of the joint percentage of occurrences s of $H_{S\,peak}$ and $T_{P\,peak}$, or C_{peak} and h_{peak}.

In addition to the contour lines, a black internal dotted line was also drawn to show the external limits of the ($H_{S\,peak}$, $T_{P\,peak}$) distribution.

5.3 Results

In this section the key results of the assessment of environmental conditions, mean and maximum loads associated with peak mooring load conditions are presented for the SWMTF and for the Bolt-2 LifeSaver device.

5.3.1 South West Mooring Test Facility (SWMTF)

Loadcell 3 was not working during most of the first SWMTF deployment after anchor drag, so results were not considered for this loadcell and this period of deployment.

The number of datasets containing peak mooring loads during the SWMTF deployments is given in Table 5.2: a range from 1 to 73 peak mooring loads have been detected, depending on the line and on the period of sea trials considered. A higher number of peak mooring loads have been observed on mooring line 1 and 3 than on mooring line 2, because mooring line 1 and 3 are facing the waves. Sea states leading to peak mooring loads account for 0.01% to 0.72% of the observed sea states. The number of sea states coming from the two main wave directions during each period of interest is summarised in Table 5.2.

During the first deployment, before and after anchor drag, a slightly higher number of waves were coming from the South than from the East. During the second deployment, the proportion of sea states coming from the South than from the East was higher than during the first deployment. The consequences of this change of direction on peak mooring loads are clear. While the duration of the second deployment was nearly half of the duration of the first deployment before anchor drag, a) more peak mooring loads have been observed on the Southerly mooring line 1 during the second deployment (70 peak mooring loads) compared to the first deployment before anchor drag (55 peak mooring loads); b) on the Easterly mooring line 3, 73 peak mooring loads have been observed during the first SWMTF deployment before anchor drag while only 22 have been observed during the second SWMTF deployment.

The percentage of peak mooring loads during the first deployment after the anchor drag was considerably lower on line 1 than during the other periods of analysis. This was not observed on the other loadcells because the number of detected peak mooring loads on line 2 is insufficient to draw a conclusion, and loadcell 3 was not working during the first deployment after anchor drag.

Table 5.2: Number/percentages of detected peak mooring loads in a period of time for the SWMTF. The total number of datasets is reminded in the last rows as well as the number of datasets associated with a range of wave direction

	First SWMTF deployment		**Second SWMTF deployment**
Line and orientation	Before anchor drag	After anchor drag	
Line 1 (185°)	55/0.29%	16/0.09%	70/0.72%
Line 2 (305°)	1/0.01%	6/0.03%	5/0.05%
Line 3 (65°)	73/0.39%	/ no data	22/0.23%
Total number of 10 minute datasets with wave data available	18,837	17,958	9,697
Total number of 10 minute datasets with $90° < D_P < 150°$	8,878/47%	7,288/41%	2,856/29%
Total number of 10 minute datasets with $150° < D_P < 210°$	9,052/48%	9,745/54%	6184/64%

Table 5.3 summarises the environmental conditions associated with peak mooring loads. This table shows that peak mooring loads occur mainly for large values of H_S, but they may occur for lower values as well.

Figure 5.4 shows the joint percentage of occurrences of wave conditions associated with peak mooring loads on the three mooring lines for the different test periods. Table 5.4 counts the number of bins populated in the wave scatter diagrams by the wave conditions associated with peak mooring loads.

Figure 5.4 and Table 5.4 indicate that some sea states are more frequently associated with peak mooring loads. More than 15% of the peak mooring loads were observed on all mooring lines for different combinations of H_S and T_P within the scatter diagram, and not on the external contour line showing the limit of the general environment conditions.

Table 5.3: Variations of the environmental conditions associated with peak mooring loads for the SWMTF

		First deployment								**Second deployment**			
		Before anchor drag				After anchor drag							
		Min	Mean	Max	Std	Min	Mean	Max	Std	Min	Mean	Max	Std
Line 1	H_S (m)	0.66	1.57	2.78	0.56	0.69	1.65	2.45	0.44	0.66	1.69	3.31	0.60
	H_{max} (m)	1.05	2.49	4.30	0.84	1.03	2.58	3.73	0.70	1.40	2.89	4.96	0.87
	T_Z (s)	4.1	5.5	7.6	0.8	4.5	5.6	6.4	0.5	3.6	5.4	7.3	0.9
	T_P (s)	3.7	6.4	8.3	1.1	4.7	6.1	7.7	0.8	4.1	6.6	9.8	1.2
	C (m/s)	-0.18	0.05	0.23	0.11	-0.18	-0.04	0.36	0.13	-0.18	0.05	0.31	0.11
	h (m)	28.1	30.4	32.5	1.2	29.0	31.2	32.6	1.2	28.2	30.4	32.8	1.3
Line 2	H_S (m)	0.82	0.82	0.82	0	0.38	0.50	0.81	0.18	0.54	0.68	1.04	0.20
	H_{max} (m)	1.38	1.38	1.38	0	0.62	0.86	1.13	0.21	/ no valid data			
	T_Z (s)	3.7	3.7	3.7	0	4.0	4.8	5.4	0.5	2.8	3.3	4.5	0.7
	T_P (s)	3.8	3.8	3.8	0	2.7	5.3	8.1	2.1	2.7	3.8	6.1	1.5
	C (m/s)	0.24	0.24	0.24	0	-0.14	-0.05	0.19	0.13	0.13	0.26	0.37	0.11
	h (m)	27.9	27.9	27.9	0	29.3	31.5	32.8	1.2	28.8	29.6	31.0	0.9
Line 3	H_S (m)	0.45	1.98	2.93	0.46	/ no data				0.70	1.70	3.05	0.64
	H_{max} (m)	0.82	3.03	4.69	0.70					2.10	3.36	4.87	1.07
	T_Z (s)	3.8	5.6	7.2	0.6					3.1	5.1	7.0	1.0
	T_P (s)	3.9	6.4	7.7	0.6					2.7	5.8	8.5	1.4
	C (m/s)	-0.18	0.12	0.32	0.14					-0.07	0.14	0.38	0.11
	h (m)	27.9	30.4	32.8	1.4					28.1	29.6	32.7	1.1

Table 5.4: Number of bins generated in the ($H_{S\ peak}$, $T_{P\ peak}$) scatter diagram for SWMTF. The number of bins populated in the (H_S, T_P) scatter diagram is reminded in the last row

	First SWMTF deployment		**Second SWMTF deployment**
	Before anchor drag	After anchor drag	
Line 1	13	7	15
Line 2	1	5	3
Line 3	12	/ no data	12
General interpolated wave conditions	41	37	37

Figure 5.5 plots a vector $H_{S\ vec}$ (red dots) with an amplitude equal to H_S and a direction equal to D_P. In Figure 5.5j-l, the three mooring lines are drawn (blue lines), while in Figure 5.5a-i only the mooring line of interest is drawn. Figure 5.5j-l plots $H_{S\ vec}$ for the general environmental conditions, while Figure 5.5a-i plots $H_{S\ vec}$ for the wave conditions associated with peak mooring loads on the different mooring lines and for the different period of analysis.

Figure 5.5j and l indicate that during the first deployment before anchor drag, most of the sea states were coming from the East, which is close to the direction of line 3, while during the second SWMTF deployment, most of the sea states were coming from the South, which is the exact direction of mooring line 1.

Peak mooring loads occur on mooring line 1 mainly for a Southerly wave direction while they occur on mooring line 3 mainly for an Easterly wave direction, close to the line direction but not aligned with it. Peak mooring loads generally occurred for higher H_S on line 3 than on line 1.

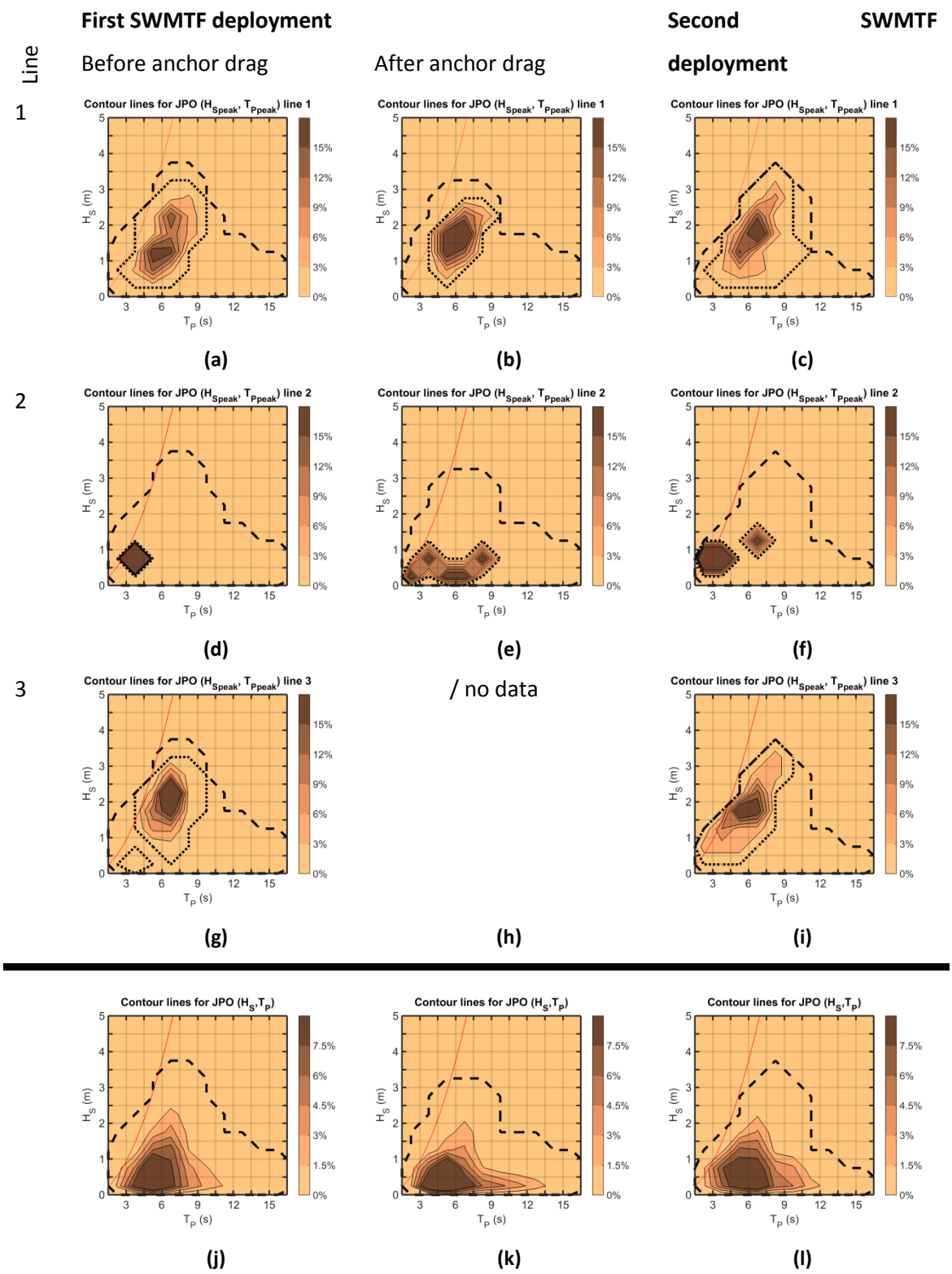

Figure 5.4: Scatter plots of the waves conditions associated with peak mooring loads ($H_{S\ peak}$, $T_{P\ peak}$) for the SWMTF for the three mooring lines. General environmental conditions (H_S, T_P) are reminded in j-l. The black external dashed line is the limit of the general interpolated wave conditions. The black internal dotted line in (a-i) is the limit of the wave conditions associated with peak mooring loads. The red line shows the average wave steepness limit.

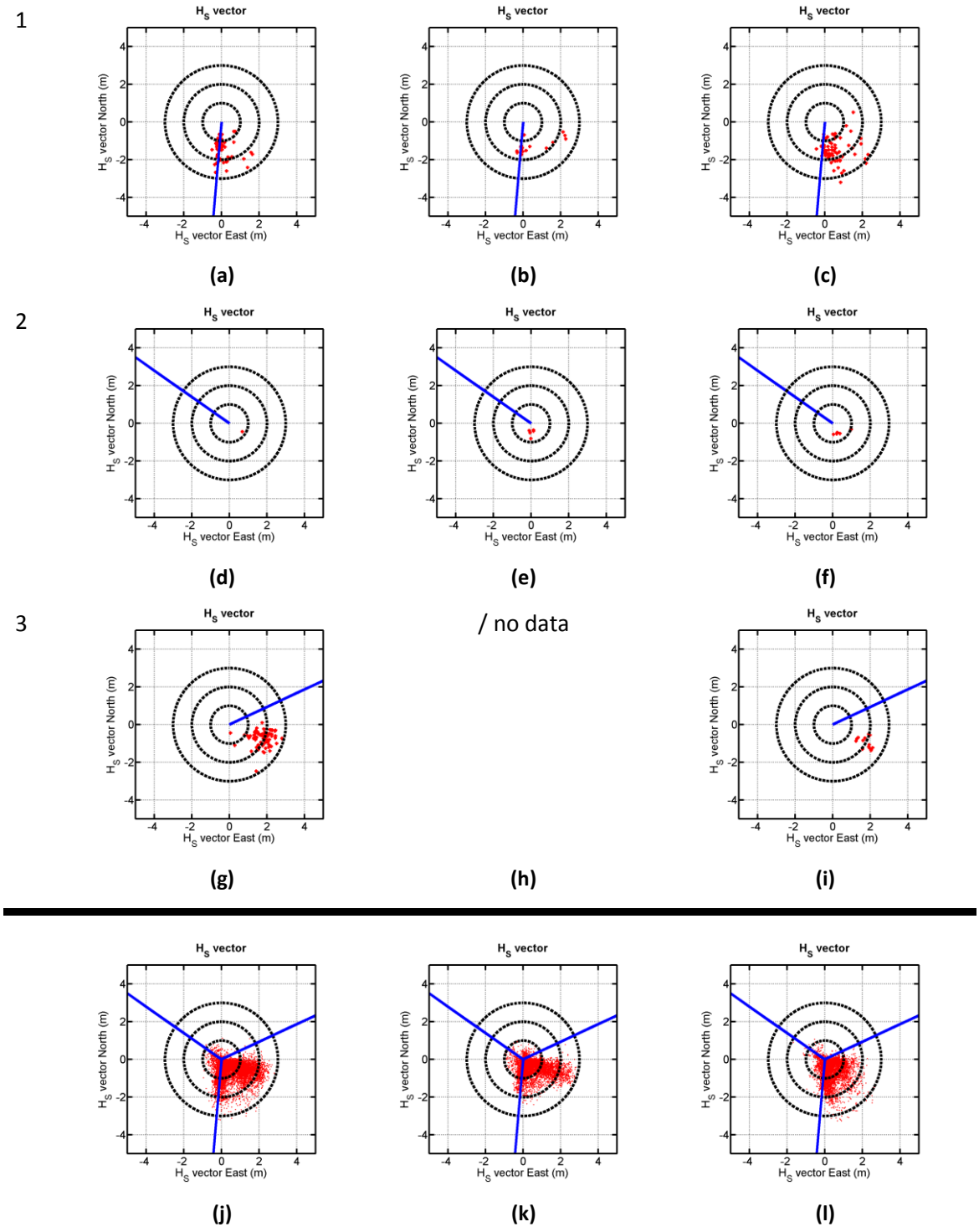

Figure 5.5: Direction of wave conditions associated with peak mooring loads $D_{P\ peak}$ for the SWMTF for the three mooring lines. General environmental conditions D_P are reminded in j-l. Blue lines indicate the mooring line orientation . The wave direction is the direction from which the waves are coming.

Figure 5.6 shows the joint percentage of occurrences of tidal conditions associated with peak mooring loads on all mooring lines and for the different test periods. On mooring line 1 and 3 during the first SWMTF deployment before anchor drag and during the second SWMTF deployment, more peak mooring loads were detected for low tidal heights while the general conditions indicate that high tidal heights were more frequent. However, this was not the case on line 1 during the first deployment after anchor drag, when most of the peak loads occurred for high tides.

Table 5.5 counts the number of bins populated in the tidal scatter diagram. It displays the number of different tidal combinations (*C*, *h*) leading to peak mooring loads. Peak mooring loads with occurrences higher than 7.5% were observed on line 1 and on line 3 for two different combinations of *h* and *C*, one for low tide, the other for high tide. The number of occurrences of peak mooring loads on line 2 was too low to draw any conclusion.

Figure 5.7 shows the current directions associated with peak mooring loads on all mooring lines and for the different test periods. Peak mooring loads do not seem to be associated to any particular current direction.

Table 5.5: Number of bins generated in the scatter diagram of the tidal conditions associated with peak mooring loads (C_{peak} , h_{Ppeak}). The number of bins generated in the (*C*, *h*) scatter diagram is reminded in the last row

	First SWMTF deployment		**Second SWMTF deployment**
	Before anchor drag	After anchor drag	
Line 1	18	10	25
Line 2	1	2	4
Line 3	25	/ no data	15
General interpolated tidal conditions	50	67	49

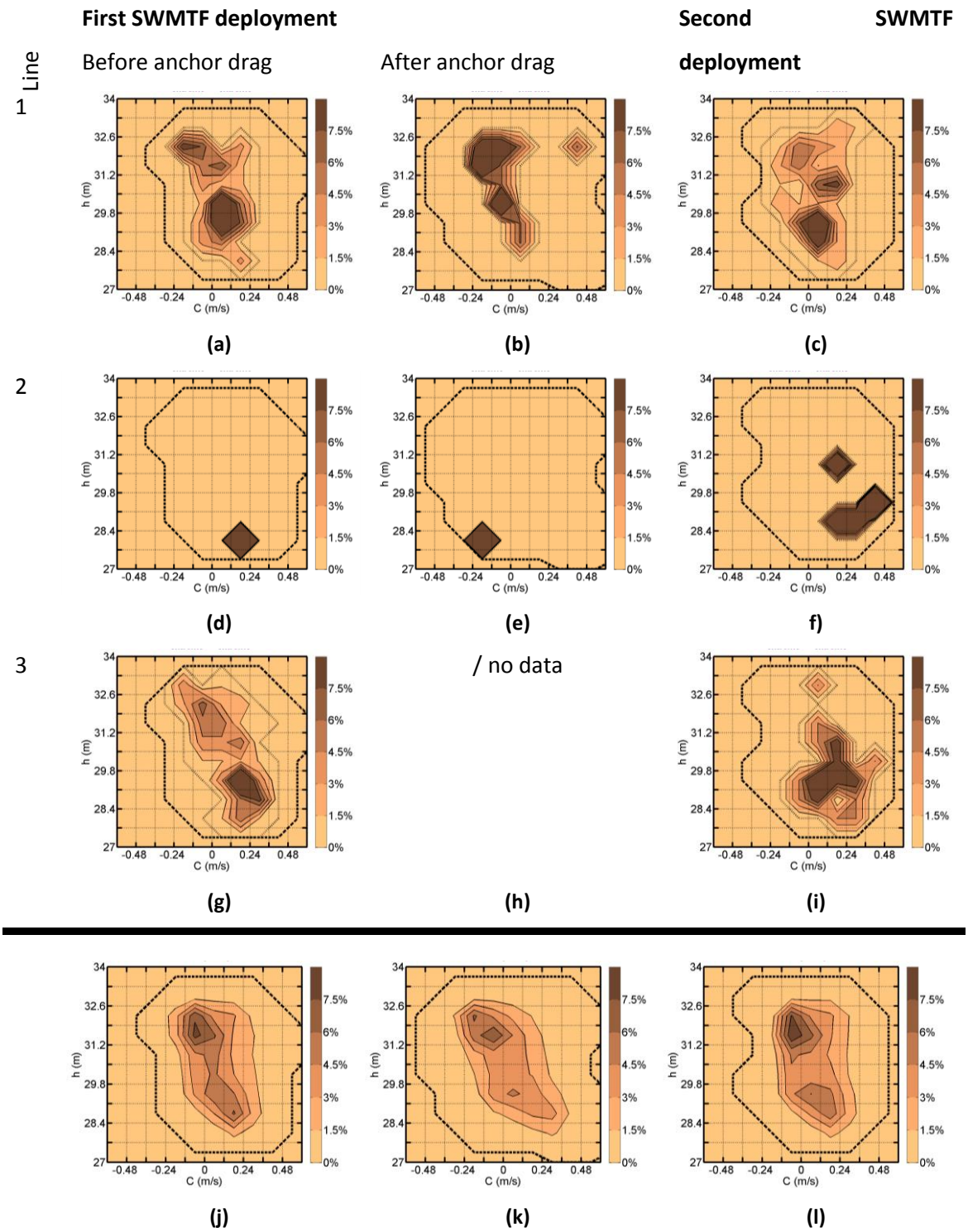

Figure 5.6: Scatter plots of the tidal conditions associated with peak mooring loads (h_{peak}, C_{peak}) for the SWMTF and for the three mooring lines. General environmental conditions (*C, h*) are reminded in j-l. The black external dashed line is the limit of the general tidal conditions. The black internal dotted line in (a-i) is the limit of the tidal conditions associated with peak mooring loads

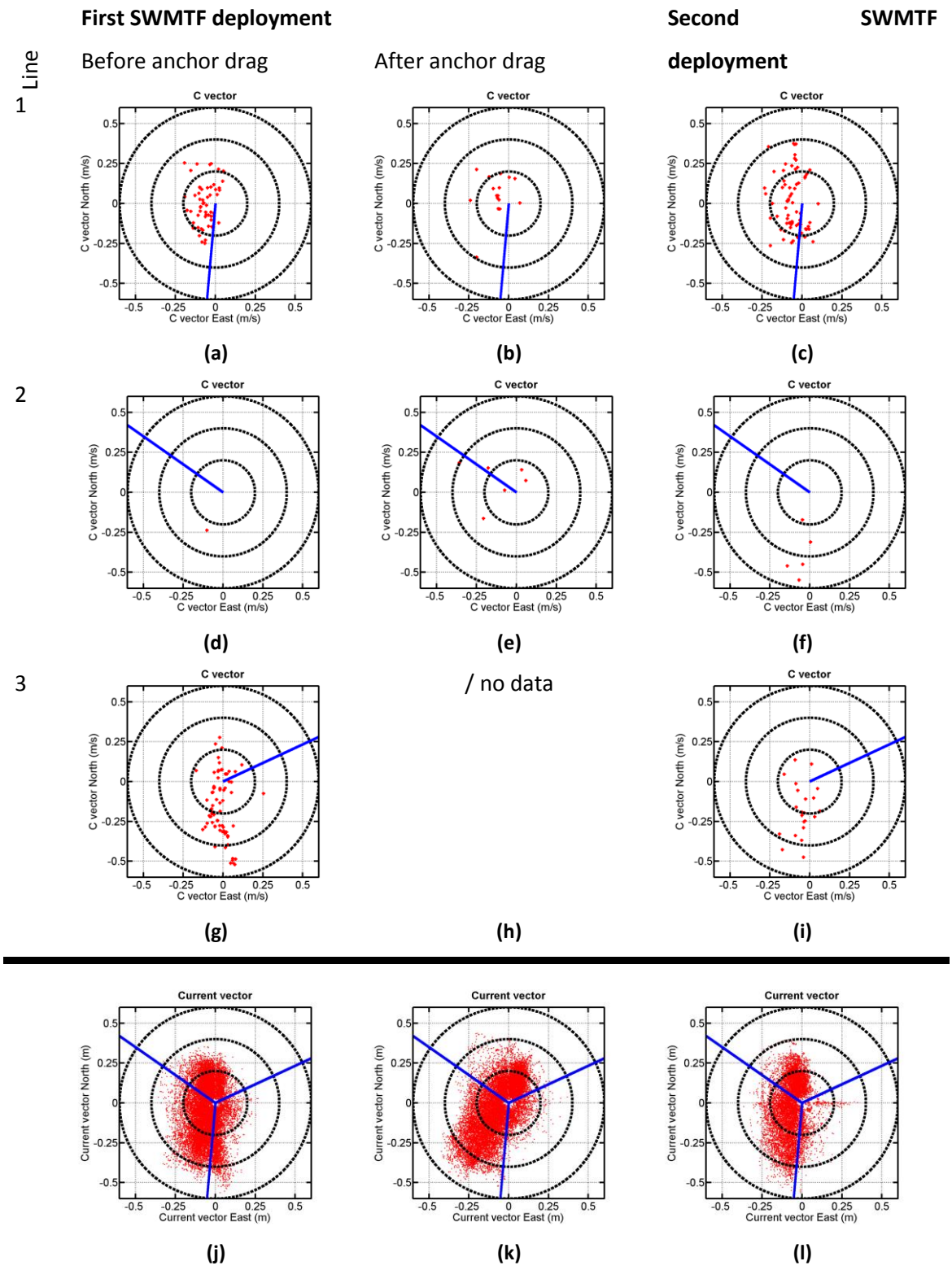

Figure 5.7: Direction of tidal conditions associated with peak mooring loads C_{Dir_max} in a period of time for the SWMTF for the three mooring lines. General environmental conditions C_{Dir} are reminded in j-l. Blue lines indicate the mooring line orientation. The current direction is the direction from which the current is coming.

The amplitude and number of peak mooring loads need to be particularly assessed, because of their consequences on mooring survivability and fatigue. Mooring loads with an amplitude close to the MBL divided by a safety factor can potentially cause a failure of the mooring, while mooring loads over a certain percentage of the MBL will need less cycles to damage the rope than mooring loads with a lower amplitude. However, mooring loads with a lower amplitude can still be harmful if they repeat themselves (S-N curves).

Figure 5.8 shows the peak mooring loads on the different mooring lines and during the different SWMTF deployments for a particular range of wave conditions. On mooring line 2, the peak mooring loads are always below 10 kN. On mooring line 1 and 3, some peak mooring loads are over 50 kN for the first SWMTF deployment before anchor drag, in both cases for high but not the highest measured H_S. For the first SWMTF deployment after anchor drag and the second SWMTF deployment, peak mooring loads do not exceed 20 kN. These amplitudes are largely below the MBL (460 and 520 kN for the first and second deployment respectively) and the number of occurrences of these peak mooring loads is largely below the thousands of cycles necessary for fatigue damage. This is discussed in more details in 7.1.2.2.

Figure 5.9 shows the values of the peak load and their associated wave direction. Figure 5.10 shows the values of the peak load and their associated current direction. Figure 5.11 shows the values of the mean load when peak loads occurred and the associated wave direction. Figure 5.12 the values of the mean load when peak loads occurred and the associated current direction. The maximum and mean loads for the general data are also reminded (green dots) to compare peak loads with the rest of the data.

Figure 5.9 shows that on mooring line 1 and 3, the mooring loads with the highest amplitude are peak loads, but that other mooring loads with lower amplitude are also peak loads. Peaks loads occur for wave direction close to the mooring line orientation.

Figure 5.10 indicates that peak loads occurred for any current direction. Figure 5.11 and Figure 5.12 show that the mean loads during peak loads are varying over a wide range and no pattern can be clearly identified.

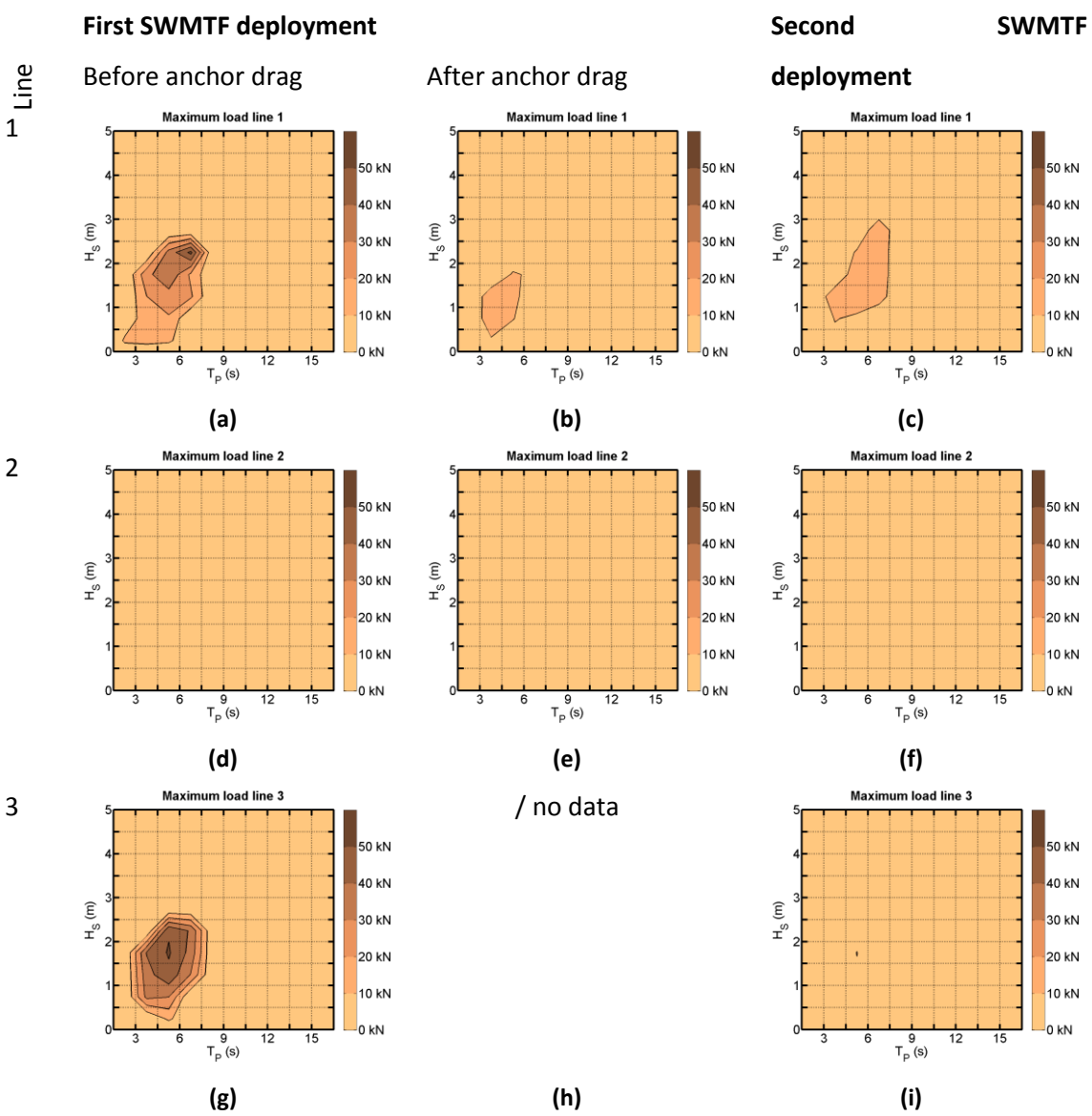

Figure 5.8: Peak mooring loads for a given sea state range for the SWMTF for the three mooring lines

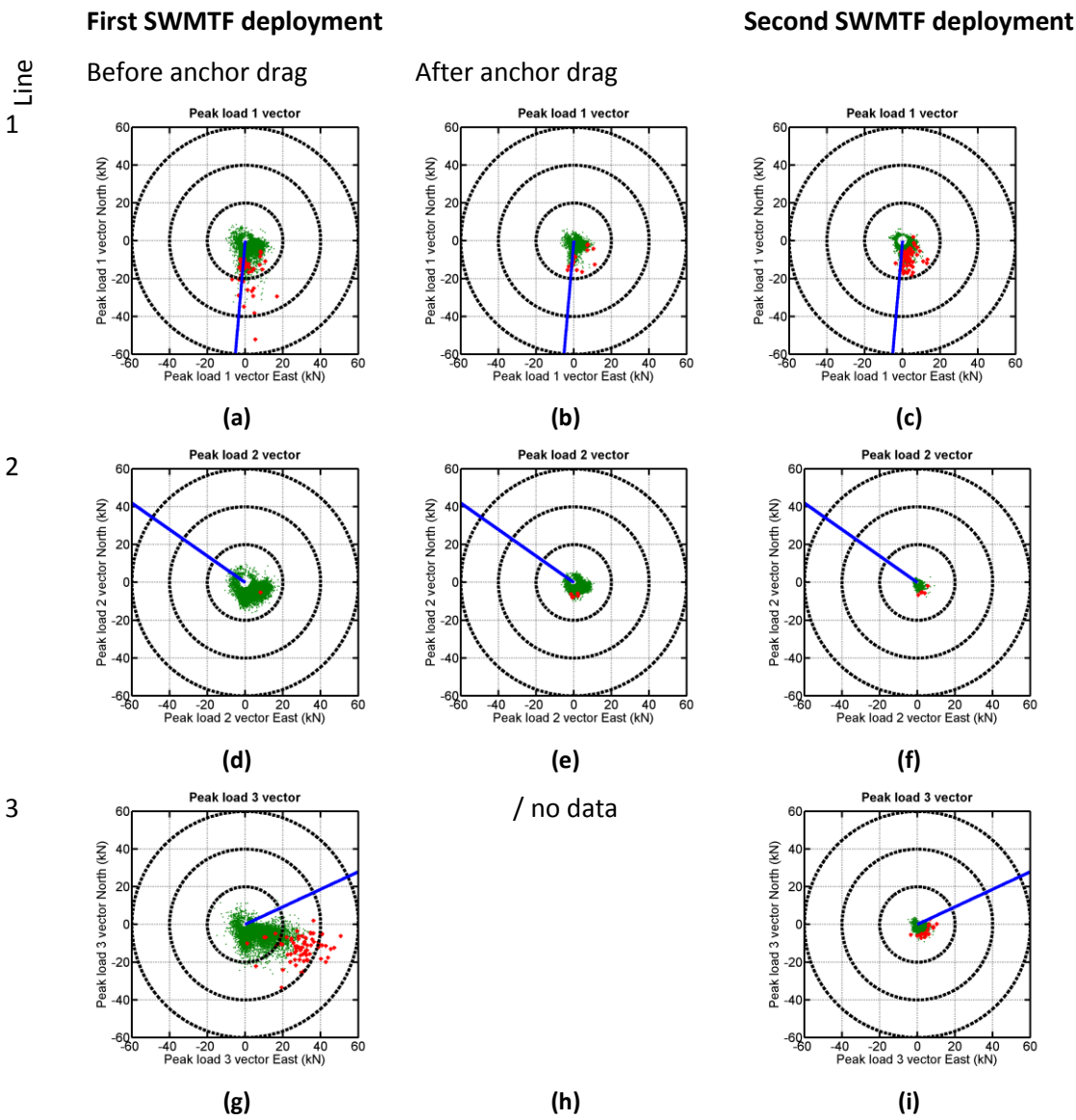

Figure 5.9: Maximum mooring loads and associated wave direction $D_{P\ peak}$ associated with peak mooring loads (red dots) and for the general environmental conditions (green dots) for the SWMTF for the three mooring lines. Blue lines indicate the mooring line orientation. The wave direction is the direction from which the waves are coming.

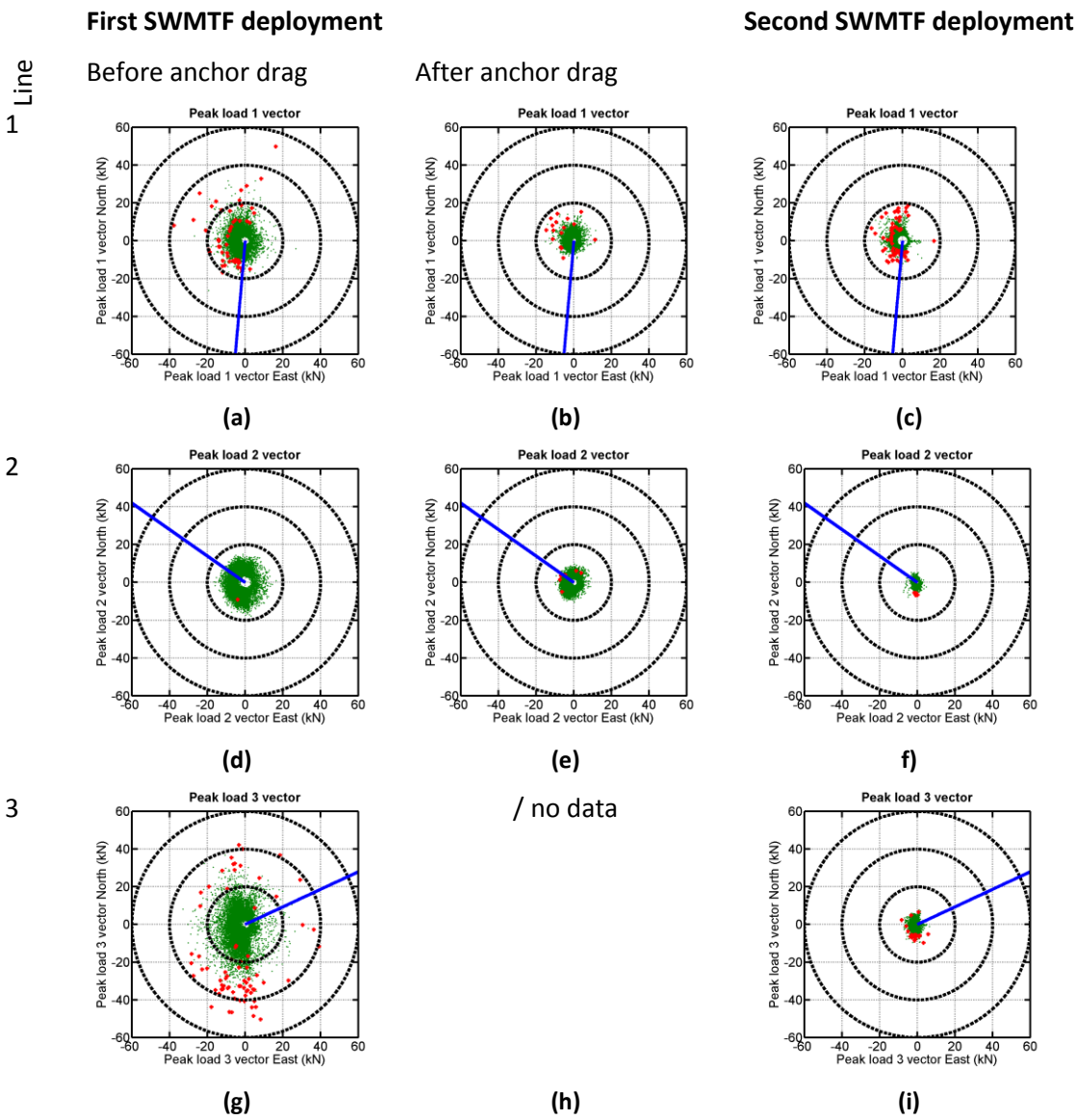

Figure 5.10: Maximum mooring loads and associated current direction associated with peak mooring loads C_{Dir_max} (red dots) and for the general environmental conditions C_{Dir} (green dots) for the SWMTF for the three mooring lines. Blue lines indicate the mooring line orientation. The current direction is the direction from which the current is coming.

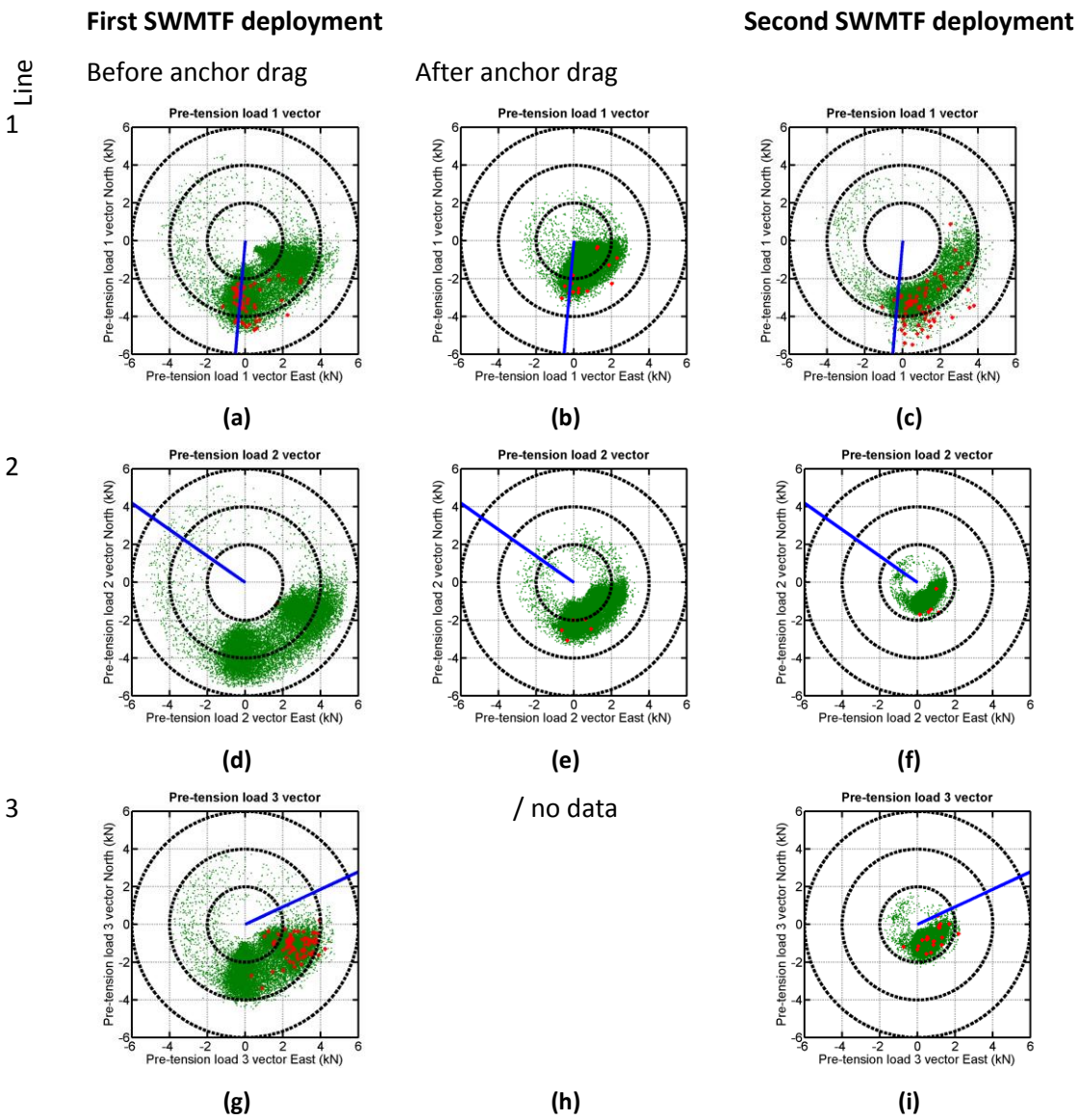

Figure 5.11: Mean mooring loads and associated wave direction associated with peak mooring loads $D_{P\ peak}$ (red dots) and for the general environmental conditions D_P (green dots) for the SWMTF for the three mooring lines. Blue lines indicate the mooring line orientation. The wave direction is the direction from which the waves are coming.

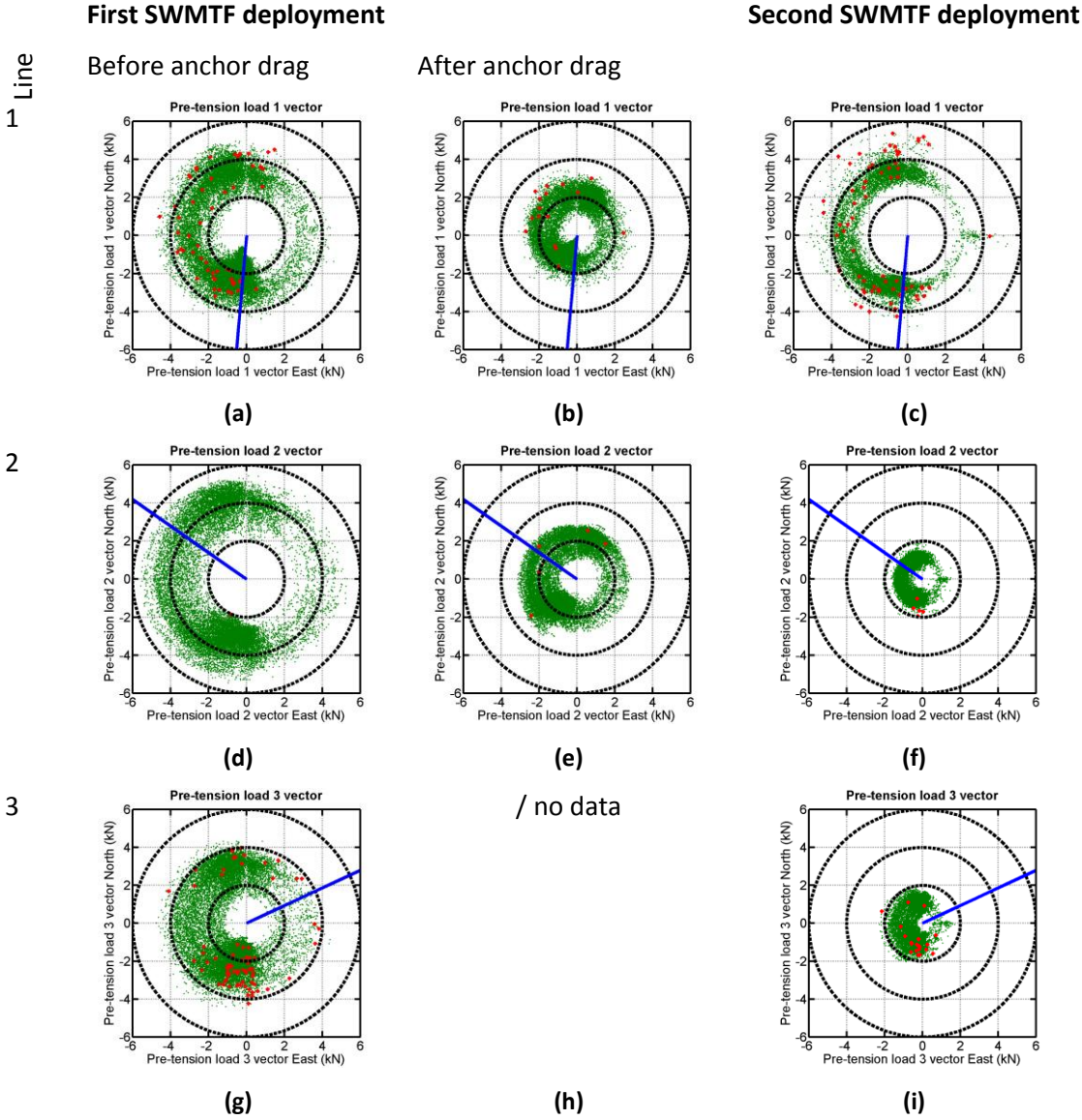

Figure 5.12: Mean mooring loads and associated current direction associated with peak mooring loads C_{Dir_max} (red dots) and for the general environmental conditions C_{Dir} (green dots) for the SWMTF for the three mooring lines. Blue lines indicate the mooring line orientation. The current direction is the direction from which the current is coming.

Figure 5.13 shows the distributions of the peak loads for the different lines and periods of analysis, and reminds the distribution of the general maximum loads. The peak loads are over their threshold values (τ was equal to 9.3 kN for the first SWMTF deployment before anchor drag, 6.1 kN after anchor drag and 5.5 kN for the second SWMTF deployment). The distributions are decreasing regularly for their higher values. For mooring line 1, most of the peak mooring loads have amplitudes between 5 and 20 kN. The number of occurrences of peak loads on line 2 is too low to draw any conclusion. The value of the peak load is significantly decreasing on line 3 in the second SWMTF deployment compared to the first SWMTF deployment before anchor drag.

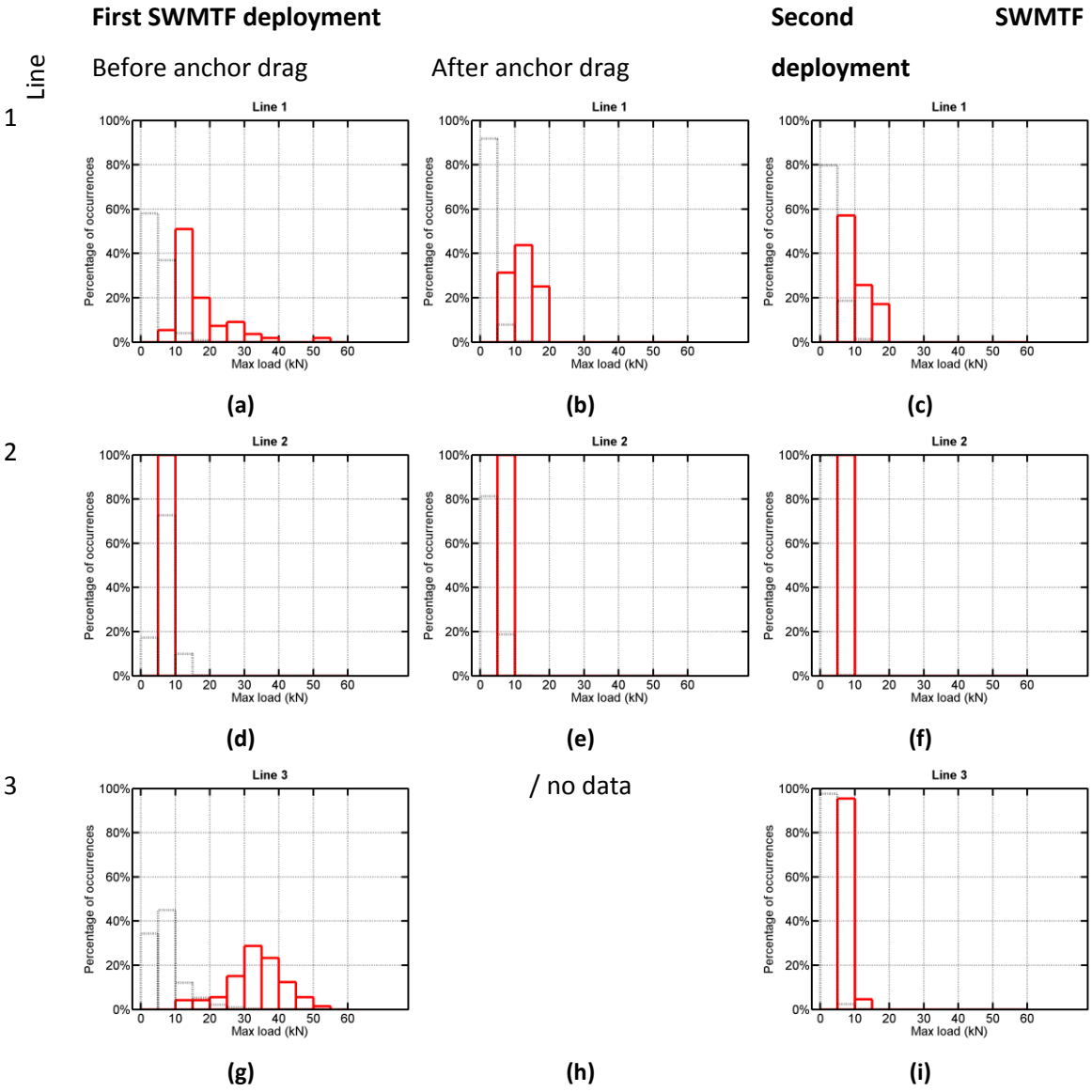

Figure 5.13: Distribution of the peak load for the SWMTF for the three mooring lines (Red lines) and distribution of the all maximum loads during this period of time on this mooring line (Black dotted lines)

Figure 5.14 shows the distribution of the mean loads when peak loads occurred for the different mooring lines and during the different period of analysis. The distribution of the general mean loads is also reminded. The shape of the distribution of the mean tension associated with peak mooring load is similar to the shape of the distribution of the general mean tension, but the distributions associated with peak mooring loads are generally centred on a higher value of mean load.

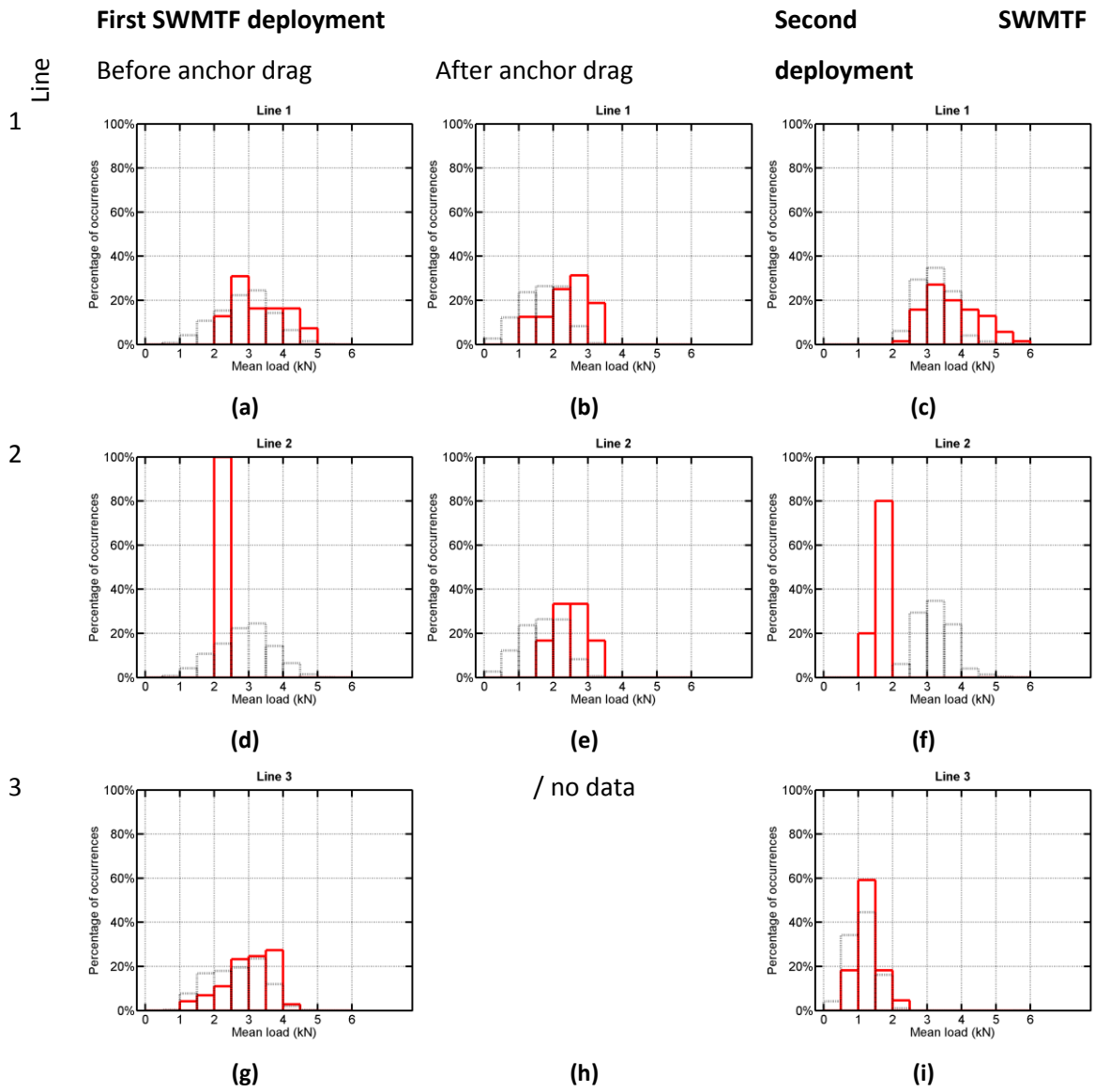

Figure 5.14: Distribution of the mean loads during peak load for the SWMTF for the three mooring lines (Red lines) and distribution of all mean loads during this period of time on this mooring line (Black dotted lines)

5.3.2 FaBTest: Bolt-2 LifeSaver device

The number and the percentage of dataset containing peak mooring loads during the Bolt-2 LifeSaver deployment are given in Table 5.6. A range from 0 (line 3) to 23 (line 1) peak mooring loads have been detected, which corresponds to 0% to 0.40% of the datasets.

Peak mooring loads were mainly detected on mooring line 1 and 5 which are facing the waves. However, more than the double of peak mooring loads have been detected on mooring line 1 (24 peak mooring loads) compared to mooring line 5 (11 peak mooring loads).

The number of sea states coming from the South was more than double those coming from the East.

Table 5.6: Number/percentages of detected peak mooring loads for the five lines of Bolt-2 LifeSaver device. The total number of datasets is reminded in the last rows as well as the number of datasets associated with a wave direction D_{mean}

Line (Orientation °)	**Number of peak loads / percentage of datasets containing peak loads**
Line 1 (136°)	23/0.47%
Line 2 (64°)	1/0.02%
Line 3 (352°)	0/0%
Line 4 (280°)	1/0.02%
Line 5 (208°)	11/0.23%
Total number of datasets after correction and with wave available at the same time	4,878
Total number of datasets with 120° < D_{mean} < 150°	745/15%
Total number of datasets with 180° < D_{mean} < 210°	2,060/42%

The variations of the environmental conditions associated with peak mooring loads at Bolt-2 LifeSaver are summarised in Table 5.7. Only one occurrence of peak load was recorded on mooring lines 2 and 4, which explains why the standard deviation of the statistical wave parameters is zero. No occurrence of peak load was recorded on mooring line 3. On mooring line 1 and 5, peak loads were detected for medium sea states, with H_S as low as 1.6 m but also for energetic sea states, with H_S above 3 m.

Table 5.7: Variations of the environmental conditions associated with peak mooring loads at Bolt-2 Life-Saver

		Min	Mean	Max	Std
Line 1	H_S (m)	1.5796	2.3272	3.5831	0.5474
	H_{max} (m)	2.4766	3.6427	6.3469	1.0112
	T_Z (s)	4.4553	5.2178	6.8506	0.6154
	T_P (s)	5.1437	6.8312	10.5693	1.3437
Line 2	H_S (m)	2.1969	2.1969	2.1969	0
	H_{max} (m)	3.0751	3.0751	3.0751	0
	T_Z (s)	5.5235	5.5235	5.5235	0
	T_P (s)	8.2967	8.2967	8.2967	0
Line 3	/ no peak mooring load				
Line 4	H_S (m)	3.3678	3.3678	3.3678	0
	H_{max} (m)	4.3360	4.3360	4.3360	0
	T_Z (s)	6.1628	6.1628	6.1628	0
	T_P (s)	9.3226	9.3226	9.3226	0
Line 5	H_S (m)	1.6406	2.8429	4.1934	0.9731
	H_{max} (m)	2.6377	4.2765	6.9961	1.5472
	T_Z (s)	4.5898	5.8850	7.1215	0.9341
	T_P (s)	5.8077	8.2649	9.9536	1.5155

Figure 5.15 shows the joint percentage of occurrences of wave conditions associated with peak mooring loads on the five mooring lines. Table 5.8 counts the number of bins populated in the wave scatter diagram.

Table 5.8: Number of bins generated in the scatter diagram of the wave conditions associated with peak mooring loads ($H_{S\,peak}$, $T_{P\,peak}$) for Bolt-2 LifeSaver device. The number of bins generated in the (H_S, T_P) scatter diagram is reminded in the last row

Line	Number of bins generated in the scatter diagram
Line 1	8
Line 2	1
Line 3	0
Line 4	1
Line 5	8
General wave conditions	44

Figure 5.15 and Table 5.8 indicate that some wave conditions are more often associated with peak mooring loads. More than 7.5% of the peak mooring loads were observed on mooring lines 1 and 5 for different combinations of H_S and T_P within the scatter diagram, and not on the external contour line. On mooring line 5, more than 7.5% of the peak mooring loads were also observed for the highest measured value of H_S.

Figure 5.16a-e shows D_{mean} and H_S for each mooring line when peak mooring loads were detected. The general wave conditions are reminded in Figure 5.16f. Peak mooring loads occurred on mooring line 5 only when the waves were closely aligned with the mooring line while they occur for a wider range of wave directions on line 1.

The peak mooring loads have been assessed in Figure 5.17. The peak mooring loads are over 50 kN in line 1 and 5 (when the MBL is 672 kN), in both cases for high but not the highest measured H_S. Only one peak mooring load was detected on line 2 to 4 which is not sufficient to draw conclusions.

Figure 5.18 shows the distribution of the peak loads on each mooring line and compared it with the distribution of the maximum loads during the whole test. Peak loads have an amplitude over 30 kN, because of the parameter τ (equal to 35.3 kN). On line 1 and 5, which are the more exposed mooring lines, the distribution of the peak loads is relatively flat, meaning that a similar number of occurrences of peak loads were detected with values between 30-40 kN and between 60-70 kN.

Figure 5.19 shows the distribution of the mean loads when peak loads were detected. The distribution of mean loads during the whole test is also reminded. The shape of the distribution associated with peak mooring load is similar to the shape of all mean loads, however the distribution associated with peak loads is shifted by 5 kN on line 1 and 10 kN on line 5, meaning that mean load is higher when peak loads are detected.

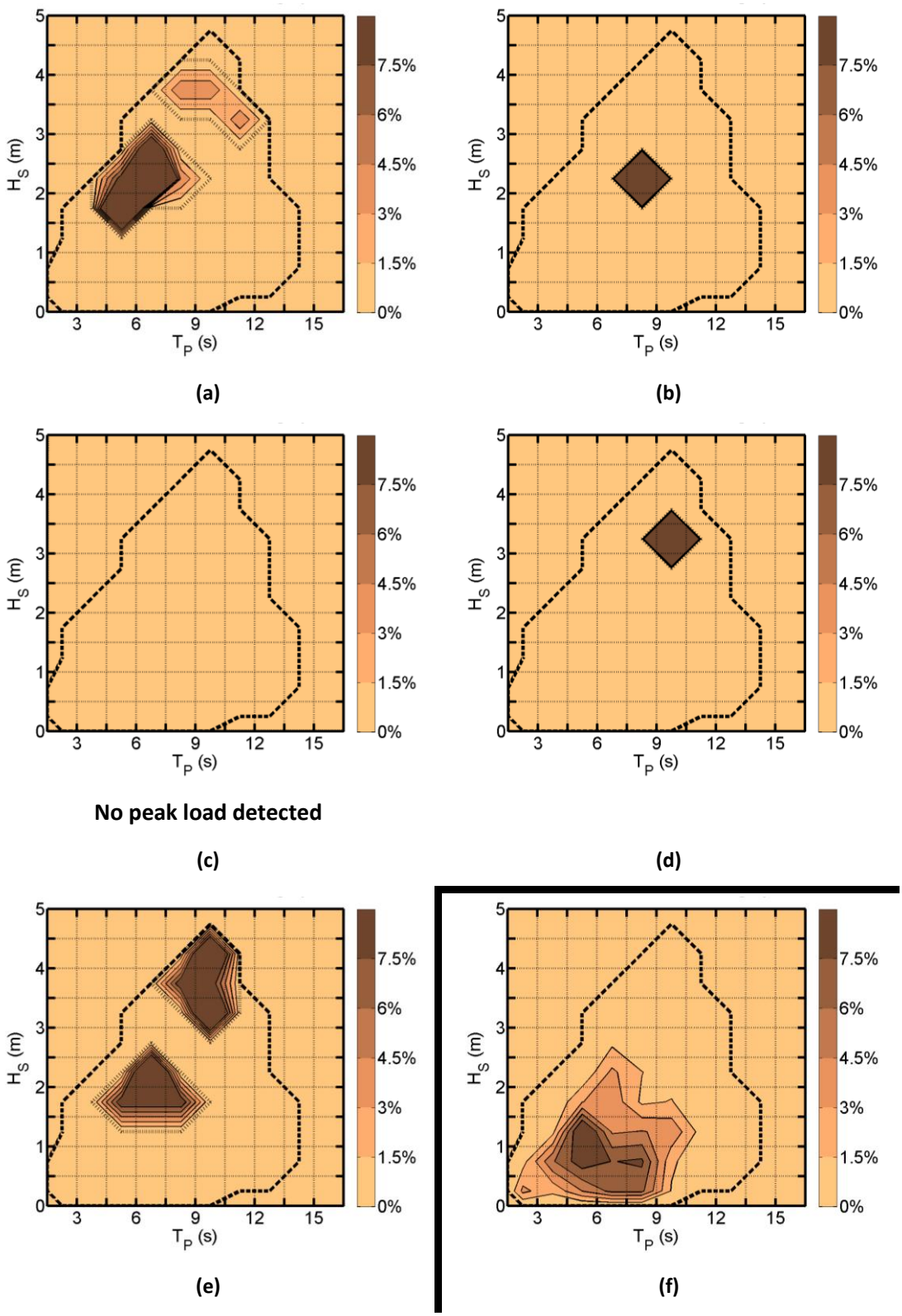

Figure 5.15: Scatter plots of the wave conditions associated with peak mooring loads (H_{Speak}, T_{Ppeak}) for the five lines (a-e) of Bolt-2 LifeSaver device. General environmental conditions (H_S, T_P) are reminded in f. The black external dashed line is the limit of the general wave conditions. The black internal dotted line (a-e) is the limit of the wave conditions associated with peak mooring loads

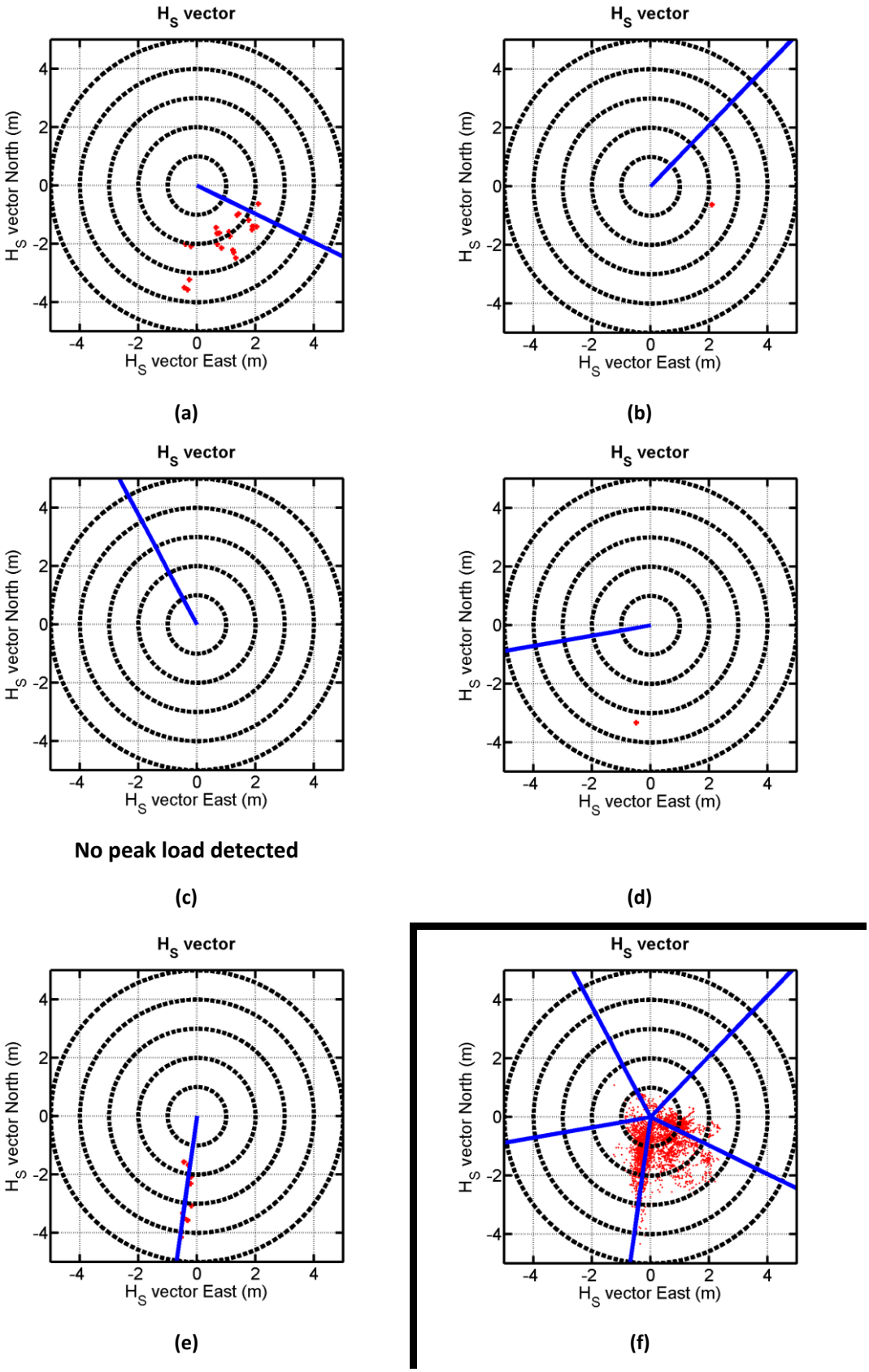

Figure 5.16: Directionality of wave conditions associated with peak mooring loads (H_{Speak}, $D_{mean\ peak}$) for the five lines (a-e) of Bolt-2 LifeSaver device. General environmental conditions D_{mean} are reminded in f. Blue lines indicate the mooring line orientation. The wave direction is the direction from which the waves are coming.

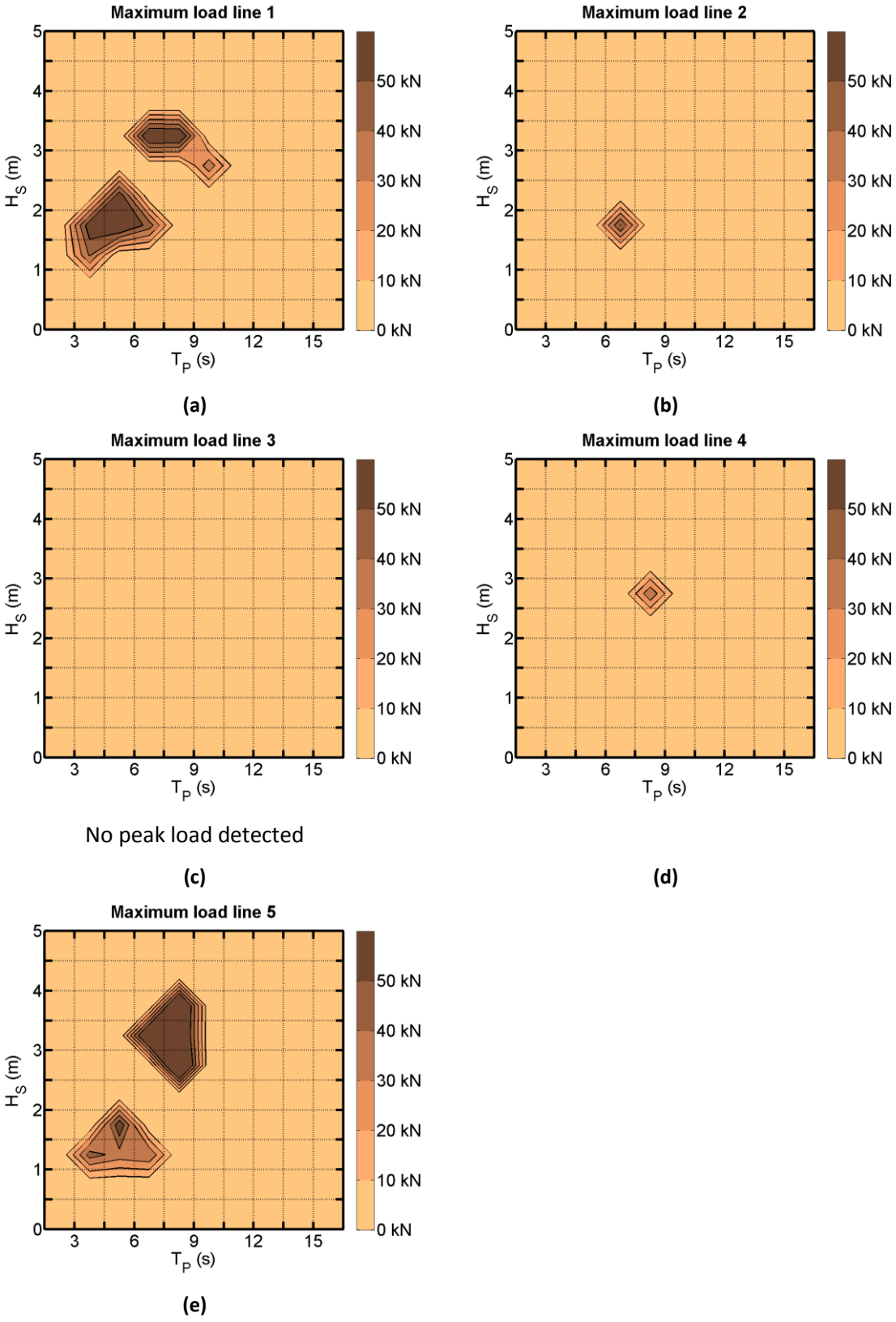

Figure 5.17: Peak mooring loads for a range of sea state for the five lines (a-e) of Bolt-2 LifeSaver device.

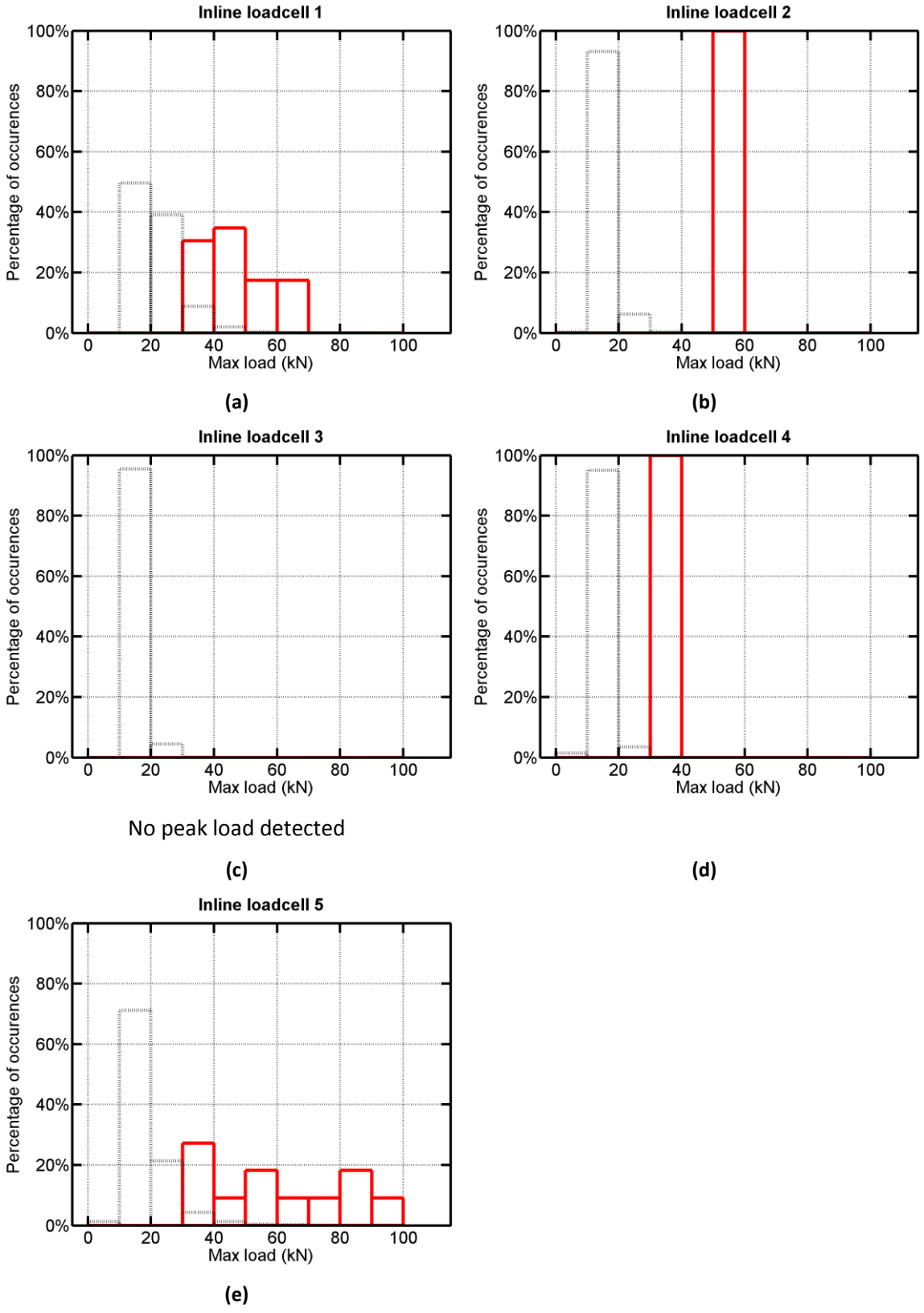

Figure 5.18: Distribution of the peak load at Bolt2-LifeSaver for the five mooring lines (a-e). Red lines: distribution of the peak load. Black dotted lines: distribution of all maximum loads during this period of time on this mooring line

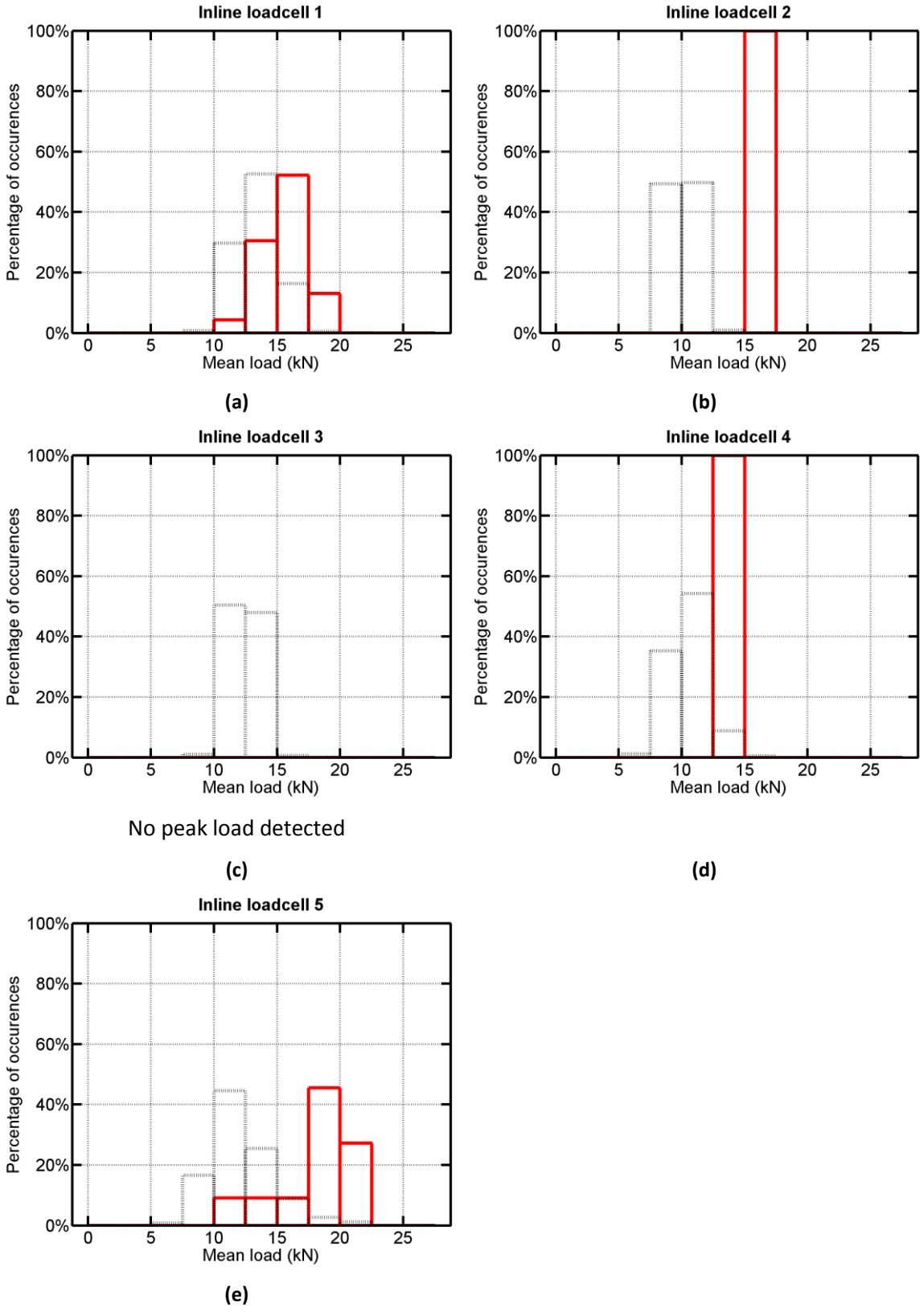

Figure 5.19: Distribution of the mean loads during peak load at Bolt-2 LifeSaver for the five mooring lines (a-e). Red lines: distribution of the mean loads during peak load. Black dotted lines: distribution of the mean of all loads during this period of time on this mooring line

5.4 Comparison with general environmental conditions

The number of occurrences of peak mooring loads relatively to the wave conditions indicates that peak mooring loads are more likely to occur for large, but not necessarily the maximum H_S. This can be clearly seen at both installations in Figure 5.4 (SWMTF) and Figure 5.15 (Bolt 2 Lifesaver).

It should be noted that the points inside the scatter diagram are points in less steep sea states, compared to the point on or close to the contour line. However, it does not mean that steep waves are less likely in this kind of sea states. Actually, steep waves in not so steep seas may be more likely than steep waves in steep seas. This point has been already discussed in HSE (2006). However, for the set of data presented in this thesis, it is difficult to verify if steep waves occurred directly at the buoy and if they were the reasons behind the peak mooring loads (see 1.2). The heave motion is the only indicator of the surface elevation. However, because of non-linearities, the heave motion may be lower the surface elevation.

Peak mooring loads can occur for low value of H_S if the mooring line is aligned with the wave direction. Figure 4.40 (SWMTF) and Figure 5.16 (Bolt 2 Lifesaver) plot a vector $H_{S\,vec}$ (red dots) with an amplitude equal to H_S and a direction equal to the peak direction D_P or the mean direction D_{mean} respectively. The mooring lines are drawn to compare the mooring line orientation with the wave direction. The plots for the general environmental conditions are reminded to facilitate the comparison with the wave conditions associated with peak mooring loads.

It was shown in the previous chapter that two typical wave conditions are occurring for the SWMTF and FaBTest. For the SWMTF one wave condition has waves coming from the East (SWMTF), the other has waves coming from the South. H_S can be high for both wave conditions. At FaBTest, one wave condition has waves coming from the South East, with small associated H_S, the other has waves coming from the South, with higher associated H_S.

The mooring configuration of SWMTF was orientated to have the highest easterly H_S sea states between the mooring lines 1 and 3. The consequences of this choice can be observed on Figure 4.40. Figure 4.40 indicates that no waves were able to align with

line 3, resulting in peak mooring loads only for higher H_S values. In Figure 4.40, the waves coming from the South are able to align with line 1 resulting in peak mooring loads even at low H_S, with wave heights below 1 m. Similarly, the mooring configuration of Bolt 2 Lifesaver was oriented to have the Easterly primary storm between the mooring lines 1 and 2, and the Southerly secondary storm between the mooring lines 1 and 5. Figure 5.16 indicates that storms could align sometimes with mooring line 1 and more often with mooring line 5. The consequence of this alignment is peak mooring loads occurring for low values of H_S. On mooring line 1, peak mooring loads also occurred for waves not aligned but in a close direction of the mooring line, for higher values of H_S.

The relative directionality of the waves and of the mooring lines can explain the difference in the number of occurrences of peak mooring loads for the different mooring lines. For the SWMTF, the significantly lower number of peak mooring loads in line 2 can be explained by the fact that mooring line 2 is not facing the wave direction. Similarly, at Bolt-2 LifeSaver wave energy device, the low number of peak mooring loads in line 2 to 4 is due to the directions of these mooring lines, not facing the waves.

For the SWMTF, the high number of occurrences of peak mooring loads in line 1 compared to line 3 during the second deployment can be explained by the high number of sea states coming from the South during this deployment and consequently facing line 1. The similar number of occurrences of peak mooring loads in line 1 and 3 during the first deployment before anchor drag could be explained by a similar number of waves coming from the South and from the East, facing line 1 and 3 respectively.

Tidal variations have also been investigated. Based on the SWMTF results (Figure 5.6), it can be observed that peak mooring loads are occurring both for low and high tide, and for any current direction. The number of occurrences of low tidal conditions is less frequent than high tidal conditions; however the number of occurrences of peak mooring loads is higher for low tidal conditions for the first SWMTF deployment before anchor drag and for the second SWMTF deployment.

A priori, at low tides, the pre-tension in the mooring system is reduced, and this could lead to mooring line becoming slack followed by snap loads. However, the number of peak load at SWMTF after the anchor drag was highly reduced, when the wave

conditions were similar with the wave conditions before the anchor drag and the main difference was a lower mooring pre-tension.

Two main hypotheses could explain the tidal ranges associated with peak mooring loads:

a) Peak mooring loads are more likely to occur for a particular pre-tension associated with the mooring properties, which would explain why they mainly occur for low water depth before anchor drag and for high water depth after anchor drag. However, this result has been observed only on one mooring line and for a limited period of test, so more data are required to validate this hypothesis.

b) This result is just coincidental and the waves are the main driver of the peak mooring loads. Tidal elevation has a low or no influence on peak mooring loads.

In both cases, the mooring system design should be carefully designed for all tide conditions.

The mooring load amplitude is one of the main governing factors for fatigue analysis. However, other factors should be taken into account for fatigue analysis, such as cycle count. Figure 5.8 and Figure 5.17 indicate the maximum mooring load amplitude which was measured in all mooring lines for a given sea state for the SWMTF and Bolt-2 LifeSaver respectively. It should be noted that the highest amplitudes of mooring loads were not observed on the H_S and T_P wave scatter diagram contour line, but as well within the scatter diagram. The amplitude was however low in terms of percentage of the MBL, below 11% of the MBL for the SWMTF, and below 14% of the MBL at Bolt 2 Lifesaver, which means that the highest measured peak loads were not harmful for the survivability of the mooring system, and would be for the fatigue only if they repeat themselves a high number of times, depending on the R-N curve of the fibre ropes. The available R-N curves for Nylon (Ridge, 2010) require extrapolation for low values of tensions such as the one measured during the field tests. This is discussed in more details in 7.1.2.2.

One of the limitations of this study is that the two test sites used for this study are close to each other, with similar sheltered wave conditions and similar tidal conditions, and installed for a short period of time. They also both use similar multi-leg catenary

moorings. The positive point is that some confidence can be gained in the results by observing similar results at both facilities, and by comparing and explaining the differences. One of the main differences between both facilities is that FaBTest is in a more exposed location. Another difference is that Bolt-2 LifeSaver device uses more catenary mooring lines than the SWMTF buoy, and as a consequence less peak mooring loads are observed on the mooring lines.

This chapter has assessed the influence of environmental conditions on peak mooring loads and has shown that some particular environmental conditions are more likely to trigger peak mooring loads.

Chapter 6. Numerical model validation for mooring systems: Method and application for wave energy converters

This chapter presents tank test results for a scale model of the buoy and mooring used at the South West Mooring Test Facility (SWMTF). More generally, this chapter aims to present methods and procedures which will allow the effective validation of numerical models to enable the development of appropriate mooring systems in wave energy applications. The methods used for these tank tests are methods which have been widely used by the offshore oil and gas industry and are still used to investigate a particular problem. The main difference lies in the type of mooring investigated: in this study, the mooring is particularly compliant, allowing highly dynamic motions of the floating structure, especially in pitch.

Tank tests and numerical models can be used in combination with field tests to improve the understanding of dynamic mooring system. Tank tests give results under a perfectly controlled environment, and the corresponding numerical model can be used to investigate further parameters. However, none of them replace field tests, with inherent installation and operation inaccuracies, ageing and other long-term effects, and very large range of environmental conditions.

Preliminary static, quasi-static, decay, regular and irregular wave tests were conducted on a 1:5 scale model, using the Ifremer basin in Brest. A corresponding numerical model was developed with a time-domain mooring modelling tool, inputting hydrodynamic data from a radiation/diffraction potential modelling program.
After the calibration of several hydrodynamic parameters (added mass, damping and mean drift), the numerical model results are compared with the experimental results, from the tank. A quick comparison is also made with the field test results.

6.1 Experimental set-up and modelling of the mooring system

This section describes the experimental set-up and the numerical modelling of the mooring system. The properties of the basin and its instrumentation are described, the choice of scale is explained, and the scaled properties of the buoy and its mooring are detailed. Finally, the inputs of the numerical model are defined.

6.1.1 Experimental set-up

The tank tests were performed in the Ifremer deep water wave basin in Brest, France. This tank uses sea water with a density of 1,026 kg/m^3 at 17.2°C, and 35.6% salinity (averages based on three sample measurements during the test period using the method described by Sharqawy, Lienhard and Zubair (2010)). The basin is 50 m long, 12.5 m wide and 10 m deep for the first three quarters of its length, where the model is installed. The wave generator is able to generate waves with maximum heights of 0.5 m and with periods from 0.8 to 3.5 s. The mooring loads were recorded with axial load cells installed on the top of each mooring line. Six degree of freedom motions at the centre of gravity of the buoy were determined using a Qualysis video motion tracking system with reflecting targets mounted on the top of the buoy (Figure 6.4a). Surface elevations were measured with servo wave gauges, installed as shown in Figure 6.4b. All measured signals were time synchronised and recorded at 100 Hz.

The scale of the model was determined by the dimensions of the tank, particularly its width. An initial full-scale static numerical investigation with OrcaFlex was carried out to estimate the length of mooring line constantly resting on the seabed for a range of surge/sway (+/-30 m) and heave (+/-15 m) buoy motions. An explanation of OrcaFlex functioning has been given in 2.4.3.3. These motions were the largest observed motions during the sea trials of the SWMTF. The portion of mooring line which rests on the seabed during large displacements does not significantly interfere with the hydrodynamic behaviour of the system and can therefore be truncated. Consequently, the elasticity of the truncated part of the mooring lines is not considered in the numerical model. This could have been taken into account by adding linear springs at the line end on the seabed. The results of this preliminary study indicated that a Froude model scale of 1:5 with a water depth of 5.95 m was feasible. A false floor was installed in the tank to achieve the desired water depth

(Figure 6.4c). Truncated mooring lines were simplified and scaled (Table 6.1). For example, on the full scale SWMTF mooring, section 4 of the mooring line is made of a DN24 open link chain and of a 9.5 tonnef shackle. In the scale model mooring, only a chain was used while taking into account the weight of the shackle. The drag and inertia coefficients for the mooring lines were taken from DNV standards (DNV-OS-E301, 2013) for the nylon lines and from the OrcaFlex manual (Orcina, 2014) for the chains. The axial stiffness of three samples extracted from the used model rope was quantified using tension testing equipment at Ifremer (Weller, et al. in review). The yarns demonstrated axial stiffness values between 10.0 and 12.6 kN when subjected to scaled (by N/Tex, Tex being a measurement unit for linear density in textile applications and N/Tex being a normalised value of material strength) loading using a 25 s oscillation period. An average value of 10.873 kN was used in the numerical model, while the scaled value of the stiffness of the rope used at the SWMTF ranges between 7.1 and 7.8 kN. This scale is just for static or slowly varying loads. It would be interesting in the future to evaluate the dynamic scaling, in particular for further investigations evaluating peak mooring loads. These tank tests were conducted for moderate sea states and not aiming to investigate the extreme loads.

The model was orientated with mooring lines 1 and 3 facing the wave symmetrically, and all tests were carried out with a wave incidence angle equal to zero (Figure 6.4b). Table 6.2, adapted from Le Roux (2012), and Figure 6.4a give details about the scale model properties.

Table 6.1: Properties of the original mooring lines and of the simplified, scaled and truncated mooring lines where C_{Dn} and C_{Mn} are normal drag and inertia coefficients, C_{Da} and C_{Ma} are axial drag and inertia coefficients. E: Young Modulus, A: rope section area

Section: top(1) to bottom (4)	Components of full scale SWMTF mooring	Properties of the scaled mooring lines								
		Section simplified mooring	Length (m)	Nominal diameter (m)	Weight (N/m)		Axial stiffness (*EA*, kN)	Drag coefficient		Inertia coefficient	
					In air	In water		C_{Dn}	C_{Da}	C_{Mn}	C_{Ma}
1	Swinging arm 4x9.5 tonnef shackle rope thimble load cell 10 tonnefswivel 25 tonnef shackle large rope thimble	Chain	0.259	0.008	17.191	14.994	6464	1	0.4	1	0.07
2	Nylon rope: Bridon Superline 44mm diameter	Rope	4.0	0.009	0.235	0.0417	Scaled value for full scale facility:7.1-7.8 Tank (mean): 10.873	1.6	0	1	0
3	2x9.5 tonnef shackle 10 tonnef swivel 25 tonnef shackle large rope thimble	Chain	0.126	0.006	17.515	15.279	3.636×10^6	1	0.4	1	0.07
4	DN24 open link chain 9.5 tonnef shackle	Chain	5.672	0.0049	4.520	3.942	2.0505×10^6	1	0.4	1	0.08

Table 6.2: Full scale and theoretical and measured model buoy properties. COG = centre of gravity

	Full scale SWMTF values	Theoretical scaled values	Measured scaled values	Relative error
Mass (kg)	3,108	24.86	24.86	0%
Distance between COG and bottom of keel (m)	1.13	0.2260	0.2262	0.09%
Moment of inertia I_{xx} (kg.m^2)	4,260.75	1.3634	1.4141	3.72%
Moment of inertia I_{zz} (kg.m^2)	1,178.83	0.3772	0.3963	5.06%

6.1.2 Modelling of the mooring system

Mooring system software such as OrcaFlex requires the specification of hydrodynamic parameters. Hydrostar, a radiation/diffraction potential code, was used to calculate the hydrodynamic properties for a simplified hull shape (Figure 6.4d) and for each angular wave frequency, from 0.11 to 13.42 rad/s, in increments of 0.11 rad/s. This simplified shape does not include the vertical triangular braces at the bottom of the buoy (Figure 6.4 a), therefore the added mass and hydrodynamic damping associated with these features are not accounted for. The frequency-dependent data calculated for each of the 6 degrees of freedom of the buoy were:

a) the load Response Amplitude Operators (RAOs) and associated phases at the metacentre at the equilibrium position of the buoy (Figure 6.1),

b) the added masses at the centre of gravity (COG) of the buoy (Figure 6.2),

c) the radiation damping values at the COG of the buoy (Figure 6.2), and

d) the Quadratic Transfer Functions (QTFs) at the metacentre at the equilibrium of the buoy (Figure 6.3).

The viscous damping cannot be calculated by radiation/diffraction potential codes. It should be noted that the metacentre has been chosen for some calculations while the centre of gravity is more commonly used (for example by WAMIT).

The natural and resonance periods of the floating structure were also provided in Table 6.3.

Amplitude **Phase**

X

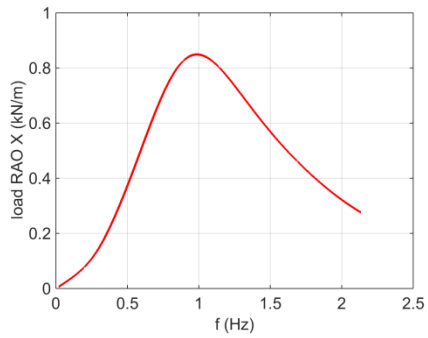

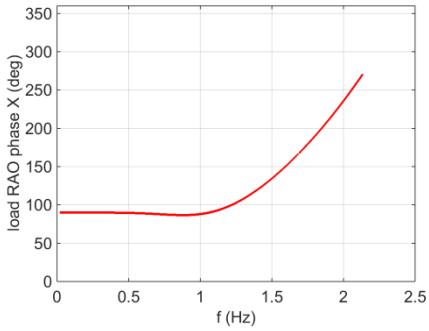

Z

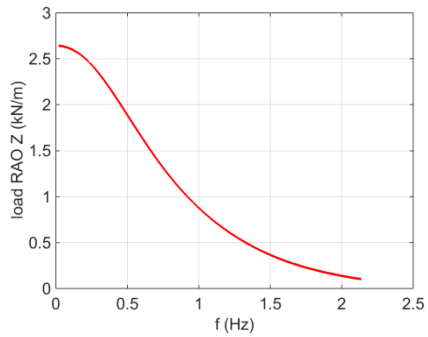

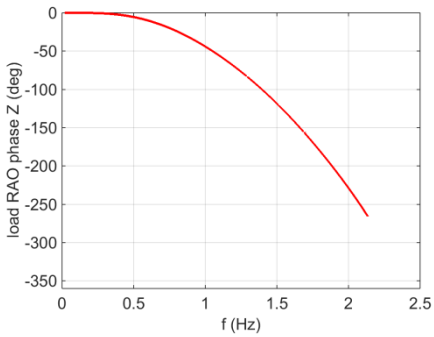

pitch

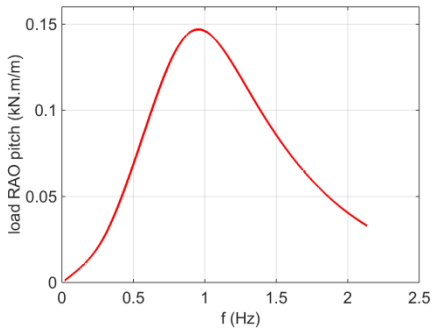

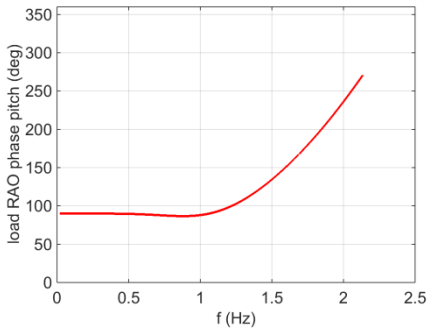

Figure 6.1: Model scale load RAOs and associated phases for the surge, heave and pitch motion as calculated by the radiation/diffraction potential code Hydrostar

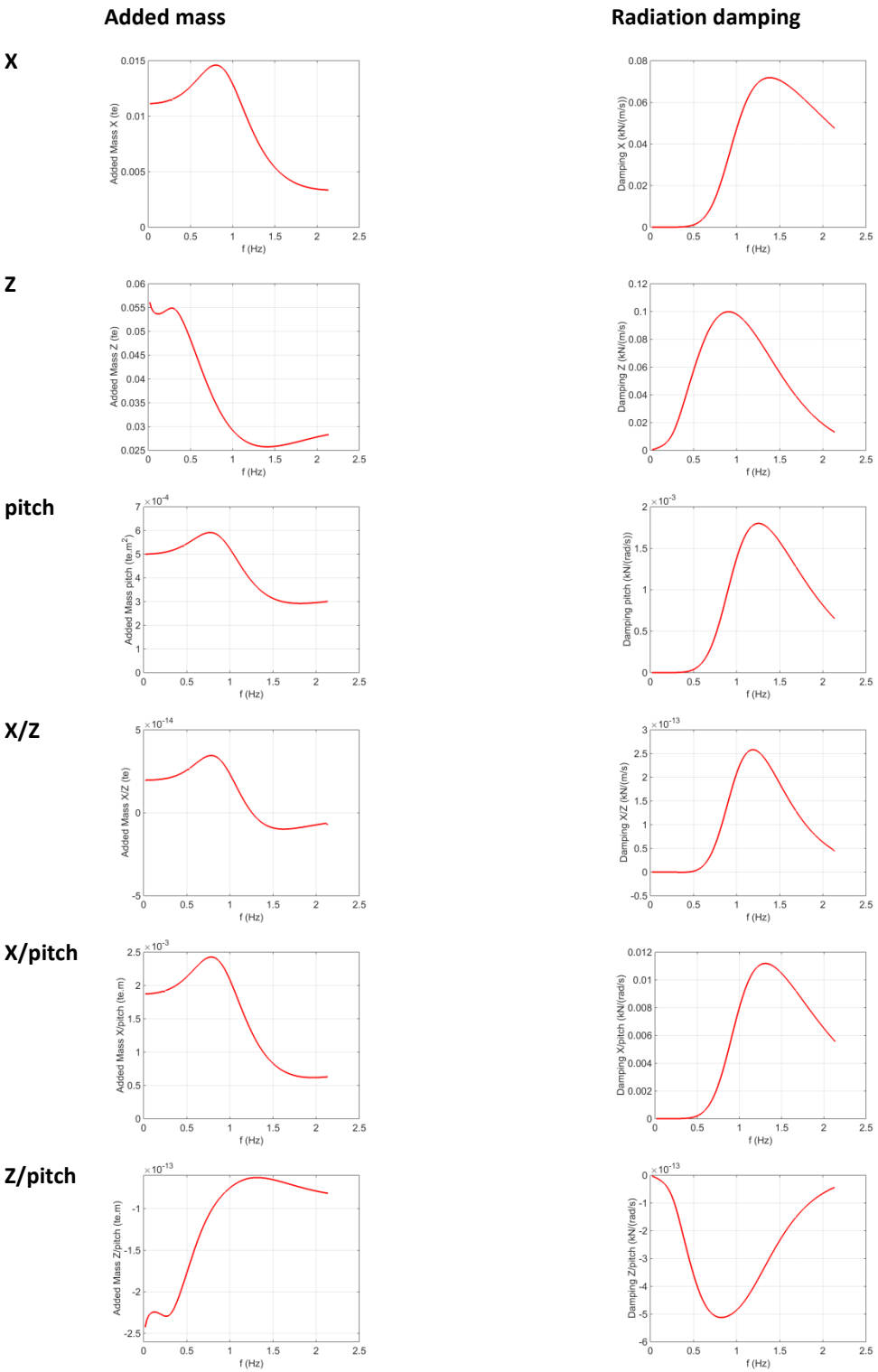

Figure 6.2: Model scale added mass and radiation damping for the surge, heave and pitch motion, and for the interactions between these motions as calculated by the radiation/diffraction potential code Hydrostar

X

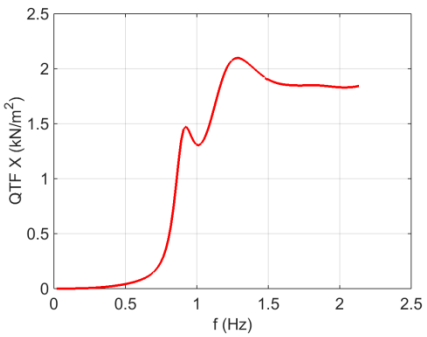

Z

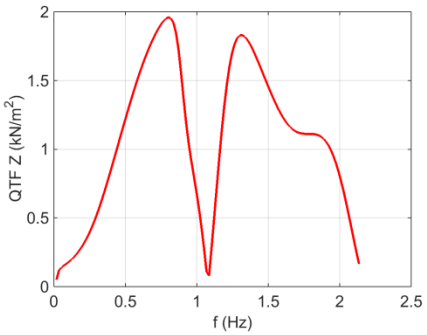

pitch

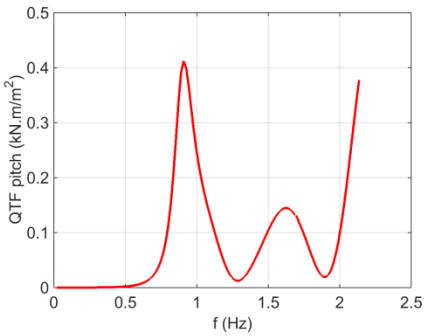

Figure 6.3: Model scale QTF for the surge, heave and pitch motion as calculated by the radiation/diffraction potential code Hydrostar

Table 6.3: Model scale natural and resonance period and associated frequency for the SWMTF floating structure as calculated by radiation/diffraction potential codes

	Natural period (Le Roux, 2012) Period/frequency	**Resonance period (Soulé and Le Boulluec, 2013) Period/frequency**
Surge/sway	11.09 s / 0.09 Hz	/
Heave	0.89 s / 1.12 Hz	0.94 s / 1.06 Hz
Roll/pitch	1.07 s / 0.93 Hz	1.12 s / 0.89 Hz
Yaw	2.82 s / 0.35 Hz	/

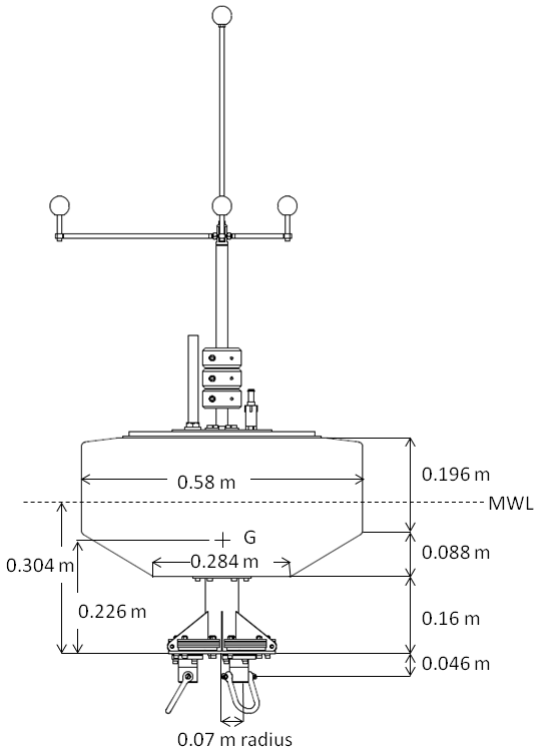

(a)

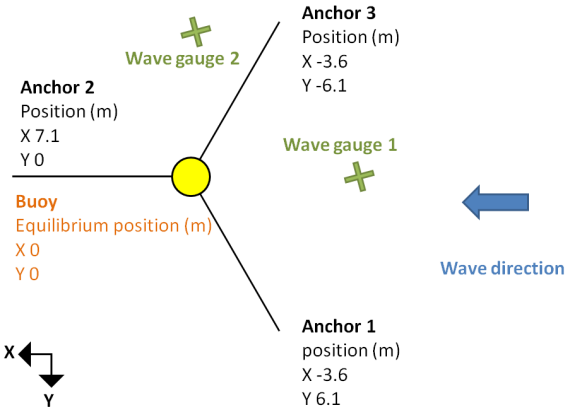

(b)

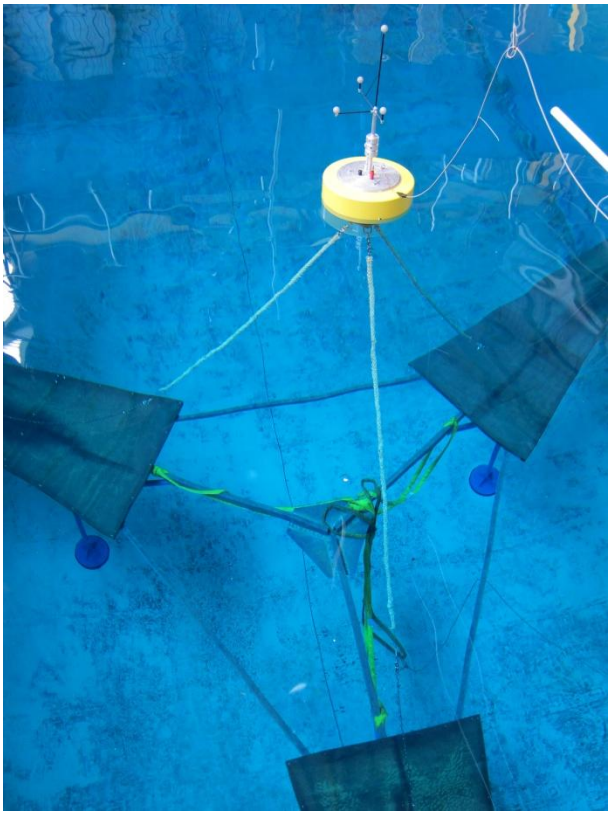

(c)

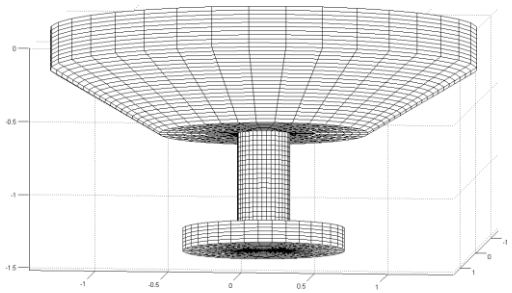

(d)

Figure 6.4: Wave basin installation and numerical model settings of the SWMTF : a) side view of the scaled buoy and dimensions, b) top view of the truncated mooring and of the wave gauge layout, c) photograph in the basin, with the false floor and d) buoy hull mesh used for the radiation/diffraction potential analysis

To simplify the OrcaFlex calculations, Newman's approximation was used for the QTFs. This approximation considered that the full QTFs should not influence significantly the behaviour of the device; consequently only the mean drift forces are required to estimate the second order motion of the floating structure. De Hauteclocque et al. (2012) discussed the differences in results using different methods to calculate the second-order low frequency loads in shallow water and found that the two key parameters for a proper estimation of the behaviour of the moored system are the water depth and the resonance period: the Newman approximation can give accurate results for a compliant system in deep water. For this experiment, the low Ursell number (Eq(6.1)) and the low wave steepness (shown in detail for the regular waves in Figure 6.10) indicates that the conditions are linear (linear wave theory, DNV-RP-C205, from DNV, 2010). Furthermore, the mooring system is highly compliant, and its resonance periods, highlighted by the regular wave tests are relatively small.
In order to validate this assumption, model runs with the full QTFs will be compared with a model using the Newman's approximation in subsection 6.2.4.

The numerical model was run using an implicit integration method, with a time step of 0.01s. Accuracy of the results with the implicit integration method was assessed by comparing them with results using the explicit integration method.

$$Ur_{\max} = \frac{H_{\max}\lambda_{\max}^2}{8\pi^2 h^3} = \frac{0.5\times 5.2^2}{8\pi^2 5.95^3} = 0.00081 << 1 \tag{6.1}$$

where H_{max} is the highest wave height used for regular wave tests, λ_{max} is the longest wave length used for regular wave tests and h is the water depth.

6.2 Validation results

This section will present results from the different tests. The aim of this series of tests is to obtain an accurate model in realistic sea states. As shown in Figure 6.5, each test will provide different information about the hydrodynamics of the buoy and its mooring. This information will then be used to finely calibrate the numerical model and correct potential inaccuracies. The calibration of the model will be done using best fit models a) for the surge added mass, quadratic damping and linear damping using the decay test results and b) for the pitch quadratic damping and surge QTFs using the regular wave test results. The drag forces applied on the mooring lines are assumed to be correct.

The numerical model is built using the potential radiation-diffraction theory. Consequently, the buoy properties (RAOs, added mass...) have been calculated for a constant draft and for infinitesimally small waves. As discussed previously, the Newman's approximation has been used for the QTFs to simplify the calculations.

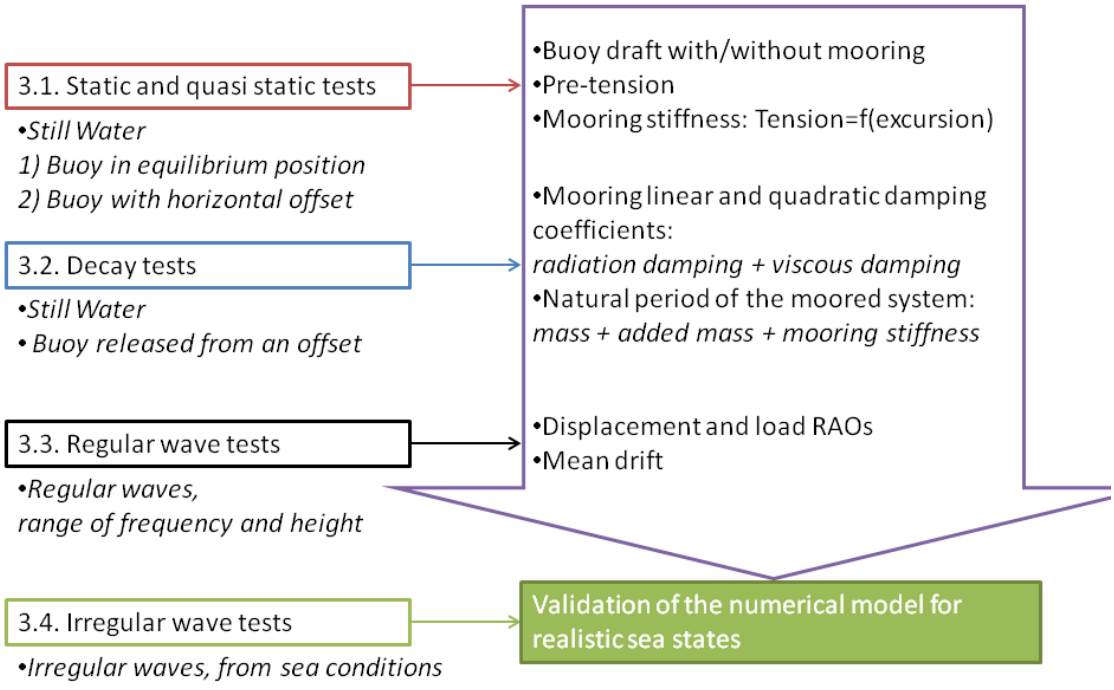

Figure 6.5: Range of tests needed to validate a numerical model with experimental data

6.2.1 Static and quasi static tests

Static tests were conducted in still water conditions to determine the buoy draft, with and without mooring lines in place. In free-floating conditions, before attaching the mooring lines, the centre of gravity of the buoy was at 0.078 m below the mean water level in the basin. This distance was set in the numerical model. After the attachment of the mooring lines, the centre of gravity was 0.10 m below the mean water level and the mooring pre-tension was 18 N in both the basin and the numerical model.

Quasi-static tests were used to identify the horizontal stiffness characteristics of the mooring system, by determining the relationship between the buoy horizontal position and the mooring line tensions. The model was placed in the basin in still water conditions. The buoy was held in different surge positions and the mooring tensions were measured for each surge position.

The results of the quasi-static tests are presented in Figure 6.6a, indicating the tension in the mooring lines for a given surge offset. The results of the tank tests and of the numerical model show an excellent agreement with a relative error not exceeding 6% (Figure 6.6b).

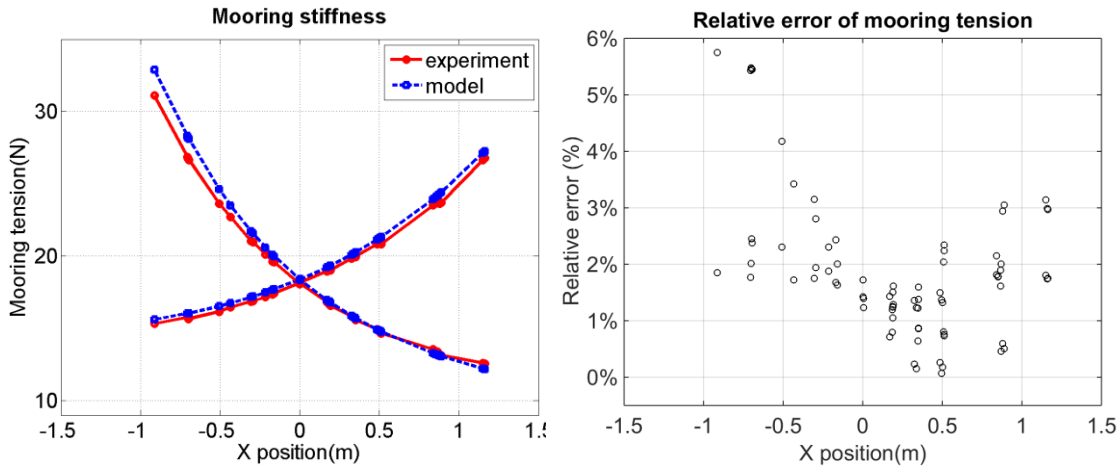

Figure 6.6: SWMTF model mooring stiffness: a) comparison of the experimental (red circles and solid line) and modelled (blue circles and dashed line) mooring load/buoy surge offset relationship and b) relative error in mooring tension between experimental and modelled values

6.2.2 Decay tests

Decay tests were carried out to evaluate the linear and quadratic damping and the added mass of the buoy from its natural period. Decay tests involve moving the moored buoy from its equilibrium position in one degree of freedom and then releasing it. The buoy moves at its natural frequency for this degree of freedom, and the amplitude of motion decreases because of the damping of the system. A Matlab code called Wave Analysis for Fatigue and Oceanography, usually referred to as WAFO (Wave Analysis for Fatigue and Oceanography ,WAFO group, 2011), was used to detect peaks and troughs in the decay time series. The first decay oscillation was ignored for calculation, because the buoy may have experienced additional damping due to the release of the mooring. For each decay test, the subsequent 5 peaks and 5 troughs were used to calculate the natural period and damping coefficients. The amplitude of release used for the numerical model was the mean amplitude after the first oscillation during the tank tests. The amplitudes of release and after one oscillation during tank tests are given in Table 6.4 (surge) and Table 6.5 (pitch).

Table 6.4: Results for the surge decay tests: amplitude of release and after one oscillation, natural period T_m, linear damping p_1 and quadratic damping p_2, and norm of the residuals associated with the damping linear fit

		Surge	Mean	Standard deviation
Amplitude of release(m) / amplitude after 1 oscillation (m)	Exp. 1	-0.69/-0.076	Mean(abs) = 0.70/0.084	Std(abs) = 0.075/0.0078
	Exp. 2	-0.59/-0.083		
	Exp. 3	-0.82/-0.074		
	Exp. 4	0.70/0.092		
	Exp. 5	0.67/0.090		
	Exp. 6	0.73/0.090		
Natural period T_m (s)	Exp. 1	11.06	11.11	0.0447
	Exp. 2	11.09		
	Exp. 3	11.11		
	Exp. 4	11.14		
	Exp. 5	11.10		
	Exp. 6	11.19		
p_1 (s^{-1})	Exp. 1	0.03133	0.0393	0.0127
	Exp. 2	0.02737		
	Exp. 3	0.02688		
	Exp. 4	0.04234		
	Exp. 5	0.05554		
	Exp. 6	0.05249		
p_2 (m^{-1})	Exp. 1	4.876	5.0949	0.3036
	Exp. 2	4.643		
	Exp. 3	5.119		
	Exp. 4	5.227		
	Exp. 5	5.523		
	Exp. 6	5.181		
Norm of the residuals	Exp. 1	0.05360	0.1041	0.0750
	Exp. 2	0.03701		
	Exp. 3	0.03732		
	Exp. 4	0.1121		
	Exp. 5	0.2150		
	Exp. 6	0.1697		

Table 6.5: Results for the pitch decay tests: amplitude of release, natural period T_m, linear damping p_1 and quadratic damping p_2, and norm of the residuals associated with the damping linear fit. Exp = experiment

		Pitch	Mean	Standard deviation
Amplitude of release(°) / amplitude after 1 oscillation (°)	Exp. 1	-7.3/-4.0	Mean(abs) = 3.7/2.3	Std(abs) = 2.1/1.1
	Exp. 2	-3.0/-2.1		
	Exp. 3	-3.6/-2.4		
	Exp. 4	-3.2/-2.2		
	Exp. 5	1.6/0.93		
Natural period T_m (s)	Exp. 1	1.070	/	/
	Exp. 2	1.080		
	Exp. 3	1.095		
	Exp. 4	1.120		
	Exp. 5	1.088		
p_1 (s^{-1})	Exp. 1	/	/	/
	Exp. 2	/		
	Exp. 3	-0.5105		
	Exp. 4	/		
	Exp. 5	0.01242		
p_2 (rad^{-1})	Exp. 1	/	/	/
	Exp. 2	/		
	Exp. 3	0.9197		
	Exp. 4	/		
	Exp. 5	0.3268		
Norm of the residuals	Exp. 1	/	/	/
	Exp. 2	/		
	Exp. 3	0.8512		
	Exp. 4	/		
	Exp. 5	0.1585		

The assumption is made that the natural period depends mainly on the stiffness of the moored system, its mass and added mass. However, the experimental value includes the damping from the mooring system, which may not be negligible and may be frequency dependent for a relatively small buoy. Quasi static tests indicated that the stiffness of the mooring system in the numerical model is very close to the experimental stiffness, and the model buoy was weighed before the tank tests, as shown in Table 6.2, with a perfect agreement between the experimental and

numerical values. By elimination of the other parameters, this means that the natural period is aiming to validate the value of added mass calculated by the radiation-diffraction code. The natural period was calculated as the mean time between similar extreme values (peak or trough).

The radiation damping forces depend linearly on the magnitude of relative velocity between the sea and the buoy, and the viscous damping by a quadratic relationship. The overall damping was calculated for the tank tests and for the numerical model, and was separated into a linear and a quadratic coefficient: $p_1 + p_2|\xi_j|i\omega$, with ξ_j the motion amplitude in one degree of freedom and ω the angular frequency. p_1 and p_2 are coefficients which can be calculated using the relation described by Faltinsen (1990), assuming the damping to be constant with respect to the oscillation amplitude (Eq.(6.2)):

$$\frac{2}{T_m}\log\left(\frac{X_{n-1}}{X_{n+1}}\right) = p_1 + \frac{16}{3}\frac{X_n}{T_m}p_2 \tag{6.2}$$

where X_n is the amplitude of the nth oscillation and T_m is the natural period of oscillation. Figure 6.7a and b illustrate this method: a) extremes are detected, and b) $\frac{2}{T_m}\log\left(\frac{X_{n-1}}{X_{n+1}}\right)$ is plotted against $\frac{16}{3}\frac{X_n}{T_m}$, allowing the calculation of p_1 and p_2 by linear regression using a least square method. The norm of the residual was calculated to give an indication of the goodness of the fit.

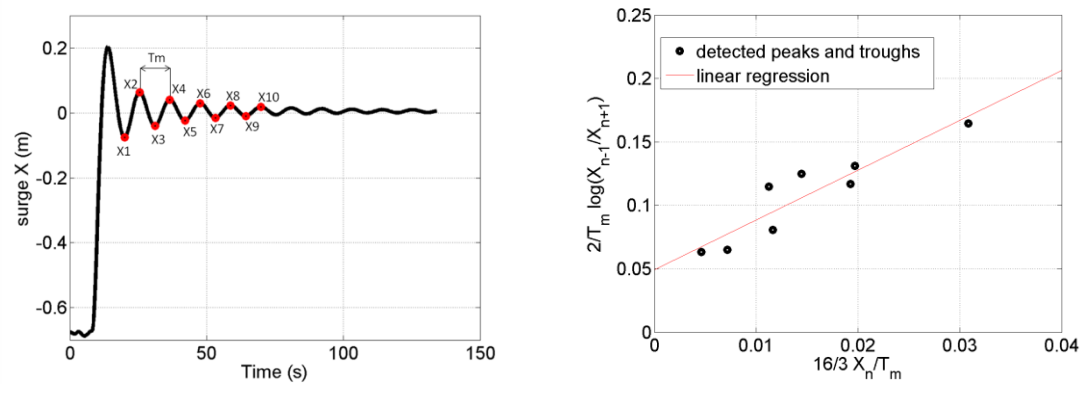

(a) **(b)**

Figure 6.7: Example of calculation of the natural period and linear and quadratic damping based on tank test results: a) detection of peaks and troughs and calculation of the natural period, b) calculation of the linear p_1 and quadratic p_2 damping coefficients using a linear fit; norm of the residua l = 0.036

Decay results from the tank tests and from the initial numerical model are presented in Figure 6.8a and b and Table 6.4 to 6.5. Test repeatability was evaluated using the standard deviations of natural period, damping coefficients and norms of the residuals between the different experiments. Table 6.4 indicates that for the different surge decay tests, similar results were obtained for the natural period and the quadratic damping coefficients, and more variability was observed for the linear damping coefficients. Because of this repeatability, the values chosen to calibrate the numerical model are the mean values of natural period and damping coefficients over the six experiments. The pitch decay tests provide a larger range of natural period and damping values for the different experiments. This lack of repeatability may be due to a coupling of the pitch motion with the surge motion, as seen in Figure 6.8b. This coupling can be due to a similar behaviour in surge and pitch, as shown in Figure 6.1, with similar resonance period and similar phases. For the decay motion tests, large amplitudes of the surge motion - up to 0.4 m for a 8° pitch motion (amplitude peak to peak)- are observed and the pitch motion does not oscillate around zero. Because of this lack of repeatability, the pitch motion properties could not be evaluated accurately and the experimental values could not be used to calibrate the numerical model. Several methods have been developed to investigate coupled motions, for example by Liagre and Niedzwecki (2003) and could be used for further investigations.

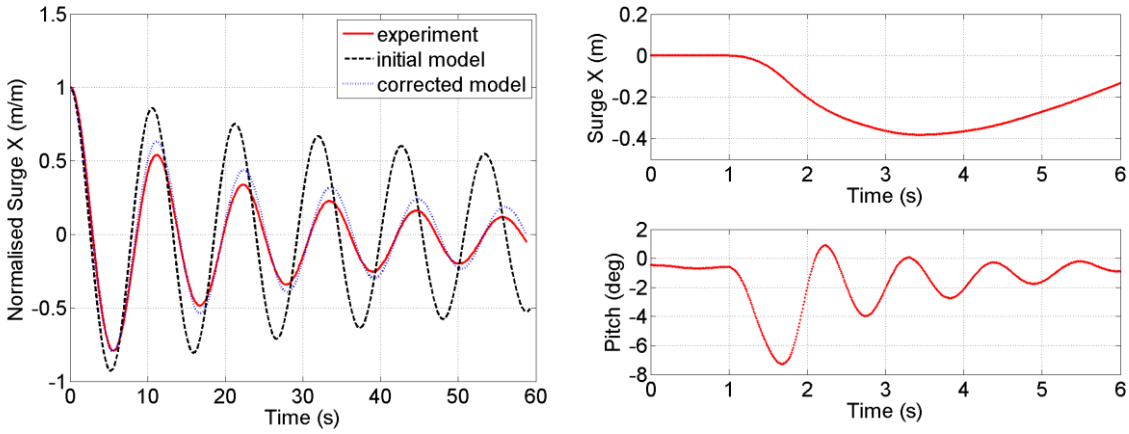

Figure 6.8: Time-series of decay tests in a) surge, with comparison between the experimental values (red solid line), initial (dashed black line) and corrected numerical model (blue dotted line) and in b) pitch, with a plot of the experimental surge motion to show the coupling between surge and pitch

Table 6.6: Comparison of experimental and numerical results: natural period T_m, linear damping p_1 and quadratic damping p_2 for surge decay

	Values measured from tank	Initial numerical model: value/relative error	Corrected numerical model: value/relative error
Natural Period T_m (s)	11.11	10.68/4%	11.20/1%
p_1 (s^{-1})	0.0393	0.0008/98%	0.0426/ 8%
p_2 (m^{-1})	5.0949	1.0503/79%	4.7488/7%

The initial numerical model was underestimating the damping of the system and the natural period in surge (Figure 6.8a, Table 6.6). The inaccuracies in the added mass and linear damping may have been due to the simplified hull shape or the inabilities of the radiation-diffraction model to evaluate viscous damping. Following an iterative process, the added mass, linear and quadratic damping values were adjusted until the numerical natural periods and damping coefficients matched the experimental values:

a) The surge added mass is multiplied by coefficients between 1 and 1.5 for all the wave frequencies and simulations are run with these corrected added masses; the natural period is calculated for each added mass simulation and plotted against the multiplying coefficients (Figure 6.9a). A linear fit estimates the value of the multiplying coefficient which leads to a similar experimental and modelled natural period. The mass of the buoy was 24.86 kg and the added mass was varying between 3.36 and 14.6 kg (surge/sway) and 25.7 and 56.1 kg (heave). A multiplying coefficient of 1.5 for the added mass would then consequently be a large multiplying coefficient, because the order of magnitude of the mass and added mass is similar, meaning that either the added mass has not been properly calculated, either, and more likely, other effects such as damping were having an influence on the natural period.

b) Additional quadratic damping value is added to the numerical model with values between 0 and the total quadratic damping value, p_2, calculated from the tank tests. Simulations are run with this additional damping. The quadratic damping coefficient, p_2, is calculated for each simulation and plotted against the additional quadratic damping (Figure 6.9b). A linear fit gives the value of additional damping which leads to a similar experimental and modelled quadratic damping, p_2.

c) Additional linear damping is slowly increased in the numerical model. For each value of additional linear damping, the linear damping coefficient, p_1, is calculated and

plotted against the value of additional linear damping (Figure 6.9c). Following a similar method than previously, a value of additional linear damping is chosen for further calculations.

Calibrations are summarised in Table 6.7. The added mass multiplying coefficient is relatively high, which could mean that the difference in natural period between the numerical model and the tank test could be due to something else than the added mass. For the surge, the corrected model shows a good agreement with the experimental data, as seen in Figure 6.8a or Table 6.6, with less than 8% relative error between the measured and modelled natural periods and damping values.

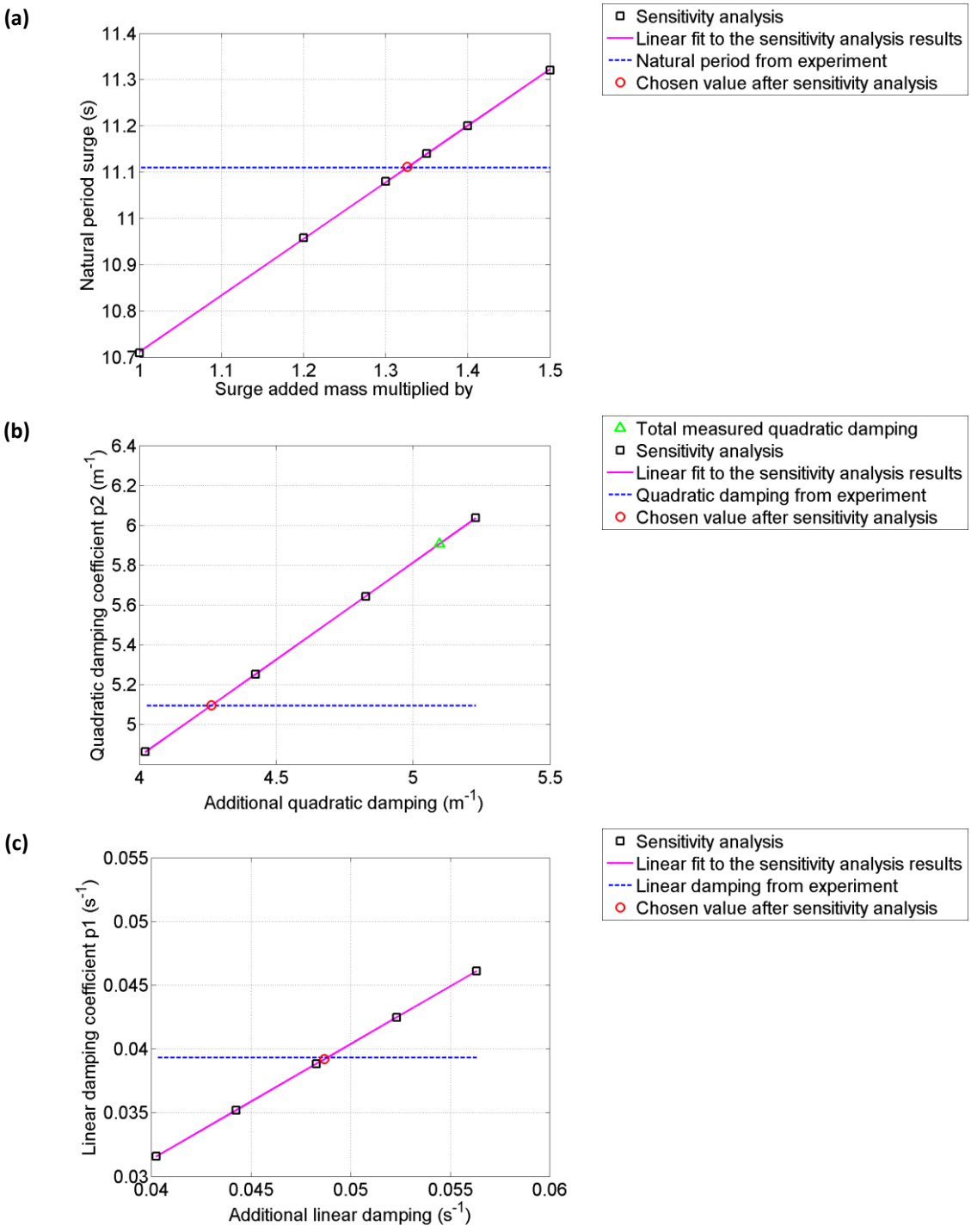

Figure 6.9: Sensitivity analysis for the surge decay: a) for the added mass; b) for the quadratic damping; c) for the linear damping

Table 6.7: Correction implemented on added mass, linear damping p_1 and quadratic damping p_2 for the surge motion

Added mass multiplied by	Additional Linear damping p_1 (s^{-1})	Additional Quadratic Damping p_2(m^{-1})
1.3262	0.0487	4.2639

6.2.3 Regular waves tests

Regular wave tests aim to evaluate Response Amplitude Operators (RAOs) of the buoy motions together with the mean drift for a large range of wave periods and wave steepness values. The RAOs are transfer functions indicating the response of the buoy in each degree of freedom for a range of wave frequencies. Results from the regular wave tests will additionally be used to evaluate the damping of the pitch motion.

A total of 36 different tests were carried out using sinusoidal waves with wave periods and wave heights from 0.88 s to 2.3 s and from 0.03 m to 0.5 m respectively as shown in Figure 6.10. These tests correspond to waves with a period from 1.97 s to 5.14 s and a height from 1.5 m to 2.5 m at full scale, which are operational sea states at the SWMTF site, but not extreme sea states. The choice of wave period and wave frequency was limited by the wave-breaking limit (H/λ=0.14 in deep water with H is the wave height and λ is the wave length) as well as the performance of the tank. Non-linear effects can be considered in waves if (Sarpkaya and Isaacson, 1981, Eq. (6.3)):

$$\frac{H}{\lambda} > \frac{1}{2}\left(\frac{H}{\lambda}\right)_{\max} \text{ with } \left(\frac{H}{\lambda}\right)_{\max} \text{ at the wave breaking limit} \qquad (6.3)$$

$$\text{Hence } \frac{H}{\lambda} > \frac{1}{2}0.14 \text{ in deep water}$$

The mooring system behaviour for steep waves was separately investigated (filled circles in Figure 6.10), while the behaviour for waves with small amplitudes was used to determine the validity of response predictions based on linear wave theory. Wave periods near the resonance periods of the system were investigated in detail. The tests were run for a duration of at least 10 wave periods in order to observe the steady response of the floating structure.

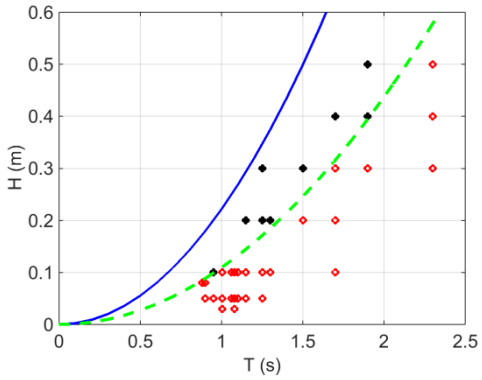

Figure 6.10: Tests in regular waves: Wave height *H* and wave period *T* used for the tank tests: the green dotted line is separating the steep and the linear waves, and the blue solid line is separating steep waves and breaking waves (with the hypothesis of deep water). The black filled circles indicate steep waves while the red hollow circles indicate linear waves.

Time series of experimental and modelled wave elevations and buoy motions are analysed using a least squares fit method to estimate the amplitude, period and phase. It would actually have been better – simpler and safer - to use a FFT procedure, which is a standard procedure. The time-series are fitted to a cosine as described in Eq.(6.4) and Eq.(6.5) and shown in Figure 6.11a. The mean of the motion, which is also the mean drift, was removed before the fit. The covariance between the original data and the fitted curves was indicating the correlation between the data.

$$Wavefit(t) = \frac{H_w}{2}\cos(\omega_w t + \varphi_w) \tag{6.4}$$

$$Motionfit(t) = \frac{H_m}{2}\cos(\omega_w t + \varphi_m) \tag{6.5}$$

Very good agreement was achieved for the heave, pitch and the waves, with values over 99% for the correlation coefficient between the data and the fit for the numerical and experimental heave, and over 83% for the pitch. The only fit which has a significantly lower correlation coefficient was for the experimental surge motion, with correlation values down to 42% for combinations of low wave periods and wave heights as shown in Figure 6.11b. In these cases, a low frequency surge motion was observed in the tank (Figure 6.11c). This low frequency motion may have been due to the transient state of the wave motion, when the wave train reaches the body which is not moving. Consequently, the slow drift forces suddenly increase, before decaying.

The solution to validate the fit was to filter the surge motion with a moving average using 250 data points – 2.5 s, which removes the slow motion of the buoy and not the wave frequency motion which as a shorter period. The filtered data and the fit show correlation coefficients over 97%, which validates the fit.

The RAOs were then calculated as H_m/H_w and the associated phases as φ_m-φ_w. The mean drift was divided by the square of the wave amplitude because the drift forces are proportional to the wave amplitude squared.

Results (model scales) for the regular waves are presented in Figure 6.12 (mean drift) and Figure 6.13 (motion RAOs and phases). Red circle markers indicate values measured during the experiment and black diamond markers values calculated by the initial numerical model. Filled markers are used for data obtained with steep waves, as defined previously.

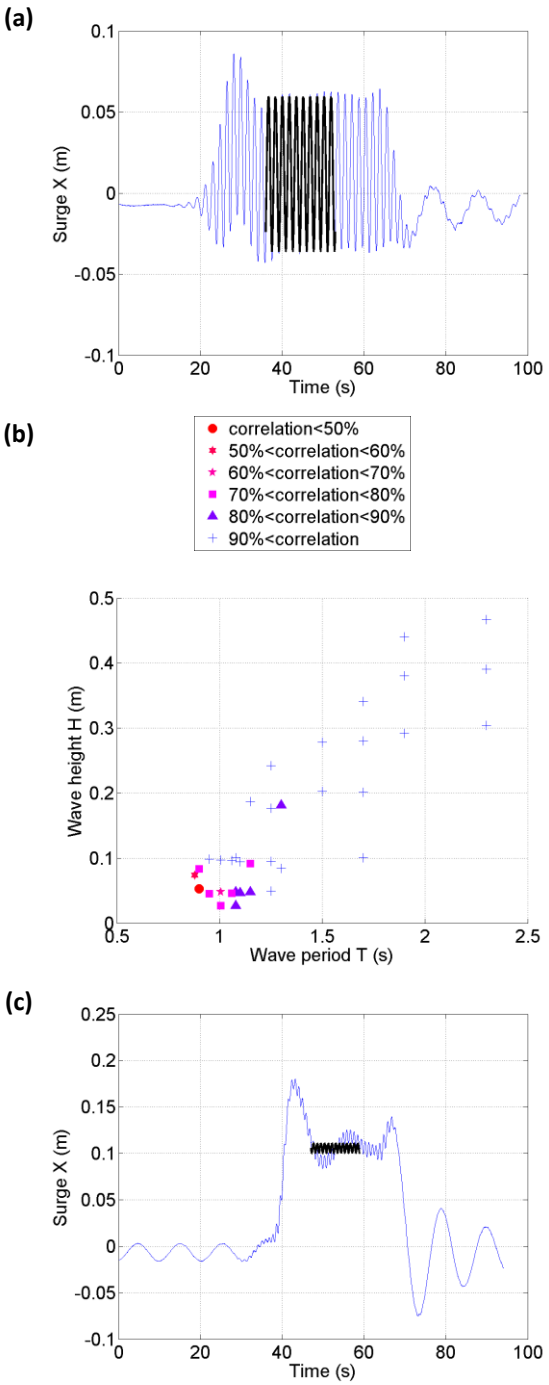

Figure 6.11: Examples of fit of the experimental surge motion: a) for *H* = 0.1 m and *T* = 1.7 s (blue line: signal, black line: fit); b) Summary of the correlation coefficient between the fit and the experimental values c) Examples of fit for *H* = 0.05 m and *T* = 0.9 s where a low frequency motion on the X axis can be observed (blue line: signal, black line: fit)

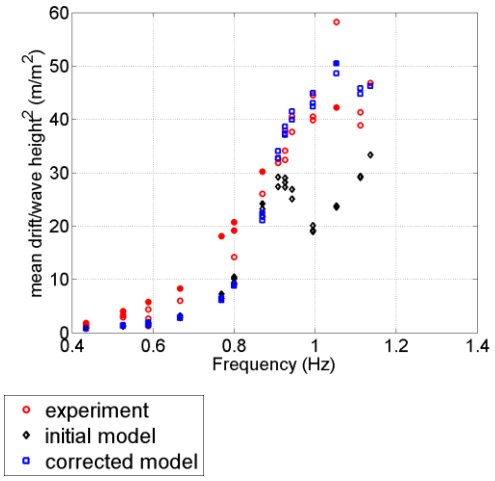

Figure 6.12: Mean drift divided by the square of the wave amplitude for different wave frequencies and wave steepness values.

For wave frequencies over 0.9 Hz, the modelled mean drift (Figure 6.12) was underestimated by the initial numerical model and actually appeared to decrease between 0.9 and 1 Hz for the initial numerical model, with a minimum value at 19 m/m^2 at 1 Hz while the minimum experimental value is at 40 m/m^2. This decrease originates from the potential radiation-diffraction code which calculated the mean drift forces with this shape before inputting them into the numerical model. This was possibly due to the heave and pitch resonance of the moored system at this frequency (Figure 6.13, Table 6.3). The mooring linearised stiffness could have been included in the QTF calculation to avoid this discrepancy. A methodology to correct the QTFs will be proposed below.

Response Amplitude Operators (RAO) analysis are used to describe the first order motions. The main result from the RAO analysis is that the initial modelled pitch RAOs are largely overestimating the pitch RAOs around the resonant frequency f = 0.9 Hz. The maximum modelled value at this frequency was equal to 843°/m (8.43°/cm) while the maximum experimental value was equal to 521°/m (5.21°/cm). These values seem at first unrealistic because too high but results were obtained for very small wave heights and are presented at the model scale. For example, for the highest experimental value, H was equal to 0.03 m (3 cm) and T was equal to 1.08 s meaning that the buoy was pitching with an amplitude peak to peak of 521°/m x 0.03 m = 15.6° (Figure 6.14). These results confirm the highly dynamic behaviour of the mooring system.

The high values in the initial numerical model are due to the lack of damping in pitch, with quadratic damping forces not considered in the numerical model at this stage as described in the previous section. A methodology to add quadratic damping will be proposed below.

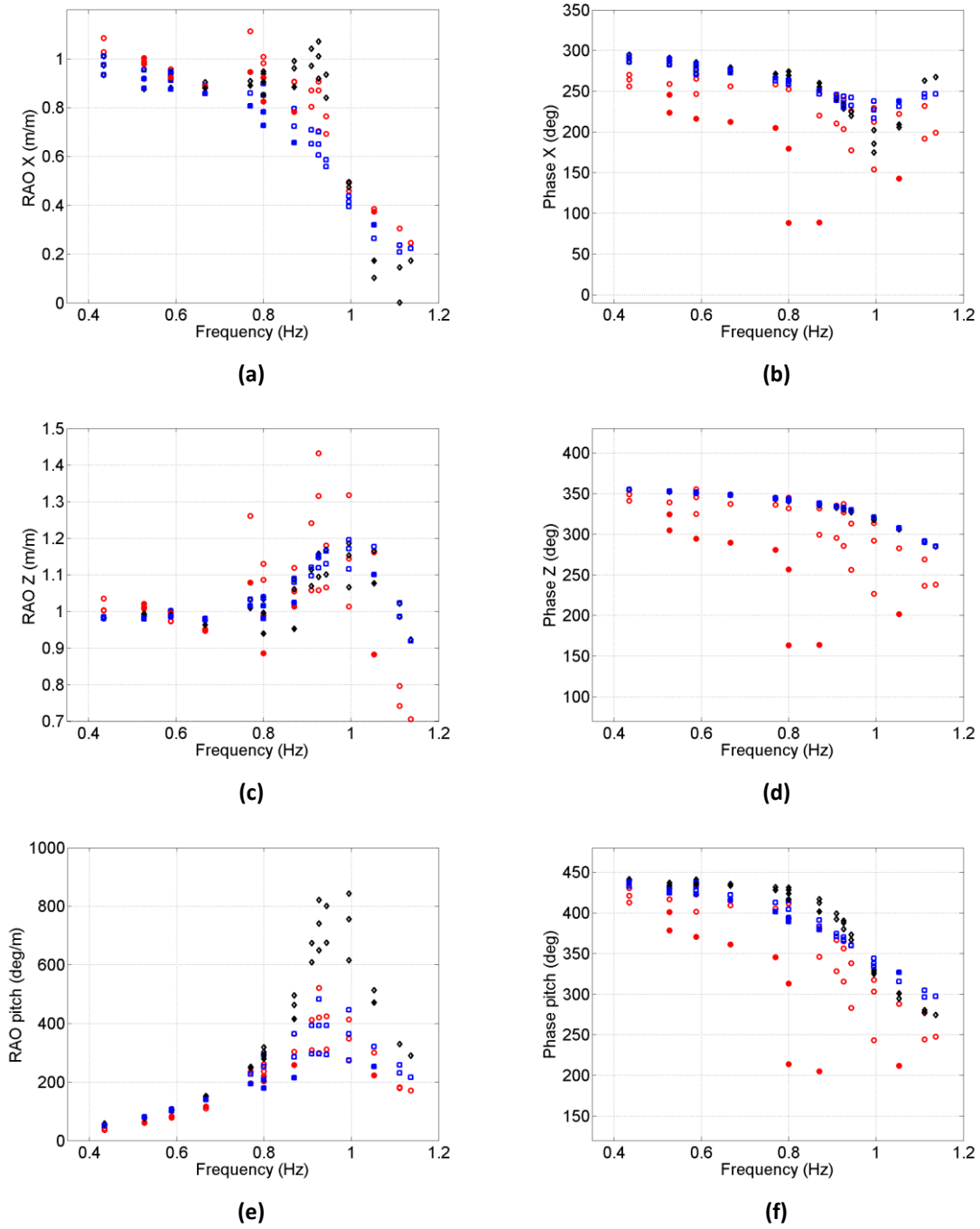

Figure 6.13: Motion RAOs for the surge, heave and pitch (from top to bottom): amplitudes (left) and phases (right)

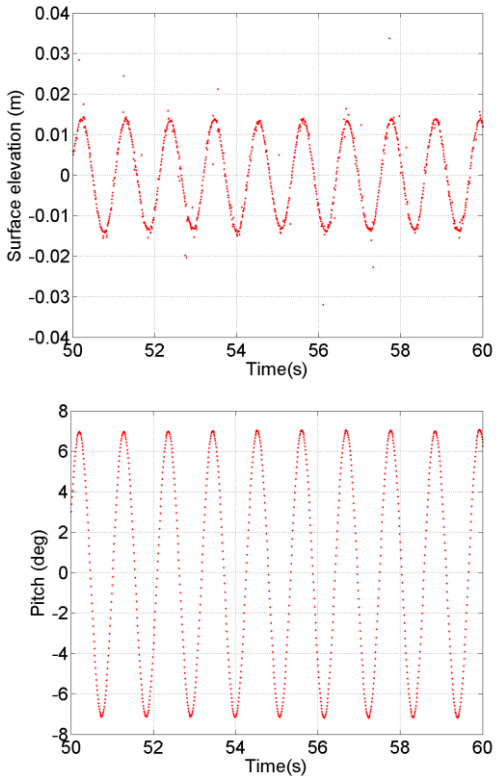

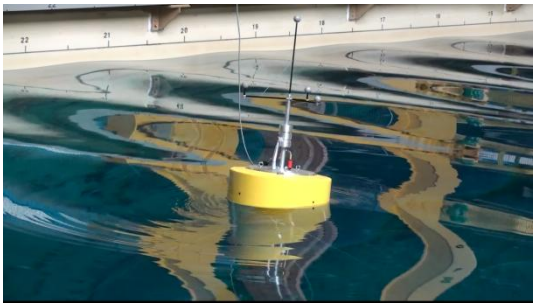

(a) **(b)**

Figure 6.14: Regular wave tank test with the highest pitch RAO (*H* = 0.03 m and *T* = 1.08 s). a) Time series of the surface elevation and pitch motion, b) Picture of the buoy at its maximum pitch RAO

A discontinuity in the modelled QTF data was observed between 0.9 and 1 Hz (Figure 6.12). There is actually some unknown on this discontinuity of the QTFs. This discontinuity was not observed on the measured data. Further measured data would be required to validate this continuity or discontinuity. This discontinuity could have physical reason with the buoy being out of phase with the waves for frequency below 1 Hz and in phase for the frequencies over 1 Hz. This discontinuity was corrected but this was actually maybe not necessary. The correction removes the discontinuity in the QTFs and is explained below.

Calibration of the mean drift forces in the surge direction

The mean drift values in surge were corrected by calibrating the mean wave drift force values in the surge direction (Figure 6.15):

a) The mean drift forces are multiplied by different coefficients between 0.5 and 10. Each regular tank test is replicated in the numerical model for the different input values of mean drift forces and mean drift is calculated for each test.

b) For each test over 0.85 Hz, the difference between the mean drift for the experiment and for the numerical model is plotted against the different multiplying coefficients. A linear fit is applied to select the value which equates the difference to zero.

c) The values to equate the difference to zero in each test are plotted against the wave frequency. A smoothing spline is fitted to these values, and interpolated multiplying coefficients are output.

d) The initial mean drift force is multiplied by the interpolated multiplying coefficients. However, for wave frequencies outside of the range used in this study, the validity of the modelling of the mean drift is not known. For low frequencies, the difference of mean drift between the numerical model and the experiment tends towards zero, but for high frequencies, further investigations are required to validate the modelling of the mean drift. Once the numerical model has been corrected, the experiment (red circles) and the model (blue squares) were giving similar results in the considered range of steep and linear waves (Figure 6.12).

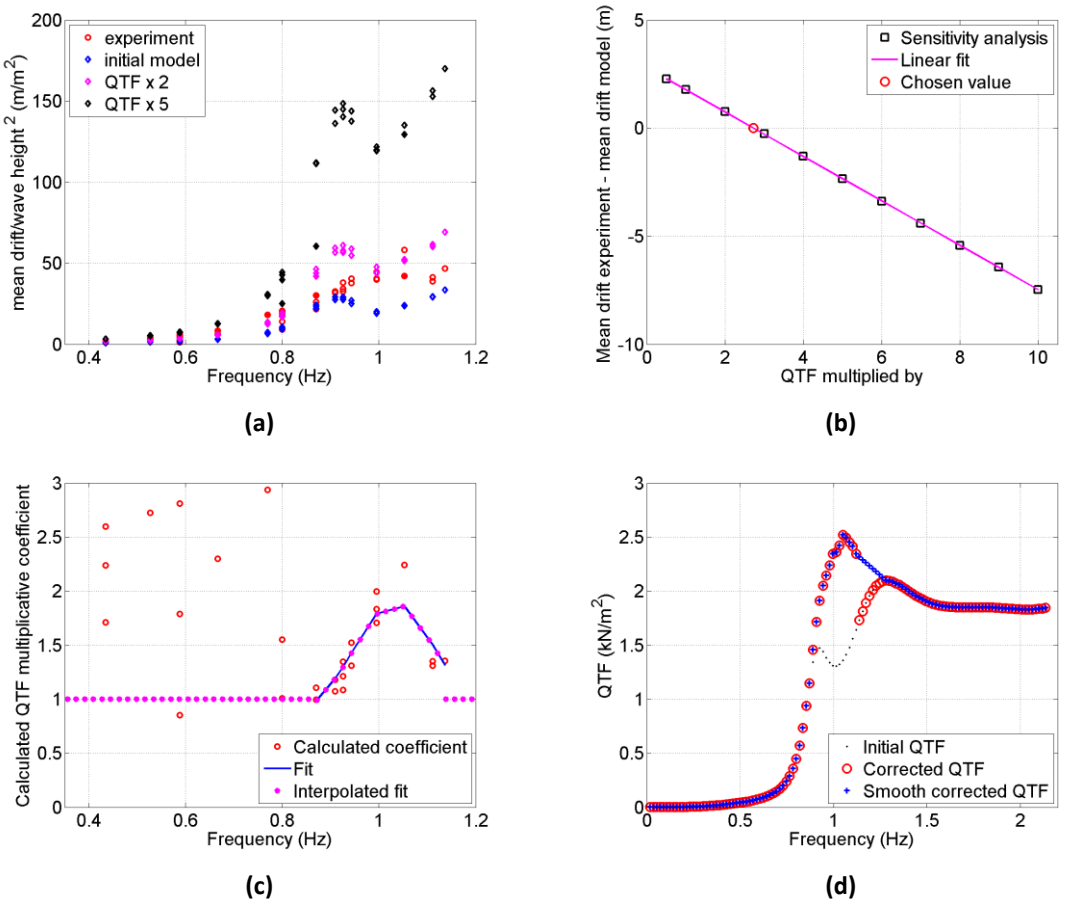

Figure 6.15: Sensitivity analysis for the surge mean drift forces for the linear waves: a) calculation of the mean drift for all sea states with the mean drift forces multiplied by different coefficients; b) for a given sea state, calculation of the corrective mean drift force multiplicative factor which leads to equal experimental and numerical mean drift (here for H = 0.6 m and T = 1.9 s); c) for frequencies over 0.85 Hz, fit of the corrective multiplicative factors; d) Corrected mean drift forces and smoothing of the values

Calibration of the quadratic pitch damping

Quadratic pitch damping was added using a sensitivity analysis (Figure 6.16):

a) Several values of quadratic damping are considered between 0 and 0.0035 (kN.m)/(rad/s)^2, numerical models are run with these different values for all regular sea states and pitch RAOs are calculated.

b) The sum over the different sea states of the absolute value of the difference between the numerical and the experimental pitch RAO is calculated for each considered quadratic damping values. The sea states are separated between linear waves and steep waves. The relationship between the sum and the quadratic damping is highlighted by a second order polynomial fit line, and the minimum of this line is calculated, giving the optimum quadratic damping value.

This method assumes that the pitch linear damping value in the numerical model is correct. The RAOs for the corrected numerical model are plotted in Figure 6.13 with blue squares. The addition of quadratic pitch damping also leads to a better fit of the modelled surge RAOs and improves the modelled heave RAOs near the pitch resonance.

After correction, the modelled mean drift (Figure 6.12) and RAOs amplitudes and phases (Figure 6.13) are in good agreement with the experimental values. The amplitudes and phases of the corrected modelled RAOs indicate no significant difference in prediction for linear or steep waves.

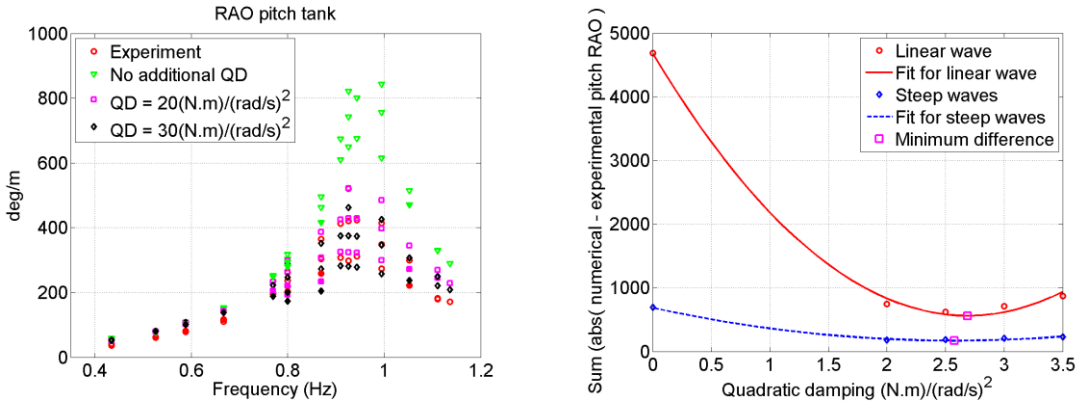

Figure 6.16: Sensitivity analysis for the pitch additional quadratic damping: a) calculation of pitch RAO for different values of additional quadratic damping for all sea states. QD stands for additional quadratic damping; b) minimisation of the sum of the absolute value of the difference between experimental and numerical pitch RAOs

6.2.4 Irregular wave tests

Irregular wave tests were used to validate the numerical model for realistic sea states. The wave elevation input signals for the tank were scaled time series of water surface elevation recorded at 2 Hz during sea tests at the SWMTF. Beam 3 of the ADCP was used for this record.

In order to have a first look at the data, the data have been taken as provided by the ADCP. In consequence, no correction was added to the measured time series of surface elevation, to take into account the tilt of the ADCP. The inputs used for the numerical models were waves measured at 100 Hz during the tank tests. Spikes in these inputs were removed in the time domain: if the absolute difference between two adjacent points was higher than 5 times the standard deviation of the signal or

three times the absolute difference of the two preceding adjacent points, the last point was removed (Figure 6.17a).

Finally the corrected signal was re-sampled at 4 Hz to simplify OrcaFlex calculations (Figure 6.17c). Three different sea states (Table 6.8) were chosen, with a duration of approximately 500 s each (model scale). In order to leave some initial time to let the model settle into its drifted position, the first 95 s were discarded. Figure 6.18 indicates that this was enough time for the body to settle around its mean surge position. The correlation coefficients between the experiment, the numerical model and the standard deviations for surge, heave and pitch motions as well as mooring loads were calculated for durations of 350 s. Times over 445 s were discarded to have time series of similar duration for the different tests.

The choice of the sea states for tank test has been based on several considerations: a) sea states with this combination of H_S and T_P frequently occur at the South West Mooring Test Facility; Case 1 and 3 were chosen with similar significant wave heights, which are close to the maximum capability of the basin, and with different wave periods. Case 2 was chosen because its wave period is close to the resonance in pitch. b) the water depth is similar for all 3 sea states, around 30 m at the full scale facility; c) the wave direction is similar for all 3 sea states and with the waves coming from the East at the full scale facility (105° clockwise from the North, when line 3 was at 65° and line 1 and 185°).

(a)

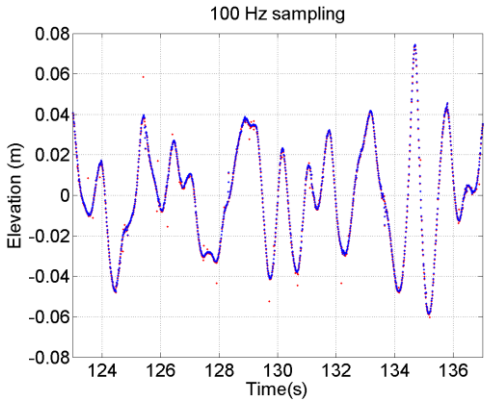

(b)

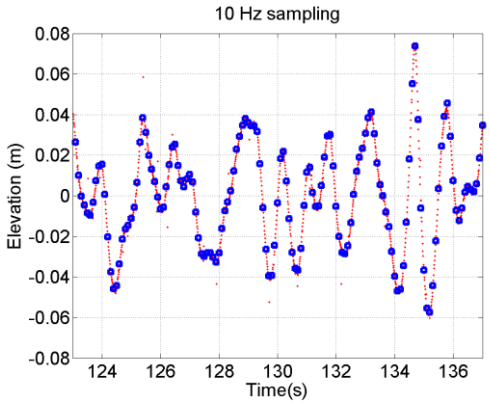

(c)

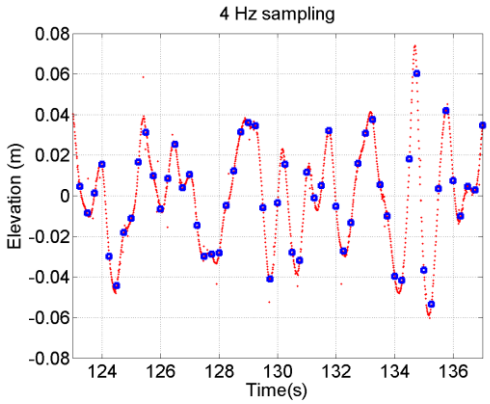

Figure 6.17: Example of different sampling frequencies for the wave inputs for Case 2. The red dots are the signal measured during the experiment and the blue dots are for the corrected signal used as an input in the numerical model with different sampling frequencies: a) 100 Hz, b) 10 Hz, c) 4 Hz

Table 6.8: Statistical properties of the irregular sea states as calculated by WavesMon, the ADCP firmware using the field data, and plot of the field data spectrum with WAFO function dat2spec (WAFO group, 2011)

Case	*Date*	H_S (m)	T_P (s)	H_S *full scale (m)*	T_P *full scale(s)*	*Spectrum model scale based on field test data*
1	07/10/2010 12:38:46	0.23	1.88	1.15	4.20	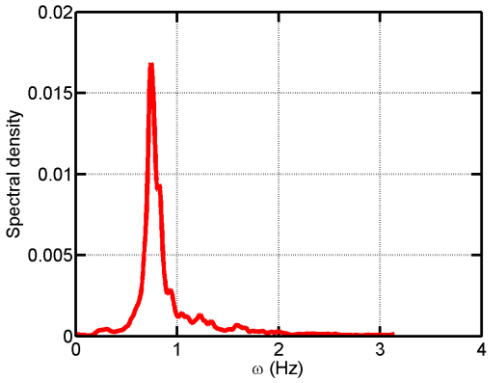
2	25/09/2010 01:57:10	0.10	1.30	0.50	2.91	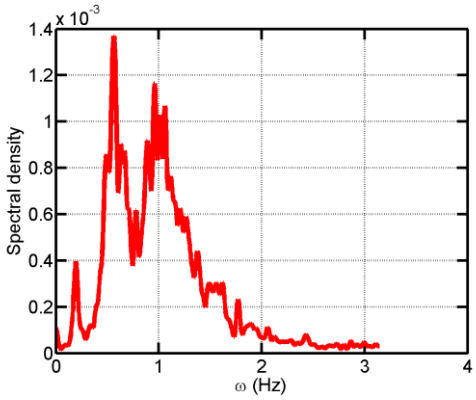
3	31/10/2010 16:13:43	0.29	2.91	1.45	6.51	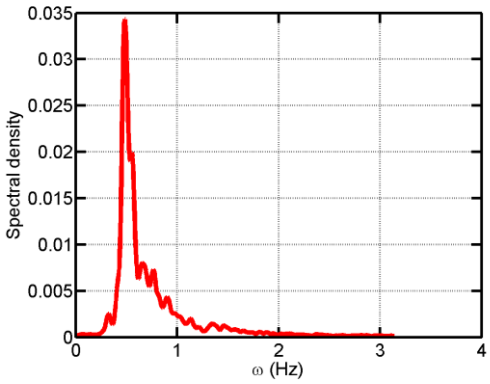

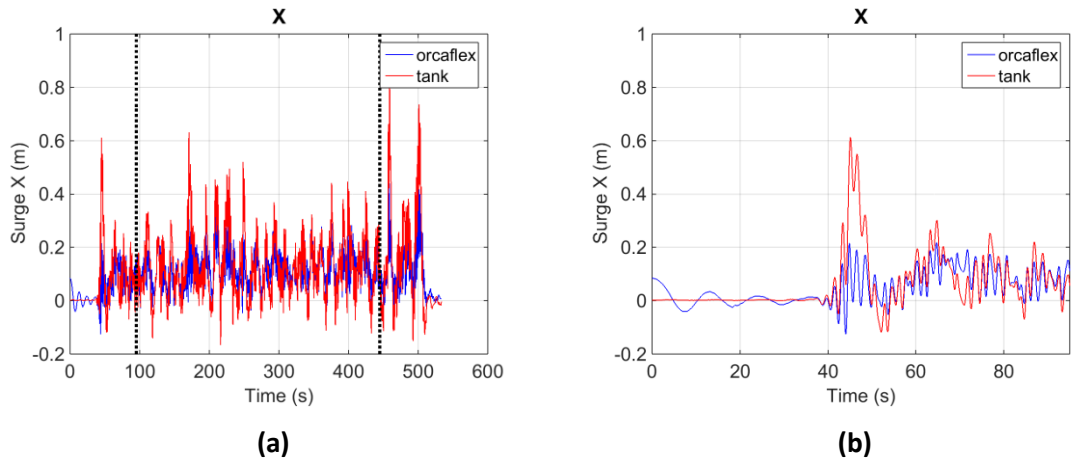

Figure 6.18: Example of surge motion for case 1 for the whole test (a) and for the first 95 s (b)

Data were chosen during the two first months of operations to avoid discrepancies due to operation (e.g. loadcell failure). More sea states would be required to draw general conclusions, these sea states are just intended to show an example of the capability of the numerical model.

An example of wave elevation time-series, positions and mooring loads recorded during the experiment and input or computed by the numerical model is given in Figure 6.17c, Figure 6.19 and Figure 6.20 respectively. The correlation, evaluated with the covariance, between the measured and the input wave signal was over 0.99 for the three tests (Table 6.9). The heave and pitch motions are accurately replicated by the numerical model (Figure 6.19b and c). Correlation coefficients - larger than 0.96 for the heave motion and than 0.82 for the pitch motion - support this finding, although the numerical model slightly under-damps the pitch motion.

For example in case 2 (Table 6.8), the standard deviation of the experimental pitch motion was 5.1° when the standard deviation of the modelled motion was 5.4°. This may be due to the fact that quadratic damping only was added to the system and linear damping could not be checked. Some differences can be observed in the surge motion, due to differences in the drift motion. In the example given in Figure 6.19a, the buoy is reaching nearly the same minimum surge position; -0.063 m for the experiment and -0.046 m for the numerical model. Larger differences can be observed; for example, at t = 132 s, the surge position is equal to 0.044 m in the experiment and 0.082 m in the numerical model. Despite these inaccuracies, the correlation coefficients are always larger than 0.77 for the surge motion.

Mooring loads are compared between the tank tests and the numerical model in Figure 6.20 and Table 6.9. These indicate that loads are replicated with a correlation coefficient over 0.75. Loads are underestimated by the model, as shown by the standard deviations. For example, for case 2, the standard deviation in Line 1 was 1.7 N for the experiment when it was 1.3 N for the numerical model. This may be due to the underestimation of the surge motion, which may be due to the possible discrepancies in the model highlighted before: for example, overestimation of the added mass, difficulty to estimate the pitch viscous damping, or unknown in the QTF estimations.

The surge motion during the irregular wave tests is compared with the stiffness of the mooring system, as shown in Figure 6.21. These plots indicate that the buoy oscillates around its quasi-static position, and the difference between the quasi-static position and the actual position is due to the dynamic behaviour of the moored system. This plot shows the importance of the dynamic behaviour.

Maximum mooring loads are compared in Table 6.10. For example, the maximum mooring load on line 1 for case 2 was 27.4 N for the experiment and 25.9 N for the numerical model. These results indicate that the numerical model, in this setup, tends to underestimate the mooring loads, by 17% in the worst case. However, the differences between the dynamic part of the load (maximum load minus mean load) is much higher as shown in Table 6.11 and can be up to 39%. This is one of the main inaccuracies of this numerical model.

The influence of the re-sampling of the wave input in the numerical model has been assessed in Table 6.12. This table compares the correlation coefficients, standard deviations and maximum loads for different wave frequency input: 4 Hz, 10 Hz, and 100 Hz. A higher sampling frequency mainly has an influence on the surge motion, with a) a higher correlation coefficient between the modelled motion and the experimental motion (100 Hz, correlation coefficient up to 0.8218) than with a sampling frequency of 4 Hz (0.8041), and b) a lower relative error between standard deviations (up to 2.4% difference between the 4 Hz and 100 Hz input). It also has a small influence on the maximum load estimation, which may be underestimated by up to 2% with the 4 Hz input compared to the 100 Hz input.

Because of the relatively small differences between the results obtained with the 4 Hz and the 100 Hz wave input, the 4 Hz wave input has been used for all further calculations presented in this thesis in order to reduce the computation time.

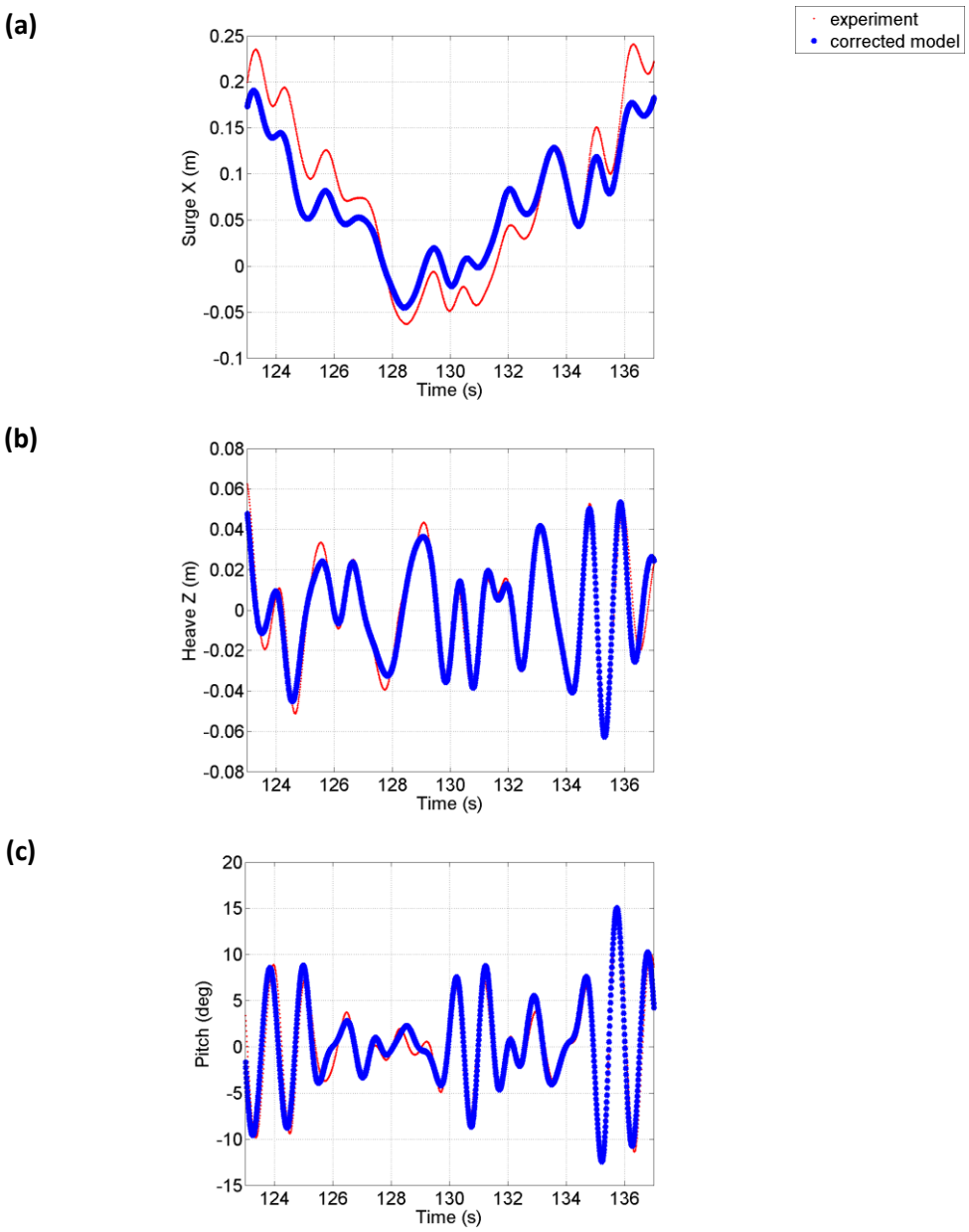

Figure 6.19: Example of motion time series for Case 2: a) surge motion, b) heave motion and c) pitch motion. Red line: experiment, thick blue line: numerical model with a 4 Hz sampling frequency wave input

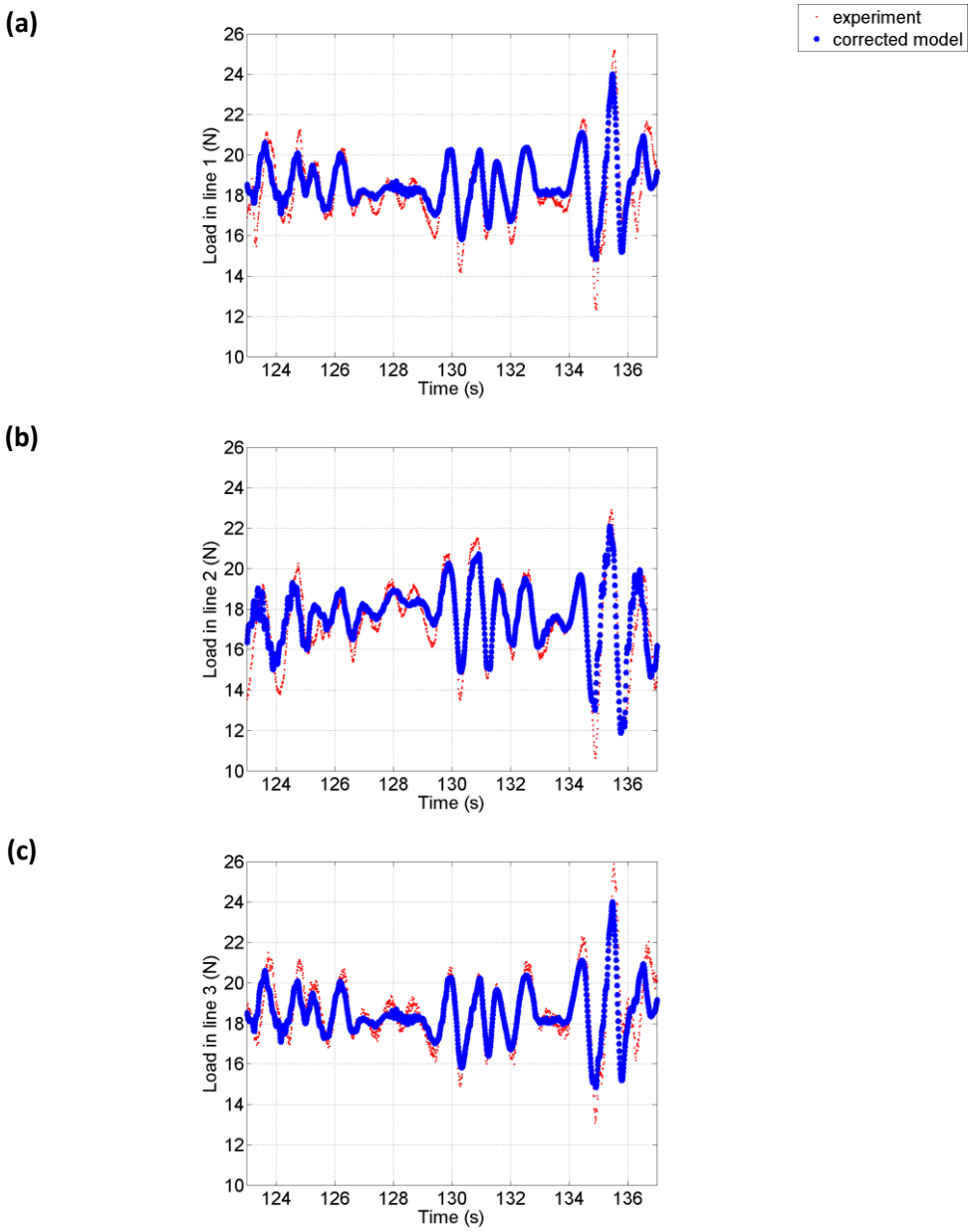

Figure 6.20: Example of mooring load time series for Case 2: a) in the front line 1, b) in the back line 2, c) in the other front line 3. Red line: experiment, thick blue line: numerical model with a 4 Hz sampling frequency wave input

(a)

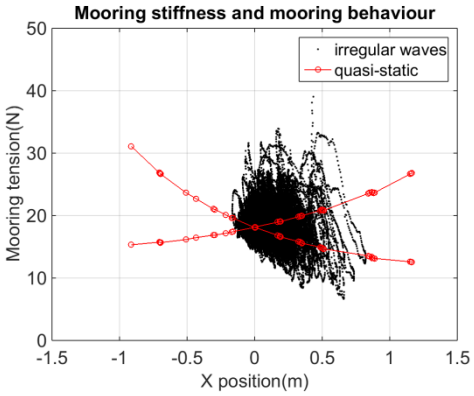

(b)

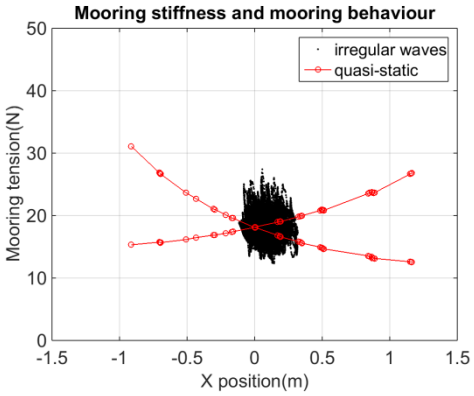

(c)

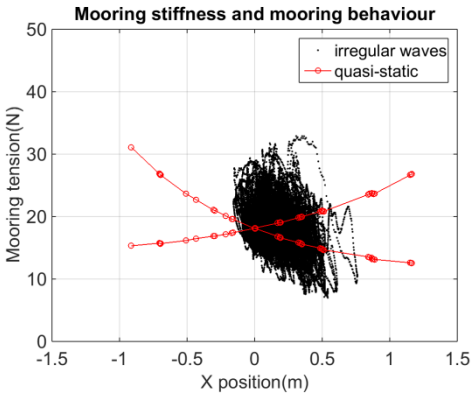

Figure 6.21: Comparison of the observed buoy motions during irregular waves and quasi-static mooring line behaviour for a) Case 1, b) Case 2, c) Case 3 for mooring line 1 with a 4 Hz sampling frequency wave input

Table 6.9: Comparison of experimental measurements and final numerical model results for the wave elevation, buoy motions and mooring loads with a 4 Hz sampling frequency wave input

	Wave	**Motion**			**Load in mooring line**		
Correlation coefficients between the experiment and the corrected numerical model							
Case	*Elevation*	*X*	*Z*	*pitch*	*Line 1*	*Line 2*	*Line 3*
1	0.99	0.79	0.96	0.91	0.76	0.84	0.77
2	0.99	0.93	0.96	0.92	0.83	0.85	0.80
3	0.99	0.77	0.96	0.82	0.75	0.79	0.75
Standard deviations: experiment/corrected numerical model/relative error							
Case	*Elevation (m)*	*X (m)*	*Z (m)*	*Pitch (deg)*	*Line 1 (N)*	*Line 2 (N)*	*Line 3 (N)*
1	0.054/0.053/1%	0.118/0.070/41%	0.052/0.053/2%	6.2/7.2/15%	2.7/2.0/28%	2.8/2.1/26%	2.8/2.0/29%
2	0.028/0.028/1%	0.073/0.053/27%	0.028/0.027/3%	5.1/5.4/5%	1.7/1.3/26%	2.2/1.6/27%	1.7/1.3/25%
3	0.077/0.078/1%	0.136/0.098/28%	0.077/0.078/1%	6.8/7.7/13%	3.3/2.4/28%	3.2/2.4/23%	3.4/2.4/30%

Table 6.10: Comparison of maximum mooring loads for the different cases and the different mooring lines with a 4 Hz sampling frequency wave input

Case		Line 1 (N)	Line 2 (N)	Line 3 (N)
1	Experiment	33.9	31.2	34.9
	Corrected Model	28.9	25.9	28.9
	Relative error	15%	8%	12%
2	Experiment	27.4	25.0	27.7
	Corrected Model	25.9	23.7	28.2
	Relative error	17%	5%	6%
3	Experiment	32.9	29.8	33.7
	Corrected Model	28.9	25.2	28.9
	Relative error	17%	9%	14%

Table 6.11: Comparison of the dynamic part of the loads (max - mean) for the different cases and the different mooring lines with a 4 Hz sampling frequency wave input

Case		Line 1 (N)	Line 2 (N)	Line 3 (N)
1	Experiment	15.4	14.1	15.9
	Corrected Model	10.1	8.7	10.1
	Relative error	34%	38%	36%
2	Experiment	9.1	7.6	9.0
	Corrected Model	6.6	6.1	6.6
	Relative error	27%	19%	26%
3	Experiment	14.6	14.4	15.6
	Corrected Model	10.7	8.2	10.7
	Relative error	27%	43%	32%

Table 6.12: Comparison of correlation coefficients, standard deviations and maximum loads between the numerical model results using different sampling frequencies for the wave input and the experimental results for the wave elevation, buoy motions and mooring loads for Case 1

	Wave	**Motion**			**Load in mooring line**		
Correlation coefficients between the experiment and the corrected numerical model/relative error with 100 Hz input							
Freq wave input	Elevation	X	Z	Pitch	Line 1	Line 2	Line 3
4 Hz	0.9927/0.40%	0.8041/2.15%	0.9629/0.01%	0.9089/0.12%	0.7611/0.17%	0.8396/0.25%	0.7728/0.03%
10 Hz	0.9962/0.05%	0.8122/1.17%	0.9626/0.02%	0.9075/0.03%	0.7589/0.12%	0.8408/0.11%	0.7719/0.09%
100 Hz	0.9967/0%	0.8218/0%	0.9628/0%	0.9078/0%	0.7598/0%	0.8417/0%	0.7726/0%
Standard deviations/relative error with 100 Hz input							
4 Hz	0.0532/0%	0.0695/2.4%	0.0527/0%	7.1691/0.08%	1.9636/0.01%	2.0721/0.14%	1.9635/0.01%
10 Hz	0.0532/0%	0.0712/0%	0.0526/0.19%	7.1651/0.02%	1.9607/0.14%	2.0679/0.06%	1.9607/0.14%
100 Hz	0.0532/0%	0.0712/0%	0.0527/0%	7.1635/0%	1.9634/0%	2.0692/0%	1.9634/0%
Maximum/relative error with 100 Hz input							
4 Hz	/	/	/	/	28.9/1.92%	25.9/1.08%	28.9/1.92%
10 Hz	/	/	/	/	29.5/0.01%	26.2/0.05%	29.5/0.01%
100 Hz	/	/	/	/	29.4/0%	26.2/0%	29.4/0%

One of the assumptions made for the numerical model was to use the Newman's approximation to simplify the Quadratic Transfer Function (QTF) calculations. The QTFs are used to model the second order motion. Table 6.13 and Figure 6.22 compared the results for the numerical model for Case 1 using the Newman's approximation and the full QTFs with and without corrected surge mean drift forces, and the results from the experiment. Correlation coefficients between the numerical models and the experiment are calculated for the motions and mooring loads and are lower when the full QTF are used, especially for the surge (without diagonal corrections, 0.73 with the full QTF and 0.81 with the Newman's approximation) and pitch motion (without diagonal corrections, 0.76 with the full QTF and 0.91 with the Newman's approximation). The mean surge motion and mean loads are similarly estimated by the numerical model with corrections using the Newman's approximation or the full QTFs. The mean surge motion is improved by the use of the corrected mean drift values, for both models using the Newman's approximation or the full QTFs, by reducing the relative error from 23% to 8-9%. The maximum loads and standard deviations of the loads are generally slightly better estimated by the numerical model using the full QTFs, with or without diagonal correction. To summarise, the use of the full QTFs instead of the use of the Newman's approximation does not significantly improve the results (estimation of the mean, max and standard deviations of the motions and loads) and even leads to lower correlation coefficients between the experimental and the modelled value.

Table 6.13: Comparison of correlation coefficients between the numerical model results using the Newman's approximation (before and after correction of the mean drift) and using the full QTFs for the buoy motions and mooring loads for Case 1 with a 4 Hz sampling frequency wave input

	Motion			Load in mooring line		
Correlation coefficients between the experiment and the numerical model						
Method of calculation	X	Z	pitch	Line 1	Line 2	Line 3
Newman's approximation original	0.8087	0.9628	0.9094	0.7593	0.8414	0.7702
Newman's approximation corrected	0.8041	0.9629	0.9089	0.7611	0.8396	0.7728
Full QTFs	0.7281	0.9627	0.7569	0.7206	0.8040	0.7239
Full QTFs diagonal corrected	0.7189	0.9627	0.7320	0.7104	0.8046	0.7189
Mean values/relative error with experiment						
Method of calculation	X (m)			Line 1 (N)	Line 2 (N)	Line 3 (N)
Newman's approximation original	0.099/23%			18.7/1%	17.4/2%	18.7/2%
Newman's approximation corrected	0.118/9%			18.8/1%	17.2/1%	18.8/1%
Full QTFs	0.099/23%			18.9/2%	17.6/3%	18.9/0%
Full QTFs diagonal corrected	0.119/8%			19.0/3%	17.5/2%	19.1/1%
Experiment	0.129			18.5	17.1	19.0
Max values/relative error with experiment						
Method of calculation				Line 1 (N)	Line 2 (N)	Line 3 (N)
Newman's approximation original				28.9/15%	26.3/16%	28.9/17%
Newman's approximation corrected				28.9/15%	25.9/17%	28.9/17%
Full QTFs				32.8/3%	29.7/5%	29.5/16%
Full QTFs diagonal corrected				33.0/3%	27.4/12%	29.5/15%
Experiment				33.9	31.2	34.9
Std values/relative error with experiment						
Method of calculation	X (m)	Z (m)	Pitch (°)	Line 1 (N)	Line 2 (N)	Line 3 (N)
Newman's approximation original	0.065/45%	0.053/2%	7.2/16%	2.0/28%	2.1/25%	2.0/30%
Newman's approximation corrected	0.070/41%	0.053/2%	7.2/16%	2.0/28%	2.1/26%	2.0/29%
Full QTFs	0.066/44%	0.053/2%	5.6/10%	2.1/23%	2.2/20%	2.1/23%
Full QTFs diagonal corrected	0.066/44%	0.053/2%	5.5/11%	2.1/23%	2.2/21%	2.1/23%
Experiment	0.118	0.052	6.2	2.7	2.8	2.8

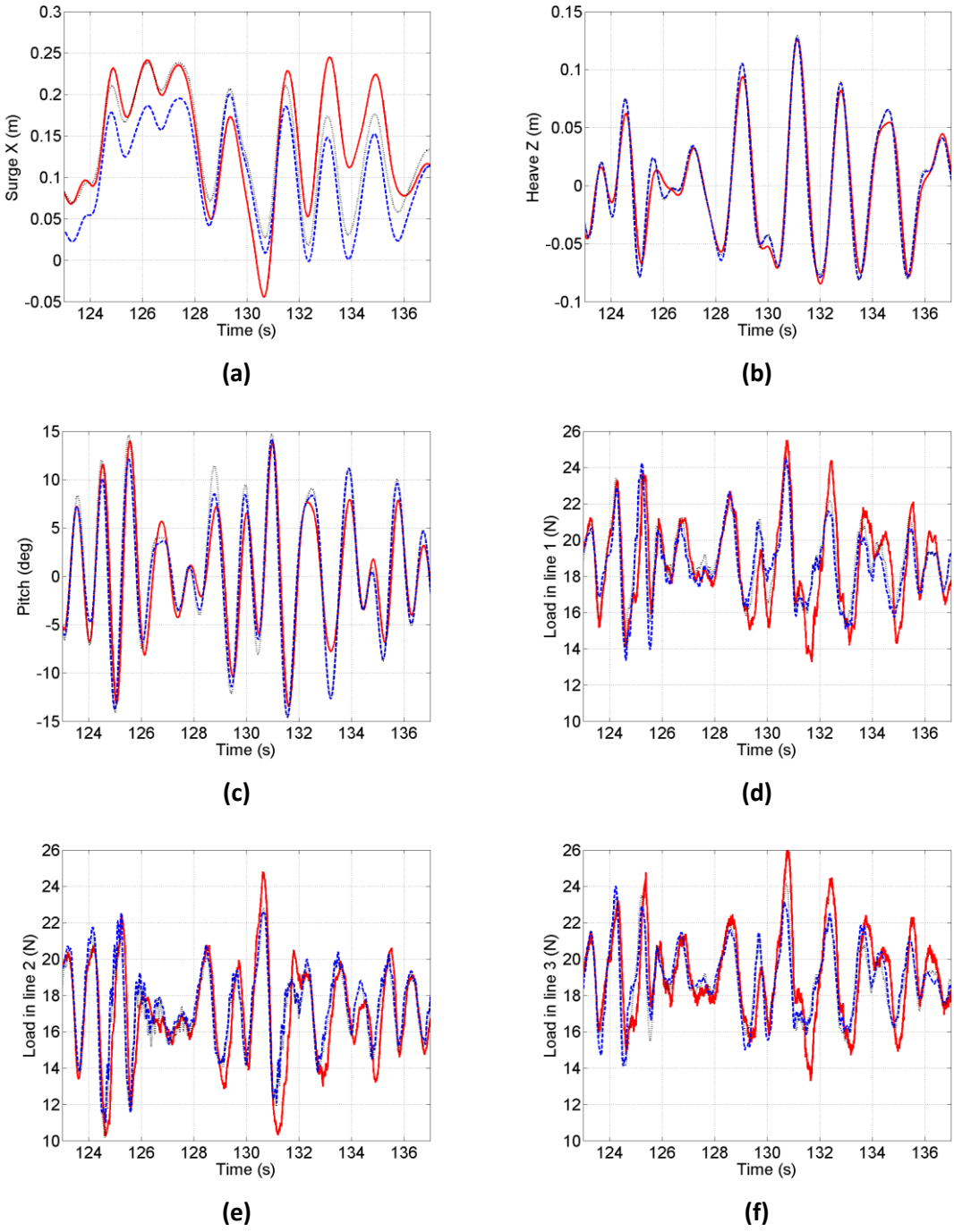

Figure 6.22: Example of time series for Case 2 using different parameters for the numerical model: a) surge motion, b) heave motion, c) pitch motion, load d) in the front line 1, e) in the back line 2, f) in the other front line 3. Solid red line: experiment; blue dashed line: numerical model with full QTFs, black dotted line: numerical model using Newman's approximation with diagonal corrections. Both numerical models used a 4 Hz sampling frequency wave input.

The motions and loads obtained with the tank tests are compared with the results in the field at the SWMTF (Figure 6.23, Table 6.14). Results are presented at the model scale. It should be noted that the wave elevation used as an input in the tank test at the position (0,0,0) (static position of the buoy) was the elevation measured by beam 3

of the acoustic Doppler current profiler (ADCP), several meters away from the buoy. Consequently, the phases of the loads and motions are different. Also the wave direction was slightly different: in the tank, waves were coming exactly between the two front mooring lines, and there was no directional spread. In the field, waves were coming 20° from the middle of the front lines, closer to line 3.

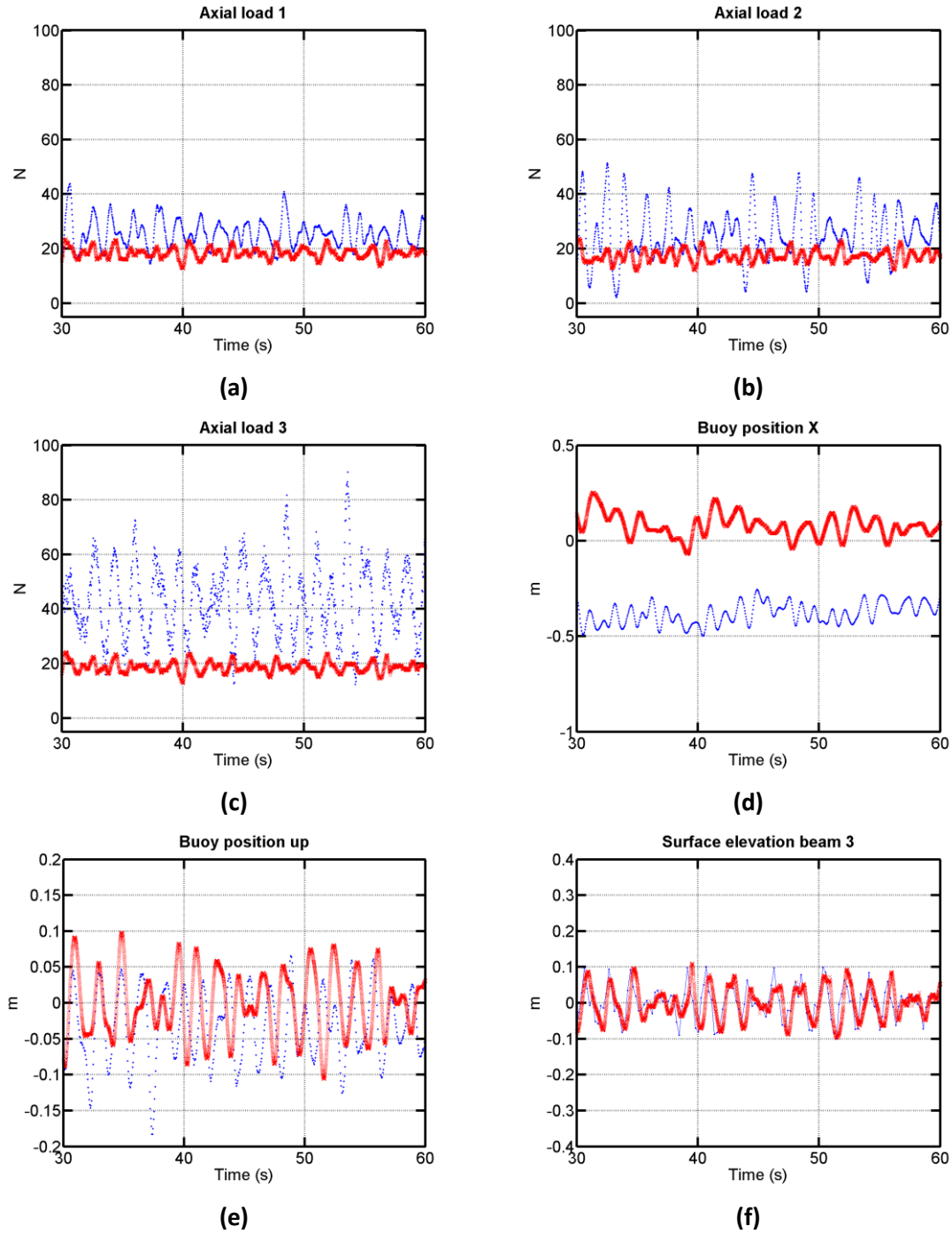

Figure 6.23: Example of time series for Case 1 of (a-c) mooring loads, (d-e) motion and (f) waves for the experiment in the tank (red thick) and the experiment in the field (blue dots). Results are shown at model scale. Red line: laboratory experiment, thick blue line: field tests

Table 6.14: Comparison of mean and standard deviations between the tank test results and the field test results for the wave elevation, buoy motions and mooring loads. Results are given at the model scale. Loads in line 3 drifted in the field.

	Wave	**Motion**		**Load in mooring line**		
Mean field/tank/relative error						
Case		X (m)		Line 1 (N)	Line 2 (N)	*Line 3 (N)*
1		-0.388/0.129/133%		26.6/18.5/30%	25.2/17.1/32%	*44.3/19.0/57%*
2		-0.314/0.075/124%		23.9/18.3/23%	27.6/17.4/37%	*32.9/18.6/43%*
3		-0.155/0.169/209%		17.6/18.3/4%	28.1/15.5/45%	*60.9/18.2/70%*
Max field/tank/relative error						
Case				Line 1 (N)	Line 2 (N)	*Line 3 (N)*
1				62.3/33.9/46%	67.7/31.2/54%	*133.0/34.9/74%*
2				36.0/27.4/24%	45.6/25.0/45%	*76.8/27.7/64%*
3				38.0/32.9/13%	78.7/29.8/62%	*154.2/33.7/78%*
Standard deviation field/tank/relative error						
Case	Elevation (m)	X (m)	Z (m)	Line 1 (N)	Line 2 (N)	*Line 3 (N)*
1	0.059/0.054/10%	0.059/0.118/100%	0.054/0.052/4%	6.2/2.7/56%	10.4/2.8/73%	*15.8/2.8/82%*
2	0.030/0.028/8%	0.046/0.073/57%	0.030/0.028/5%	2.9/1.7/41%	5.9/2.2/63%	*8.2/1.7/79%*
3	0.085/0.077/9%	0.062/0.136/120%	0.062/0.077/24%	5.3/3.3/37%	10.5/3.2/70%	*16.5/3.4/79%*

The mean load is higher in line 3 in the field tests because the measurements for this loadcell drifted.

Figure 6.23a-c and Table 6.14 indicate that the mooring load mean, maximum and standard deviation in line 1 and 2 are higher in the field, up to 45% higher for the mean load, 73% for the standard deviation of the load and 62% for the maximum loads.

Figure 6.23d and Table 6.14 also show that there is an offset in the mean buoy position by up to 0.5 m between the field and tank results. Figure 6.23d-e and Table 6.14 indicate that the variations in the mean buoy position are higher for the tank tests, with a standard deviation of the surge motion 57% to 120% higher for the tank tests than for the field tests.

One of the main reasons which could explain the differences in mooring loads and buoy position is the inaccurate positioning of an anchor, as explained by Harnois, Parish and Johanning (2012) and shown in Figure 6.24, based on results of the first SWMTF deployment. All methods seem to indicate that the target position of the North West anchor (anchor 2) has not been achieved.

However, Figure 6.24 indicates that the different methods to evaluate the anchor positions give significantly different results. This figure also indicates that the anchor position is difficult to estimate using numerical methods because only its distance to the buoy can be easily estimated.

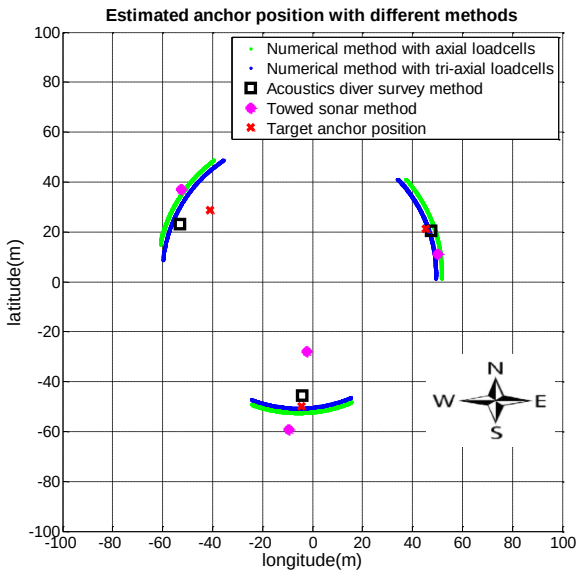

Figure 6.24: Estimated and target anchor position at SWMTF

In order to assess the consequences of inaccuracies in anchor positioning on mean and maximum load, a sensitivity study has been run using Case 1, moving the position of the back anchor (anchor 2) - which is the anchor which was suspected to be inaccurately installed in the field -, and observing the mooring loads.

The anchor positions which have been investigated are presented in Table 6.15. The anchor was moved a) along the mooring line axis, b) perpendicularly to it, and c) circularly around its original position. For a circular motion, the distance between the point (0,0) and the anchor point was always the same.

The variations (relative error between the results for the initial anchor position and the results with the modified anchor position) in mean, maximum and standard deviations of the mooring loads (model scale) for the different anchor positions are shown in Figure 6.25-26 for the three kinds of anchor move (parallel, perpendicular and circular). Unsurprisingly, results indicate that if the anchor is closer to the buoy, mean and maximum mooring loads are decreasing as well as their variations.

Based on these results, the distance in the field between the targeted and real position of anchor 2 is estimated. It was assumed that the other anchors were at their correct positions and that anchor 2 moved along the anchor line axis. This last assumption can be supported by the method of installation of drag embedment anchor: anchors are dropped on the seabed then dragged along their line axis until they are embedded.

The measured mooring loads suggest that the achieved position of anchor 2 was further from the buoy than its expected position. A second order polynomial was fitted to the mean, maximum and standard deviation load relative error presented in Figure 6.25-26. The polynomial root indicating that the anchor moved away from the centre was considered (Table 6.16).

Results generally indicate that anchor 2 was 1 or 2 m away from its position (model scale), which corresponds to the results presented by Harnois et al (2012) and shown in Figure 6.24 (anchor 2 been 10 m away full scale). The variations between the different cases may be due to the incorrect positioning of another anchor.

The result of this sensitivity study confirms that the incorrect position of anchor 2 may be the main source of difference between the results of tank test/numerical model and field tests.

Table 6.15: Anchor positions considered for the sensitivity analysis conducted with the numerical model (model scale). Blue dots show the original anchor positions, and the red dot the moved anchor position

Anchor position			
X (m)	Y (m)		Anchor motion type
5.1-9.1	0	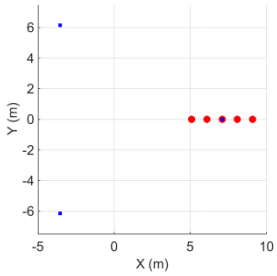	Parallel
7.1	0-4	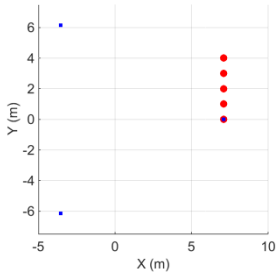	Perpendicular
Rotation around (0,0)		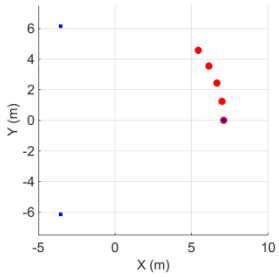	Circular

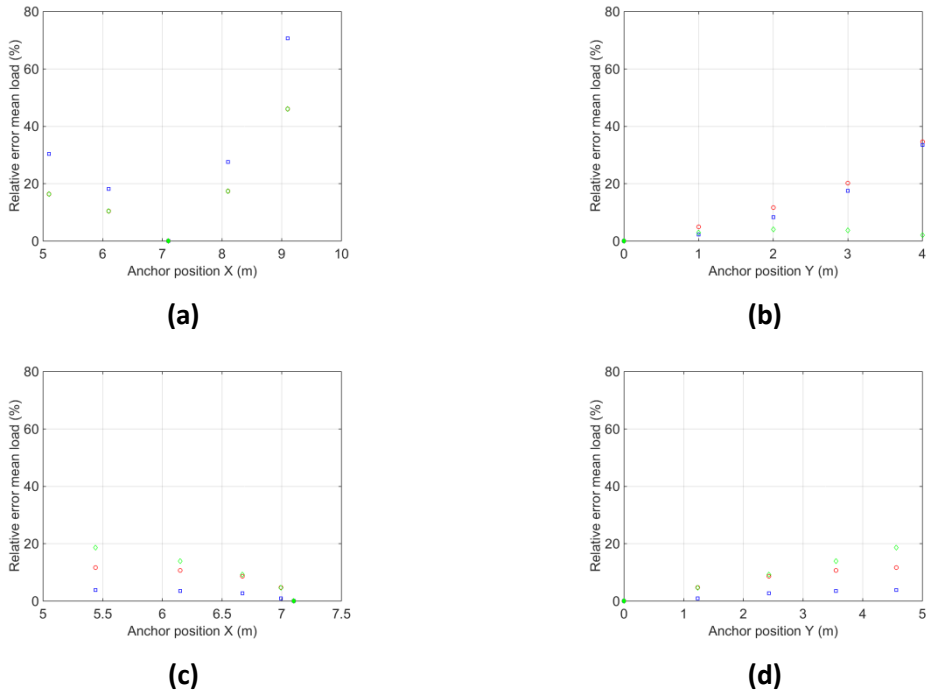

Figure 6.25: Variations in mean mooring load for different anchor position (model scale). a) anchor 2 moving along the x axis, b) along the y axis, c) and d) circularly, c) showing the X anchor position and d) the Y anchor position. Red circles: line 1, blue squares: line 2, green diamonds: line 3

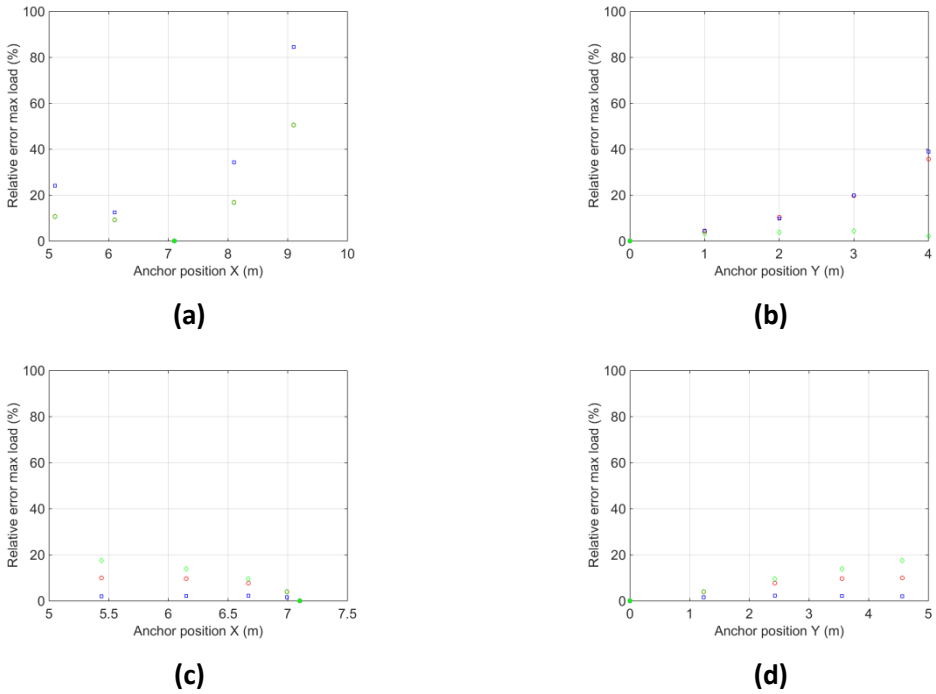

Figure 6.26: Variations in maximum mooring load for different anchor position (model scale). a) anchor moving along the x axis, b) along the y axis, c) and d) circularly. Red circles: line 1, blue squares: line 2, green diamonds: line 3

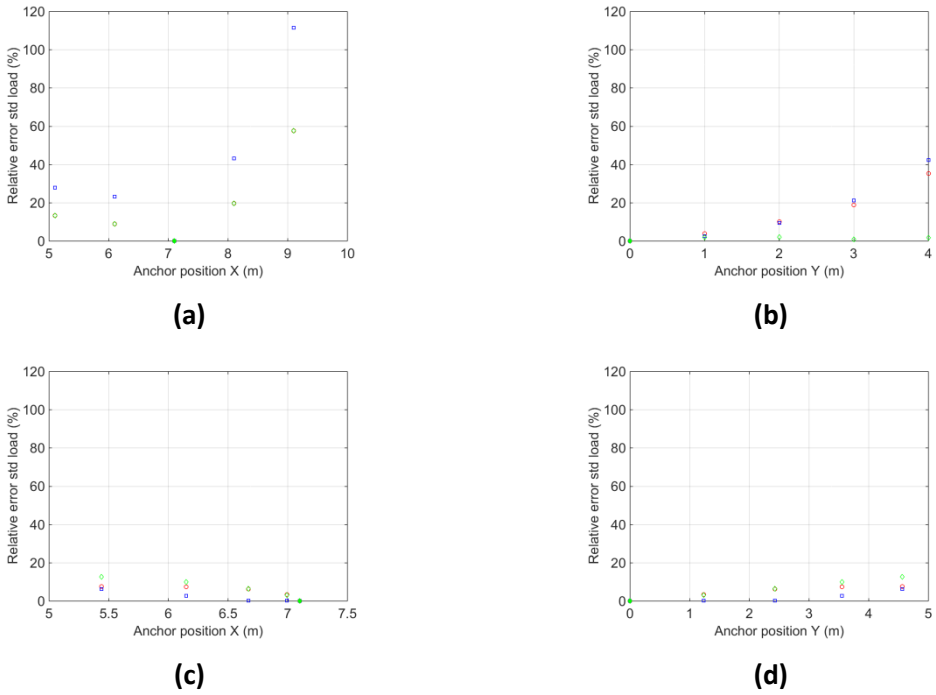

Figure 6.27: Variations in standard deviations mooring load for different anchor position (model scale). a) anchor moving along the x axis, b) along the y axis, c) and d) circularly. Red circles: line 1, blue squares: line 2, green diamonds: line 3

Table 6.16: Estimation of anchor 2 additional distance to the centre (being aligned on the x axis with its expected position) using the relative error in mean, maximum and standard deviation of mooring loads on the three mooring lines. Results are at model scale.

	Load in mooring line		
Estimation of anchor 2 move using mean relative error			
Case	Line 1 (N)	Line 2 (N)	Line 3 (N)
1	1.51	1.14	2.32
2	1.24	1.28	1.94
3	<0	1.48	2.64
Estimation of anchor 2 move using max relative error			
Case	Line 1 (N)	Line 2 (N)	Line 3 (N)
1	1.92	1.47	2.62
2	1.20	1.28	2.39
3	0.69	1.62	2.71
Estimation of anchor 2 move using std relative error			
Case	Line 1 (N)	Line 2 (N)	Line 3 (N)
1	2.00	1.50	2.55
2	1.62	1.34	2.50
3	1.50	1.45	2.50

For this study, scaling effects are minimised by using a relatively large scale, and ensuring that the type of flow is similar for the model scale, and for the full scale device.

However, it was not possible to find a rope with an exact 1:5 Froude scale stiffness. A sensitivity analysis has been run with the numerical model in order to assess the influence of mooring stiffness on the mooring behaviour. The numerical model has been run with the irregular waves used in Case 2 (Table 6.8) using different rope stiffness, up to 10 times smaller or 100 times higher than the stiffness used in the final model (10.873 kN), named below the reference stiffness. The correlation coefficients between the time-series of motion and loads of the models with a given stiffness and with the reference stiffness were calculated. Results were normalised by dividing them by the reference stiffness results and are presented in Figure 6.28a. The correlation coefficients between the reference and the modified models for the mooring loads dropped down to 0.85 when the stiffness is divided by 10, but no significant changes are observed in terms of motions and loads otherwise. Similarly, for each model with a given stiffness, the maximum load was evaluated and normalised by the maximum load for the reference stiffness and results are presented in Figure 6.28b. The maximum modelled mooring loads dropped down in line 1 for the most compliant rope.

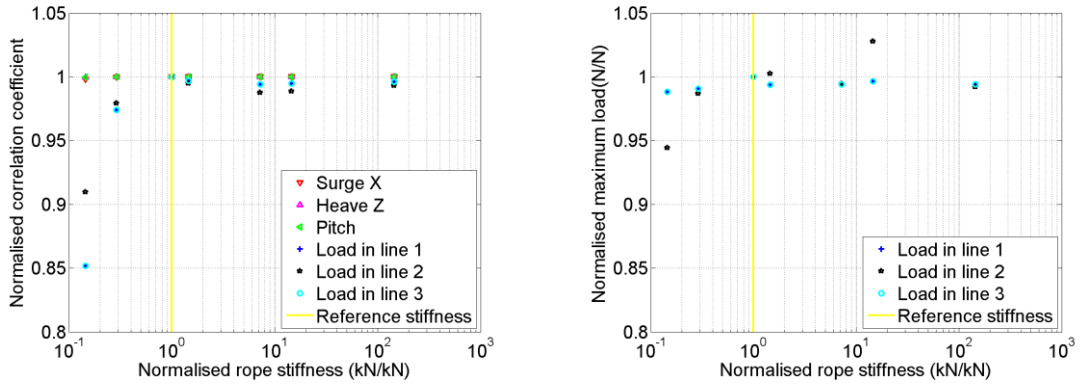

(a) **(b)**

Figure 6.28: Variations in motions and loads for Case 2 with models using different rope stiffness: a) Normalised correlation coefficient between the model with a given stiffness and the model used in this study; b) Normalised maximum mooring load with the models using different stiffness

6.3 Conclusion

This chapter describes the detailed building of a numerical model of a wave energy mooring system using tank test results. The mooring system used for this study was a 1:5 scale model catenary mooring system made of chains and representations of nylon mooring ropes.

Static and quasi-static tests were used to check the buoy draft and the tension characteristics of the mooring system. The decay tests were used to estimate the overall damping and the added mass of the system. Regular wave tests were used to obtain the buoy motion RAOs, their phases and the buoy mean drift. The irregular wave tests have been performed to replicate real sea conditions at model scale, and to compare experimental with modelled results for motions and mooring loads. Results for irregular wave tests aim to validate the numerical model for representative operational sea conditions. Despite some inaccuracies, which have been quantified, such a model gives some confidence in the ability of the numerical model to predict mooring loads at an early design stage. However, the errors are still large, especially in the prediction of the dynamic loads – up to 43%.

The numerical model presented here will be used for further research into mooring systems, for example to improve the understanding of extreme mooring loads. This understanding is fundamental for the design of a mooring system. In particular, further tank tests have been conducted using different materials in order to simulate marine growth and assess the different parameters associated with it: change of mooring stiffness, addition of mooring mass, increase in mooring line diameter and drag coefficient.

This model can also be used to improve the understanding of the hydrodynamics of the full scale SWMTF mooring system. Simulating real wave conditions will allow a better understanding of the mechanisms involved in extreme mooring loads, for example wave grouping or acceleration in buoy movements, and consequently an improvement of the mooring design. However, several barriers have been highlighted; for example; the anchor position (Harnois, 2012) was not accurate at the full scale facility, leading to a different pre-tension at the facility than the design one.

At the moment, the model can be used as a reference before conducting any engineering changes at the full scale facility, for example changing the rope materials to investigate fibre rope behaviour in long-term real sea conditions.

The methodology presented in this paper can be used by wave energy developers in the development of cost effective mooring systems which will contribute to the efficiency of wave energy devices. Tank tests are at the moment essential to improve the modelling of new designs of mooring systems; however they are expensive and time-consuming. Numerical models contribute to improve the understanding of the mooring behaviour, to reduce the unknowns and consequently build a cost-effective mooring system, specifically designed for a given wave energy device and installation site. However, inaccuracies occurring during field tests need to be considered.

Chapter 7. Discussion

This chapter will discuss the results presented in this thesis. It aims to assess the confidence levels of the results, and to highlight their importance, use and limitations. Furthermore it also puts the results into context and discusses how these results could benefit the improvement of Marine Renewable Energy (MRE) mooring design.

The challenges inherent to field tests will be emphasized, as the quality of results from the field tests directly depends on these challenges. Section 7.1 starts by investigating how representative of MRE field tests are the two case studies presented in this thesis. The challenges caused by instrumentations, installation and operations, and test sites will also be described.

In Section 7.2 the methodology to detect peak mooring loads and analyse their corresponding environmental conditions will be discussed. Firstly, the methodology will be compared with other available methodologies to investigate large mooring loads. Secondly, the choice of the significant wave height H_S and of the peak period T_P which were used in the methodology will be discussed, as well as the choice of other statistical wave parameters. Lastly, the interactions between the wave and current will be evaluated as they may have biased the results presented in this thesis.

Recommendations for the improvement of MRE mooring systems and the development of MRE standards will be presented in Section 7.3. In particular, the reduction of the amplitude of peak mooring loads would require a better understanding of the dynamics of MRE mooring systems. This could be achieved with an investigation of the time series of mooring loads, wave elevation and buoy position. A preliminary investigation is conducted in this chapter in order to highlight the importance of this step and to show that a systematic methodology to investigate time series needs to be developed.

The validation of the numerical model of the South West Mooring Test Facility (SWMTF) is discussed in Section 7.4. The limitations of the numerical model are highlighted. This section also emphasizes how numerical models should be used in combination with field tests and tank tests to improve the understanding of the dynamics of mooring systems.

7.1 Challenges of the field tests

This section aims to discuss the challenges associated with field tests and the factors which could bias the results from field tests.

The instrumentation which was used during field tests is assessed to ensure that the instrumentation can capture the physical phenomenon of interest. The inaccuracies of the mooring properties due to installation and their modifications during operation are evaluated. The differences between test sites are highlighted, and the parameters making a test site challenging are pointed out. The lack of PTO on the SWMTF buoy, and the absence of consideration of the PTO states for the Bolt-2 Lifesaver are discussed.

7.1.1 Contribution of the instrumentation to uncertainties

The instruments discussed in this section are the instruments used for wave measurements and mooring load recording.

Instruments measure a given physical quantity. They need to be correctly dimensioned beforehand in order to not miss a physical phenomenon which may not be reproduced for a long period of time – in this case the peak mooring loads. The instrument acquisition frequency, range and accuracy will be discussed below.

Instruments need to be robust to survive the aggressive sea conditions (corrosion, storms...), as a replacement may have to wait for days, until a replacement piece is received and until sea states are consistently calm enough to allow an operation boat to be sent. The weather window of calm sea states has to be sufficiently long, especially if the test site is far from the shore and/or from harbour facilities. That is why faulty equipment needs to be quickly detected. An immediate or frequent data transfer to the shore would allow an immediate monitoring of the instruments and the immediate detection of faulty equipment.

GPS, accelerometer/gyroscope and compass data have not been used for peak load assessment in this thesis (see 1.2). They only have been used to show qualitative example of data and indicate further work. Their measurement precision should be assessed in the future if they are used for quantitative assessment. GPS is likely to be fairly accurate, but as mentioned before, the integration of the acceleration and rotational velocity is likely to introduce errors in the measurements.

7.1.1.1 Acquisition frequency

Loadcells

The influence of the mooring loadcell sampling frequency on the accuracy of the recorded peak mooring load was assessed.

DNV-RP-C205 (DNV, 2010) suggests that the sampling frequency should be 10 times higher than the upper frequency of the phenomenon of interest, peak mooring loads in this case. However, the frequency of peak mooring load is not known exactly - peak mooring loads are known to be of very short duration - so this method cannot be applied and the continuity in the measurements will be qualitatively observed instead.

Figure 7.1 shows an example of a time series of a mooring load measured at 200 Hz (red dots) on Bolt-2 LifeSaver mooring system. The load seems to have been nearly fully captured, with a relative continuity in the data. The exact maximum is not likely to have been captured but the dispersion of the data indicates that the real maximum is not expected to be more than 1 or 2% higher than the estimated maximum.

It could also be noticed that the mooring load is not increasing or decreasing regularly (Figure 7.1-Figure 7.2), which may be due to the lifting of the catenary chains.

This example was used to estimate the maximum loads which would have been measured with synchronised loadcells sampling data at a lower frequency:

a) One point out of ten was selected. This simulates the measurement of a 20 Hz loadcell (with the assumption that the 20 and 200 Hz measurements are synchronised). 20 Hz was chosen because it is the acquisition frequency of the mooring loadcells for the SWMTF.

There are ten possible ways of selecting one point out of ten: selecting the points 1, 11, 21, 31, or selecting the points 2, 12, 22, 32, and so on. Depending on the combination of points chosen, the estimation of the maximum mooring load at 20 Hz is likely to differ from the record at 200 Hz.

b) The combination giving the lowest estimate of the maximum load was selected and this estimate of the maximum load was compared to the highest measured load with the initial 200 Hz frequency. The lowest estimate was chosen for comparison as it would be the worst evaluation of the peak load due to the lower acquisition frequency for synchronised instruments.

Figure 7.1a-b shows two combinations of 20 Hz sampling (blue circle). In Figure 7.1a, the maximum amplitude is similarly estimated at 20 and 200 Hz, while in Figure 7.1b, the combination leading to the lowest estimation of the maximum amplitude is shown. This process was repeated for different sampling frequencies. Results are presented in Table 7.1 and indicate that in this example, the lowest estimation of the maximum mooring load at 20 Hz was in the worst case underestimating by 2.41% the value of the maximum amplitude at 200 Hz. For this example a sampling frequency of 2 Hz would satisfy the requirement to measure the loads with a maximum error of 10%, whereas 10 Hz would be required to record the maximum load with a maximum error of 5%.

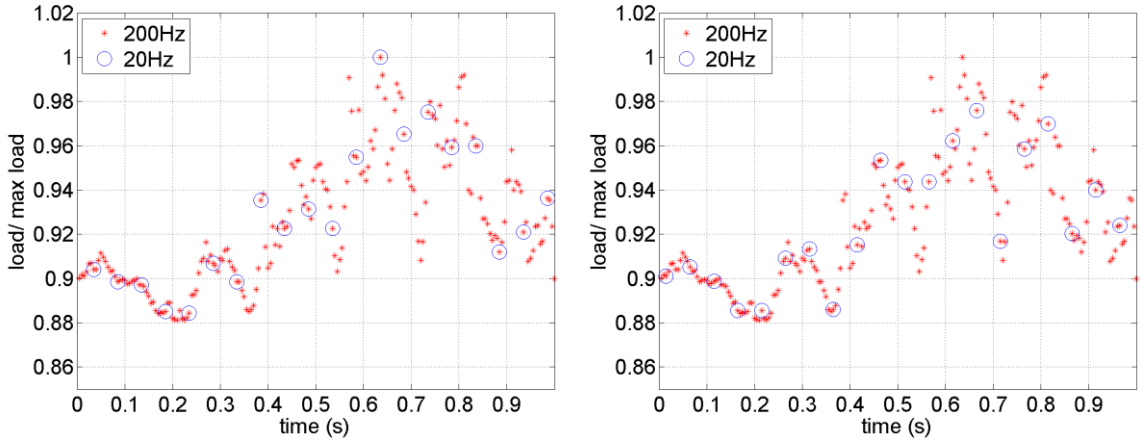

Figure 7.1: Examples of mooring load at Bolt-2 LifeSaver on mooring line 3 on the 30/04/2012 between 14:19:03 and 14:19:04; a) sampling giving the same estimation of maximum mooring load amplitude at 20 and 200 Hz, b) sampling giving a lowest estimation of maximum mooring load amplitude at 20 Hz compared to the 200 Hz measurement

Table 7.1: Example of accuracy of the lowest estimation of maximum mooring load with different sample frequencies

Frequency (Hz)	Lowest estimation of the maximum mooring load (kN)	Relative error in percentage compared to 200 Hz initial estimation
200	*28.83*	*0%*
100	28.60	0.80%
50	28.57	0.90%
20	28.14	2.41%
10	27.64	4.15%
5	27.09	6.06%
2	26.19	9.18%
1	25.40	11.89%

The aim of this methodology is to ensure that loadcells were able to accurately measure mooring loads, especially peak mooring loads. Hence this method is repeated for the mooring load with the highest measured load amplitude during the field tests on the 22/11/2012 at 11:56, which was also a peak mooring load. Results are presented in Figure 7.2 and Table 7.2. Results are in the same order of magnitude than the previous results. This method needs to be repeated several times to quantify more accurately the relative error obtained with a 20 Hz sampling compared to a 200 Hz sampling and to gain more confidence in the results presented here, which are just an indicative and qualitative estimation of relevant sampling frequency.

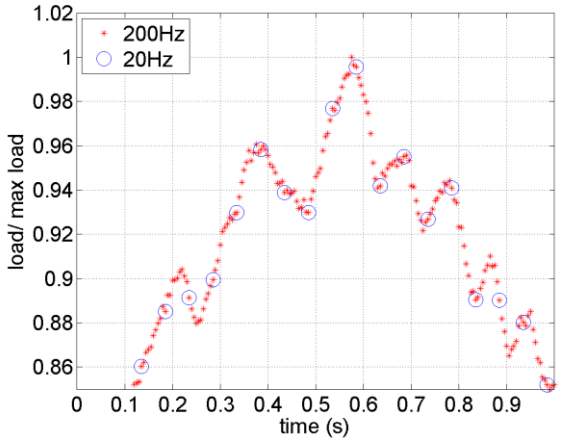

Figure 7.2: Highest mooring load recorded at Bolt-2 LifeSaver on mooring line 5 on the 22/11/2012 between 11:56:47 and 12:16:47; red dots are for the original 200 Hz sampling, blue dots are for a re-sampling at 20 Hz.

Table 7.2: Example of accuracy of the lowest estimation of maximum mooring load with different sample frequencies for the highest mooring load measured during Bolt-2 LifeSaver test

Frequency (Hz)	Lowest estimation of the maximum mooring load (kN)	Relative error in percentage compared to 200 Hz initial estimation
200	*91.24*	*0%*
100	90.92	0.34%
50	90.53	0.77%
20	89.69	1.70%
10	87.95	3.60%
5	85.93	5.82%
2	84.10	7.83%
1	71.87	21.23%

These results indicate that the loadcells used for the SWMTF and at the Bolt-2 LifeSaver device seem to have a sufficient acquisition frequency. The acquisition frequency of 200 Hz at the Bolt-2 LifeSaver device captures most of the dynamics of the mooring load. With the lowest acquisition frequency of 20 Hz for the SWMTF, a close estimation of the maximum amplitude is still provided.

Wave sensors

An acquisition frequency of 2 Hz is recommended for wave sensors (EquiMar D2.2, 2011). This recommendation is probably based on the DNV-RP-C205 (DNV, 2010) standards advising that the sampling frequency should be 10 times higher than the observed phenomenon. The wave periods are between 5 and 25 s, which means that their frequency is between 0.04 and 0.2 Hz. A sampling frequency of 2 Hz, which is equal to 10 x 0.2 Hz should then be able to capture the wave elevation.

A sampling frequency of 2 Hz also verifies the Nyquist-Shannon theorem to avoid aliasing (Réfrégier, 2008). The Nyquist-Shannon theorem stipulates that the sampling frequency should be higher than twice the difference between the minimum and maximum frequencies of the signal. The difference between the minimum and maximum frequency is 0.2-0.04 = 0.16 Hz. The sampling frequency should be higher than 2 x 0.16 Hz = 0.32 Hz which is the case: the acquisition frequency of the Acoustic Doppler Current Profiler (ADCP) for the SWMTF and wave buoy at FaBTest was of 2 Hz.

Motion sensors

Motion sensors have been used in this thesis only to provide qualitative results (see 4.1.2). The GPS acquisition frequency was 10 Hz while the accelerometer and gyroscope acquisition frequency was 20 Hz. If the buoy follows the wave, its motion frequencies are similar to the wave frequency. Second order motions are for low frequencies (up to 0 Hz: mean drift) or high frequencies (up to 2 x 0.2 Hz = 0.4 Hz). Assuming there are no other non-linearities in the motion of the floating structure, the Nyquist-Shannon theorem is respected is the sampling frequency is higher than 2 x (0.4 – 0) = 0.8 Hz, which is the case.

7.1.1.2 Range and accuracy

Loadcells

For the SWMTF, the design load was 7 tonnef (69 kN). The loadcells were able to withstand a 21 tonnef load (7 tonnef x factor of safety of 3) without yielding. The strain gauges were proof tested at 150% of rated load (7 tonnef) which means that the loadcells will work up to this load rating (7 tonnef x 150% = 10.5 tonnef) and probably beyond. The maximum measured load was approximately 50 kN, and the loadcells did not show signs of saturation.

At Bolt-2 LifeSaver device, the design load was 217 kN and the selected loadcells were rated for up to 30 tonnef (294 kN). The maximum measured load was approximately 90 kN.

This means that at both facilities, for the periods of analysis shown in this thesis, the range of the loadcells was sufficient to measure the highest mooring loads.

A fine accuracy is actually wanted to estimate the mean load indicating the pre-tension of the mooring system. The precision of the loadcells used at SWMTF was of 1 kgf, which was sufficient to accurately estimate the mean tension, around 5 kN for the SWMTF. However, the precision of the loadcells used by Bolt-2 LifeSaver was rated as better than 3.7 kN, while the mean loads were in the range of 10 kN, which means that the precision may have been insufficient.

Wave sensors

The ADCP range was sufficient to cover the whole water column (RD Instruments, 2008), with a range of 39 m, while the maximum water depth was estimated at 32 m.

Each ADCP beam is divided in bins and measures the current at these bins. Each bin is a point at a different water depth in the water column where the current velocity is measured. A bin size of 1 m is recommended by EMEC standards (2009). For these tests, the bin size of the ADCP, 0.5 m, was the highest possible resolution for a 600 kHz ADCP. This means that the ADCP was measuring current velocity in the water column every 0.5 m.

Motion sensors

Motion sensors have been used in this thesis only to provide qualitative results. (see 4.1.2)The range is not an issue for the GPS data.

Assuming that the buoy follows the waves, that the waves are regular and the deep water theory is applicable, the buoy acceleration is equal to $A\omega^2$ with ω the wave angular frequency and A the wave height. For the sea states at SWMTF, the highest acceleration could then be approximately $H_S\omega^2$ = 3.5 m x (2π/ 8s)^2 = 2.2 $m.s^{-2}$ (H_S=2A and H_{max} ~ $2H_S$). This is largely below the range of the accelerometer (2g and 3g), even with the assumptions and approximations of this calculation.

Due to the inertia of the buoy (Table 6.2), the range of the gyroscope seems appropriate (+/- 50°/s for roll, pitch and +/-30°/s for yaw).

The accuracy of the GPS depends on the quality of the data (Table 3.3). It may vary from the order of magnitude of a meter to a centimetre. It is therefore important to check the quality of the data before using them.

At the moment, accelerometer and gyroscope data cannot provide accurate linear and angular positions because of inaccuracies in the integration of the original data (see 1.2).

7.1.1.3 Monitoring

Loadcells

Instruments may not work as planned. For example, a mooring load may drift until saturation (Figure 4.2b). This could be quickly detected if the mean loads in the

different mooring lines are plotted in real time or as close to real time as possible. These plots will show any offset or drift. However, this offset or drift may be difficult to interpret. An example of a slow drift without clearly understood reasons is given in 7.1.2.2.

Wave sensors

For the SWMTF, the ADCP did not provide data during some of its deployments, and this lack of data was only discovered at its recovery. Data could be gathered in real time from the ADCP by connecting it with a cable to a transmitting buoy; however the cable should not shadow the ADCP beams and the cable would be likely to be a point of failure because of fatigue or large bending.

Motion sensors

Motion sensors have been used in this thesis only to provide qualitative results.

A GPS failure occurred and resulted in a downtime in all data measurement, because the other instruments based their date on the GPS date.

Ideally, the GPS and accelerometer data could be used to verify each other but this would require the development of a method to integrate the accelerometer data.

7.1.2 Installation and operations

There are differences between the desired design of a marine renewable energy mooring and of its wave monitoring system at a given site and its property once installed. These differences may be due to inaccuracies a) during installation: for example the anchor position, the ADCP position, damages during installation or b) during operation: marine growth, ageing.

7.1.2.1 Inaccuracies during installation

Inaccuracies in the system design originating from the installation have been observed during the field tests. These inaccuracies are likely to be reproduced during other MRE installations and therefore need to be taken into account during the design phase. The two main inaccuracies are the anchor and ADCP positions.

Harnois, Parish and Johanning (2012) showed that during the first SWMTF deployment, the drifting anchor may have been installed up to 10 m off the target location and that consequently the mooring pre-tension was higher than in the original design case.

The pre-tension is critical to the mooring behaviour. Johanning (2007) showed that if the pre-tension increases, then the mooring damping increases and the highest mooring loads increase. The results of this thesis confirm this result with a reduction in peak mooring load occurrence and amplitude after the anchor drag. Systems to adjust the pre-tension - winches or tensioners - exist and are used for traditional oil and gas installations but are too costly for MRE use. More generally, the pre-tension should be checked after deployment, and if it is higher than the design one, the mooring line causing this higher pre-tension could be redeployed.

The inaccuracies in anchor positioning are due to the methodology used to install drag embedment anchors. This methodology is not highly accurate, because an accurate positioning is usually not required.

A traditional oil and gas structure can be installed in shallow or deep water for example 60-6,500 ft (20-2,000 m) in the moorings investigated by Ma, Duggal and Smedley (2013). For a traditional oil and gas mooring, the number of mooring lines and therefore of anchors is large, for example eight to ten lines in the moorings documented by Ma, et al. (2013). MRE moorings are typically installed in shallow water, for example up to 50 m at FaBTest or up to 70 m at EMEC, with a limited number of anchor lines - three for the SWMTF, five for Bolt-2 LifeSaver.

An error of 10 m in the position of an anchor in deep water has lower consequences on the mooring pre-tension than in shallow water: the ratio between the water depth and the horizontal distance between the anchor and the floating structure (scope), which leads the mooring line behaviour, is less affected by anchor inaccuracies. In addition, the mooring load is shared on more anchors in an oil and gas mooring than in a MRE mooring.

A solution to overcome this problem would be to develop anchors which can be more accurately deployed. Gravity anchors could be a solution. They can be installed in any type of seabed, while drag embedment anchors require a sandy or muddy seabed. However, they are not highly efficient in terms of weight/handling power ratio, and therefore it may be difficult to keep their weight under reasonable handling limits. The development of gravity anchor solutions which do not require a large crane capacity

could be a solution to this issue. For example, the SeaLimpet anchor developed by Gael Force is a floating anchor with chambers which can be flooded or evacuated for easy installation and retrieval. This solution has actually been tested by Ocean Power Technologies (OPT), a wave energy developer (Hydroworld, 2011). Other types of anchors could be investigated, such as piles or screw anchors but these technologies are complex and expensive to install.

The ADCP position in the horizontal plane was not known accurately. It was deployed as a gravity anchor would be deployed, by letting it down at the vertical of the boat. The tidal current during installation and the inaccuracies in the GPS position of the boat create inaccuracies in the ADCP position. The statistical parameters and spectra do not require to know the ADCP position, but in order to use the time series of elevation, the ADCP position on the seabed (in the horizontal plane) needs to be accurately known. Currently, ADCP only provides tilt and heading. The same acoustic methodology which was used to estimate the anchor position (Harnois, et al., 2012) could be used to determinate the ADCP position.

With a wave buoy, it is not possible to know the surface elevation at a given point because the wave buoy is moving with the waves.

However, knowing the surface elevation at the exact wave energy device position would improve the understanding of the interactions between the devices and the wave and could be used to improve control strategies. At the moment, the heave position of the instrumented buoy can be used to estimate the surface elevation but this estimation will be erroneous when the buoy does not follow the waves (for example for heave resonance).

7.1.2.2 Inaccuracies during operations

For the SWMTF, the mean loads measured by the inline loadcells have been decreasing in all mooring lines during the first deployment before anchor drag and increasing after (Figure 7.3). The slope of a first order polynomial fit is equal to - 0.00695 kN/day before anchor drag and + 0.00190 kN/day after. This could have been due to fibre rope change of length, marine growth, loadcell ageing or anchor drag but further proofs are required to make a definitive conclusion:

- The ropes could have been measured before and after use in order to estimate their stretching due to creep (as a result of fatigue which will be discussed below) or shrinking due to marine growth. However, this will not provide information on the real-time length of the ropes and if the length is actually linked to the slow variations in pre-tension.
- Further research is required to quantify the effect of marine growth on the mooring loads. Nevertheless, marine growth does not explain the decrease in mooring loads before anchor drag (Figure 7.3) because the marine growth was mainly mussels and the density of mussels is close to 1.4 (Woods Hole Oceanographic Institution, 1952). Marine growth is discussed in more details below as it may endanger the survivability of the mooring system.
- Measuring the calibration of the loadcells once they are recovered would have indicated whether the loadcells were the source of the slow drift. However, this calibration could not be done because the loadcells were not working anymore when they were recovered. The tri-axial loadcells also indicated a decrease in the mean loads on their y-axis before the anchor drag (Figure 4.13) while the inline loadcells indicated an increase. The difference between the inline and tri-axial measurements could indicate that the increase or decrease in mean loads did not have a physical existence and was due to the ageing of instrumentation. However, the change in trend with the anchor drag is surprising.

  More generally, problems with mooring loadcells are frequently encountered. The monitoring of mooring has been discussed by Elman, et al. (2013) and concludes that monitoring the mooring load is difficult because of the unreliability of instrumentation. Redundant inline loadcells could have been used, but this would have been a costly option and would also require additional available channels in the data acquisition system.
- The slow decrease in mooring loads could be due to the anchor starting to drag very slowly before the large anchor drag. However, this does not explain the increase in mooring loads after the anchor drag.

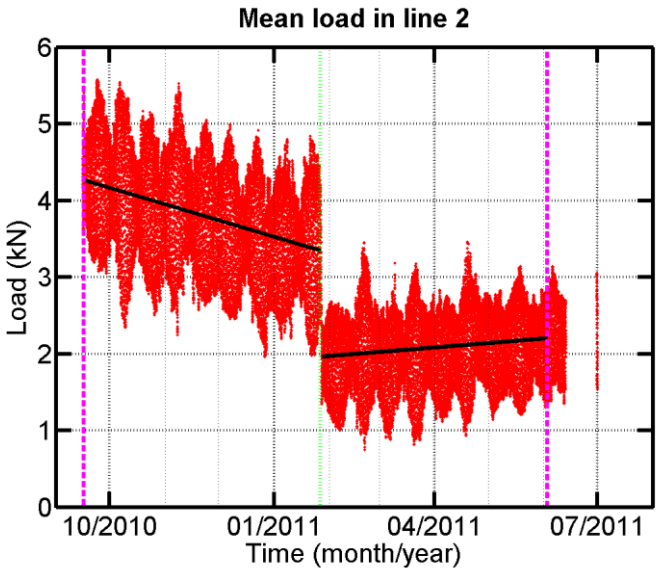

Figure 7.3: Slow decrease and increase in the mean load in line 2 during the first SWMTF deployment

Marine growth

Marine growth, also known as biofouling, can significantly change the properties of a mooring line by increasing its diameter, drag coefficient, mass and added mass (DNV, 2013) and by stiffening the line. For the SWMTF, the mooring lines were recovered after the first SWMTF deployment with an approximate diameter (including rope) of 0.15 m because of mussels around the ropes (Figure 7.4). The mussel shells were still soft when the lines were recovered but older mussels with harder and sharper shells may have cut the ropes.

(a) **(b)** **(c)**

Figure 7.4: Marine growth observed for the SWMTF during its first recovery a) on the buoy; b and c) on a mooring line (rope)

As discussed earlier, the mooring load data did not indicate when the marine growth started. Currently, the best way of monitoring marine growth is likely to be regular inspections. However, marine growth is difficult to visually detect on grounded or embedded lines.

Removing marine growth may anyway not be desirable. If it is removed from the chains, then the chains would be exposed to more corrosion.

The properties of the SWMTF rope used during the first SWMTF deployment have been studied after its retrieval and compared with the properties of a similar new rope (MERiFIC, 2013). Fibre-on-fibre friction (internal abrasion) was observed on Scanning Electron Microscope (SEM) images of fibres. Marine growth may have accelerated the fibre-on-fibre friction. The line can be protected by a jacket to avoid additional fatigue due to foreign bodies.

Fatigue

Fatigue of the synthetic mooring ropes is mainly due to internal abrasion (McKenna, Hearle and O'Hear, 2004). For both field tests, the Minimum Breaking Load (MBL) of the ropes was high because large safety factors have been applied, consequently the maximum loads did not exceed 15 % of the MBL.

Assuming that the fatigue of the Nylon ropes is similar to the fatigue of the Nylon rope studied by Ridge, Banfield and Mackay (2010), Figure 2.8 indicates that the range of load amplitude measured at both field tests is well below the amplitudes of loads creating a risk.

If the loads had been equal to 33% of the MBL, (safety factor of 3), with the assumption that the Nylon fatigue line can be linearly extrapolated, the number of cycles the Nylon line could accommodate would have been around 1,000,000,000, assuming the cycles have the same amplitude. A quick estimation of the number of cycles the rope will be exposed to during its life is done below. A more complete calculation could be done, calculating the fatigue for each sea state (Thies, et al. 2014). With waves around 5 s (the mean T_Z was between 4 and 5 s at SWMTF), assuming that the number of cycles is the same than the number of waves, in 20 years, which is the expected lifetime of a MRE, the line will accommodate 20 years x 365 days x 24 hours x 3,600 s / 5 s = 126,144,000 cycles which is largely below the maximum number of cycles the rope can accommodate.

For a MRE device, the damage can be estimated as the number of cycles the line will accommodate in 20 years divided by the number of cycles the line can accommodate in 20 years = 126,144,000/1,000,000,000 = 12.6%. Consequently the safety factor γ_F, defined in DNV-OS-E301 (DNV, 2013) as $1-d_c\gamma_F \geq 0$ with d_c the characteristic fatigue damage, can be estimated as $\gamma_F = 1/d_c$=7.9. This is lower than the safety factor of 60 recommended for polyester (in the absence of values for nylon in the standards), but in the mean time the calculation presented here is conservative mainly because it does not take into account the amplitude of the cycles. However, this result indicates that fatigue for the nylon rope may be an issue and more accurate damage estimation needs to be conducted. In addition, it may be useful for the standards to define a safety value for nylon ropes.

Fatigue of the chains may also be an issue. The maximum load was equal to 52.5 kN on SWMTF mooring and 91.2 kN on Bolt-2 Lifesaver mooring. In order to use the chain S/N curve (Figure 2.7), the maximum stress (maximum load divided by the smaller section of chain) should be calculated for the chains with the smaller diameter (which in both cases were open link).

For the SWMTF, the maximum stress is equal to

$52.5\ kN/[\pi \times (24\ mm)^2] = 29\ MPa$,

and for Bolt-2 Lifesaver to

$91.2\ kN/[\pi \times (36\ mm)^2] = 22.4\ MPa$.

Using the same simplified constant amplitude calculations than for the fibre ropes, a reading of Figure 2.3 indicates that the number of cycles these chains can handle is approximately 2.5×10^6 and 6×10^6 respectively. With the same assumption regarding the number of waves in 20 years, the lines will accommodate approximately 126,144,000 cycles in their lifetime which is over the limits of chain fatigue. A more precise calculation is actually required to conclude on this result and estimate if chains can or cannot resist fatigue for a 20 years deployment in such sea states. Chains have been widely used in the offshore oil and gas industry for longer projects.

Thies et al. (2014) ran a more accurate calculation of fatigue on the DN 24 open link chains for the SWMTF. They basically consider the number of cycles for a given sea states, and the sea states distribution for the SWMTF. They concluded that in this case

the fatigue life of chains was short, three years in the worst case after applying factors of safety. More generally, the SWMTF studies give an indication that fatigue is a concern to be carefully considered for MRE mooring systems.

Other ageing processes

Other ageing processes may compromise the durability of the mooring system. Corrosion is a well known effect (DNV, 2013) and has been accounted for during the mooring design, for example by using sacrificial anodes. Abrasion is an issue mainly for the fibre ropes, as the chains and shackles have good abrasion resistance properties. For the relatively short deployments for the SWMTF and Bolt-2 LifeSaver device, abrasion calculations have not been conducted because of the high factors of safety applied to the mooring. The mooring design ensures that the fibre ropes did not touch the seabed to avoid abrasion on them. Wear is a concern mainly for the connecting elements. Corrosion, abrasion and wear should not significantly change the behaviour of the mooring system if it has been properly designed and no failure occurred.

7.1.3 Site and device specific challenges

Results presented in this thesis are for two similar sites and mooring systems. These sites and mooring have their own particular challenges but are they representative of MRE sites and devices?

The wave directionality, the ratio between the tidal range and the water depth, and the seabed type need to taken into account as they will highly influence the mooring design.

One of the main difficulties with MRE moorings is the limited number of mooring lines. More mooring lines would mean more expensive mooring components and a higher duration of the installation. This difficulty is emphasized if the test site has several wave directions. For example, for the SWMTF, the mooring configuration was orientated to have the highest easterly H_S sea states between the mooring lines 1 and 3. However, the second predominant wave direction (South) was aligned with mooring line 1. The wave directionality is imposed by the test site but the orientation

of the mooring system and, if necessary, the addition of mooring lines could mitigate the issues due to wave directionality.

Tidal variations also need to be taken into account for the mooring design especially if the tidal range is significant in relation to the nominal water depth. Table 2.6 compares the nominal water depth and the tidal range at some nursery sites and wave energy facilities. Table 2.6 shows that nursery sites are in shallow water with a large tidal range while full scale wave energy facilities are in deeper water but with a similar tidal range. This means that the challenges associated with a large change of pre-tension caused by tidal variations is mainly an issue at the nursery sites, and is to some extent mitigated by the larger water depth of pre-commercial wave energy sites.

The choice of the tidal range is not possible at a given site but until all berths are full in a test site, the water depth can be chosen if the site offers different water depths. However the choice of the water depth may be governed by other factors.

The tidal range needs to be accommodated by the mooring system, either by a specific mooring configuration or mooring materials. For example, the mooring tethers developed by University of Exeter (Parish, 2013) can accommodate the tidal range. At the moment, chains lying on the seabed are used in catenary configurations but at high tides, when these chains are lifted, chains add weight on the floating structure, which may be prejudicial to the power production.

The seabed type will influence the choice of anchor type. Drag embedment anchor can only be used in a sandy or muddy seabed. This was the case for the SWMTF and mostly in the part of the FaBTest site where the Bolt-2 LifeSaver device was installed. However some rocks were observed in the vicinity of the anchor of line 1 for the SWMTF (Harnois, et al. 2012). The FaBTest site has areas of rocks and gravels at the North of the site (FaBTest, 2012) and one mooring line was lengthened to reach a sandy area and avoid a rocky area. In some cases, drag embedment anchors cannot be used. Hence, more expensive and/or less efficient anchors should be used. Similarly to the water depth, the type of seabed may be chosen at a test site until all berths are full, but other parameters also have to be taken into account.

There is no control on the environment during field tests. The amplitude and frequency of occurrences of storms cannot be planned. Also, to investigate different

mooring configurations or materials installed at the same location but at different times, the difference between environmental conditions need to be assessed first. At SWMTF, the difference in the numbers of sea states coming from the East or from the South clearly led to different number of peak mooring loads.

The SWMTF and Bolt-2 LifeSaver prototype differ from commercial devices. The highly dynamic behaviour of the mooring system used for the SWMTF is typical of the mooring system of a motion-dependent wave energy device such as a point absorber. However, in comparison with an operating wave energy device, the SWMTF does not have a power take-off, which would provide additional damping and modify the amplitude and velocity of the motions of the buoy, and consequently the number and amplitude of peak mooring loads. The Fred Olsen Bolt-2 LifeSaver data have been analysed regardless of the PTO states, the PTO being winches connecting the floating structure to the seabed using an intermediate submerged buoy. This information is likely to be commercially sensitive. The future commercial device is designed to accommodate five similar PTOs, but only three were installed on this prototype. These additional PTOs will modify the motions and peak mooring loads.

7.2 Peak mooring loads

This section aims to discuss the methodology developed in this thesis to detect peak mooring loads and assess the associated environmental conditions. In particular, the process to select peak mooring loads, the choice of the wave statistical parameters H_S and T_P, and the possible wave and current interactions will be discussed.

7.2.1 Selection of peak mooring loads

7.2.1.1 Thesis methodology

The methodology developed in this thesis identified datasets containing peak mooring loads. Peak mooring loads were defined as mooring loads which are peaky relatively to the other mooring loads in the dataset and which are of sufficiently large amplitude. The definition of the peak mooring load and the choice of the τ and K factors influence the results of this study

The methodology developed in this thesis aimed to detect peak mooring loads, and not snap loads or extreme mooring loads, which are difficult to measure: snap load measurement requires a loadcell whose calibration can be trusted for very low values, when the mooring line is slack, and extreme mooring load measurement requires to observe several extreme sea states (for example 10-year return period), which are rare events which were unlikely to be repeatedly observed during the short duration of the trials.

7.2.1.2 Other available methods

Other methods have been used by different authors to investigate large mooring loads. Incecik et al. (1998) investigated the distribution of the mean forces, noticed that some mean loads were grouped in the tail of the distribution and then analysed mooring loads with a mean load over a certain threshold. Parmeggiani, Kofoed and Friis-Madsen (2011) investigated the average of the $1/250^{th}$ of the highest values of each time series. This is assuming that the tail distribution of maxima is Rayleigh distributed which allows an estimation of the expected maximum –but not the real one.

Both methods are used for large floating structures moving slowly, following their second order motions.

The distributions of measured mean loads for the SWMTF (Figure 4.34 - Figure 4.35) and Bolt-2 LifeSaver (Figure 4.63 - Figure 4.64) indicate that the mean loads are regularly decreasing in the tail of the distribution making it difficult to select a threshold. Because of the dynamic behaviour of MRE devices, the average of the $1/250^{th}$ highest values of the dataset would smooth the dynamic peak loads and this method may therefore not be relevant to select the peakiest events. Moreover, this method would require reprocessing all datasets to calculate these values, which is time consuming.

7.2.1.3 Threshold method

The previous subsection shows that the choice of a threshold to isolate peak mooring load cannot be based on the mean load distribution. A threshold for the maximum load has been chosen instead to isolate a given number of datasets. For the SWMTF, a threshold has been set up at 19.3 kN to detect the same number of datasets on mooring line 1 during the first SWMTF deployment before anchor drag as with the methodology presented in this thesis.

The 55 mooring loads detected on mooring line 1 using the threshold method have been compared in Figure 7.5b with the 55 peak mooring loads using the methodology developed in this thesis (Figure 7.5a). The wave heights H_S associated with the threshold method loads are generally higher than the ones associated with the thesis methodology. The wave direction is similar in both cases. The water depths associated with the highest amplitude load method are also higher than the ones associated with the peak mooring load method.

The same threshold (19.3 kN) has been used on the other mooring lines and during the different periods of tests. The number of peak mooring loads detected is presented in Table 5.2 and compared with the number of peak mooring loads determined using the method developed in this thesis. For mooring line 3 during the first SWMTF deployment before the anchor drag, the number of mooring loads over the threshold (756) is more than 10 times higher than the number of peak mooring loads (73) using the method developed in this thesis. However, the number of mooring loads over the threshold is null during the first deployment after the anchor drag and during the second deployment on all mooring lines.

Table 7.4 shows the values of threshold which should have been set up for each mooring line and period of deployments to obtain the same number of peak mooring loads as with the method used in this thesis. The thresholds are varying between 7.36 and 31.41 kN depending on the mooring line and the period of analysis. These results indicate that the choice of a threshold is difficult and depends on the mooring properties.

Table 7.3: Number of detected peak mooring loads in a period of time for the SWMTF using the method presented in this thesis/using a threshold at 19.3 kN.

	First SWMTF deployment		**Second SWMTF deployment**
Line and orientation	Before anchor drag	After anchor drag	
Line 1 (185°)	55/55	16/0	70/0
Line 2 (305°)	1/0	6/0	5/0
Line 3 (65°)	73/756	/	22/0

Table 7.4: Threshold load which should have been applied to obtain the same number of peak mooring loads as using the method presented in this thesis/ threshold load divided by mean line tension

	First SWMTF deployment		**Second SWMTF deployment**
Line and orientation	Before anchor drag	After anchor drag	
Line 1 (185°)	19.27 kN / 6.83	13.10 kN / 7.75	11.92 kN / 3.68
Line 2 (305°)	17.41 kN / 4.63	9.97 kN / 4.79	7.41 kN / 6.50
Line 3 (65°)	31.41 kN / 11.81	/	7.36 kN / 6.51

7.2.1.4 Thesis method using the pre-tension instead of the mean load

Similarly, the method used in this thesis could be adapted by replacing the mean load term in S_{max} by the pre-tension calculated from the water level (Table 4.14). This would separate the static and dynamic load. Using the thesis methodology, the mean load was higher than the pre-tension during peak mooring loads because the mean load was including the pre-tension, and increase in mooring loads due to static and dynamic wave and current loads.

K would then be compared with $\frac{maximum\ load - pre-tension\ (from\ water\ level)}{std\ load}$ instead of with S_{max}.

This method requires the understanding of the pre-tension variations and water depth measurements or prediction. In this case, for SWMTF, the pre-tension was mainly depending on the water level.

Results are shown in Figure 7.5c and are only very slightly different from the results using the original methodology. They are slightly less occurrences for high values of H_S, and slightly more for high water depth h.

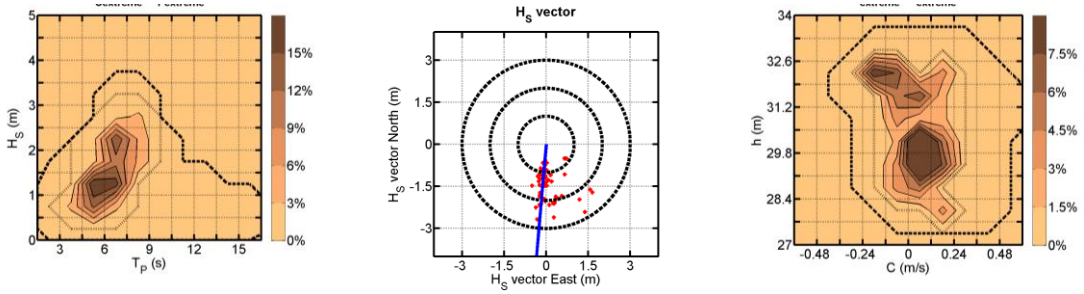

(a) Peak mooring loads using the thesis methodology

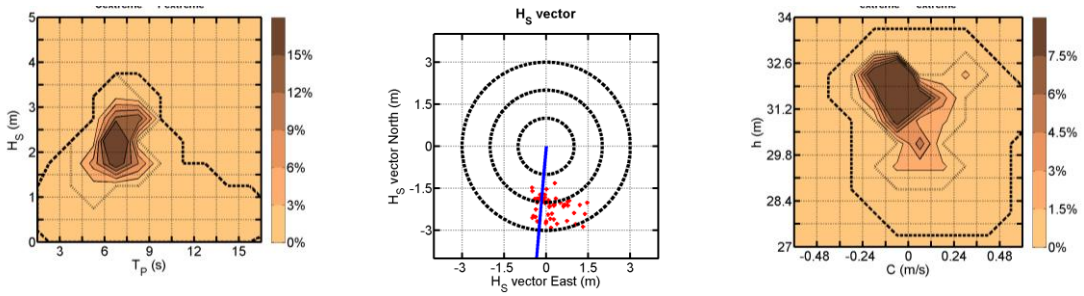

(b) 55 mooring loads with the threshold method

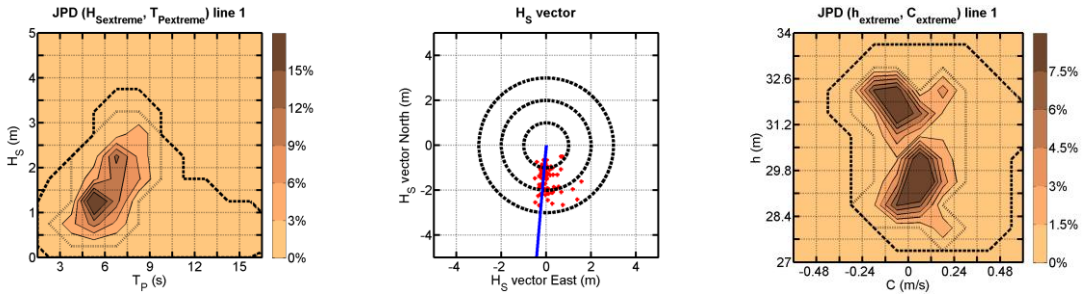

(c) Peak mooring loads using the modified thesis methodology with the pre-tension

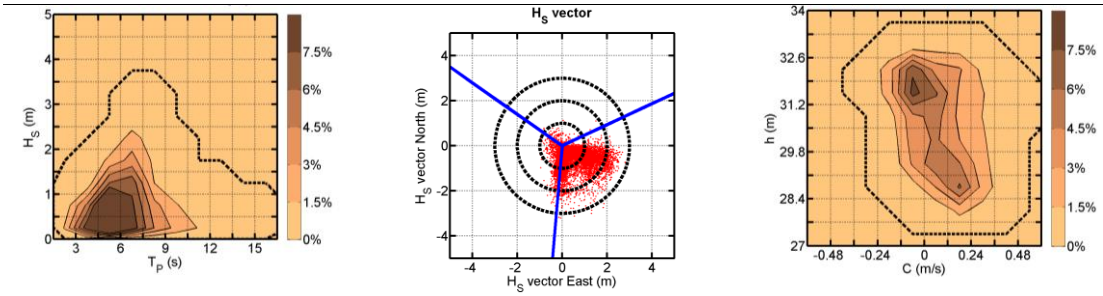

(d) environmental conditions

Figure 7.5: Comparison of the environmental conditions (from left to right: H_S/T_P, H_S/D_P, h/C) associated with peak mooring loads with different methods to detect peak mooring loads. Example during the first SWMTF deployment before anchor drag on line 1. Environmental conditions associated with a) the peak mooring loads as defined in this thesis; b) the same number of peak mooring loads defined as the loads with the highest amplitude; c) Reminder of the general interpolated environmental conditions. The wave direction is the direction from which the waves are coming.

7.2.2 Choice of wave statistical parameters for the assessment of wave conditions associated with peak mooring loads

The aim of this section is to assess if the choice of the wave statistical parameters T_P, D_P and D_{mean} in the assessment of environmental conditions associated with peak mooring loads was appropriate or if the results may be actually biased by this choice, and to investigate other wave parameters and evaluate if they would lead to similar or different results. More generally, this section aims to define which wave statistical parameters should be used in MRE mooring design standards.

In this thesis, the significant wave height H_S, the peak period T_P and the peak direction D_P (SWMTF) or the mean direction D_{mean} (FaBTest) have been chosen to describe the sea states associated with peak mooring loads because H_S and T_P are used in DNV-OS-E301 (DNV, 2013) for the choice of extreme environmental conditions for mooring design, D_P is associated with T_P and D_{mean} was the only wave direction available at FaBTest.

The relationship between T_P and D_P and the other available parameters describing the period or direction - the zero-crossing period T_Z and the mean wave direction D_{mean} respectively - is assessed using the SWMTF data. The aim is to assess if these parameters are interchangeable.

Figure 7.6 plots the interpolated values of T_P against T_Z and D_P against D_{mean} during the first SWMTF deployment before anchor drag. T_P and T_Z show a high dispersion with high values of T_P associated with low values of T_Z. D_P and D_{mean} show a fair correlation with most of the points not being dispersed. The linear relationship between the couple of parameters has been calculated using a least square method.

The relationship between T_P and T_Z and D_P and D_{mean} is considered for different values of H_S in Figure 7.7. The values which are the most dispersed correspond to the lower values of H_S. For low values of H_S, the calculation of T_P is difficult because of its definition (the frequency associated with the highest spectrum density, then when the measured spectrum is double peaked, the choice of the peak is rather random); consequently, the high values of T_P, which are occurring for the low values of H_S, are likely to be unrepresentative. D_P is depending on T_P and will be unrepresentative as well for the low values of H_S.

The peak mooring loads occurred for high values of H_S. The parameters T_P and T_Z and D_P and D_{mean} strongly depend on a linear relationship for high values of H_S. This means that these parameters could be changed in the peak mooring load assessment without major consequences on the final results.

H_{max} is not recommended as a parameter to assess the sea states leading to peak mooring loads as it is likely to be different at the ADCP and at the instrumented buoy because of the distance between the ADCP beams and the instrumented buoy and therefore of the recombination or breaking of waves in between.

Other wave parameters could be investigated in the future, such as T_{mm10}, but this parameter was not provided by the ADCP.

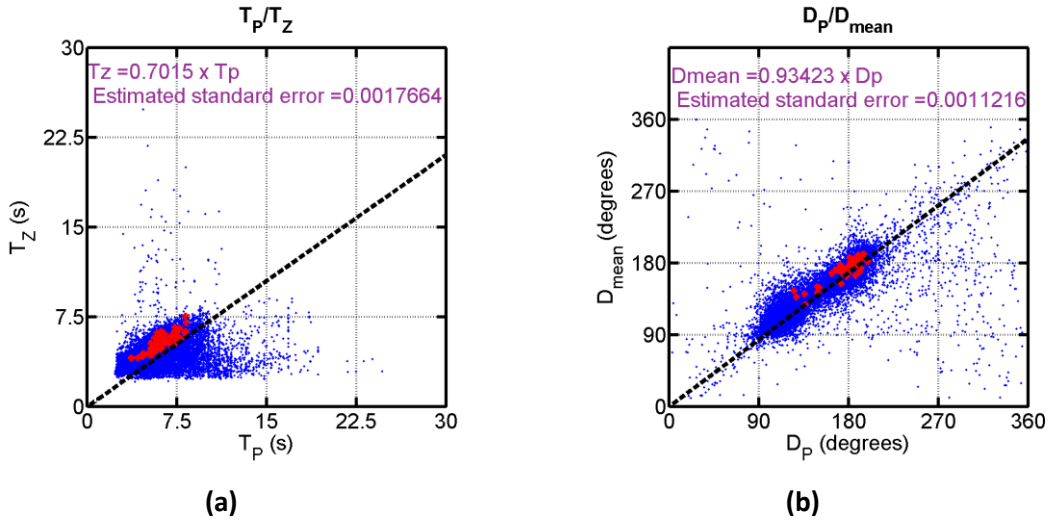

Figure 7.6: Correlation between the different statistical wave parameters for the SWMTF ADCP data during the first deployment before anchor drag a). T_Z and T_P, b) D_{mean} and D_P. Blue dots: general interpolated environmental conditions. Red dots: environmental conditions associated with peak mooring loads. Black line: best fit line for the general interpolated environment conditions

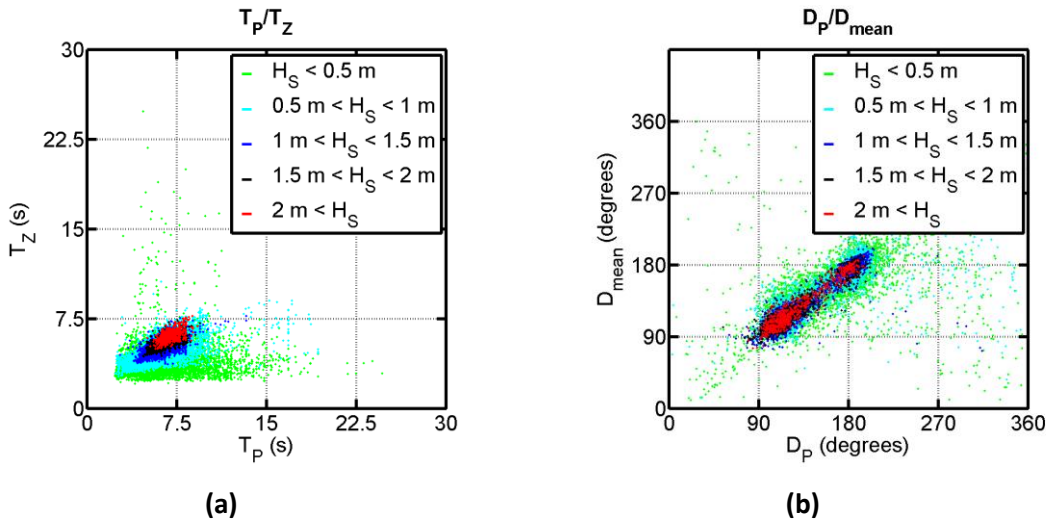

Figure 7.7: Variations of the wave periods and directions with H_S

7.2.3 Wave and current interactions

The aim of this section is to estimate if there are any interactions between the wave and the current measurements gathered from the field tests, which would bias the results. In particular the effect of current on waves will be assessed: could this effect explain why peak mooring loads occur for large but not always highest H_S, with the current reducing the amplitude of H_S or increasing T_P?

The main effect of current on waves would be to steepen the waves (Wolf and Prandle, 1999) if the current is coming from an opposite direction than the waves (opposite current), and on the contrary to reduce the steepness of the waves if the current is in the same direction than the waves (following current). One of the effects of waves on current is to add wave-induced current to wave orbital velocities.

Wave and current data were only available for the SWMTF. The data from the first SWMTF deployment before anchor drag will be used as an example for this investigation. The effect of wave or current on mooring loads will not be discussed here, but only the interactions between wave and current. For the SWMTF, current and waves were aligned when they both came from the South and they were opposed when current came from the North and wave from the South. Interactions should be observed for these two cases. In the case of Easterly waves, wave and current interactions should not be observed. The main wave and current directions for the SWMTF are summarised in Table 7.5.

Table 7.5: Wave and current main directions at SWMTF

Parameter	**Main directions**	
Waves	Easterly	Southerly
	$90° < D_P < 150°$	$150° < D_P < 210°$
Current	Southerly	Northerly
	$180° < Cur_{Dir} < 240°$	$330° < Cur_{Dir}$ or $30° < Cur_{Dir}$

Each combination of the two main wave directions and the two main current directions is investigated. For each combination, the 1,000 sea states with the lowest or with the highest current magnitude C_{Mag} were considered and the distribution of the significant wave height H_S is compared.

The distribution of the significant wave height for the different wave and current directions were plotted in Figure 7.8 for the maximum current magnitude or without current.

With the maximum current magnitudes (red lines), a lower percentage of occurrences of very low values of H_S (below 0.5 m), up to more than 10 %, is observed for all combinations of wave and current compared to the case without current. This difference is actually not due to the effect of current on waves, because it occurs for all wave and current combinations. This may be due to the influence of waves on current: the cases with minimum current speeds do not have current speeds caused by wave orbital velocities.

Unsurprisingly, the plots without current (black lines) are similar for the Easterly waves and the two current directions, and similarly, for the Southerly waves and the two current directions. However, small differences are observed between the plots, approximately up to 5%, and they may be the results of the limited number of points chosen for this analysis.

These results indicate that no strong interactions between waves and currents have been highlighted at this site and that consequently the significant wave heights H_S associated with peak mooring loads are not modified by the presence or absence of current.

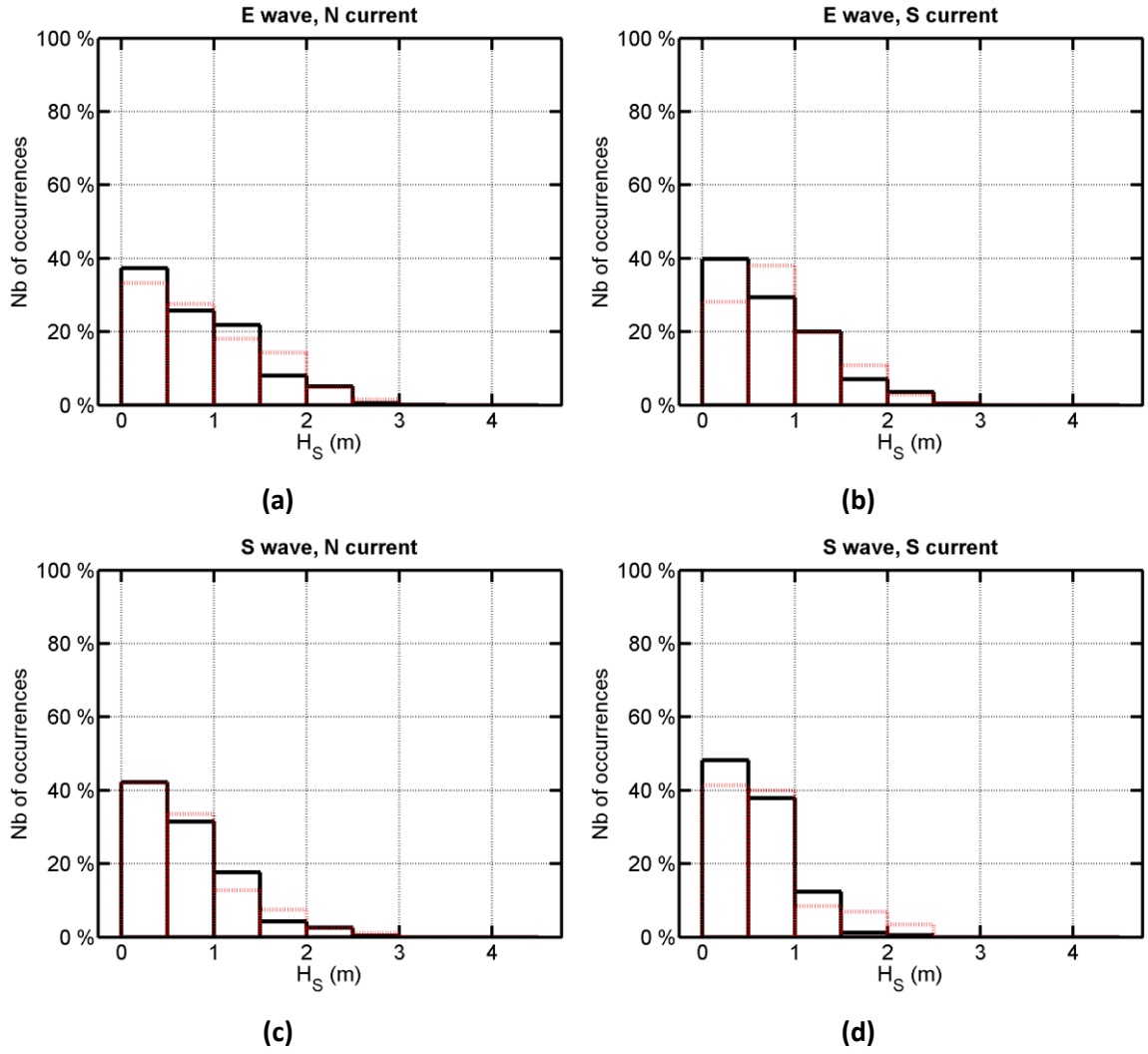

Figure 7.8: Effect of current on waves. Comparison of percentage of occurrences of significant wave height H_S with maximum (red dotted line) or without (black line) current, for different wave and current directions for the first SWMTF deployment before anchor drag. Nb: number

7.2.4 Effect of line non-linearities on S_{max}

Section 2.1.2.2 identified four different non-linear effects caused by the mooring system.

For the range of buoy excursion considered here, geometric non-linearity and non-linear stretching are small:

- The excursion of the buoy (full scale, during field tests) was in the order of magnitude of 5 m (Figure 4.20). Based on the stiffness curve of the model mooring system (Figure 6.6), in the absence of accurate field motion data, the mooring stiffness changes linearly with the excursion for this range of excursion.

- The highest recorded maximum mooring load had an amplitude of 53 kN during the first deployment and 19 kN during the second deployment. The stiffness of the rope was 858 kN during the first deployment and 687 kN during the second deployment. The maximum load was then 6% of the MBL during the first deployment and 3% of the MBL during the second deployment. For this range of load, the rope stiffness is increasing linearly with the extension (Figure 3.11)

Non-linear seabed friction has not been assessed but is likely to be small, especially for the small range of excursion observed, meaning the chain lifting was small. Consequently, peak loads are likely to be due to snap loads, caused by viscous damping. Figure 4.19 indicated that some of the observed peak loads were snap loads with the line becoming slack before being suddenly re-tensioned. It does not mean that all peak mooring loads were snap loads and further investigations would be required.

7.3 Towards improved MRE mooring design and the development of MRE mooring standards

7.3.1 Reduction of the amplitude of peak mooring loads

The amplitude of peak mooring load could be reduced in order to reduce the size of the components of a mooring and hence its price. However ropes with a smaller diameter are more exposed to surface damage as discussed by Flory and Banfield (2011) and shown in Figure 7.9. Chains are also subject to fatigue as discussed by Thies (2014) and a reduction in their diameter may not be compatible with their fatigue life.

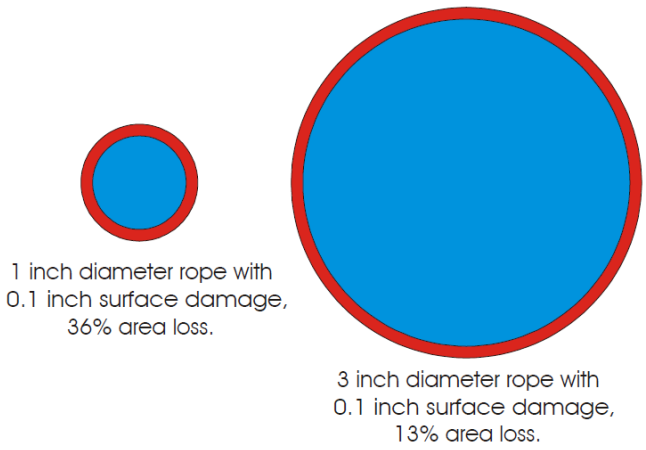

Figure 7.9: Effect of 0.1 inch surface damage on a small and a large rope

Some parameters could be investigated to reduce the amplitude of peak mooring loads:

a) A decrease of the pre-tension of the mooring system seems to reduce the amplitude of peak mooring loads, as seen by the comparison of the results before and after anchor drag during the first SWMTF deployment. A decrease of pre-tension could be achieved by increasing the rope length or moving the anchor points closer to the centre. This could be investigated during mooring design using OrcaFlex line setup wizard.

However, this should be balanced with the power production and the buoy excursion. A high pre-tension would reduce the motion of the floating structure and consequently will modify the power production. However, if the pre-tension is too low, and the buoy excursion is too large, this could be an issue for the power cable, for the PTO (for example for an “upside down yoyo” PTO as used by Bolt-2 Lifesaver), or for collision

between devices in an array. It is already difficult to achieve a sufficiently high pre-tension for low tide, while achieving a reasonably low pre-tension for high tide.

b) An increase in the number of lines could be investigated. The amplitude of mooring loads was higher on Bolt-2 LifeSaver mooring (5 mooring lines) than on SWMTF mooring (3 mooring lines) but this is because Bolt-2 LifeSaver device is installed in a more exposed environment, and is a much larger structure.
The increase of the number of mooring lines is not cost effective in terms of total price of the mooring; however, a reliable mooring system for a 20-year project will be less expensive than mooring failure. At the moment, prototypes are installed and the consequences of a mooring failure would be to obtain no field test data, and to lose the confidence of the investors and of the public.
A higher number of mooring lines may also affect the power production by restraining the motion of the floating structure. The impact of an additional mooring line on the power production needs to be evaluated during the mooring design.

c) The compliance of the mooring configuration needs to be investigated. The ropes used during the second SWMTF deployment had a lower stiffness, and the pre-tension was also lower. However, the number of peak mooring loads was only reduced in line 3 but this is likely to be due to the shortest duration of this test and the lower number of sea states coming from the East, in a similar direction as line 3. A more compliant system will have a more dynamic behaviour which may explain why more peak mooring loads have been observed on the other mooring lines.

d) If the installation site has a limited number of wave directions and a low number of mooring lines, the mooring system can be oriented to avoid the worst wave climate. This is what has been attempted for both moorings investigated in this thesis, but this was difficult because of the limited number of mooring lines and wide range of wave directions. However, the seabed properties also have to be considered, especially if drag embedment anchors, which require a cohesive soil (sand, clay...), are used, because the seabed may present some local rocky areas over the installation site, and consequently, the anchors may not be installed on some parts of the seabed.

The reduction of the amplitude of peak mooring loads is possible, but this should not be done to the detriment of survivability and durability, or to a lesser extent of power production. Survivability and durability are essential. The power production is less critical and can be reduced to some extent in order to reduce the amplitude of peak mooring loads. However, at a later stage of development, PTOs will need to be optimised in order to ensure the economic viability of the device.

7.3.2 Dynamic response and loads

This thesis has been mainly focusing on average of measured data from field test, instead of time series. This research will serve as a base for future studies looking at the critical environmental conditions identified here, aiming to understand the individual hydrodynamic behaviour of floating structures and their mooring systems leading to peak mooring loads.

The next step would be to investigate the time series of the data to understand the dynamic response and loads. This section gives a preview of the possible work to conduct. This section will investigate examples of time series of data. Further work would be to examine the time series of data in a more systematic way and understand the cause of the peak mooring loads.

Firstly two similar sea states will be compared, one led to peak mooring load whilst the other did not. Secondly, the sea state with the smallest H_S which led to peak mooring load will be examined. Data from SWMTF have been used as they also include motion data.

7.3.2.1 Why two similar cases do not lead to similar mooring loads?

The comparison of two similar cases, one leading to peak mooring loads (case 1), the other not (case 2), is aiming to highlight which parameters are worth investigating during the time series analysis of the dataset in the future. The properties of the two cases are summarised in Table 7.6. Of course, it was not possible to find two cases with exactly the same environmental statistical properties. The maximum relative difference between the environmental parameters is of 7%. H_S and H_{max} are actually

slightly higher in the case which is not leading to peak mooring load. These two cases occurred less than 1 hour apart – belonging to the same sea state- so the instrumentation and mooring are likely to be the same.

The comparison of the wave elevation between the two sets of data (Figure 7.10) is inconclusive. In both cases, large surface elevations are observed, and the waves seem to be grouped. As mentioned before, the clock of the ADCP may be not well synchronised with the clock of the SWMTF buoy, and the waves are measured at the top of a beam of the ADCP, and not at the buoy location, and are consequently different once they reach the instrumented buoy.

Figure 7.11a shows that the peak load occurred after several peaks around 10 kN alternating with null tensions followed by a peak with a small amplitude (~ 15 kN) and a null tension. This suggests that the mooring line got slack and a snap load followed. Figure 7.11b shows that for the dataset without peak load, two large loads with medium amplitude (~ 25 kN) are following each other, with low but not null loads in the 10 seconds before. Sharp increases in tensions have been observed but because of the stormy sea states, these sharp loads are not sufficiently peaky to be considered as peak loads. The value of S_{max} is below the threshold of 7.5.

In the two mooring lines which are aligned with the waves, the time series of loads are similar whether the peak mooring load occurred or not.

The time series of the position of the instrumented buoy is shown in Figure 7.12. When the peak load occurred, a large motion to the West (3 m amplitude peak to peak), to the North (6 m amplitude peak to peak) and in heave (4 m) was simultaneous to the peak load. The same sequence of motions was observed when the peak load did not occur but with a lower amplitude (West motion: 2 m, North motion: 4 m, heave motion: 3 m). Large amplitudes of motions were observed in the dataset containing the peak load, when the motion was more restrained in the dataset which does not contain the peak load.

A more systematic approach needs to be developed. The mooring load (alternating slack line/moderate loads) and motions before the peak load (dynamically moving buoy) need to be investigated.

Tank tests and numerical models could be used to gain more insight into the dynamic behaviour of the mooring system. Tank tests give a precise knowledge of the wave elevation and of the buoy position at its centre of gravity (COG) in its six degrees of

freedom (DOFs). Loadcells would also be calibrated more precisely in tank tests, indicating with certainty if a mooring line becomes slack.

Table 7.6: Two similar sea states measured on the same day at SWMTF leading to different values of maximum mooring loads

	Parameter	Peak: case 1	Not peak: case 2	Relative difference
	Date	17/11/2010 02:00-02:10	17/11/2010 02:40-02:50	$d_r = \frac{\lvert x-y \rvert}{\left(\frac{\lvert x+y \rvert}{2}\right)}$.
Wave	H_S	2.62	2.81	7%
	H_{max}	4.15	4.23	2%
	T_P	7.7	7.7	0%
	T_Z	6.53	6.24	5%
	D_P	174	185	6%
Tide	h	31.91	31.96	0%
Line 1	Max	**52.48**	**27.29**	**63%**
	Mean	4.75	4.54	5%
	Std	3.93	3.28	18%
	S_{max}	12.15	6.94	55%
Line 2	Max	12.81	12.97	1%
	Mean	3.89	3.94	1%
	Std	2.04	1.96	4%
	S_{max}	4.39	4.62	5%
Line 3	Max	19.04	18.50	3%
	Mean	3.62	3.55	2%
	Std	3.33	3.30	1%
	S_{max}	4.63	4.53	2%

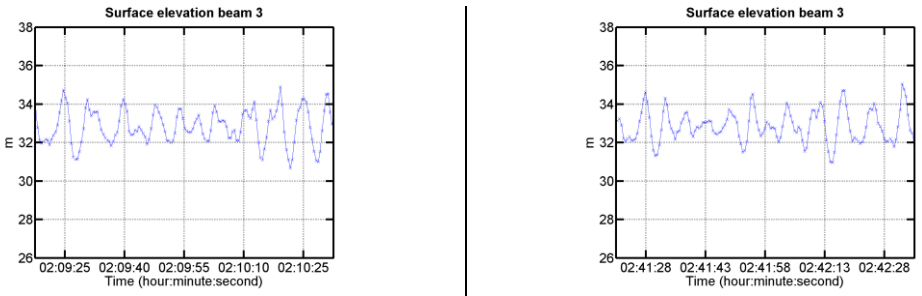

(a) **(b)**

Figure 7.10: Examples of wave elevation at beam 3 of the ADCP during 1 minute for the SWMTF on the 17/11/2010: a) case 1, b) case 2

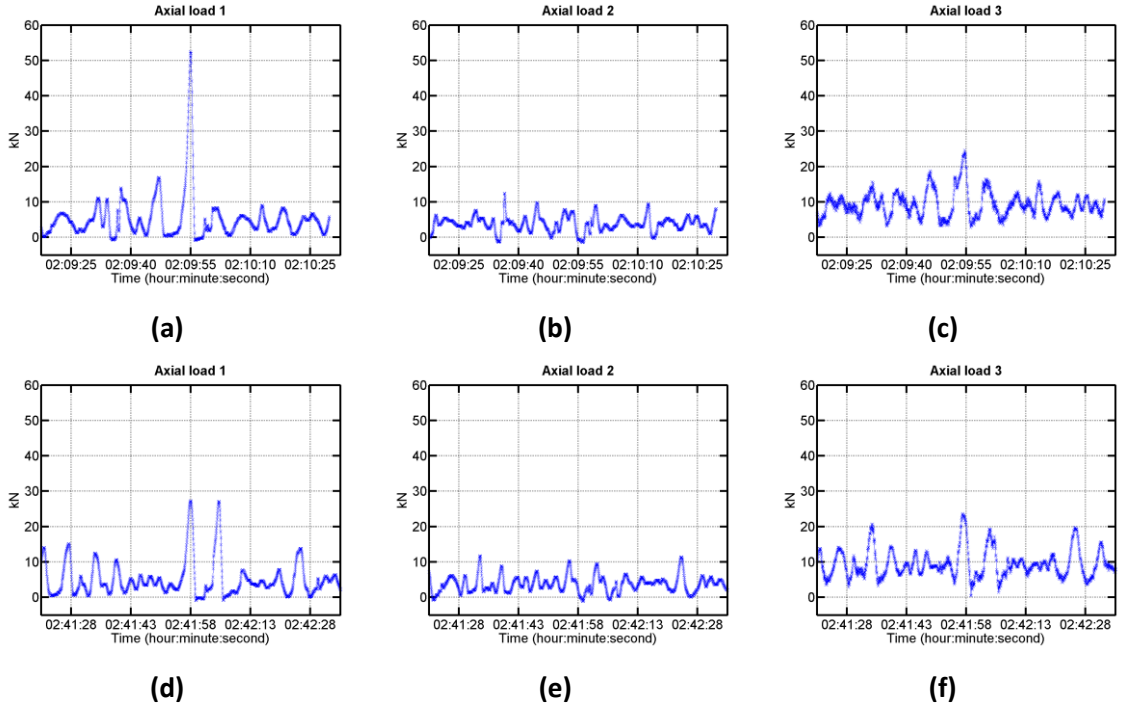

Figure 7.11: Example of mooring loads during 1 minutes in the 3 axial loadcells: (a-c) case 1 and (d-f)case 2 for the SWMTF on the 17/11/2010

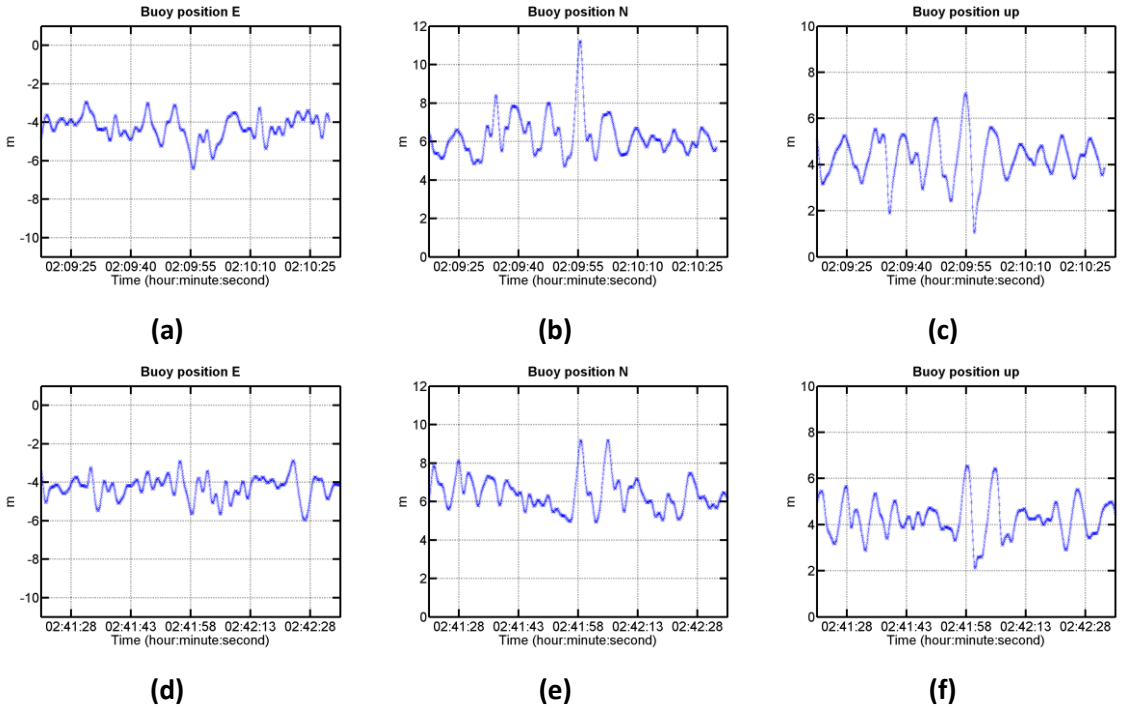

Figure 7.12: Example of SWMTF buoy motion in the 3 DOF in translation during 1 minutes: (a-c) case 1 and (d-f) case 2on the 17/11/2010. The maximum mooring load occurred at 02:09:55 (peak, case 1) and 02:41:58 (no peak, case 2).

7.3.2.2 Example of small H_S leading to peak mooring loads

Large but not necessary the highest H_S lead to peak loads. This result is not surprising and is linked to short-term variability. Short-term variability means that the maximum over a given duration for the same environmental conditions (H_S, T_P and spectrum) is not a single value but a random variable following the Extreme Value Distribution (EVD). Therefore it is advised (DNV, 2013) that the mooring design should be conducted with several (8 to 10) three hour sea states with the same environmental conditions but with different sets of random phase angles in order to provide adequate statistics.

The peak load associated with the lowest value of H_S on line 1 during the first SWMTF deployment before anchor drag has been chosen for further analysis in this subsection. It was checked in the operation log book that there were no operations at the buoy on this day.

The statistical values for this sea state are summarised in Table 7.7. In this example, the maximum load on line 1 (12.4 kN) is just over τ (9.3 kN) and the standard score of the maximum S_{max} (7.7) was just above K (7.5). Consequently, because this point is just on the edge, its quality of peak load may be criticised and that is one of the limitations of the methodology presented in this thesis. If more data would have been available, the same methodology could have been used and higher values of τ and K could have been chosen.

The wave elevation during this sea state is shown in Figure 7.13. Most of the waves are below 1 m.

The whole time series of mooring load of this dataset are shown in Figure 7.14, and a zoom on the peak load has been plotted as well. The line tension was low just before the peak. It was moderately varying before, between 0 and 5 kN mainly.

The position of the buoy is shown in Figure 7.15. The peak load was preceded by a motion towards the West (~ 1 m), towards the North (~ 2.5 m) and up (~ 1.5 m), and followed by a small motion to the East (< 1m), to the South (~ 1.5 m) and down (2 m). This is again the same sequence of motions as observed in the previous subsection. That motion could be the trigger of peak mooring loads.

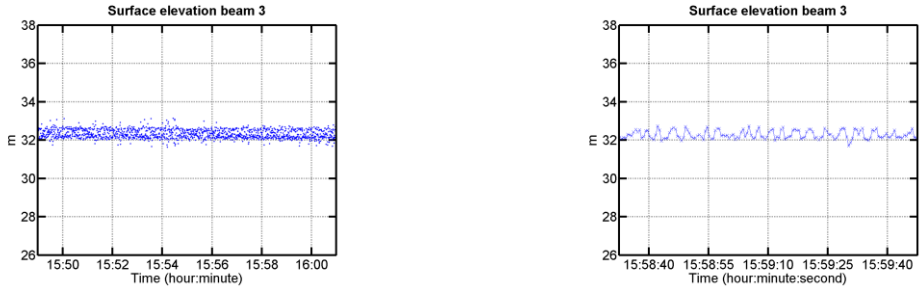

(a) **(b)**

Figure 7.13: Example of wave elevation at beam 3 of the ADCP during 10 minutes and zoom on 1 minute for the SWMTF

Table 7.7: Environmental conditions and mooring loads measured at SWMTF during a sea state with a low value of H_S leading to a peak mooring load

Parameter	**Value**		
Date	16/11/2010 15:50-16:00		
H_S	0.66 m		
H_{max}	1.05 m		
T_P	3.66 s		
T_Z	4.08 s		
D_P	178°		
h	31.4 m		
Mooring load	Line 1	Line 2	Line 3
Max (kN)	12.4	9.3	8.3
Mean (kN)	3.3	3.7	2.6
Std (kN)	1.2	1.2	1.3
S_{max}	7.7	4.7	4.3

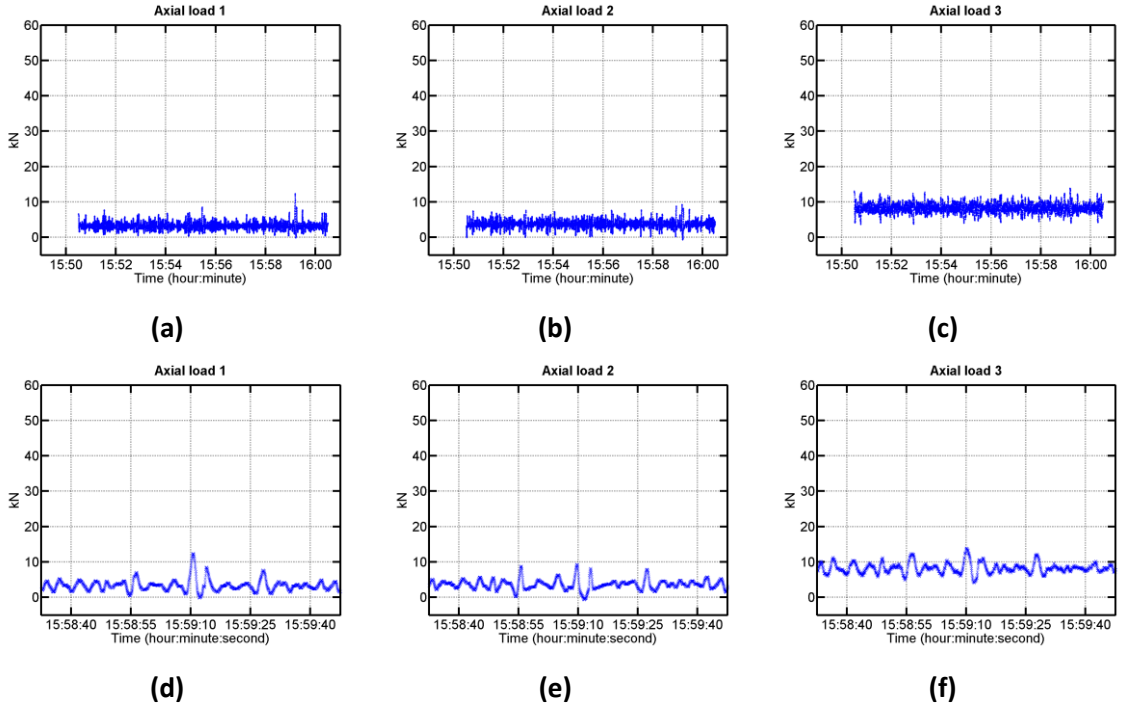

Figure 7.14: Example of mooring loads during 10 minutes in the 3 axial loadcells (a-c) and zoom on 1 minute (d-f) for the SWMTF

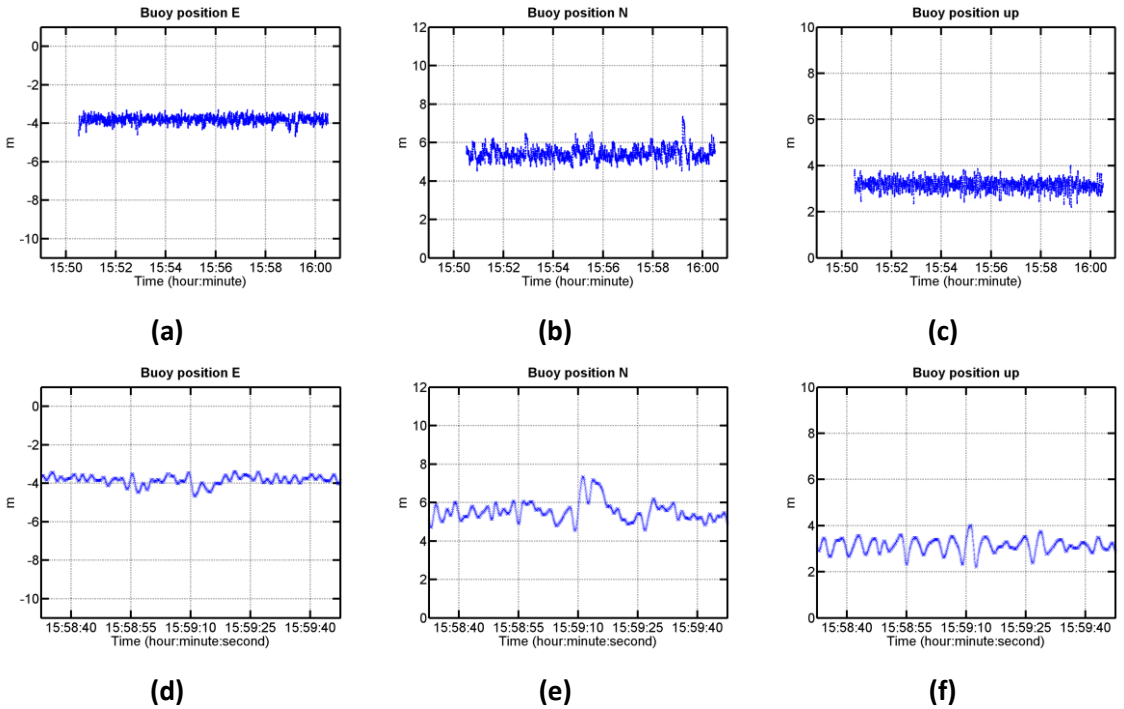

Figure 7.15: Example of SWMTF buoy motion in the three translation DOFs during 10 minutes (a-c) and zoom (d-f) on 1 minute

7.3.2.3 Relationship between the buoy motion and the quasi-static mooring line behaviour

One of the important steps for further research would be to understand the relationship between the time series of waves, the floating structure motion and the mooring loads. The time series of motions recorded during the field test could only be used for a qualitative assessment (SWMTF) (see 4.1.1.3 and 4.1.2), or these data were not available (Bolt-2 LifeSaver). This subsection aimed to show how to apply a quasi-static method to estimate the mooring loads. The buoy motion recorded during SWMTF tank test will therefore be used here as an example for a qualitative assessment. In the future, the same method can be applied to motion data which are fully validated and accurately represent the buoy motion.

The quasi-static mooring line load for a given buoy position was estimated using the numerical model in the absence of wave, and these loads were compared with the loads recorded during a tank test.

The numerical model has been used to estimate the mooring loads in each mooring line for a given static buoy position: between -0.4 and 0.9 m on the X axis in steps of 0.1 m, between 0 and 0.04 m on the Y axis in steps of 0.01 m, and between - 0.4 and 0.9 m on the Z axis in steps of 0.1 m. Buoy rotations were not considered.

The difference between the recorded and calculated loads gives an estimation of the dynamic part of the mooring load.

Figure 6.21 already showed that the dynamic part of the mooring load could be significant.

Results of the quasi-static analysis are presented in Figure 7.16 and Table 7.8. The mean load is well estimated using the quasi-static method, with a maximum relative error of 7%. However, the relative error is higher for the maximum load and the standard score of the maximum load, up to 25% and 26% respectively, and even higher for the standard deviation of loads, up to 62%. They are possible uncertainties due to the quality of the time series of motion data as discussed in 4.1.1.3 and 1.2 and the results of this study are mainly qualitative.

These results indicate that the highest mooring loads have a large dynamic contribution, about 25% of the total load in this example, and that small and fast variations of the mooring loads are also due to dynamic load.

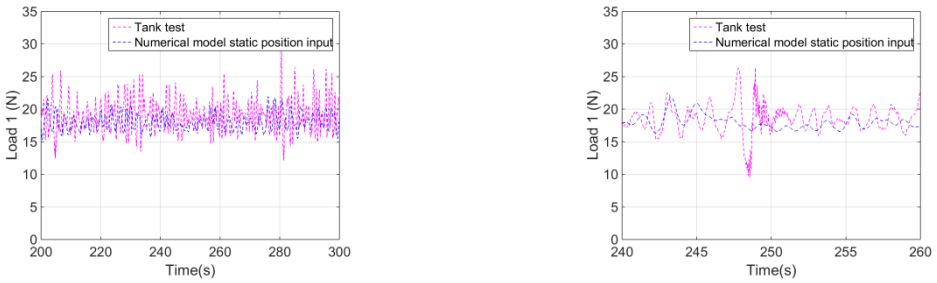

Figure 7.16: Example using Case 1 of mooring load as measured during the tank test and estimated from the motion using a quasi-static method a) for 100 s, b) zoom on 20 s

Table 7.8: Mooring loads: mean, maximum, standard deviation and S_{max} as measured during tank test and as calculated from the buoy motion using a quasi-static method

Mean load in mooring line for tank test/for quasi-static numerical model/ relative error			
Case	Line 1 (N)	Line 2 (N)	Line 3 (N)
1	0.0188/0.0180/4%	0.0172/0.0162/6%	0.0188/0.0176/6%
2	0.0185/0.0177/5%	0.0176/0.0166/6%	0.0185/0.0173/6%
3	0.0189/0.0181/4%	0.0171/0.0159/7%	0.0189/0.0178/6%
Max load in mooring line for tank test/for quasi-static numerical model/ relative error			
Case	Line 1 (N)	Line 2 (N)	Line 3 (N)
1	0.0289/0.0226/22%	0.0259/0.0193/26%	0.0289/0.0221/23%
2	0.0252/0.0196/22%	0.0238/0.0183/23%	0.0252/0.0192/24%
3	0.0296/0.0237/20%	0.0253/0.0194/23%	0.0295/0.0233/21 %
Std load in mooring line for tank test/for quasi-static numerical model/ relative error			
Case	Line 1 (N)	Line 2 (N)	Line 3 (N)
1	0.0020/9.1563e-04/53%	0.0021/9.6215e-04/54%	0.0020/8.8290e-04/55%
2	0.0013/4.9622e-04/61%	0.0016/6.2018e-04/61%	0.0013/4.8136e-04/62%
3	0.0024/0.0012/48%	0.0024/0.0012/52%	0.0024/0.0012/49%
S_{max} load in mooring line for tank test/for quasi-static numerical model/ relative error			
Case	Line 1 (N)	Line 2 (N)	Line 3 (N)
1	5.1448/5.0035/3%	4.1885/3.1777/24%	5.1450/5.0534/2%
2	5.2123/3.9152/25%	3.8577/2.8396/26%	5.2123/3.8442/26%
3	4.4552/4.4752/0 %	3.4064/2.9450/14%	4.4559/4.5108/1%

7.3.3 From peak mooring loads to extreme mooring loads and MRE mooring standards

Comparing the results of this study with the available standards is useful to suggest potential areas to further develop MRE standards. The results indicate the importance of adapting the available oil and gas mooring standards, such as DNV-OS-E301 (DNV, 2013), to highly dynamic responding moored structures, such as some MRE devices.

Both mooring systems investigated in this paper have been designed following oil and gas mooring standards. However it was not possible to use a 100-year return period contour line during the mooring design. Wave measurements or validated hindcast models should have been available for a number of years in order to estimate this contour line. As explained in 3.1.4 and 3.2.4, the SWMTF mooring was designed based on 1 year of wave measurements and the Bolt-2 Lifesaver mooring using an 8-year hindcast model. In both cases, high safety factors have been used to account for the limited amount of wave data for mooring design and for uncertainties in the rope behaviour. The target safety factor was 3 and the rope MBL was reduced to account for eye splice, water absorption, ageing and fatigue. Consequently, the final safety factor was equal to: rope initial MBL/design load = 461kN/69KN=6.7 for the first deployment at SWMTF and 520 kN/69kN =7.5 for the second deployment, and 812kN/217kN =3.7 at Bolt-2 LifeSaver. The hindcast model presented in this thesis was made available after the mooring design, and it only covers a 23 year period. This lack of wave data is an issue at many wave energy sites.

The data analysed in this thesis only covers a few months of field tests. Consequently, the extreme sea states – such as a 100-year return period sea state - were not likely to be attained and it is difficult to conclude on the behaviour of the mooring for extreme sea states. However, it should be highlighted that the difference between large H_S and extreme H_S is relatively small, the maximum H_S values following a Weibull distribution. For example, the highest H_S expected by the 23-year hindcast model was around 3.3 m when the highest hindcast H_S during the first SWMTF deployment (9 months) was around 2.6 m. For comparison, the highest measured H_S during the first SWMTF deployment was 3.3 m. This means that inaccuracies in the hindcast model should be accounted in order to use the hindcast model for mooring design.

As observed at both facilities, the peak mooring loads were not always occurring for the highest values of H_S for the different wave periods, but within the scatter diagram of the measured data. Additional data would be required in order to make sure a similar behaviour occur for the extreme sea states.

Meanwhile, the addition of H_S and T_P design values would allow a better understanding of mooring dynamics. Running more calculations during the mooring design would improve the understanding of the dynamics of the mooring system, and only require a small additional period of time.

Standards such as DNV-OS-E301 (DNV, 2013) and API RP 2SK (API, 2005) do not give specific recommendations for tidal variations but they indicate that mooring design should be done for applicable water depths and currents. These standards are designed for offshore structures, installed in area with low tidal variations. Based on the results of this study, and in the absence of final conclusions on the tidal influence of peak mooring loads, several tidal elevations should be considered for the mooring design.

7.4 Tank tests and numerical modelling

Tank tests of the SWMTF have been conducted and their results have been used to calibrate a numerical model. Results have been presented in Chapter 6. The tank tests and the validation of a numerical model gave insight into specific and more general considerations: difference between the SWMTF and a real wave energy device, validation of the numerical model for a wide range of sea states, limitation of the radiation/diffraction potential analysis, possible improvements to the numerical model, scaling limitation especially for the stiffness of the mooring rope, and combination of numerical model and tank tests to gain more insight into the behaviour of a mooring system in real sea conditions.

7.4.1 Validation of the numerical model for a wide range of sea states

It should be noted that the presented tank tests were not conducted to estimate the mooring behaviour in extreme conditions, i.e. to explore the survivability of the device, but to analyse the operational behaviour characteristics. At the SWMTF, 1-year return period sea state has an estimated significant wave height H_S of 3.5 m and peak period T_P of 7 s (Johanning, Spargo and Parish, 2008). At the 1:5 scale used in this model, this corresponds to H_S equal to 0.7 m and T_P to 3.1 s. Hydrodynamics parameters have been calculated for this range of sea states for linear and steep waves. For low wave frequencies, the RAOs and mean drift curves (Figure 6.12-Figure 6.13) converge to a constant value, with the floating structure expected to follow the waves. The results can then be extrapolated with some confidence.

The results in irregular waves give confidence in the ability of the numerical model to predict mooring loads in real sea conditions. However, additional irregular wave tests, covering a more varied range of wave conditions, would provide greater confidence in the results. For the available results, the inaccuracies have been quantified. In particular, the maximum mooring loads are underestimated by 5 to 17% (Table 6.10). Typically a safety factor of 1.4 (DNV-OS-E301, 2013) is applied. In this case, the uncertainties cut into a large part of the safety factor and this may result in insufficient reliability, because the safety factor needs to account for other uncertainties. Consequently, it would be advised either to reduce the uncertainties, either to increase the safety factor.

7.4.2 Limitation of the radiation/diffraction potential analysis and possible improvements to the numerical model

The main discrepancy which has been observed in the numerical model regards the mean drift, which is not accurately modelled especially for the highest wave frequencies, at the pitch resonance. It is however accurately modelled for the short wave frequencies which are of interest because associated with storms. This was also the case with a similar buoy during experiments performed by Cozjin, Uittenbogaard and ter Brake (2005). Cozjin et al. suggested that inaccuracies in the surge wave drift forces may be linked to inaccuracies in the first order vessel motions. In Cozjin et al and in this thesis, the first order pitch motion was overestimated by the numerical model because it was lacking viscous damping. This may have induced the inaccuracies for the surge wave drift motions. The lack of viscous damping was due to the limitations of the radiation/diffraction potential analysis which does not include viscous effects.

Cozjin et al. also noticed that the heave and pitch added mass were underestimated by a linear radiation-diffraction potential code for a similar buoy. In this thesis, it was found that the surge added mass was underestimated by the linear radiation-diffraction code. Cozjin et al. suggested that it was due to the fact that rotational accelerations in the fluid are not taken into account by this kind of code.

Furthermore, radiation/diffraction potential analysis usually used a simplified shape of the hull to reduce the computation time, but this could introduce inaccuracies for added mass and radiation parameters.

Computational Fluid Dynamics (CFD) could be the solution for the lack of viscous damping and the absence of rotational accelerations in the fluid. Bunnik et al. (2002) suggested using CFD in the future to predict viscous forces. Palm et al (2013) and Yu and Li (2011) started investigating CFD for wave energy devices. Palm et al. (2013) concluded that CFD is highly time consuming and requires validation. CFD should be looked at as a future work to improve the understanding of MRE moorings.

Numerical results could be slightly improved by using a higher time resolution for the wave input into the numerical model. The previous chapter indicated that a wave input re-sampled at 4 Hz can lead to up to 2% relative error in the surge motion. However,

these calculations are time consuming and would make the numerical model tedious to use for further investigations.

In the previous chapter, a method has been developed to adjust added mass, radiation and quadratic damping values based on natural period, linear and quadratic damping decay results respectively. However, this method was not applicable for the pitch decay tests, because the pitch motion was coupled with the surge motion and the relative contribution of pitch radiation and quadratic damping could not be determined experimentally. Because of this, the pitch radiation damping was assumed to be correct, and the pitch quadratic damping was corrected using the pitch RAO plot from the regular wave tests. Forced oscillation tests would have isolated the pitch motion but they were not conducted because of limited testing time. They should be included in future tank tests.

7.4.3 Scaling of the static stiffness of the mooring rope

A sensitivity analysis on the stiffness of the rope has been presented, as the stiffness of the rope used in the tank test was higher than the scaled value of the stiffness of the full scale rope, because of limited availability. It should be noted that only the static stiffness of the rope has been considered in the numerical model. The dynamic stiffness of the rope - higher than the static stiffness - should be considered for further investigations as it may have an influence on peak loads. The results of the sensitivity analysis in irregular waves for different rope stiffness (Figure 6.28) indicate that in this particular case, with a model stiffness of 10.873 kN when the equivalent scaled stiffness of the full scale facility was between 7.1 and 7.8 kN, small bias without considerable effect was observed for the motions and mooring. These results more generally indicate that for tank tests, when no accurate information is available on the stiffness of the mooring ropes (full scale or model scale), or when the choice of model mooring rope is limited, it is better to choose a slightly stiffer rope (within limits) than what is desired, and that this will not have a significant consequence on the tank test results.

7.4.4 Combination of numerical model and tank test to gain more insight into the behaviour of a mooring system in real sea conditions

The numerical model can be used to improve the understanding of the hydrodynamics of the full scale SWMTF mooring system. This is less time consuming (and expensive) to run different wave conditions in the numerical model than to run tank tests. The model can also be used as a reference before conducting any engineering changes at the full scale facility, for example changing the rope materials to investigate fibre rope behaviour in long-term real sea conditions.

Simulating real and rough wave conditions with the numerical model will allow a better understanding of the mechanisms involved in peak mooring loads, for example wave grouping or acceleration in buoy movements, and consequently an improvement of the mooring design.

Tank tests allow the identification of the different hydrodynamic parameters of a mooring system, for example the RAOs. One of the limitations of the tank tests is that they do not take into account some changes which occur in real sea conditions. For example at the SWMTF, the incorrect position of an anchor in the field significantly modified the mooring loads and the buoy mean position. This problem is likely to occur for other wave energy devices unless specific anchors are developed.

Another change which is not easily taken into account by the tank tests is the variations in water depth; these variations lead to change in pre-tension and consequently change in the behaviour of the mooring system. The tidal range to nominal water depth ratio is 20% at the SWMTF, and approximately 10% at full scale facilities (Wave Hub and EMEC, Table 2.6). Winches could be used on a future tank test to modify the pre-tension. A raisable floor has also been developed at Plymouth University Marine Building, in the Coastal Ocean and Sediment Transport (CoaST) laboratories in their ocean wave basin (Marine Institute Plymouth University, n.d.).

Hence tank tests and numerical models are complementary. Tank tests determine the hydrodynamic behaviour of the floating structure and mooring; numerical models allow the variation of those parameters that were fixed or not explored in the tank.

The aim in the future is to understand the inaccuracies inherent to MRE field tests and replicate them in the numerical model, in order to model what happen in reality, and compare it with what happen for the design mooring system. This would allow a more accurate calibration of safety factors.

Chapter 8. Further work and conclusion

8.1 Further work

The previous chapter identified further work which could be conducted to improve the understanding of peak mooring loads and more globally develop better MRE moorings systems. This further work is summarised below.

Firstly, further work could be conducted to improve the accuracy of the developed methodology:

- Conducting further field tests. The limited number of data collected for this thesis does not allow a conclusion on extreme mooring loads (for a 10-year return period storm for example) or on the tide influence on peak mooring loads.

- Investigating the buoy mean position and its extremes and relating it to the pre-tension and peak mooring loads. The aim is to understand the motions leading to peak mooring loads: frequency, amplitude, combination of first order and second order motions. The next step would be to improve the hull shape and mooring lines design in order to avoid such motions. This investigation has not been conducted in this thesis because the processing of the field test statistical data for motions was incorrect and these data require re-processing. The error originates from the conversion of latitude and longitude from degrees to meters and requires the reprocessing of all motion data.

- Investigating the dynamics and the mechanisms behind peak mooring loads. This requires studying the relationship between the time series of surface elevation, of the buoy motions and of the mooring loads. Some examples of the investigation which can be conducted with the time series of floating structure motions, wave elevation, and mooring loads have been presented in 7.3.2. A

methodology which looks in a systematic way at the time series from the field tests should be developed. The methodology presented in this thesis only looked at the statistical data from the field tests. Specific tank tests and numerical simulations investigating peak mooring loads could confirm the dynamic behaviour of the mooring system which leads or not to peak mooring loads. The development of more accurate numerical models, for example using CFD or Euler time-domain models including free water surface motion would also improve the modelling of peak mooring loads, and avoid the limitations of the potential theory currently used in the numerical models, leading to inaccuracies in the modelling of the second order motion.

Secondly, further work has to be considered by the MRE community in order to develop standards for MRE moorings.

- Improve the understanding of the ADCP and anchor positions. Harnois, et al. (2012) investigated several methods. The accuracy of these methods was in the order of several meters and need to be improved. Without knowing accurately the anchor position, the numerical model cannot give accurate results which can be directly compared with the field test results. Similarly, without knowing the exact ADCP position, it is difficult to accurately estimate the surface elevation at the buoy after modelling the wave propagation from the top of the beams to the buoy, and then to understand how the waves interact with the mooring system.
- Improve the understanding of the instrumented buoy position and motions. A similar method than for the wave buoys (Horwood et al., 2002) could be investigated. Without knowing accurately the buoy position, the wave elevation at the buoy are difficult to evaluate, and without knowing accurately the buoy motions, the field test results are difficult to compare with numerical results, and it is difficult for example to correlate buoy motions, mooring loads and surface elevation.
- Carrying out additional field tests with different MRE devices at different locations for longer periods would help to further improve the confidence in the results presented in this thesis and widen the applications of these results. In particular the tidal influence on peak mooring loads and the behaviour of the

mooring system under extreme conditions, such as a 10-year return period storm, could be considered.

- Develop new mooring configurations and components. Results show that chains may not be able to handle fatigue for the lifetime of a MRE device. Mooring systems could be developed without using chains, but then cost effective anchors which can accommodate vertical loads should be developed, as the main reason of using chains is to avoid vertical loads on the anchors.
- Develop more reliable mooring loadcells. Field tests show that loadcells have failed regularly, and that more confidence needs to be gained in the reading of the lowest values, which indicated that the line got slack.
- Validate the fatigue life of Nylon ropes for a high number of cycles. Results from field tests indicated that Nylon ropes should be able to accommodate fatigue for the lifetime of the MRE device. However the R-N curve for Nylon is only known for a small number of cycles. The other effects which may accelerate the degradation of the rope, such as marine growth, also need to be properly assessed.

8.2 Conclusion

This thesis investigated peak mooring loads on highly dynamic mooring systems and assessed these loads in the context of incident environmental conditions.

The aim was to try to understand when and why peak loads occur. This thesis analysed 11 and 9 months respectively of highly dynamic mooring system data from field tests from two different devices at two close locations and a large range of moderate wave conditions from tank tests for one of the device. The data were continuously sampled at high acquisition frequency so this thesis dealt with a considerable amount of data.

A numerical model of the mooring system was established using the tank test data in order to be able in the future to improve the understanding of the mooring dynamics. The aim of the field tests was to gather real data and include all effects occurring in the fields as well as the inaccuracies inherent to field tests. The tank tests have been conducted to calibrate a numerical model. Experiments and models aim to improve the mooring design and to develop more cost effective and more reliable mooring systems.

The main finding of this thesis is that peak mooring loads are likely to occur for large, but not necessarily the highest significant wave heights.

This result is consistent with the existing literature, which advises to take into account the highly dynamic behaviour of wave energy devices in mooring design. (Johanning, Smith and Wolfram, 2005; Paredes, et al. 2013). Also, the literature advises to use fibre ropes, in particular Nylon ropes, in the MRE design (Ridge, et al. 2010, Harris, Johanning and Wolfram, 2004), and the results of the field tests indicate that this choice is appropriate.

The level of inaccuracies in the field tests was an unexpected finding of this thesis. The consequences of the lack of accuracy in the anchor positions have been particularly highlighted. The consequences are high especially because of the low water depth at MRE sites: the scope of the mooring is significantly modified and consequently the mooring dynamics is also modified.

The presented work has contributed insights and methods to mitigate against peak loads. Mooring standards should account for peak mooring loads occurring for large but not extreme H_S. Different tidal range conditions should also be considered to ensure survivability for different mooring pre-tensions.

The design of MRE mooring system is challenging, mainly because of the high cost limitations, the energetic sea states, and the low water depth and large tidal range. Designing a mooring system means reaching a compromise. Overdesigning a mooring system is not cost-effective but neither is underdesigning it.

References

ABS (2012, Spring) *A History of Advancing Offshore Oil & Gas Technologies*, ABS Offshore News, pp 15-21

API (American Petroleum Institute) (2005). *API RP 2SK: Recommended Practice for Design and Analysis of Stationkeeping Systems for Floating Structures*

API (American Petroleum Institute) (2010) *API RP 2A-WSD: Planning, Designing and Constructing Fixed Offshore Platforms - Working Stress Design - Includes Supplement*

Aquamarine Power (2011) *Environmental Statement. Oyster 2 wave energy project. European Marine Energy Centre. Billia Croo, Orkney*, Xodus group, Available at: http://www.aquamarinepower.com/sites/resources/Reports/2880/Oyster%202%20Array%20Project%20ES%20-%20Main%20Document.pdf (Accessed: 4th September 2014).

Aranha, J.A.P., Pinto M.O. (2001) 'Dynamic tensions in risers and mooring lines: an algebraic approximation for harmonic excitation', *Applied Ocean Research,* 23(2), pp. 63-81.

Army, Department of (1973) *The universal grids: Universal Transverse Mercator (UTM) and Universal Polar Stereographic (UPS),* Available at: http://earth-info.nga.mil/GandG/publications/tm8358.2/TM8358_2.pdf (Accessed: 4th September 2014).

Babarit, A., Hals, J., Muliawan, M.J., Kurniawan, A., Moan, T., Krokstad, J. (2012) 'Numerical benchmarking study of a selection of wave energy converters', *Renewable Energy,* 41, pp. 44–63.

Barltrop, N.D.P. (1998) *Floating Structures: A guide for design and analysis*, Centre for Marine and Petroleum Technology, Oilfield Publications, Incorporated.

BERR (Department for Business, Enterprise and Regulatory Reform) (2008) *Atlas of UK Marine Renewable Energy Resources: Atlas pages. A strategic environmental assessment report*, UK: ABP Marine Environmental Research Ltd. Available at: http://www.renewables-atlas.info/downloads/documents/Renewable_Atlas_Pages_A4_April08.pdf (Accessed: 4th September 2014).

Bradney (1987) *A practical guide to the mooring and anchoring of small boats*, UK

Bridon (2011) *Fibre rope catalogue*, Available at: http://www.bridon.com/x/downloads/fibre/Fibre.pdf (Accessed: 4th September 2014)

Brown, D.T., Mavrakos, S. (1999) 'Comparative study on mooring line dynamic loading', *Marine Structures,* 12(3), pp. 131-151.

BS (British Standards) (1989) *BS 6349-6:1989: Maritime structures. Design of inshore moorings and floating structures.*

BS (British Standards) (2013) *BS 6349-1:2013: Maritime works. General. Code of practice for planning and design for operations*

Bunnik, T.H.J., de Boer, G., Cozijn, J.L., van der Cammen, J., van Haaften, E., ter Brake, E. (2002) 'Coupled mooring analysis in large scale model tests on a Deepwater calm buoy in mild wave conditions' , *In the Proceedings of the 21st international Conference on Offshore Mechanics and Arctic Engineering*, Oslo, Norway, 26-31 May 2002

BV (Bureau Veritas) (2012) *NR 493 DT R02 E: Classification of Mooring Systems for Permanent Offshore Units*

Carbon Trust (2006) *Future Marine Energy. Results of the Marine Energy Challenge: Cost competitiveness and growth of wave and tidal stream energy*, UK

Carnegie (2014) *CETO commercial scale unit overview*, Available at: http://www.carnegiewave.com/index.php?url=/ceto/ceto-overview (Accessed: 4th September 2014).

Cerveira, F., Fonseca, N., Pascoal, R. (2013) 'Mooring system influence on the efficiency of wave energy converters', *International Journal of Marine Energy (IJOME),* 3-4(/), pp. 65-81.

Chakrabarti, S.K. (1987) *Hydrodynamics of offshore structures*, Computational Mechanics edn., WIT Press.

Charles and Nuttall (2010) Statoil looks to test it's floating Hywind Turbines in North West Europe, Available at: http://charlesandnuttall.blogspot.se/2010/07/statoil-looks-to-test-its-floating.html (Accessed: 16th January 2015).

Christensen, L., Friis-Madsen, E., Kofoed, J.P. (2005) 'The wave energy challenge- the wave dragon case', *In the Proceedings of the PowerGen 2005 Europe Conference,* Milan, Italy, June 2005

Clément, A., McCullen, P., Falcao, A., Fiorentino, A., Gardner, F., Hammarlund, K., Lemonis, G., Lewis, T., Nielsen, K., Petroncini, S., Pontes, M.-T., Schild, B.-O., Sjöström,P., Søresen, H.C. (2002) 'Wave energy in Europe: current status and perspectives', *Renewable and Sustainable Energy Reviews,* 6(5), pp. 405–431.

Cozijn, J.L., Uittenbogaard, R., ter Brake, E. (2005) 'Heave, Roll and Pitch Damping of a Deepwater CALM Buoy with a Skirt', *In the Proceedings of the 15th International Offshore and Polar Engineering Conference*, Seoul, South Korea; 19-24 June 2005

Cruz, J. (2008) *Ocean Wave Energy - Current Status and Future Perspectives*, Springer edn

Cummins, W E. (1962) 'The impulse response function and ship motions', *Schiffstechnik*, 9, pp 101-109.

de Hauteclocque, G., Rezende, F., Waals, O., Chen, X.-B. (2012) 'Review of Approximations to Evaluate Second-Order Low-Frequency Load', *In the Proceedings of the 31st International Conference on Ocean, Offshore and Arctic Engineering (OMAE conference),* Rio de Janeiro, Brazil, 1-6 July 2012

Delft University of Technology (DUT) (2012) *SWAN User Manual,* Available at: http://falk.ucsd.edu/modeling/swanuse.pdf (Accessed: 4th September 2014).

Devine-Wright, P. (2008) 'Reconsidering public acceptance of renewable energy technologies: a critical review', in Grubb, M., Jamasb, T., Pollitt, M.G. (ed.) *Delivering a Low Carbon Electricity System. Technologies, Economics and Policy*: Cambridge University Press, Available at: http://geography.exeter.ac.uk/beyond_nimbyism/deliverables/Reconsidering_public_acceptance.pdf (Accessed: 4th September 2014).

DNV (Det Norske Veritas) (2000) *DNV-RP-E301: Design and installation of fluke anchors*

DNV (Det Norske Veritas) (2002) *DNV-RP-E302: Design and installation of plate anchors in clay*

DNV (Det Norske Veritas) (2009) *DNV-OS-E304: Offshore mooring steel wire ropes.*

DNV (Det Norske Veritas) (2010) *DNV-OS-E303: Offshore mooring fibre ropes.*

DNV (Det Norske Veritas) (2010) *DNV-RP-C205: Environmental conditions and environmental loads.*

DNV (Det Norske Veritas) (2010) *DNV-RP-F205: Global performance analysis of deepwater floating structures*

DNV (Det Norske Veritas) (2011) *DNV-OS-C101: Design of offshore steel structures, General (LRFD Method)*

DNV (Det Norske Veritas) (2013) *DNV-OS-E301: Position mooring.*

Elman,P., Elletson, P. , Bramande, J, Pinheiro, K. (2013) 'Reducing Uncertainty Through The Use Of Mooring Line Monitoring', *In the Proceedings of the Offshore Technology Conference (OTC)*, Houston, Texas, USA, 6-9 May 2013

EMEC (European Marine Energy Centre) (2009) *Guidelines for Reliability, Maintainability and Survivability of Marine Energy Conversion Systems*, UK: BSI, Available at: *http://www.emec.org.uk/guidelines-for-reliability-maintainability-and-survivability-of-marine-energy-conversion-systems/* (Accessed: 4th September 2014)

EMEC (European Marine Energy Centre) (2009) *Assessment of Performance of Tidal Energy Conversion Systems*, Available at: *http://www.emec.org.uk/assessment-of-performance-of-tidal-energy-conversion-systems/* (Accessed: 4th September 2014)

EMEC (European Marine Energy Centre) (2014) *Bluewater energy services*, Available at: *http://www.emec.org.uk/about-us/our-tidal-clients/bluewater-energy-services/* (Accessed: 4th September 2014).

EMEC (European Marine Energy Centre) (2014) *Wello Oy,* Available at: *http://www.emec.org.uk/about-us/wave-clients/wello-oy/*(Accessed: 4th September 2014).

EMU (2003) *WP 3.3 Environmental impact*, Denmark, Available at: *http://www.marinerenewables.ca/wp-content/uploads/2012/11/Environmental-Impact.pdf*

EquiMar (Equitable Testing and Evaluation of Marine Energy Extraction Devices in terms of Performance, Cost and Environmental Impact) (2009) *EquiMar deliverable D7.3.2: Consideration of the cost implications for mooring MEC devices*, UK, Available at: *https://www.wiki.ed.ac.uk/download/attachments/9142387/EquiMar-Del7-3-2.pdf?version=1* (Accessed: 4th September 2014)

EquiMar (Equitable Testing and Evaluation of Marine Energy Extraction Devices in terms of Performance, Cost and Environmental Impact) (2011) *EquiMar deliverable D2.2: Wave and Tidal Resource Characterisation*, Available at: http://www.equimar.org/equimar-project-deliverables.html (Accessed: 4th September 2014)

Ernst & Young LLP (2010) *Cost of and financial support for wave, tidal stream and tidal range generation in the UK. A report for the Department of Energy and Climate Change and the Scottish Government*, Available at: http://webarchive.nationalarchives.gov.uk/20121205174605/http:/decc.gov.uk/assets/decc/what%20we%20do/uk%20energy%20supply/energy%20mix/renewable%20energy/explained/wave_tidal/798-cost-of-and-finacial-support-for-wave-tidal-strea.pdf (Accessed: 4th September 2014).

Exsil n.v. - Koordenfabriek Van Houte n.v. (2014) *Braided or plaited*, Available at: http://www.exsil.be/#/en/rope-constructions/braided-or-plaited/ (Accessed: 4th September 2014)

FaBTest (2012) *Description of site characteristics and eligible test installations*, Available at: http://fabtest.com/sites/default/files/Appendix-9-FaB-Test-site-characteristics-05.03.2012.pdf (Accessed: 4th September 2014)

FaBTest (2014) *Guide to deployments & application process requirements*, Available at: http://fabtest.com/sites/default/files/Guide%20to%20Deployments%20and%20Application%20Process%20Requirements%20v6%20020514.pdf (Accessed: 4th September 2014).

Falcão, A.F.d.O. (2010) 'Wave energy utilization: a review of the technologies', *Renewable and Sustainable Energy Reviews*, 14(3), pp. 899–918.

Falnes, J., Løvseth, J. (1991) 'Ocean wave energy', *Energy Policy,* 19, pp. 768-775

Falnes, J. (1993). 'Small is beautiful: How to make wave energy economic', *In the Proceedings of the European Wave Energy Symposium*, Edinburgh, Scotland, 21-24 July 1993

Falnes, J. (2007) 'A review of wave-energy extraction ', *Marine Structures,* 20(4), pp. 185–201, Available at: http://www.ewp.rpi.edu/hartford/~ottj/ET/Other/Wave%20Energy%20Sources/16.Falnes%20Johnannes%20-%20A%20review%20of%20wave-energy%20extraction.pdf (Accessed: 4th September 2014).

Faltinsen, O.M. (1990) *Sea Loads on Ships and Offshore Structures*, Cambridge University Press edn., Cambridge, UK

Fitzgerald, J., Bergdahl, L. (2007) 'Considering Mooring Cables for Offshore Wave Energy Converters', *In the Proceedings of the 7th European Wave and Tidal Energy Conference (EWTEC)*, Porto, Portugal, 11-14 September 2007

Fitzgerald, J., Bergdahl, L (2008) 'Including moorings in the assessment of a generic offshore wave energy converter: A frequency domain approach', *Marine Structures* , 21(1), pp. 23–46.

Flory, J.F., Banfield, S.J.(2011) 'Fiber rope myths', *In the Proceedings of the OCEANS Conference,* Waikoloa, HI, USA, 19-22 September 2011

Forestier, J.M., Holmes, B., Barrett, S., Lewis, A.W.(2007) 'Value and Validation of Small Scale Physical Model Tests of Floating Wave Energy Converters', *In the Proceedings of the 7th European Wave and Tidal Energy Conference (EWTEC),* Porto, Portugal, 11-14 September 2007

Free Flow Energy Inc (2009) *Assess the Design/Inspection Criteria/Standards for Wave and/or Current Energy Generating Devices*, USA, Available at: http://large.stanford.edu/courses/2011/ph240/yan1/docs/FinalReport.pdf (Accessed: 4th September 2014)

Frigaard, P., (1989) 'Wave loads on cylinders', *In the Proceedings of CEEC Comet Seminar on wave and ice forces on offshore structures,* Salford, UK, April 1989, Available at: http://vbn.aau.dk/files/49966848/wave_loads_on_cylinders.pdf (Accessed: 4th September 2014)

Friis-Madsen, E., Sørensen, H.C., Parmeggiani, S. (2012) 'The development of a 1.5 MW Wave Dragon North Sea Demonstrator', *In the Proceedings of the International Conference on Ocean Energy (ICOE),* Dublin, Ireland, 17-19 October 2012

Fugro (2010) *SEAWATCH Mini II Buoy*, Available at: http://www.geos.com/downloads/flyers/oceanographic-buoys/seawatch-mini-ii-buoy (Accessed: 4th September 2014)

Gao, Z., Moan, T.(2009) 'Mooring system analysis of multiple wave energy converters in a farm configuration', *In the Proceedings of the 8th European Wave and Tidal Energy Conference (EWTEC)*, Uppsala, Sweden, 7-10 September 2009

Garrad Hassan (2008) *Development of wave energy in the South West*, UK Available at: http://www.wavehub.co.uk/wp-content/uploads/2011/06/2008-February-Development-of-Wave-Energy-in-the-South-West.pdf (Accessed: 4th September 2014)

Goda, Y. (1977) *Numerical experiments on statistical variability of ocean waves,* Japan: the port and harbour research institute, ministry of transport, Available at: http://www.pari.go.jp/cgi-bin/search-en/detail.cgi?id=1977060160201 (Accessed: 4th September 2014)

Hansen, L.K., Hammarlund, K., Sørensen, H.C., Christensen, L. 'Public acceptance of wave energy'. *In the Proceedings of the 5th European Wave Energy Conference*, Cork, Ireland, 17-20 September 2003

Harnois, V., Parish, D., Johanning, L. (2012) 'Physical measurement of a slow drag of a drag embedment anchor during sea trials', *In the Proceedings of the International Conference on Ocean Energy (ICOE),* Dublin, Ireland, 17-19 October 2012

Harnois, V., Weller, S.D., Johanning, L., Thies, P.R., Le Boulluec, M., Le Roux, D. Soulé, V., Ohana J. (In corrections) 'Numerical model validation for mooring systems: Method and application for wave energy converters'

Harnois, V., Smith, H.C.M., Benjamins, S., Johanning, L. (In Review) 'Assessment of risk of entanglement of marine animals due to Marine Renewable Energy mooring systems'

Harnois, V., Johanning, L., Thies, P.R., Bjerke, I. (In Progress) 'The influence of environmental conditions on the peak mooring loads'

Harris, R.E, Johanning, L., Wolfram, J. (2004) 'Mooring systems for wave energy converters: A review of design issues and choices', *In the Proceedings of the 3rd International Conference on Marine Renewable Energy (MAREC)*, Blyth, UK, 7-9 July 2004

Hasham, N. (2008) *$5m Port Kembla wave generator wrecked*, Illawara Mercury, 14 May 2008, Available at: http://www.illawarramercury.com.au/news/local/news/general/5m-port-kembla-wave-generator-wrecked/1830582.aspx (Accessed: 4th September 2014)

Haver, S. (1987) 'On the joint distribution of heights and periods of sea waves', *Ocean Engineering,* 14(5), pp. 359-376.

Hayward, J., Osman, P. (2011) The potential of wave energy, Australia: CSIRO, Available at: http://www.garnautreview.org.au/update-2011/commissioned-work/potential-wave-energy.pdf (Accessed: 4th September 2014).

Hjetland, E., Bjerke, I., Tjensvoll, G., Sjolte, J. (2011) 'A brief introduction to the bolt-2-wave project' , *In the Proceedings of the 9th European Wave and Tidal Energy Conference (EWTEC),* Southampton, UK, 5-9 September 2011

HM Government (2010) *Marine Energy Action Plan 2010; Executive Summary & Recommendations*, UK: Department of Energy and Climate Change (DECC), Available at: http://regensw.s3.amazonaws.com/1275819743_963.pdf (Accessed: 4th September 2014).

Holthuijsen, L.H. (2007) *Waves in Oceanic and Coastal Waters*, Cambridge University Press edn.

Horwood, J.M.K, Belmont, M.R., Thurley, R.W.F. (2002) 'A novel design for surface following buoys for oceanography and wave prediction', *Journal of Measurement and Control,* 35(6), pp. 176-180

HSE (Health & Safety Executive) (1995) *Offshore Installations: guidance on design, construction and certification*, HSE books.

HSE (Health & Safety Executive) (1998) *An Experimental, Theoretical and Full-Scale Investigation on the Snap Loading of Marine Cables: Main Report*, UK: HSE books, Available at: http://www.hse.gov.uk/research/othpdf/500-599/oth558.pdf (Accessed: 4th September 2014)

HSE (Health & Safety Executive) (2005) *Wave slap loading on FPSO bows*, UK: HSE books, Available at: http://www.hse.gov.uk/research/rrpdf/rr324.pdf (Accessed: 15th December 2014)

Huang, M., Aggidis, G.A. (2008) 'Developments, Expectations of Wave Energy Converters and Mooring Anchors in the UK', *Journal of Ocean University of China ,* 7(1), pp. 10-16.

Huse, E. (1991) 'New developments in prediction of mooring system damping', *In the Proceedings of the 23th Offshore Technology Conference (OTC),* Houston, Texas, USA, 6-9 May 1991

Hydroworld (2011) Gael Force Group supplies SeaLimpet mooring device to OPT, 13 September 2011, Available at: http://www.hydroworld.com/articles/2011/09/gael-force-group-supplies-sealimpet-mooring-device-to-opt.html (Accessed: 4th September 2014)

IALA AISM (International Association of Marine Aids to Navigation and Lighthouse Authorities) (2001) *Guidelines on synthetic mooring lines*, France.

IEA (International Energy Agency) (2006) *Renewable Energy: RD&D Priorities. Insights from IEA Technology Programmes* Available at: http://www.iea.org/publications/freepublications/publication/renewenergy.pdf (Accessed: 4th September 2014)

Incecik, A., Bowers, J., Mould, G., Yilmaz, O (1998) 'Response-based extreme value analysis of moored offshore structures due to wave, wind, and current', *Journal of Marine Science and Technology,* 3(3), pp. 145-150.

Isherwood R M (1987) 'A Revised Parameterisation of the JONSWAP Spectrum', *Applied Ocean Research*, 9(1), pp 47-50.

ISO (International Organization for Standardization) (2005) *ISO 19901-1:2005: Petroleum and natural gas industries -- Specific requirements for offshore structures - Part 1: Metocean design and operating considerations*

ISO (International Organization for Standardization) (2013) *ISO 19901-7:2013: Petroleum and natural gas industries -- Specific requirements for offshore structures - Part 7: Stationkeeping systems for floating offshore structures and mobile offshore units*

Johanning, L. (n.d. a) *Lecture notes "Moorings for Marine Energy Converters",* University of Exeter

Johanning, L. (n.d. b) *Lecture notes "Dynamic mooring approach / OrcaFlex",* University of Exeter

Johanning, L., Wolfram, J. 'Challenging tasks for floating WECs'. *In the Proceedings of the International Symposium on Fluid Machinery for Wave and Tidal Energy: State of the Art and New Developments*, London, UK, 2005

Johanning, L., Smith, G.H., Wolfram, J. (2005) 'Towards design standards for WEC moorings', *In the Proceedings of the 6th European Wave and Tidal Energy Conference (EWTEC)*, Glasgow, UK, 29 August – 2 September 2005

Johanning, L., Smith, G.H., Wolfram, J. (2006) 'Interaction between mooring line damping and response frequency as a result of stiffness alteration in surge', *In the Proceedings of the 25th International Conference on Offshore Mechanics and Arctic Engineering (OMAE)*, Hamburg, Germany, 4- 9 June 2006.

Johanning, L., Smith, G.H., Wolfram, J. (2007) 'Measurements of static and dynamic mooring line damping and their importance for floating WEC devices', *Ocean Engineering,* 34(14-15), pp. 1918-1934.

Johanning, L., Smith, G.H. 'Station keeping study for WEC devices including compliant chain, compliant hybrid and taut arrangement'. *In the Proceedings of the 27th Offshore and Arctic Marine Engineering Symposium,* Estoril, Portugal, 15- 20 June 2008

Johanning, L., Spargo, A.W., Parish, D. 'Large scale mooring test facility – A technical note', *In the Proceedings of the 2nd International Conference on Ocean Energy (ICOE)*, Brest, France, 15-17 October 2008

Johanning, L., Parish, D. (2012) *Mooring Limb*. US Patent 20120298028 A1, Available at: *http://www.google.com/patents/US20120298028* (Accessed: 4th September 2014)

JP KENNY (2009) *SW Wave Hub – Metocean Design basis* , UK, Available at: http://www.wavehub.co.uk/wp-content/uploads/2011/06/S18-2009.04.29-Metoc-Design-Basis-Report-Rev-1-FINAL.pdf (Accessed: 4th September 2014)

Kuik, A.J., van Vledder, G.P., Holthuijsen, L.H. (1988) ' A Method for the Routine Analysis of Pitch-and-Roll Buoy Wave Data', *Journal of Physical Oceanography,* 18(7), pp. 1020-1034.

Lane, C., Wood, G. (2009) 'Capitalist Diversity and Diversity Within Capitalism', *Economy and Society,* 38(4), pp. 531-551.

Lavelle, J., Kofoed, J.P. (2011) *Power Production Analysis of the OE Buoy WEC for the CORES Project.*, Department of Civil Engineering, Aalborg University, Aalborg: DCE Technical Reports, no. 119*,* Available at: http://vbn.aau.dk/files/61595716/Power_Production_Analysis_of_the_OE_Buoy_WEC_for_the_CORES_Project.pdf (Accessed: 4th September 2014).

Lawrence, J., Kofoed-Hansen, H., Chevalier, C. (2009) 'High-resolution metocean modelling at EMEC's (UK) marine energy test sites' , *In the Proceedings of the 8th European Wave and Tidal Energy Conference (EWTEC)*, Uppsala, Sweden, 7-10 September 2009

Le Méhauté, B. (1976) *An introduction to hydrodynamics and water waves,* Springer

Le Roux, D. (2012) *MSc Thesis (in French) Rapport de Projet de fin d'études. Etude d'un ancrage textile pour la bouée SWMTF destinée à l'analyse du comportement des systèmes houlomoteurs.*

Liagre, P.F., Niedzwecki, J.M. (2003) 'Estimating nonlinear coupled frequency-dependent parameters in offshore engineering', *Applied Ocean Research,* 25, pp. 1-19.

Lynn, P.A. (2013) *Electricity from Wave and Tide: An Introduction to Marine Energy*, John Wiley & Sons edn., UK.

Ma K., Duggal A., Smedley P.A., l'Hostis, D., Shu, H. (2013) 'Historical review on integrity issues of permanent mooring systems', *In the Proceedings of the Offshore Technology Conference (OTC)*, Houston, Texas, USA, 6-9 May 2013

Marine Institute Plymouth University. (n.d.), *Plymouth University New Marine Building*, Available at: http://www.plymouth.ac.uk/files/extranet/docs/MARINST/Marine%20Building%20Brochure.pdf (Accessed: 4th September 2014)

Masciola, M., Robertson, A., Jonkman, J., Driscoll, F. (2011) 'Investigation of a FAST-OrcaFlex coupling module for integrating turbine and mooring dynamics of offshore floating wind turbines ', *In the Proceedings of the International Conference on Offshore Wind Energy and Ocean Energy,* Beijing, China, 31 October-2 November 2011, Available at: *http://www.nrel.gov/docs/fy12osti/52896.pdf* (Accessed: 4th September 2014)

Mc Evoy, P. (2012) 'Combined Elastomeric & Thermoplastic Mooring Tethers', *In the Proceedings of the International Conference on Ocean Energy (ICOE),* Dublin, Ireland, 17-19 October 2012

McKenna, H.A., Hearle, J.W.S., O'Hear, N., (2004) *Handbook of Fibre Rope Technology,* Woodhead Publishing edn

MERiFIC (Marine Energy in Far Peripheral and Island Communities) (2012) *National Policy Framework for Marine Renewable Energy within the United Kingdom, Task 4.1.1 of WP4 from the MERiFIC Project* , University of Exeter, Available at: *http://www.merific.eu/files/2012/09/4.1.1-National-Policy-Framework-for-Marine-Renewable-Energy-within-the-United-Kingdom.pdf* (Accessed: 4th September 2014).

MERiFIC (Marine Energy in Far Peripheral and Island Communities) (2013) *Politiques publiques de soutien aux projets d'énergies marines renouvelables (EMR) et cadres réglementaires régissant le secteur en France. Livrable 4.1.1 du WP4 du projet MERiFIC (in French)*, Parc naturel marin d'Iroise et UMR/AMURE, Available at: http://www.merific.eu/files/2012/06/4.1.1-Politiques-publiques-de-soutien-aux-projects-denergies-marines-renouvalables.pdf (Accessed: 4th September 2014).

MERiFIC (Marine Energy in Far Peripheral and Island Communities) (2013) *MERiFIC Deliverable 3.5.2: Guidance on the use of synthetic fibre ropes for marine energy devices*, University of Exeter, Available at: http://www.merific.eu/files/2012/06/D3-5-2_Guidance-on-the-use-of-synthetic-fibre-ropes-for-marine-energy-devices.pdf (Accessed: 4th September 2014).

Molin, B. (2002) *Hydrodynamique des structures offshore (in French)*, Technip edn

Murphy, L.M., Edwards, P.L. (2003) *Bridging the Valley of Death: Transitioning from Public to Private Sector Financing*, USA: NREL (National Renewable Energy Laboratory), Available at: http://www.nrel.gov/docs/gen/fy03/34036.pdf (Accessed: 4th September 2014)

NCEL (Navy Civil Engineer Laboratory) (1987) *Drag embedment anchors for Navy moorings. Techdata Sheet 83-08R*, USA.

Ocean Power Technologies (2014) *Mark 3 Powerbuoy,* Available at: http://www.oceanpowertechnologies.com/mark3.html (Accessed: 4th September 2014).

Orcina (2010) 'Dynamic analysis and control of offshore marine systems using OrcaFlex', *SuperGen 7th Doctoral Training Programme Workshop 'Control of Wave and Tidal Energy Converters,'* Lancaster University, UK, 26 February 2010, Available at: http://www.engineering.lancs.ac.uk/lureg/events/ORCAFLEX%20ORCINA.pdf (Accessed: 4th September 2014)

Orcina (2014) *OrcaFlex manual, version 9.7.a,* Available at: http://www.orcina.com/SoftwareProducts/OrcaFlex/Documentation/OrcaFlex.pdf (Accessed: 4th September 2014)

Palm, J., Eskilsson, C., Paredes, G.M., Bergdahl, L. (2013) 'CFD Simulation of a Moored FloatingWave Energy Converter', *In the Proceedings of the 10th European Wave and Tidal Energy Conference (EWTEC)*, Aalborg, Denmark, 2-5 September 2013

Paredes, G.M., Bergdahl, L., Palm, J., Eskilsson, C., Pinto, F.T. (2013) 'Station keeping design for floating wave energy devices compared to floating offshore oil and gas platforms', *In the Proceedings of the 10th European Wave and Tidal Energy Conference (EWTEC)*, Aalborg, Denmark, 2-5 September 2013

Parish, D. (2013) 'Development of the Exeter Mooring Tether. A novel mooring tether for marine energy converter applications and other highly dynamic offshore systems', *PhD seminar, University of Exeter, Penryn, UK,* 19 September 2013

Parmeggiani, S., Kofoed, J.P., Friis-Madsen, E. (2011) 'Extreme Loads on the Mooring Lines and Survivability Mode for the Wave Dragon Wave Energy Converter', *In the Proceedings of the World Renewable Energy Congress 2011*, Linköping, Sweden, 8-11 May 2011

Parmegianni, S. (2013) *Modelling and Testing of Wave Dragon Wave Energy Converter Towards Full Scale Deployment – Analysis of Overtopping Performance and Mooring Load Response*, PhD thesis, Department of Civil Engineering, Aalborg University, Aalborg.

PCCI (2009) *Wave and current energy generating devices criteria and standards*, USA, Available at: http://oregonwave.org/oceanic/wp-content/uploads/2013/05/Wave-and-Current-Energy-Generating-Devices-MMS-2009.pdf (Accessed: 4th September 2014)

Pelamis (2014) *Development History,* Available at: http://www.pelamiswave.com/development-history (Accessed: 4th September 2014).

Peng, W., Lee, K.-H., Shin, S.-H., Mizutani, N (2013) 'Numerical simulation of interactions between water waves and inclined-moored submerged floating breakwaters', *Coastal engineering,* 82, pp. 76–87.

Ponomarev, M., Johanning, L.,Parish, D.N. (2010) 'Enhancing precision and reliability of tri-axial load cells formooring load measurements', *In the Proceedings of the 3rd International Conference on Ocean Energy (ICOE),* Bilbao, Spain, 6-8 October 2010

Principle (2014) *Windfloat*, Available at: *http://www.principlepowerinc.com/products/windfloat.html* (Accessed: 4th September 2014).

RD Instruments (1996) *Acoustic Doppler Current Profiler. Principles of operations. A practical Primer*, Available at: *ftp://www.comm-tec.com/support/RDI/Misc_Docs/Broadband%20Primer.pdf* (Accessed: 4th September 2014)

RD Instruments (2003) *Waves User's Guide*, Available at: ftp://www.comm-tec.com/oops/wavesmon/Waves%20Users%20Guide_Oct03.pdf (Accessed: 4th September 2014)

RD Instruments (2009) *Workhorse Sentinel. Self-contained 1200, 600, 300 kHz ADCP*, Available at: *http://www.rdinstruments.com/datasheets/wh_sentinel.pdf* (Accessed: 4th September 2014)

RD Instruments (n.d.) *Waves primer: Wave measurements and the RDI ADCP waves array technique*, Available at: http://www.rdinstruments.com/pdfs/waves_primer.pdf (Accessed: 19th March 2015)

RD Instruments (2011) *WavesMon v3.08 User's Guide*, Available at: *http://new.comm-tec.com/Docs/Manuali/RDI/WavesMon%20Users%20Guide.pdf* (Accessed: 4th September 2014).

Réfrégier, P. (2008) *Lecture notes "Traitement du signal"*, Ecole Centrale Marseille

renewableUK (2010) *Channelling the energy. A way forward for the UK wave & tidal industry towards 2020*, UK, Available at: *http://www.renewableuk.com/en/publications/index.cfm/Wave-and-Tidal-Channelling-the-Energy* (Accessed: 4th September 2014).

renewable UK (2013) *Wave and Tidal Energy in the UK. Conquering Challenges, Generating Growth*, UK, Available at: *http://www.renewableuk.com/en/publications/index.cfm/wave-and-tidal-energy-in-the-uk-2013* (Accessed: 4th September 2014)

Ricci, P., Rico, A., Ruiz-Minguela, P., Boscolo, F., Villate, J.L. (2012) 'Design, Modelling and Analysis of an Integrated Mooring System for Wave Energy Arrays', *In the Proceedings of the International Conference on Ocean Energy (ICOE),* Dublin, Ireland, 17-19 October 2012

Ridge, I.M.L., Banfield, S.J., Mackay, J. (2010) 'Nylon Fibre Rope Moorings for Wave Energy Converters', *In the Proceedings of the OCEANS conference*, Seattle, Washington, 20-23 September 2010

Sanmuganathan, V. (2009) *Seawatch Mini II buoy, User Manual.*

Sarpkaya, T., Isaacson, M.I. (1981) *Mechanics of wave forces on offshore structures*, Van Nostrand Reinhold edn., New York, USA

SEAI (Sustainable Energy Authority of Ireland) (2012) *Resource Characterisation of the Galway Bay 1/4 Scale Wave Energy Test Site*

SeaWeb Aquaculture Clearinghouse (2004) *At a Crossroads: Will Aquaculture Fulfill the Promise of the Blue Revolution?*, Available at: *http://www.seaweb.org/resources/documents/reports_crossroads.pdf* (Accessed: 4th September 2014)

Sharqawy, M.H., Lienhard, V.J.H., Zubair, S.M. (2010) 'Thermophysical properties of seawater: a review of existing correlations and data', *Desalination and Water Treatment,* 16(/), pp. 354-380.

SI Ocean (2013) *Ocean Energy Technology: Gaps and Barriers*, Available at: *http://www.si-ocean.eu/en/upload/docs/WP3/Gaps%20and%20Barriers%20Report%20FV.pdf* (Accessed: 4th September 2014).)

Sjolte, J., Bjerke, I. K., Tjensvoll, G., Molinas, M. 'Summary of Performance After One Year of Operation with the Lifesaver Wave Energy Converter System', *In the Proceedings of the 10th European Wave and Tidal Energy Conference (EWTEC)*, Aalborg, Denmark, 2-5 September 2013

Sjolte, J. Bjerke, I, Hjetland, E., Tjensvoll, G. (2013) 'All-Electric Wave Energy Power Take Off Generator Optimized by High Overspeed', *In the Proceedings of the 10th European Wave and Tidal Energy Conference (EWTEC)*, Aalborg, Denmark, 2-5 September 2013

Soulé, V., Le Boulluec, M. (2013) 'Réponse à la houle de la bouée; Etude hydrodynamique aux premier et second ordres' (in French),

South West of England Regional Development Agency (SWRDA) (2006) *Wave Hub Environmental Statement* , UK: Halcrow Group Limited, Available at: *http://www.wavehub.co.uk/wp-content/uploads/2011/06/Environmental-Statement-June-2006.pdf* (Accessed: 4th September 2014)

Strainstall (2014), *Type 5395 Underwater Load Shackles*, Available at:*http://www.strainstall.com/files/1413/5972/8812/Underwater_Load_Shackle_-_Type_5395.pdf* (Accessed: 4th September 2014).

Tension Technology International (2014) *Rope constructions*, Available at: http://www.tensiontech.com/tools_guides/rope_constructions.html (Accessed: 4th September 2014).

Terray, E.A., Brumley, B.H., Strong, B. (1999) 'Measuring waves and currents with an upward-looking ADCP', *In the Proceedings of the IEEE 6th Conference on Current Measurement,* San Diego, USA, 11-13 March 1999, Available at: www.rdinstruments.com/rr/reports/uplook.DOC (Accessed: 16th December 2014).

Thies, P.R., Johanning, L., Gordelier, T. (2013) 'Component reliability testing for wave energy converters: Rationale and implementation', *In the Proceedings of the 10th European Wave and Tidal Energy Conference (EWTEC)*, Aalborg, Denmark, 2-5 September 2013

Thies, P.R., Johanning, L., Harnois, V., Smith, H.C.M., Parish, D.N. (2013) 'Mooring line fatigue damage evaluation for floating marine energy converters: Field measurements and prediction', *Renewable Energy,* 63, pp. 133-144.

van Nieuwkoop, J.C., Smith, H. C., Smith, G.H., Johanning, L. (2012) 'Application and evaluation of a long term hindcast dataset for wave resources and extreme wave conditions on the Cornish coast', *Renewable Energy ,* 58, pp. 1-14.

Vicente, P.C., Falcão, A.F.O., Justino, P.A.P. (2011) 'Non-linear Slack-Mooring Modelling of a Floating Two-Body Wave Energy Converter', *In the Proceedings of the 9th European Wave and Tidal Energy Conference (EWTEC),* Southampton, UK, 5-9 September 2011

Viking moorings (n.d.) *Section 4 Wire ropes*, Available at: http://files.vikingseatech.com/dokumenter/wire/wire.pdf (Accessed: 4th September 2014)

Vryhof anchors (2010) *Anchor manual 2010. The guide to anchoring*, The Netherlands, Available at: http://www.vryhof.com/anchor_manual.pdf (Accessed: 4th September 2014)

WAFO group (2011) *WAFO A Matlab Toolbox for Analysis of Random Waves and Loads*, Available at: *http://www.maths.lth.se/matstat/wafo/documentation/wafotutor25.pdf* (Accessed: 4th September 2014)

Waveplam (2009) *Del. 2.2. Non-technical barriers to wave energy implementation*, Available at: *http://www.waveplam.eu/files/downloads/Waveplam_Del_2-2_Non-technological-barriers.pdf* (Accessed: 4th September 2014).

Wave Hub (2013) *Marine licence approved for first Wave Hub deployment,* Available at: *http://www.wavehub.co.uk/news/press-releases/marine-licence-approved-for-first-wave-hub-deployment/* (Accessed: 4th September 2014).

Webster, W.C (1995) 'Mooring-induced damping', *Ocean Engineering,* 22(6), pp. 571-591.

Weller, S.D., Davies, P., Vickers, A.W., Johanning, L. (In review) 'Synthetic Rope Responses in the Context of Load History: The Influence of Aging'

Wello (2014) *Penguin,* Available at: *http://www.wello.eu/penguin.php* (Accessed: 4th September 2014).

Wichers, J.E.W. (1979) 'Slowly oscillating mooring forces in single point mooring systems', *In the Proceedings of the Second International Conference on Behaviour of Offshore Structures (BOSS),* London, UK, 28-31 August 1979

Wichers J.E.W. (2013), *Guide to Simple Point Moorings*, Available at: http://www.wmooring.com/files/Guide_to_Single_Point_Moorings.pdf Accessed: 20th January 2015).

Winterstein, S., Ude, T.C., Cornell, C.A., Bjerager, P., Haver, S. (1993) 'Environmental Parameters for Extreme Response: Inverse FORM with Omission Sensitivity', *In the Proceedings of the 6th International Conference on Structural Safety & Reliability (ICOSSAR)*, Innsbruck, Austria, 9-13 August 1993

Wolf, J., Prandle, D. (1999) 'Some observations of wave-current interaction"', *Coastal Engineering,* 37(3-4), pp. 471-485.

Woods Hole Oceanographic Institution (1952) 'Chapter I. The effects of fouling', in Bureau of Ships, Navy Department (ed.) *Marine fouling and its prevention.* USA: US Naval Institute, pp. 3-19*,* Available at: *https://darchive.mblwhoilibrary.org/bitstream/handle/1912/191/chapter%201.pdf?sequence=8* (Accessed: 4th September 2014).

Yu, Y., Li ,Y. (2011) 'Preliminary results of a RANS simulation for a floating point absorber wave energy system under extreme wave conditions' *In the Proceedings of the 30th International Conference on Ocean, Offshore and Arctic Engineering (OMAE conference),* Rotterdam, The Netherlands, 19-24 June 2011

Zanuttigh, B., Angelelli, E., Kofoed, J.P (2013) 'Effects of mooring systems on the performance of a wave activated body energy converter', *Renewable Energy,* 57, pp. 422-431

Zhao, J., Zhang, L., Wu, H. (2012) 'Motion Performance and Mooring System of a Floating Offshore Wind Turbine', *Journal of Marine Science and Application,* 11(3), pp. 328-334.

Appendix 1

List of publications

A.1. Journal publications

Harnois, V., Weller, S.D., Johanning, L., Thies, P.R., Le Boulluec, M., Le Roux, D. Soulé, V., Ohana J. (2015) 'Numerical model validation for mooring systems: Method and application for wave energy converters', *Renewable Energy*, 75, pp. 869-887

Harnois, V., Johanning, L., Thies, P.R., Bjerke, I. (In Progress) 'On peak mooring loads and the influence of environmental conditions for marine energy converters'

Harnois, V., Smith, H.C.M., Benjamins, S., Johanning, L. (Accepted for publication in the International Journal of Marine Energy) 'Assessment of risk of entanglement of marine animals due to Marine Renewable Energy mooring systems'

Thies, P.R., Johanning, L., **Harnois, V.**, Smith, H.C., Parish, D.N. (2013) 'Mooring line fatigue damage evaluation for floating marine energy converters: Field measurements and prediction', *Renewable Energy* , 63, pp. 133-144

A.2. Conference publications

Harnois, V., Parish, D., Johanning, L. (2012) 'Physical measurement of a slow drag of a drag embedment anchor during sea trials', *In the Proceedings of the International Conference on Ocean Energy (ICOE),* Dublin, Ireland, 17-19 October 2012

Weller, S., Davies, P., Thies, P.R., Johanning, L., **Harnois, V.** (2012) 'Durability of synthetic mooring lines for ocean energy devices', *In the Proceedings of the International Conference on Ocean Energy (ICOE),* Dublin, Ireland, 17-19 October 2012

Harnois, V., Johanning, L., Thies, P.R. (2013) 'Wave Conditions Inducing Extreme Mooring Loads on a Dynamically Responding Moored Structure', *In the Proceedings of the 10th European Wave and Tidal Energy Conference (EWTEC),* Aalborg, Denmark, 2-5 September 2013

Weller, S.D., Thies, P.R., Gordelier, T., **Harnois, V.**, Parish, D. and Johanning, L. (2014) 'Navigating the Valley of Death: Reducing Reliability Uncertainties for Marine Renewable Energy', *In the Proceedings of ASRANet Offshore Renewable Energy conference*, Glasgow, UK, 15-17th September 2014